Dissertation zur Erlangung des Doktorgrades
der Fakultät für Chemie und Pharmazie
der Ludwig-Maximilians-Universität München

Structure and Reactivity of *s*-Triazine-Based Compounds in C/N/H Chemistry

Fabian Karl Keßler

aus
Augsburg, Deutschland

2019

Erklärung

Diese Dissertation wurde im Sinne von § 7 der Promotionsordnung vom 28. November 2011 von Herrn Prof. Dr. Wolfgang Schnick betreut.

Eidesstattliche Versicherung

Diese Dissertation wurde eigenständig und ohne unerlaubte Hilfe erarbeitet.

München, 30.10.2019

.....

Fabian Karl Keßler

Dissertation eingereicht am	05.08.2019
1. Gutachter:	Prof. Dr. W. Schnick
2. Gutachter:	Prof. Dr. B. V. Lotsch
Mündliche Prüfung am	22.10.2019

Danksagung

Eine Arbeit wie diese ist niemals das Werk eines Einzelnen, insofern möchte ich an dieser Stelle meinen Dank all jenen ausdrücken, die mich auf diesem Weg begleitet und unterstützt haben.

Zuvordest möchte ich Herrn Prof. Dr. Wolfgang Schnick für die Möglichkeit danken, diese Arbeit in seiner Arbeitsgruppe anzufertigen, ebenso wie für die Betreuung und Anleitung die mir im Verlauf dieser Arbeit zuteil wurde. Insbesondere bedanke ich mich für die eingeräumte Gestaltungsfreiheit, sowie für beständige Ermutigung und Unterstützung.

Frau Prof. Dr. Bettina Lotsch danke ich herzlichst für die Übernahme des Koreferats dieser Arbeit.

Herrn PD Dr. Constantin Hoch, Herrn Prof Dr. Heinz Langhals, Herrn Prof. Dr. Thomas Klapötke und Herrn Prof. Dr. Hans-Christian Böttcher möchte ich meinen Dank für die Bereitschaft aussprechen, sich als weitere Prüfer meiner Doktorarbeit zur Verfügung gestellt zu haben.

Ganz besonderen Dank möchte ich Herrn Sebastian Schmiechen, der mich in die Welt der Festkörperchemie eingeführt hat und Frau Nicole Braml, die mir die C/N/H-Chemie nahe gebracht und mir gerade zu Beginn meiner eigenen Arbeiten in diesem Themenbereich eine unverzichtbare Hilfe war, aussprechen. Ohne eure Anleitung wäre ich nicht dort, wo ich heute bin.

Weiterhin möchte ich meinen Vorgängern im Bereich der C/N/H-Chemie, Dr. Nicole Braml, Dr. Eva Wirnhier, Dr. Sophia Makowski, Dr. Andreas Sattler und Prof. Dr. Bettina Lotsch für all die Vorarbeiten danken, auf denen ich aufbauen konnte, die mir Orientierung und Inspiration geboten haben und auf diesem Weg den Verlauf meiner Doktorarbeit ganz wesentlich geformt haben.

Zahlreichen Personen bin ich darüber hinaus für ganz konkrete Hilfestellungen und Unterstützung bei diversesten Problemstellungen dankbar. Zuallererst sei hierbei Herr PD Dr. Constantin Hoch genannt, dem ich für seine Hilfe und Anleitung bei etlichen kristallographischen Problemen herzlichst danken möchte. Herrn Prof. Dr. Jürgen Senker, Frau Dr. Maria Mesch und Frau Beate Bojer möchte ich meinen Dank für die Hilfe bei der NMR-spektroskopischen Charakterisierung von C/N/H-Verbindungen und die Aufnahme diesbezüglicher Messungen aussprechen. Für weitere Hilfestellung hinsichtlich der Planung und Auswertung von NMR-Experimenten ergeht mein herzlicher Dank an Herrn Thomas Bräuniger. Ganz herzlich möchte ich mich außerdem bei Herrn Dr. Markus Döblinger für die gemeinsame Planung und Durchführung von TEM-Experimenten bedanken. Herrn Wolfgang Wünschheim und Herrn Thomas Miller bin ich außerordentlich dankbar für die Unterstützung in allerlei technischen Belangen.

Meinen Kooperationspartnern in München und Leipzig möchte ich für die fruchtbare Zusammenarbeit danken: Herrn Prof. Dr. Christian Ochsenfeld, Herrn Dr. Asbjörn Burow und Herrn Gökcen Savasci für quantenchemische Berechnungen und Herrn Prof. Dr. Oliver Oeckler, Herrn. Dr.

Tobias Rosenthal und Herrn Peter Schultz für die Aufnahme und Auswertung von Synchrotron-Beugungsdatensätzen.

Ich danke außerdem der Schar fleißiger Praktikanten, welche mich im Laufe meiner Doktorarbeit unterstützt haben und an die ich mein Wissen weitergeben durfte: Lucie Thomas, Sebastian Häringer, Marie Däntl, Frank Schäfer, Thaddäus Koller und Alexander Schuhbeck.

Für die Durchführung zahlloser Messungen und die Unterstützung bei der Auswertung und Interpretation der Ergebnisse ergeht mein verbindlichster Dank an: Dr. Peter Mayer und Arthur Haffner für Einkristall-Beugungsexperimente, Marion Sokoll für FT-IR-Aufnahmen, Christian Minke für Festkörper-NMR-Spektroskopie und Rasterelektronenmikroskopie, Susanne Ebert und Robert Eicher für CHNS-Elementaranalytik, Jaroslava Obel für ICP-AES-Messungen, Brigritte Breitenstein und Sonja Kosak für massenspektrometrische Untersuchungen, Sascha Harm für DSC/TG-Aufnahmen und Anna-Katharina Hatz für impedanzspektroskopische Messungen.

Jenseits der reinen Wissenschaft möchte ich mich ganz besonders bei meinen Laborkollegen Sascha Harm, Jonny Sappl, Anna-Katharina Hatz und Christian Minke, sowie all den zahlreichen Bacheloranden, F-Praktikanten und Masteranden, mit denen ich im Verlauf der letzten fünf Jahre das Labor teilen durfte, für die angenehme und entspannte Arbeitsatmosphäre und zahllose amüsante Unterhaltungen im und außerhalb des Labors bedanken.

Darüber hinaus danke ich an dieser Stelle allen gegenwärtigen und ehemaligen Mitgliedern der Arbeitskreise Schnick, Johrendt und Lotsch, die ich als ungemein herzliche, hilfsbereite und angenehme Kollegen kennen lernen durfte: Dr. Dominik Baumann, Dr. Eva-Maria Bertschler, Dr. Philipp Bielec, Jakob Blahusch, Dr. Nicole Braml, Dr. Thomas Bräuniger, Leo Diehl, Dr. Dajana Durach, Lucien Eisenburger, Eugenia Elzer, Florian Engelsberger, Dr. Erik Flügel, Dr. Gina Friederichs, Lisa Gamperl, Tobias Giftthaler, Kerstin Gottschling, Arthur Haffner, Sascha Harm, Anna-Katharina Hatz, Dr. Jonas Häusler, PD Dr. Constantin Hoch, Dr. Katrin Horky, Dr. Franziska Hummel, Dr. Simon Kloß, Dr. Claudia Lermer, Catrin Löhnert, Olga Lorenz, Dr. Christian Maak, Mathias Mallmann, Dr. Olaf Alberto von Mankowski, Dr. Alexej Marchuk, Christian Minke, Dr. Lukas Neudert, Robin Niklaus, Dr. Ursula Pachmayr, Dr. Simon Peschke, Dr. Christine Pösl, Reinhard Pritzl, Florian Pucher, Dr. Philipp Pust, Tobias Rackl, Dr. Annekathrin Ranft, Dr. Dieter Rau, Bettina Rendenbach, Jonathan Sappl, Hendrik Schlomberg, Dr. Sebastian Schmiechen, Stefanie Schneider, Dr. Katharina Schwinghammer, Juliane Stahl, Dr. Linus Stegbauer, Dr. Philipp Strobel, Dr. Christine Stürzer, Dr. Tobias Stürzer, Dr. Katalin Szendrei-Temesi, Dr. Frank Tambornino, Stefan Trenker, Sebastian Vogel, Peter Wagatha, Sophia Wandelt, Valentin Weippert, Sebastian Wendl, Dr. Erwin Wiesenmayer, Dr. Matthias Wörsching, Wolfgang Wünschheim und Otto Zeman.

Ein ganz herzliches Dankeschön ergeht an meine Studienkollegen Philipp Angloher, Martin Reynders, Sabine Auras, Juliane Stahl, Patrick Jüstel, Leonhard Kick, Martin Grundei, Anselm Gruber, Anne Schultz, Patricia Liebhäuser, Thomas Rösener und Kerstin Sigl, die mich nicht nur während meiner

Doktorarbeit, sondern bereits zuvor durchs Studium – alles in allem also ein volles Jahrzehnt – begleitet haben und die als meine Freunde zu zählen ich mich außerordentlich glücklich schätze.

Schlussendlich möchte ich selbstverständlich auch meiner gesamten Familie danken – insbesondere meinen Eltern Marion und Wilhelm Keßler, sowie meiner Schwester Nina – die mich in all diesen Jahren immer vorbehaltslos und uneingeschränkt unterstützt und bekräftigt haben und mir so erst ermöglicht haben, mein Studium und meine Promotion zum Abschluss zu bringen.

Inhalt

1. Introduction

It seems only appropriate to begin this thesis with the mention of *Justus Liebig*, since it was *Liebig* with whom the entire field of C/N/H chemistry began. Although the initial discovery of the thermal transformation of mercury(II) thiocyanate, $Hg(SCN)_2$, to a carbon nitride type material—an experiment that became famous as a fairground attraction by the name of 'Pharaoh's serpents' due to the snake-like shape of the formed structures—is attributed to *Jöns Jakob Berzelius*, it was *Liebig* who first published an extensive work on a wide range of these compounds in 1834.[1] In this, *Liebig* reported not only on *Berzelius'* material, which he named melon (or mellon in later publications),[2,3] but also a series of related compounds by the names of melamine, melam, ammeline, ammelide and melonkalium. These non-systematic names—originating from a time before nomenclature conventions were established—are still in use. *Liebig* himself declared that they were not deduced from the color or any property of the compounds, but chosen arbitrarily since he deemed them as good as any.[1]

These compounds, initially characterized only by their elemental composition and reaction behavior, share the common feature of one of two molecular building blocks, which themselves are closely related: the triazine ring, C_3N_3, also known as *s*-triazine, *sym*-triazine, 1,3,5-triazine or cyanuric nucleus; and the heptazine ring, C_6N_7, which also goes by the names of *s*- or *sym*-heptazine, tri-*s*-triazine, 1,3,4,6,7,9,9b-heptaazaphenalene or cyameluric nucleus. Both of these are comprised of six-membered aromatic rings with alternating C and N atoms, the triazine ring being comprised of one such unit, while the heptazine ring is formed from three fused rings (Figure 1.1). Such systems are exclusively composed of C-N bonds, which exhibit relatively high bond dissociation energies as compared to C-C, C-H or N-N bonds due to the significant difference in electronegativity between C and N that leads to the formal oxidation states of C^{+IV} and N^{-III}. This results in compounds exhibiting the remarkable thermal and oxidative stability as well as chemical inertness that characterize this group of materials.[4] Both of these nuclei possess three 'outer' carbon atoms that are available for either terminal groups such as hydrogen, amino, keto or halogenide moieties, resulting in a variety of monomeric molecular species; or for bonds towards bridging

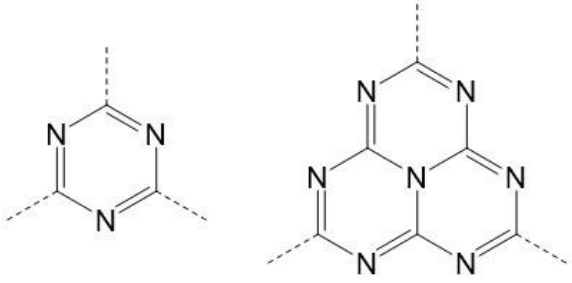

Figure 1.1: Fundamental building blocks of C/N/H chemistry. Left: triazine nucleus; right: heptazine nucleus.

imide groups or (supposedly) tertiary N atoms, which join together several such ring systems, resulting in dimeric, oligomeric or 1D or 2D polymeric compounds.

Following *Liebig's* initial discoveries, a large number of further C/N/H compounds was described, such as potassium hydromelonate, $K_3C_6N_7(NCN)_3$ by *Gmelin*,[5] cyameluric acid, $C_6N_7H_3O_3$ by *Henneberg*[6] or melem, $C_6N_7(NH_2)_3$ by *Klason*.[7,8] Throughout the 19th century, this substance class was subject of—at times rather heated—discussions and sparked great interest regarding the composition and structural identity of its representatives. A number of noteworthy contributions was made in the early 20th century. *Franklin* proposed the concept of amminocarbonic acids for C/N/H compounds, interpreting them as de-ammonation products of a hypothetical ammono-orthocarbonic acid, $C(NH_2)_4$, or, vice versa, as adducts of the also hypothetical final de-ammonation product carbon nitride, C_3N_4, and ammonia in specific stoichiometric ratios.[9] This concept is derived from the analogous concept for aquocarbonic acids that interprets carbonic acid, H_2CO_3, and carbonic anhydride, CO_2, as dehydration products of orthocarbonic acid, $C(OH)_4$, although the substance class of 'ammonocarbonic acids' is much larger. Table 1.1 lists the most common representatives of this class in the form of ammonia adducts of C_3N_4.

Table 1.1: Common C/N/H compounds described as "ammonocarbonic acids" according to *Franklin*.

C/N/H compound	sum formula	x C_3N_4 · y NH_3
guanidine	CN_3H_5	1 C_3N_4 · 5 NH_3
biguanide	$C_2N_5H_7$	1 C_3N_4 · 3.5 NH_3
cyanamide	CN_2H_2	1 C_3N_4 · 2 NH_3
dicyandiamide	$C_2N_4H_4$	1 C_3N_4 · 2 NH_3
melamine	$C_3N_3H_6$	1 C_3N_4 · 2 NH_3
melam	$C_6N_{11}H_9$	1 C_3N_4 · 1.5 NH_3
melem	$C_6N_{10}H_6$	1 C_3N_4 · 1 NH_3
melon	$C_6N_9H_3$	1 C_3N_4 · 0.5 NH_3
poly(triazine imide)	$C_6N_9H_3$	1 C_3N_4 · 0.5 NH_3
dicyanimide	C_2N_3H	1 C_3N_4 · 0.5 NH_3
hydromelonic acid	$C_9N_{13}H_3$	1 C_3N_4 · 0.33 NH_3

Pauling and *Sturdivant* introduced the heptazine or cyameluric nucleus as a building block for various C/N/H compounds—such as melon or hydromelonic acid—whose structure had been a mystery for more than a century.[10] Prior structure propositions based on interconnected triazine nuclei had not been able to account for the acidity and hydrolysis reaction behavior of these compounds. The existence of this nucleus, proposed based on quantum-mechanical calculations, could later be verified by structural data obtained from X-ray diffractometry. On the basis of this proposed structure, *Redemann* and *Lucas* established the molecular structures of melam, melem and melon.[11] Melam, $C_6N_{11}H_9$, can be described as tetraaminodicyanurimide, $[C_3N_3(NH_2)_2]_2NH$, while melem, $C_6N_{10}H_6$, is cyameluryl triamide, $C_6N_7(NH_2)_3$. For melon, two different structures based on the cyameluric nucleus were proposed, the first consisting of three nuclei connected by imide bridges in a cyclic arrangement, while in the second model the building blocks are arranged in (infinite) linear chains.

Interest in C/N/H chemistry somewhat abated in the second half of the 20th century. A noteworthy exception to this are *Finkel'shtein* and coworkers, who investigated this substance class intensely throughout the 60s and 70s.[12,13] While their studies were primarily spectroscopic in nature[14-16]—with a focus on IR, Raman and UV-Vis spectroscopy—they also made a number of mentionable preparative contributions in the form of molecular as well as ionic C/N/H compounds and their derivatives.[17,18] Further investigations included studies in the thermal properties[19,20] and solubility[21] of these substances as well as quantum-mechanical calculations of spectra and properties,[22] thus contributing greatly to the methodology of C/N/H compound characterization and synthesis.

Renewed interest in C/N/H chemistry was sparked by a series of publications by *Liu* and *Cohen* in the last decade of the century.[23-26] Their calculations predicted a bulk modulus for β-C_3N_4—a hypothetical carbon nitride compound with a structure analogous to β-Si_3N_4—that exceeded the bulk modulus of diamond. This material constant as a measure of the compressibility of a solid material under hydrostatic pressure is related to the material hardness on a microscopic level and assuming a simple, ideal, defect-free system.[23] On a macroscopic scale, however, the complex property 'hardness', which cannot be physically exactly defined, also depends on other properties such as the shear modulus, which describes the behavior of the material when exposed to shear forces. However, it can be tempting to use hardness and bulk modulus interchangeably, not least because they are experimentally strongly correlated. For example, diamond, the hardest known material, does also possess the highest bulk modulus. β-C_3N_4 was thus interpreted as a material with the potential to exceed diamond in hardness or at least a novel super-hard material. This prospect started a veritable rush towards the preparation of this phase, sometimes called the 'harder-than-diamond fever'.

A broad array of methods was applied for the preparation of this material, ranging from conventional synthetic approaches such as pyrolysis of nitrogen-rich organic precursors[27,28] to more exotic, physico-chemical methods like shockwave decomposition,[29] chemical vapor deposition,[30] ion beam deposition, reactive sputtering[31] and laser techniques.[32] However, most of these attempts yielded either amorphous powders of undefined composition or thin films of nitrogen-doped, mainly sp^2-hybridized carbon. Although claims of the successful synthesis of β-C_3N_4 have frequently been made, no unambiguous evidence for these could be presented.[33]

As for structurally related diamond, quantum-mechanical calculations predict metastability for β-C_3N_4. *Teter* and *Hemley* postulated four additional C_3N_4 modifications beside the β-phase: an α-phase structurally related to β-C_3N_4, a planar graphitic C_3N_4-phase, a pseudocubic structure based on α-$CdIn_2Se_4$ and a willemite-II-like cubic structure.[34] Of these, the former two are energetically favored compared to β-C_3N_4, with graphitic C_3N_4 representing the energetic minimum under ambient conditions. The cubic *c*-C_3N_4 that might possess a bulk modulus exceeding that of the β-phase, is predicted to become energetically favorable under elevated pressure. A diamond analogous synthetic approach starting from graphitic C_3N_4 thus appeared a feasible route to low-compressibility carbon

nitride phases. C/N/H compounds, especially *Liebig's* highly condensed melon, were seen as promising precursor materials for this g-C_3N_4.

Various different structure models were proposed for g-C_3N_4. While initially a triazine-based model was assumed, quantum-chemical calculations by *Kroke* showed a model based on the heptazine nucleus to be energetically favorable.[35] This model, comprised of heptazine nuclei interconnected by tertiary nitrogen atoms, is identical with a structure proposed by *Redemann* and *Lucas* in 1940 for an extended version of their cyclic melon structure.[11] Both models are depicted in Figure 1.2.

Based on the works of *Franklin* as well as *Redemann* and *Lucas*, *Komatsu* conducted a series of experiments to synthesize polymeric carbon nitrides starting from molecular precursors. In these simple setups, triazine or heptazine derivatives in various combinations were heated to elevated temperatures in sealed autoclaves. Based on mass spectrometry, IR spectroscopy and elemental analyses, imide bridged chains of aminoheptazine[36] as well as triangular arrangements of heptazine rings interconnected by tertiary nitrogen atoms, consisting of five by five units[37], were proposed as structures for the obtained products. Both of these arrangements are in agreement with *Redemann's* structure propositions for melon. Further experiments of the series were claimed to have yielded carbon nitrides with a composition close to $CN_{1.0}$ and a structure, in which heptazine rings are interconnected by sp^2-hybridized carbon atoms,[38] or extended sheets of imide bridged triazine rings[39] that show great similarity to *Teter's* model.[34] While all of these products exhibited poor crystallinity and no unambiguous validation of the structure models was possible, it is the simplicity of the synthesis routes—especially in comparison with the abovementioned methods—that makes these experiments noteworthy and emphasizes the potential of triazine- and heptazine-based small molecules.

Throughout the first decade of the 21st century, the 'harder-than-diamond fever' abated—in parts, because further calculations had shown that the bulk modulus of the respective C_3N_4 modification might be slightly less than the one of diamond and the significantly lower shear modulus would make the material less hard than expected; in parts because the hope of finding a synthetic approach towards

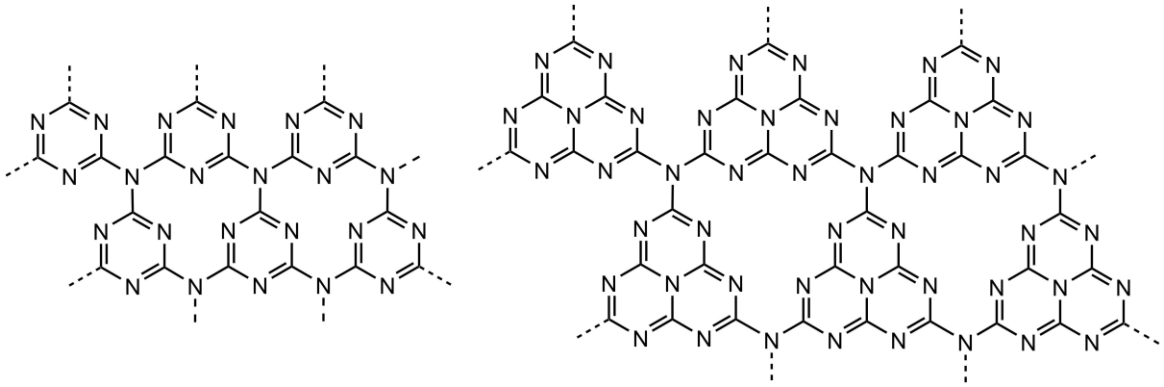

Figure 1.2: Models for hypothetical graphitic C_3N_4. Left: triazine-based model according to *Teter* and *Hemley*. Right: heptazine-based model according to *Kroke*.

the still unknown compound dwindled. The focus of C/N/H research shifted towards material properties of the compounds, which had frequently been obtained in the endeavors to synthesize graphitic C_3N_4. In particular the polymeric materials—which supposedly are all closely related to melon—exhibited a band gap of interesting width and thus quickly became known as inexpensive, abundant, and easily accessible metal-free semiconductor materials. Application began to move more and more into the center of scientific attention. *Antonietti* and coworkers reported on catalytic activity of a mesoporous C/N/H material in various organic reactions. This 'mpg-C_3N_4' was successfully shown to catalyze Friedel-Crafts type substitution reactions on benzene with various acylation and alkylation reagents, CO_2 activation for the oxidation of benzene to phenol, as well as cyclotrimerization of alkynes and nitriles.[40-43] With specific applications in mind, the relevance of material optimization in contrast to development of new materials grew. Techniques such as nanocasting to obtain C/N/H material nanoparticles or the application of silica nanoparticle hard templates for the synthesis of mesoporous monoliths or films were successfully used to enhance surface areas and electronic properties of the dedicated catalyst materials.[44]

The groundbreaking discovery, which set the almost exclusive course in C/N/H chemistry for the following decade and until today, however, was the finding of photocatalytic activity of melon by *Wang* and coworkers.[45] A plethora of materials, with TiO_2 possibly the most prominent among them, has been proposed and investigated as potential photocatalysts, however, C/N/H materials—melon in particular—show a range of favorable properties that distinguish them amongst these alternative candidates. First of all, they show a remarkable thermal as well as chemical stability, with thermal degradation of melon only setting in around 700 °C. As metal-free photocatalyst materials they are independent of critical raw materials such as noble metals or rare earth elements, inexpensive due to the abundance of the comprising elements and simplicity of the synthesis process, and non-toxic as well as environmentally friendly. Raw melon exhibits only moderate solar conversion efficiency, which is attributed to a wide bandgap, high rates of charge recombination and insufficient number of surface active sites.[46] However, as for organic catalysis, the efficiency can be increased by nanostructurization, increase of surface area or doping. Another intensely studied optimization approach is the formation of heterojunction materials and nanocomposites to alleviate these drawbacks. Potential candidate materials for these are carbon-based materials such as fullerenes, carbon nanotubes or quantum dots, noble metal nanodots as well as various transition metal oxides and sulfides.[47-50]

The most important field of application for C/N/H photocatalyst materials is water splitting. The separation of hydrogen and oxygen driven by solar energy has the potential to become an important asset in the transition in energy generation from fossil fuels to renewable energy sources, as it allows the fixation of abundant solar energy in the storable form of chemical energy. Hydrogen is a very favorable storage form in this, since with hydrogen fuel cells a technically mature and highly efficient technology for the conversion into electric energy is available. Alternatively, solar fuels can be

generated through photocatalytic reduction of CO_2. Realization of this reaction is more complex than for water splitting, since it is based on a multi-electron transfer process. It would, however, simultaneously allow to remove greenhouse active CO_2 from the atmosphere and yield small hydrocarbons such as methane, methanol or formaldehyde, which find application not only in energy generation, but also organic synthesis.[51,52] C/N/H materials exhibit a conduction band edge being sufficiently negative to facilitate this process, making them promising photocatalysts for this process, although fast recombination of charge carriers within the material somewhat hampers the catalytic efficiency and necessitates co-catalysts or heterojunction materials. Both of these processes, light-driven water splitting as well as CO_2 reduction, take place analogously in green plants during photosynthesis, earning the here described processes the moniker of 'artificial photosynthesis'. Another promising application for C/N/H photocatalysts is degradation of organic pollutants for the remediation of industrial wastewater. Photocatalysts can initiate this process by generation of reactive oxygen species such as $^{\bullet}OH$ or $^{\bullet}O_2^+$ from either H_2O itself or through activation of added H_2O_2.[48,51-53] Since this technology is developed with organic dyes in mind, experiments usually apply rhodamine B (RhB), methyl orange (MO) or methylene blue (MB) as test systems. Further potential applications include N_2 photofixation, antimicrobial films and fungicides.[54]

An unfortunate development that came along with the reorientation of C/N/H chemistry towards application is a certain decay in usage of nomenclature. Since the investigated materials often are of undefined composition and characterization became less and less important, the term 'g-C_3N_4' became common to describe these compounds, even though they contain significant amounts of hydrogen and the C:N ratio deviates from 3:4. This custom is a regrettable continuation of the disreputable earlier trend to declare compounds to be *Teter* and *Hemley's* long sought-after 'graphitic C_3N_4', which later turned out to differ from this model in composition as well as structure. Presumably, the materials investigated for photocatalytic applications, which usually are polymeric, heptazine-based compounds, could all be described as melon—which has been accepted as a material of ill-defined composition and consisting of several polymorphs since the days of *Franklin* and *Redemann* and *Lucas*. It is thus all the more incomprehensible, from where the urge to denote these materials as a pure carbon nitride results. The use of this misleading denotation is therefore to be strongly discouraged. It does, however, deserve mention that in recent years more and more groups refrain from the denotation 'g-C_3N_4' and instead denote their materials as 'polymeric carbon nitride' (PCN), a much more suitable term for these structurally unidentified compounds.[47,55-57]

The possibly most important concept in C/N/H chemistry is the concept of a reaction cascade linking amino-terminated triazine and heptazine compounds via a series of consecutive condensation reactions that transform each of these compounds into the respective next higher condensed compound under elimination of ammonia (Figure 1.3). This concept was initially introduced by *Franklin* in his treatise on C/N/H compounds as ammonocarbonic acids.[9] In this, he explicated that C/N/H compounds of higher degrees of condensation—according to the interpretation of these

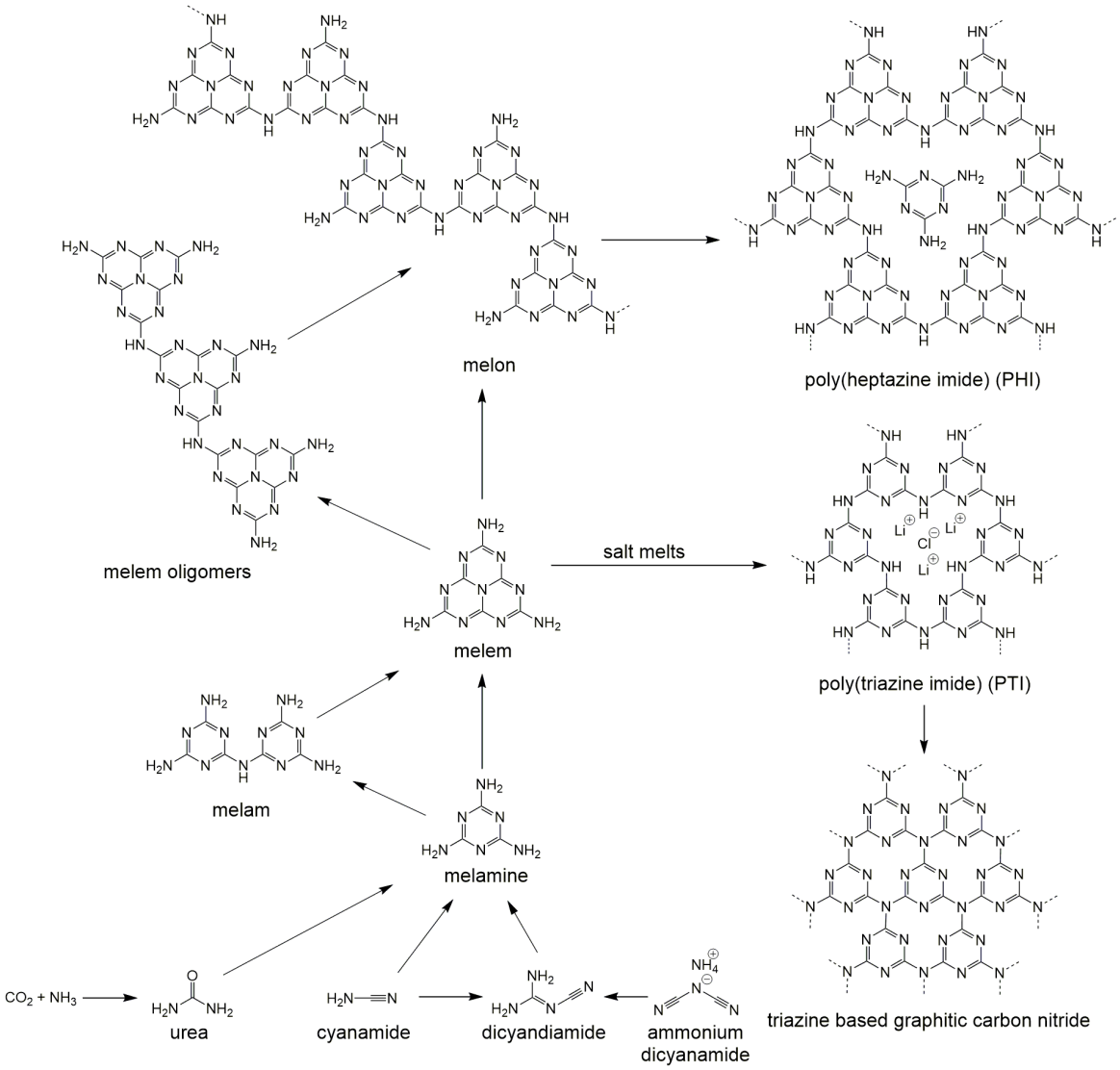

Figure 1.3: Condensation cascade of C/N/H compounds.

compounds as adducts of C_3N_4 and NH_3—can not only formally be seen as deammonation products of less condensed compounds, but that most of these conversions have actually been experimentally observed. *May* studied the pyrolysis of melamine and was able to detect melam, melem and melon alongside defined amounts of ammonia at successively higher temperatures.[58] Quantification of liberated ammonia showed the gas volume to be well in line with expectations according to *Franklin's* concept. While the constituents of the condensation cascade are known since *Liebig's* days, still not all of the involved steps have unambiguously been identified.

Franklin started his scheme with a number of small, non-cyclic molecules, such as hypothetical ammono-orthocarbonic acid or cyanamide and dicyandiamide. While these molecules without a doubt represent important precursor compounds, they are typically not included in the condensation cascade. The starting point is instead represented by melamine, the least condensed compound to contain the triazine building block. At temperatures around 350 °C, melamine is supposed to dimerize and form melam under elimination of ammonia, which, however, is quickly converted to heptazine-

based melem and is thus difficult to isolate. However, the discovery of several melamine-melem adducts led to speculations, whether melam actually is an intermediate or rather a side product formed under certain specific conditions, while the reaction proceeds via an imminent melamine-to-melem conversion mechanism.[59] Monomeric melem undergoes polymerization towards 1D polymeric melon at temperatures around 450 °C. Melem dimers and trimers, which can be isolated at reduced reaction temperatures, are typically not interpreted as unique species and are often neglected from the condensation cascade, although they are distinguishable from polymeric melon in their properties.[60] The generally accepted structure of melon, which still contains one amino group per heptazine unit that could be eliminated in further condensation reactions, would suggest condensation towards a 2D extended polymer to take place when further elevating the temperature. However, no such reaction can be observed. Instead, melon decomposes at temperatures above 650 °C, forming a mixture of various gaseous products and leaving no solid residue. A 2D extended polymer as part of the condensation cascade has only been reported in poly(heptazine imide), which has been obtained as a minor side phase alongside melon in reactions at elevated pressure and temperatures close to the decomposition temperature.[61] Condensation schemes as depicted in literature often conclude with a triazine- or heptazine-based C_3N_4 compound as the final product of the cascade. While this is in accordance with *Franklin's* concept, no such reaction has yet been experimentally observed.

Melamine, triamino-*s*-triazine, $C_3N_6H_6$, is the simplest and most intensely investigated C/N/H compound. *Liebig* initially synthesized melamine from potassium thiocyanate and ammonium chloride. Nowadays, laboratory synthesis of melamine typically starts from cyanamide, CN_2H_2, which trimerizes to form melamine, or dicyandiamide, $C_2N_4H_4$, from which the reaction pathway supposedly runs via cyanamide, as well. These three compounds share the same composition, thus—in contrast to most other conversions discussed here—this reaction is no condensation and does not liberate ammonia. Industrially, melamine is obtained from urea. Various high- or low-pressure processes are applied, which are often directly coupled to urea synthesis from ammonia and carbon dioxide within the same plant.[62] Melamine is an industrially relevant material with global annual production surpassing 2 million tons.[63] Its most important application is in melamine-formaldehyde resins, which find use in surface coating, laminating and adhesives, as plastic tableware and dirt-removing sponges.[64-67] Furthermore, melamine and derivatives have been investigated as flame retarding impregnation materials, since they not only possess a high thermal stability that allows them to act as 'heat sinks', but also release flame suppressing nitrogen upon decomposition.[68-70] It deserves mention, that melamine was also the first C/N/H compound to be structurally elucidated by X-ray diffractometry. *Hughes* described a monoclinic structure comprised of planar rings that are interconnected by hydrogen bridge bonds.[71] Very uniform bond lengths and angles indicated complete resonance of the double bonds within the triazine ring, i.e. the triazine ring as an aromatic system.

Melam, $C_6N_{11}H_9$, is the dimer of melamine, two amino-terminated triazine rings linked by a bridging imide group. The condensation mechanism, by which two molecules of melamine should form melam and one equivalent of ammonia, is obvious. However, thermal condensation of melamine typically yields melem with melam occurring as a side phase at best. Preparative approaches that proved feasible to obtain phase pure melam include autoclave reactions, in which elevated ammonia pressure inhibits the formation of melem (which would be accompanied by further ammonia evolution),[72] or the neutralization of melamium halide salts, which are readily obtained from the reaction of dicyandiamide with ammonium halides.[73] Although melam was first mentioned by *Liebig*, the crystal structure was only elucidated a decade ago.[74] Melam features a torsion angle of 11° to 14° between the two triazine ring planes. This results in a helical crystal structure, which is not determined by van-der-Waals interactions, but rather dominated by a network of hydrogen bridge interactions. Melam thus contrasts other C/N/H compounds, in which the planarity of the respective ring systems often results in layered structures. Industrial applications of melam are scarce. Although there are reports

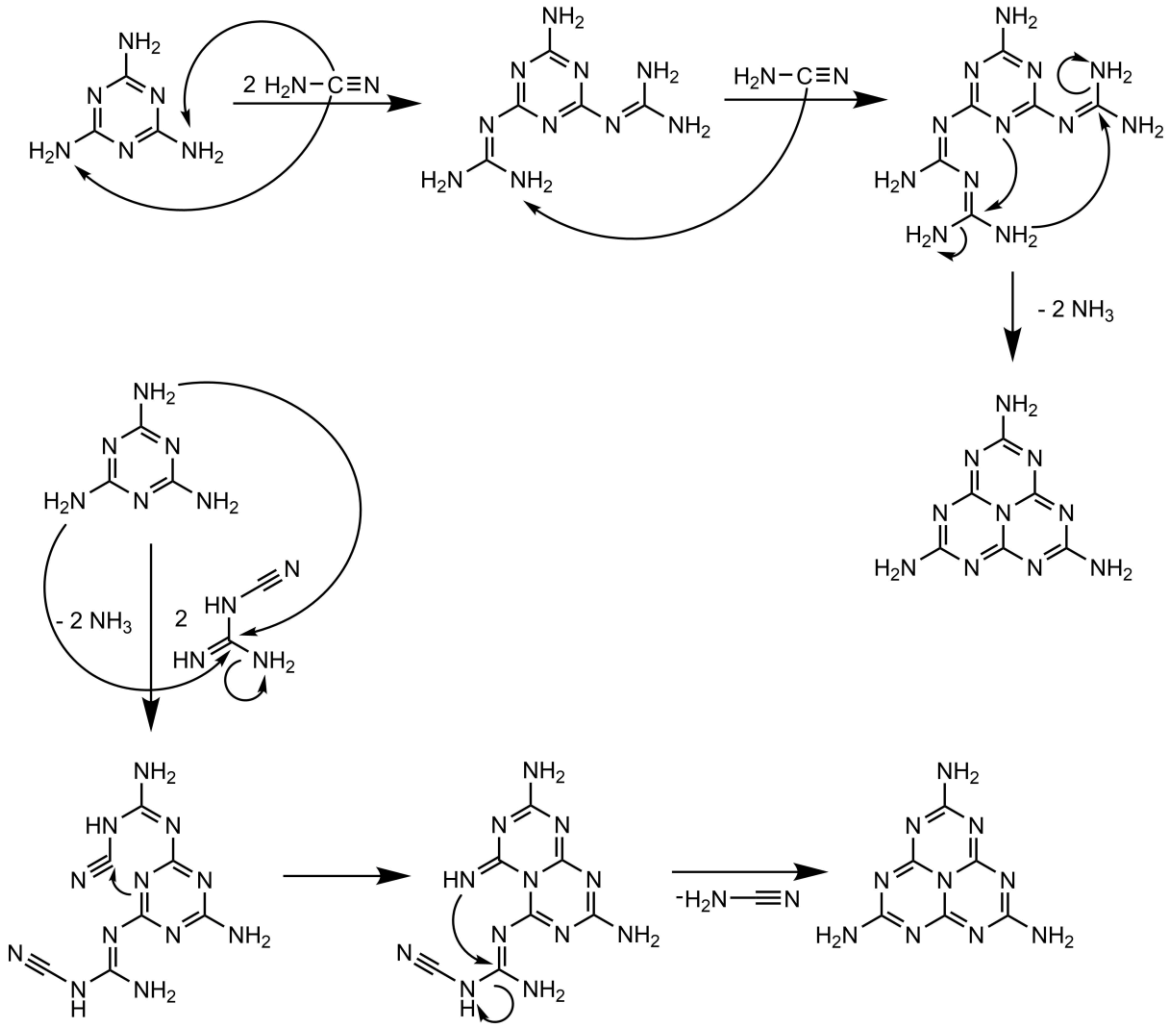

Figure 1.4: Possible reaction mechanisms for the formation of heptazine-based melem from triazine-based melamine. Top: mechanism proposed by May.[58] Bottom: mechanism proposed by Shahbaz et al.[76]

of melam as nitridation agent in steel surface hardening as well as of applicability as flame retardant, the relevance of melam is negligible.

Formation of melem, triamino-*s*-heptazine, $C_6N_{10}H_6$, from melamine sets in above a temperature of about 360 °C. As postulated by *Pauling*, melem is comprised of the cyameluric nucleus terminated by three amino groups. Melem appears to be a thermodynamic sink, being thermally stable up to 450 °C and being facilely obtained through thermal condensation. The mechanism for the formation of the heptazine nucleus from triazine-based starting materials in the formation of melem has been the subject of much discussion and has not been unambiguously determined.[58,75,76] Furthermore, the models found in literature assume melamine as the imminent triazine-based precursor for melem (Figure 1.4). However, this does not account for an alternative pathway, which assumes melam as a reactive intermediate. Experimental evidence for both proposed reaction pathways has been reported in the form of melamine-melem adducts on the one hand[59]—proving the parallel existence of melamine and melem—and melam-melem adducts on the other.[72] The crystal structure of melem has been studied by X-ray powder as well as single crystal diffractometry.[77,78] It is comprised of two different kinds of stacked layers, which are tilted towards each other with an angle of ca. 40°. Melem molecules are almost perfectly planar and stacked with an interlayer distance of 327 pm, which is close to the van-der-Waals distance found for graphite and thus interpreted as mainly determined by these interactions. Like melam, melem has no industrial relevance.

The final product of the condensation cascade, melon, poly(aminoimino)heptazine, '$C_6N_9H_3$', is a 1D polymeric material comprised of imide bridged heptazine building blocks. However, 'melon' does not necessarily describe a single compound of defined composition. The degree of polymerization within the material is rather low, with melon prepared according to standard procedures—i.e. heating of less condensed C/N/H precursors to temperatures between 450 and 650°C for several hours—possessing chain lengths no longer than ten units.[36] Furthermore, the completeness of the condensation process strongly depends on reaction conditions. At lower temperatures, oligomers of two or three units are obtained,[60] while elevated temperatures and pressure promote the condensation. Additionally, it cannot be excluded that the circular form of melon proposed by *Redemann* and *Lucas* contributes to the overall composition as well. The nominal sum formula $C_6N_9H_3$ assumes an infinite polymer. Thus, materials of short chain lengths would show higher nitrogen and hydrogen contents. This leads to varying compositions depending strongly on the preparation of the material. Furthermore, melon is difficult to characterize due to its insolubility in polar as well as apolar solvents and its notorious amorphicity. A crystal structure of melon could be elucidated for a particular crystalline and highly condensed material that was obtained from sealed ampoules at 630 °C under autogenous pressure, through a complementary approach of electron diffraction, X-ray powder diffraction and solid-state NMR spectroscopy.[79] The structure is comprised of zigzag strands arranged in layers with close distances between the strands that allow for the formation of hydrogen bridge bonds. While this results in a structure that is well-ordered in two dimensions, the respective layers are only connected

by weak dispersion forces. Thus, melon exhibits a pronounced stacking disorder along the crystallographic *c* direction. 2D solid-state NMR spectroscopy and force field calculations allowed for the elucidation of this disorder.[80] It could be deduced that melon layers, while showing no ordered stacking pattern, are arranged in a manner to reduce heptazine overlap between successive layers. Melon as obtained from conventional thermal condensation synthesis is a material of pale to bright yellow color (Figure 1.5), which corresponds to a band gap of ~2.7 eV.[45] It is generally assumed that this results from an extended conjugated π-system along the strands of imide bridged heptazines. It is this bandgap width that makes melon particularly suitable for the abovementioned water splitting process, since the bandgap is sufficiently narrow to allow absorption throughout a major range of the solar spectrum, but wide enough to catalyze the reduction of H^+ as well as the oxidation of O^{2-}.

Figure 1.5: C/N/H materials of different degrees of condensation. From left to right: melamine, melem, and melon.

Poly(heptazine imide) (PHI) with intercalated melamine, $C_{12}N_{17}H_3{\cdot}C_3N_6H_6$, represents the only 2D extended polymer that has been obtained directly from thermal condensation of C/N/H materials. However, no synthetic approach to quantitatively obtain this product is known. Instead, the material was only found as a minor side phase in melon syntheses under harsh experimental conditions, similar to the synthesis of abovementioned 'crystalline' melon and its 2D structure determined by electron diffraction.[61] Analogous to melon, PHI is a planar, layered material with no covalent bonds between distinct sheets. The layers are formed from heptazine nuclei, which are each connected to three adjacent heptazine building blocks through imide bridging. This results in a porous network, in which six nuclei, respectively, are arranged in a triangular motif with a melamine molecule, only connected to the network via hydrogen bonds, located in the central cavity. Recently, a C/N/H compound sharing the PHI heptazine network, however with potassium ions intercalated within the cavities, was obtained from triazole or tetrazole starting materials in eutectic LiCl/KCl salt melts.[81,82] These cavities appear to be accessible for ion exchange, which allowed for the synthesis of several other poly(heptazine imide) compounds with various mono- and divalent metal cations.[83] These materials proved promising for photocatalyst applications in water splitting as well as in photooxidation of organic molecules.[84-86] With photocatalytic efficiencies exceeding those of benchmark material melon and the ability to decouple reduction and oxidation reaction through a stable radical K-PHI$^{\bullet-}$,[87] they have received wide attention throughout the photocatalyst community.

Another 2D extended polymeric C/N/H material, although not directly obtainable from thermal condensation of small precursor molecules, is poly(triazine imide) (PTI). PTI shares the network connectivity of PHI, however, comprises triazine rings interconnected by imide bridges instead of

heptazine building blocks. The material was initially reported as the product of the reaction of melamine and cyanuric acid under high pressure conditions in a piston cylinder apparatus and contained HCl intercalated within the cavities, however, received little attention due to the complicated synthesis process.[88] A more facile approach was found in an ionothermal synthesis route applying eutectic LiCl/KCl salt melts.[89] Although the recovered product was initially misidentified as heptazine-based graphitic C_3N_4, a more thorough investigation using powder X-ray and electron diffraction data as well as solid-state NMR spectroscopy correctly established the identity of the compound.[90] PTI obtained from LiCl/KCl salt melt intercalates Li^+ and Cl^- ions within its channels as well as partially substitutes imido group protons for additional Li^+ ions. The disordered H/Li substructure could be elucidated by 2D multinuclear solid-state NMR spectroscopy.[91] Substituting LiCl/KCl by LiBr/KBr yielded a structurally identical compound with intercalated Li^+ and Br^- ions. No such substitution was possible for an analogous fluoride compound, although ion exchange in PTI/Li^+Br^- with ammonium fluoride yielded PTI/Li^+F^-.[92] PTI also showed to be a promising material for photocatalysis. While PTI itself already exceeds melon in photocatalyic activity towards hydrogen evolution, further improvement of the efficiency has been achieved through doping with structurally related organic heterocycles or through nanostructurization via exfoliation of PTI sheets.[93,94] Furthermore, it could be shown that the bandgap of PTI/Li^+Cl^- depends on the Li^+ content, which can be tuned by post synthesis Li^+ extraction, thus allowing for systematic bandgap tuning.[95]

Ionothermal synthesis supposedly also opened an approach towards a carbon nitride material of even higher degree of condensation. Triazine-based graphitic C_3N_4 (TGCN), the carbon nitride modification postulated by *Teter* and *Hemley* has reportedly been found as a side phase in PTI syntheses in LiBr/KBr melts.[96] The compound, which formed thin films at the interface between the melt and the ampoule wall, could be obtained as macroscopic flakes up to several hundred layers thick. The structure, which was elucidated through electron diffractometry, consists of corrugated layers of triazine rings connected by tertiary N atoms. No quantitative synthesis of TGCN has been reported in literature. The compound is nevertheless of great interest due to its close relation to graphene on the one hand as well as in regard of the longtime search for C_3N_4 started by the 'harder-than-diamond-fever'.

Apart from these compounds, which are exclusively composed of carbon, nitrogen and hydrogen, a variety of derivatives based on the triazine or heptazine nucleus terminated by functional groups containing 'heteroatoms' exists. Many of them are similar in properties to pure C/N/H compounds or represent important intermediates or starting materials and thus deserve brief mention in this place.

Ammeline, ammelide and cyanuric acid are hydrolysis products of melamine with one, two or three of the terminal amino groups formally replaced by hydroxy groups, resulting in sum formulas of $C_3N_5H_5O$ for ammeline, $C_3N_4H_4O_2$ for ammelide and $C_3N_3H_3O_3$ for cyanuric acid (Figure 1.6). Ammeline and ammelide date back to *Liebig's* original publication on C/N/H compounds.[1] Ammeline was initially obtained through basic hydrolysis of melam in aqueous KOH followed by precipitation through neutralization. However, various other facile synthesis routes starting from dicyadiamide or

biguanide and cyanic acid, cyanuric acid, urea or urethane have been reported.[97,98] Unlike melamine, ammeline possesses no industrial relevance and has mainly been studied due to its appearance as disturbing impurity in melamine-formaldehyde resin fabrication. No crystallographic structure of ammeline is known. The question of tautomerism, however, has been extensively studied in solid state as well as in aqueous solution. Quantum-chemical calculations as well as spectroscopic experiments were able to establish a preference for the keto tautomer both in solid state and solution, while the hydroxy form is energetically preferred in the gas phase.[99,100]

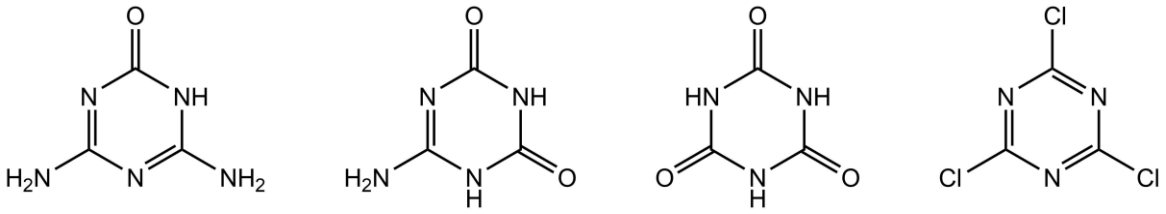

Figure 1.6: Heteroatom-substituted triazine compounds. From left to right: ammeline, ammelide, cyanuric acid, cyanuric chloride.

Ammelide could be synthesized by *Liebig* through acidic hydrolysis of melam, melamine or ammeline in concentrated nitric or sulfuric acid. Further synthesis routes described in literature name ammelide as a decomposition product of carbamide or biuret when heated to temperatures around 200 °C[101] as well as the hydrolysis of 2-amino-4,6-dichloro-*s*-triazine.[102] In many respects, ammelide resembles ammeline and both compounds are often investigated simultaneously. Like ammeline, ammelide can appear as an impurity in melamine-formaldehyde resin formation. Both materials are decomposition products of the herbicide atrazine (1-chloro-3-ethylamino-5-isopropylamino-2,4,6-triazine).[103,104] In recent years, a multitude of methods for the parallel quantification of melamine, ammeline, ammelide and cyanuric acid has been under investigation as a consequence of the food adulteration scandals of 2007 and 2008.[105]

Cyanuric acid is one of the longest known triazine-based compounds and, in fact, has been reported on even before *Liebig's* groundbreaking work on C/N/H compounds. Early mentions date back to *Scheele* in 1776, Wöhler in 1829 and *Sérullas* in 1830.[106-108] However, since the compound is potentially formed in nature from isocyanic acid, it might actually exist since prebiotic times.[107] Various synthetic approaches have been realized. *Sérrulas* hydrolyzed cyanuric chloride, while *Wöhler* thermally decomposed urea and uric acid. Acidic hydrolysis of melamine is also feasible and has been industrially realized. Nowadays, however, commercial synthesis of cyanuric acid usually follows *Wöhler's* approach and uses urea as a starting material.[109] As with its synthesis, cyanuric acid was one of the first triazine-based compounds to be crystallographically elucidated, predating the elucidation of the melamine structure by three years.[110,111] The crystal structure, which was later revised by the same author, is comprised of planar sheets of cyanuric acid molecules, which form a tight network of N–H–O hydrogen bridges.[112] It is noteworthy that very short and consistent C-O bond lengths were found in the structure, which indicate the prevalence of the keto tautomer in

cyanuric acid. This is in accordance with IR-spectroscopic data.[113] The most common application of cyanuric acid is in disinfection of swimming pools, in which bactericidal chlorine is stabilized through the formation of chlorinated intermediates and its release retarded to increase the depletion time.[114] As a starting material for organic synthesis, cyanuric acid has been valued for a long time for its three functionalities, e.g. in the formation of esters.[115,116]

Of even greater preparative importance is cyanuric chloride, $C_3N_3Cl_3$. This tri-chlorinated triazine derivative exhibits strong reactivity towards nucleophilic substitution reactions due to favorable Cl^- leaving groups.[117] Cyanuric chloride reacts with various amines, including ammonia, as well as aliphatic and aromatic alcohols. Like cyanuric acid and melamine, its discovery dates back to the first half of the 19th century.[118] For the initial synthesis, *Sérullas* reacted chlorine with hydrocyanic acid to obtain cyanogen chloride, which is able to undergo trimerization to form cyanuric chloride. The same synthesis route is still applied in industrial-scale production of the compound. The main application for cyanuric chloride is as a precursor for pesticides and herbicides, primarily atrazines, which accounted for about 70 % of the annual global production of 200.000 tons in 2005.[109] Further applications include dye fabrication and use as crosslinking agents, e.g. in the formation of covalent triazine frameworks (CTFs).[119,120]

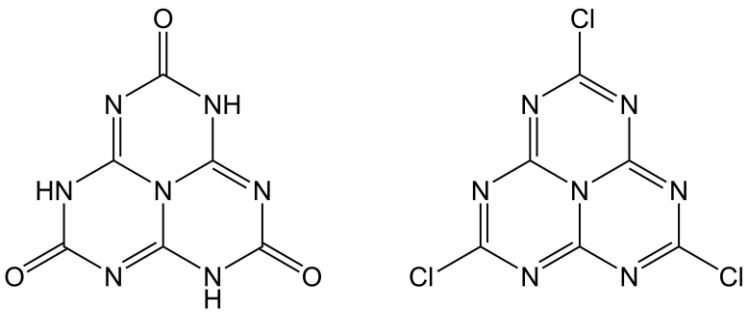

Figure 1.7: Heteroatom-substituted heptazine compounds. Left: cyameluric acid; right: cyameluric chloride.

Analogous to cyanuric acid and cyanuric chloride, the respective heptazine-based equivalents, cyameluric acid and cyameluric chloride exist (Figure 1.7). The former has been known for over 150 years, when it has first been prepared by *Henneberg* through alkaline decomposition of potassium cyamelurate.[6] The compound featured prominently in the structure elucidation of the heptazine—or cyameluric—nucleus[10,11] and although it is of little practical relevance, it has been studied intensely in more recent years regarding its keto/hydroxy tautomerism. Quantum-chemical calculations predicted a preference of the keto form,[121,122] which was later confirmed experimentally. Crystal structures were elucidated for cyameluric acid as well as the compound's trihydrate and DMF solvate, all of which crystallize in the symmetric trioxo form.[123-125] Cyameluric chloride, on the other hand, has received much less attention. It was supposedly first synthesized by *Redemann* and *Lucas* from phosphorus pentachloride and potassium cyamelurate or cyameluric acid.[11] The crystal structure of cyameluric chloride was established in 2002, representing the first functionalized heptazine derivative to be crystallographically characterized.[35] The compound forms a layered structure of distorted heptazine rings, which are arranged in triangular motifs and connected through rather short Cl-N donor-acceptor interactions.[126] Cyameluric chloride finds little application in preparative chemistry,

although it has been shown to readily undergo nucleophilic substitution reactions and can be used to obtain a variety of heptazine derivatives.[127]

Besides the here presented covalent C/N/H materials and derivatives, a veritable plethora of ionic triazine- or heptazine-based compounds has been reported on. These salts have often been proposed as potential starting materials for functional C/N/H materials and have also been successfully applied as such. However, studies concerning ionic C/N/H compounds tend to focus primarily on their crystallographic structures to elucidate fundamental questions of C/N/H compound constitution. Quite some of these compounds date back to the beginning of C/N/H material research in the 19th and early 20th century, when the elucidation of a novel compound's reaction behavior towards certain standard compounds—such as mineral acids or alkaline solutions—was part of standard characterization processes. It is, however, debatable whether these salts were obtained phase pure and most often they were no subject to further characterization. Modern state of knowledge is thus primarily based on crystallographic studies from more recent years applying state-of-the-art X-ray diffractometry techniques.

In these ionic compounds, triazine- or heptazine-based ions can appear as cations as well as anions. While cations are typically realized through ring protonation in the abovementioned molecular C/N/H species, charges in anions are usually located on negatively charged functional groups. A number of the most noteworthy anionic and cationic C/N/H compounds is shown in Figures 1.8 and 1.9. Furthermore, a surprisingly large number of adduct compounds exist, in which uncharged species appear next to cationic or anionic C/N/H building blocks.

The first salt-like compounds to find mention in literature were (hydro)melonates, so called because they were thought to be salts of a 'hydromelonic acid' when the constitution and structure of melon were yet unknown. The melonate anion is comprised of a heptazine nucleus terminated by three cyanamido moieties. These cyanamides are easily deprotonated, resulting in an anion carrying three negative charges. Potassium melonate, $K_3[C_6N_7(NCN)_3]$, was initially described by *Gmelin*, who obtained it as a side product in the synthesis of KSCN, and later studied by *Liebig*, who reacted melon in molten KSCN.[2,5] The crystallographic structure of the respective pentahydrate, however, was only

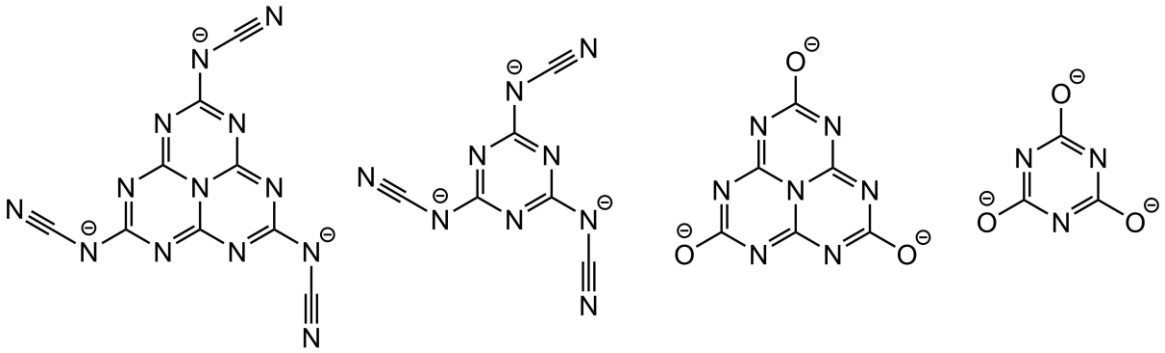

Figure 1.8: Anionic C/N/H ions. From left to right: melonate, tricyanomelaminate, cyamelurate, cyanurate.

elucidated in 2005, showing planar sheets of anions with K^+ cations intercalated between the layers.[128] Anhydrous potassium melonate, $K_3[C_6N_7(NCN)_3]$, prepared by *Liebig's* method, was structurally elucidated a few years later, showing melonate ions that lack C_{3h} symmetry due to a side chain turned by 180°. In the 1970s, various organic and inorganic melonate salts were synthesized and studied spectroscopically by *Finkel'shtein et al.*, including alkaline earth, first row transition metal and main group metal salts.[20,129] Structural elucidation of melonate salts was mainly conducted within the last decade. Lithium melonate, nickel melonate as well as several silver melonates and melonate adducts have been prepared through ion exchange in $K_3[C_6N_7(NCN)_3]$ either in solution or applying ion exchange resins.[130,131] The same methods were successfully used in the synthesis of heavy alkali melonates $Rb_3[C_6N_7(NCN)_3]\cdot 3H_2O$ and $Cs_3[C_6N_7(NCN)_3]\cdot 3H_2O$ as well as the protonated melonate $Ca[HC_6N_7(NCN)_3]\cdot 7H_2O$.[132,133] Rare-earth melonates $LnC_6N_7(NCN)_3\cdot xH_2O$ (Ln = La, Ce, Pr, Nd, Sm, Eu, Tb; x = 8–12) were prepared through ion exchange in ammonium melonate either in heated solution or under hydrothermal conditions in autoclaves.[134]

The melonate-analogous triazine compounds were named tricyanomelaminates. Like the melonate anion, tricyanomelaminate is terminated by three cyanamido moieties and thus carries three negative charges. For a long time, the only known tricyanomelaminate was trisodium tricyanomelaminate, $Na_3C_6N_9$, which was synthesized by *Madelung* via thermally induced trimerization of sodium dicyanamide,[135] and whose trihydrate was structurally elucidated by *Hoard*.[136] More recently, the crystal structures of both the trihydrate and the anhydrous substance have been revised and elucidated using advanced structure elucidation methods.[137,138] These structures differ greatly, with the trihydrate showing planar arrangement of C_{3h} symmetric anions, while side chains are turned out of threefold symmetry and molecules are tilted towards each other for $Na_3C_6N_9$. Other tricyanomelaminates could be obtained through ion exchange in $Na_3C_6N_9$. Potassium and rubidium salts were obtained using ion exchange resins, but form monohydrates instead of trihydrates.[139] Cu^{2+}, Ni^{2+}, Co^{2+}, and Cd^{2+} salts of tricyanomelaminate form extended sheets of metal-coordinating networks.[140] On the other hand, anhydrous potassium and rubidium tricyanomelaminates were obtained analogously to the sodium salt through trimerization of the respective dicyanamide salt.[141] These salts are isotypic to each other, however, deviate from the structure of the sodium salt. Especially interesting is a group of non-metal tricyanomelaminates—namely the ammonium, guanidinium and melaminium salt—which have been prepared through ion exchange.[142] These compounds consist exclusively of carbon, nitrogen and hydrogen and show complete C-N alternation as is required for C/N/H compounds, and thus allow for novel C-N-H ratios unobtainable through conventional thermal condensation of covalent compounds.

As Brønsted acidic compounds, cyanuric acid and cyameluric acid both form a plethora of inorganic salts. The oldest and most common synthesis route for these is neutralization of aqueous solutions of the respective acid with a base containing the desired counter ion. Consequently, cyanurates are primarily known for alkali or alkaline earth metals. Other salts that have been reported very early on include ammonium, silver, lead, and copper salts.[143,144] It is noteworthy that many of these salts are mixed salts including multiple different cations. A more modern synthetic approach is solid-state metathesis, typically between alkali cyanurates and metal halides. Cyclotrimerization of alkali cyanates in metal halide melts proved similarly effective. Thus obtained cyanurate salts have recently shown to be promising materials for luminescence or non-linear optical applications and thus received scientific attention.[145-147] Cyamelurates, which have already been mentioned by *Liebig*, have been studied only superficially and literature on them is scarce. Throughout the 1970s, *Finkel'shtein et al.* synthesized a number of alkali (Na, K), alkaline earth (Mg, Ca, Ba), transition (Mn, Cr, Fe, Co, Ni, Cu, Zn, Ag, Cd) and main group (Al, Pb, Bi) metal salts of cyameluric acid and characterized them IR-spectroscopically and thermogravimetrically.[148,149] Elucidation of the crystallographic structure via X-ray diffractometry was performed for the alkali cyamelurates $M_3[C_6N_7O_3]\cdot nH_2O$ (M = Li, Na, K, Rb, Cs; n = 3-6) was well as the mono- and dipotassium salts $K[H_2C_6N_7O_3]\cdot 2H_2O$ and $K_2[HC_6N_7O_3]\cdot H_2O$.[150,151] It could be shown that in fully deprotonated species the trihydroxy tautomeric form is dominant, while the mono- and di-substituted salts preferred the keto form.

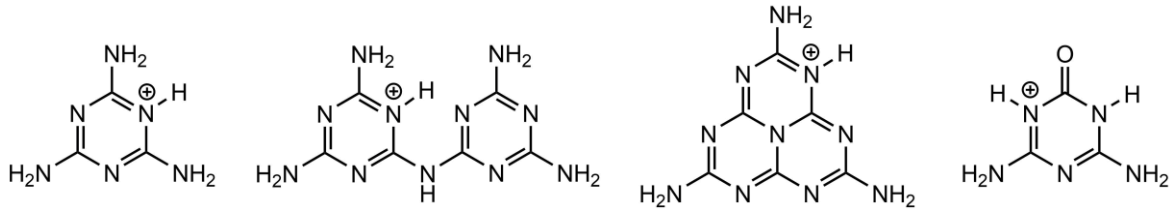

Figure 1.9: Cationic C/N/H ions. From left to right: melaminium, melamium, melemium, ammelinium.

Cationic C/N/H ions exist for all molecular species described in the condensation cascade, namely melamine, melam and melem, but also for derivatives such as ammeline. They are typically formed through protonation of the ring nitrogen atoms, which are more basic than the terminal amino groups. While monoprotonated cations are the most common, di- or trications have been reported as well.

It comes as little surprise that of melamine, the most prominent representative of the C/N/H compound group, the by far largest number of salts has been prepared. These comprise salts of mineral acids, such as melaminium sulfate, melaminium chloride or melaminium nitrate,[152-156] but also various organic salts such as phthalates, benzoates or citrates,[157,158] or salts containing complex inorganic anions, e.g. melaminium hexachlorodicuprate or melaminium β-octamolybdate[159,160] to name but a few. The most commonly applied synthesis routes are rather simple. Typically, melamine is dissolved in the respective concentrated or diluted acid, or mixed with a salt containing the desired anion in hydrochloric acid. However, there have also been reports of solid-state reactions between melamine and the respective ammonium salt,[73,153] or ion exchange in solution in preformed

melaminium salts, such as melaminium perchlorate.[155] As is typical for C/N/H compounds, melaminium salts show extensive hydrogen bonding as well as π-stacking, which appear to be the dominating structure-directing forces, while anions only play an ancillary role. Apart from their interesting structural characteristics, melaminium salts have also been studied for various applications. As very nitrogen-rich compounds, melaminium salts with anions such as nitrate, nitramide or nitroformate have been investigated as energetic materials.[155,161] Melaminium molybdates or phosphates have been discussed as flame or smoke retardant materials, since they combine the favorable, flame-suppressing properties of C/N/H compounds, which have been mentioned above, with specific desirable properties of the respective anion.[162,163] Furthermore, melaminium salts have been identified as potential candidates for crystals exhibiting nonlinear optical (NLO) properties due to their delocalized electron systems and numerous donor-acceptor interactions.[164,165]

In contrast, only a limited number of melamium salts has been elucidated. *Finkel'shtein et al.* reported on the synthesis of melamium chloride, sulfate, nitrate, phosphate and perchlorate.[166] However, of these only melamium perchlorate, $C_6N_{11}H_{11}(ClO_4)_2{\cdot}2H_2O$, could be reproduced and structurally elucidated.[74] Melam is known to be hydrolyzed to ammeline by strong acids, thus it is highly likely that the obtained compounds, which were prepared by dissolving melam in the respective acid and for which no characterization was reported, are in fact ammelinium salts. For some of the reported melamium salts this was experimentally confirmed later.[167] Apart from these compounds, the only melamium salts mentioned in literature are a melamium chloride ammonium chloride adduct as well as a melamium thiocyanate melamine adduct.[73] These were synthesized through thermal condensation of melamine in the presence of ammonium chloride, and through pyrolysis of thiourea in a closed system, respectively.

The study of melemium salts has begun only very recently. Literature names melemium sulfate, $(H_2C_6N_7(NH_2)_3)SO_4 \cdot 2H_2O$, melemium perchlorate, $(HC_6N_7(NH_2)_3)ClO_4 \cdot H_2O$, triple protonated melemium hydrogensulfate $H_3C_6N_7(NH_2)_3(HSO_4)_3$ and two melemium methylsulfonate salts of different composition, $H_2C_6N_7(NH_2)_3(SO_3CH_3)_2{\cdot}H_2O$ and $HC_6N_7(NH_2)_3H_2C_6N_7(NH_2)_3(SO_3CH_3)_3{\cdot}H_2O$.[168-170] All of these were prepared through treatment of pre-synthesized melem with the respective strong acid. In the cases of methylsulfonic acid and sulfuric acid, the formed reaction product heavily depended on the concentration of the acid. As can be seen from the sum formulas, mono-, di- or triprotonated melemium anions can be formed in this process. In contrast to triazine rings, which offer only three ring N atoms that can be protonated, six possible protonation sites in heptazine-based melem lead to a multitude of possible protonation patterns and thus different tautomers. Interestingly, while protonation generally takes place in a way that aims to maximize distance between separate protonation sites, this trend could not be observed in all of the elucidated structures. Two different protonation patterns were observed for the different melemium

methylsulfonates, respectively, which allow the conclusion that these tautomers are rather similar in energy.

It is conspicuous that melamine and cyanuric acid display diametrically opposed reaction behavior in the formation of salts. The obvious explanation for melamine exclusively taking the role of a cation and cyanuric acid only existing as an anion is obviously caused by their different acidity and basicity. However, this raises the question of the reaction behavior of the intermediate hydrolysis/ammonolysis products ammeline and ammelide. In general, ammeline shows similar reaction behavior to melamine while ammelide tends to react similarly to cyanuric acid. In the case of ammeline, this is also true concerning the formation of ionic compounds. Several salts with cationic ammelinium have been described, however, none comprising a deprotonated ammeline anion. Ammelinium chloride, bromide and nitrate have been obtained through hydrolysis of melam in the respective acid and were structurally elucidated by single crystal X-ray diffractometry.[167] The sulfate and nitrate salts were furthermore prepared by acidic hydrolysis of 4,4',6,6'-tetramino(azo)-1,3,5-triazine and successively used in ion exchange reactions to obtain the perchlorate and 5-tetrazolate salts.[171] These compounds have been studied as potential energy-rich materials. Concerning ammelide, neither anionic nor cationic salts are known, so no evidence exists whether the compound tends towards the melamine or cyanuric acid reaction behavior in the formation of ionic compounds.

C/N/H chemistry, which had been neglected for more than a century, experienced a phenomenal revival during the last three decades and although there has always been a driving force towards a certain specific goal, it is remarkable how diverse this field of research has become—in respect of the studied compounds but also regarding the deployed methodology and preparative approaches. In more recent years, however, a tendency towards a more streamlined view on C/N/H chemistry and materials has taken root. Research became focused not only on the goal of photocatalysis, but also on a single material—namely melon, more often denoted as g-C_3N_4 or PCN. Nowadays, the vast majority of C/N/H research is concerned with material optimization towards photocatalytic applications, either through nanostructurization to increase the surface area, or through formation of nanocomposites and heterojunctions to improve electronic properties. Little, however, is done towards optimization of the material itself and other materials apart from melon are rarely included in these studies. Considering the mediocre intrinsic properties of melon, this waste of potential is hardly understandable. The examples of poly(triazine imide) and potassium poly(heptazine imide) have shown, that especially 2D extended materials show a dramatically higher photocatalytic efficiency than 1D extended melon and the recent discovery of triazine-based graphitic carbon nitride proved once again that the search for novel C/N/H materials has not been completed. With these prospects, it is all the more curious that application-oriented groups so often limit themselves to PCN, a material that is not even properly understood. Just as surprising is the lack of interest concerning the identity of the material, which is often only characterized superficially or not at all. This impedes any directed attempts at material optimization and condemns scientists to tedious trial-and-error approaches.

This thesis aims to contribute to the plurality of triazine- and heptazine-based compounds and further the understanding of the material class by investigating formation mechanisms and structure-directing interactions. A special focus lies on the until now only rudimentarily investigated group of melam and melamium compounds. The three central aspects of C/N/H chemistry this thesis is dedicated to are:

- The transition from triazine-based compounds to heptazine-based compounds and vice versa, and the mechanisms behind those
- The influence of (inorganic) salts on the reaction behavior of C/N/H compounds, their incorporation, and their respective role in the reaction process
- The role in and respective influence on the crystallographic structure of different kinds of intra- and intermolecular interactions, namely hydrogen bridge bonds, π-stacking and ionic interactions

To this end, various novel polymeric, molecular and ionic triazine-based compounds are prepared and characterized crystallographically and spectroscopically. These compounds are structurally elucidated in detail, intra- and intermolecular interactions identified and compared to related compounds. In the case of PTI, a mechanistic study is performed to elucidate the formation mechanism.

[1] J. Liebig, "Ueber einige Stickstoff-Verbindungen", *Ann. Pharm.* **1834**, *10*, 1-47.

[2] J. Liebig, "Ueber Mellon und Mellonverbindungen", *Justus Liebigs Ann. Chem.* **1844**, *50*, 337-363.

[3] J. Liebig, "Ueber die Constitution der Mellonverbindungen", *Justus Liebigs Ann. Chem.* **1855**, *95*, 257-282.

[4] E. Kroke, M. Schwarz, "Novel group 14 nitrides", *Coord. Chem. Rev.* **2004**, *248*, 493-532.

[5] L. Gmelin, "Ueber einige Verbindungen des Melon's", *Ann. Pharm.* **1835**, *15*, 252-258.

[6] W. Henneberg, "Ueber einige Zersetzungsproducte des Mellonkaliums", *Ann. Chem. Pharm.* **1850**, *73*, 228-255.

[7] P. Klason, "Ueber Cyanursäure, Di- und Trithiocyansäure", *J. Prakt. Chem.* **1885**, *33*, 116-131.

[8] P. Klason, "Ueber Melamverbindungen", *J. Prakt. Chem.* **1885**, *33*, 285-289.

[9] E. C. Franklin, "THE AMMONO CARBONIC ACIDS", *J. Am. Chem. Soc.* **1922**, *44*, 486-509.

[10] L. Pauling, J. H. Sturdivant, "The Structure of Cyameluric Acid, Hydromelonic Acid and Related Substances", *Proc. Natl. Acad. Sci. USA* **1937**, *23*, 615-620.

[11] C. E. Redemann, H. J. Lucas, "Some Derivatives of Cyameluric Acid and Probable Structures of Melam, Melem and Melon", *J. Am. Chem. Soc.* **1940**, *62*, 842-846.

[12] A. I. Finkel'shtein, E. N. Boitsov, "The Molecular Structure of 1,3,5-Triazine and its Derivatives", *Russ. Chem. Rev.* **1962**, *31*, 712-720.

[13] A. I. Finkel'shtein, N. V. Spiridonova, "Chemical Properties and Molecular Structure of Derivatives of sym-heptazine[1,3,4,6,7,9,9b-heptaazaphenalene, tri-1,3,5-triazine]", *Russ. Chem. Rev.* **1964**, *33*, 400-405.

[14] V. V. Khorosheva, A. I. Finkel'shtein, "Spectroscopic study of melon", *Zh. Fiz. Khim.* **1962**, *36*, 1055-1057.

[15] N. I. Zhogrova, N. V. Spiridonova, A. I. Finkel'shtein, "Vibrational spectra and molecular structure of cyameluric acid salts", *Zh. Prikl. Spektrosk.* **1973**, *19*, 153-154.

[16] A. I. Finkel'shtein, S. G. Fedoruk, "Study of the interaction of ligands with anion in hydromelonates of ammine complexes using vibrational and electronic spectra", *Zh. Prikl. Spektrosk.* **1983**, *39*, 606-609.

[17] N. V. Spiridonova, A. I. Finkel'shtein, "Melam synthesis and its physical and chemical properties", *Khim. Geterotsikl. Soedin.* **1966**, 126-129.

[18] V. A. Gal'perin, A. I. Finkel'shtein, N. K. Gavrilova, "Synthesis of melam from melamine", *Zh. Org. Khim.* **1971**, *7*, 2431-2432.

[19] A. I. Finkel'shtein, N. V. Spiridonova, "Products of thermal conversion of some derivatives of sym-heptazine as studied by means of infrared spectra", *Zh. Org. Khim.* **1965**, *1*, 606-609.

[20] S. G. Fedoruk, A. I. Finkel'shtein, N. V. Spiridonova, "Synthesis and study of the thermal properties of hydromelonate salts with organic bases", *Tr. Khim. Khim. Tekhnol.* **1975**, *5*, 106-109.

[21] N. V. Spiridonova, A. I. Finkel'shtein, "Solubility of some derivatives of sym-heptazine", *Tr. Khim. Khim. Tekhnol.* **1967**, *1*, 38-40.

[22] E. M. Moncharzh, N. K. Gavrilova, V. A. Gal'perin, A. I. Finkel'shtein, "Calculation of the structure and electronic spectra of melam and its ions", *Zh. Strukt. Khim.* **1982**, *23*, 152-154.

[23] A. Y. Liu, M. L. Cohen, "Prediction of New Low Compressibility Solids", *Science* **1989**, *245*, 841-842.

[24] A. Y. Liu, M. L. Cohen, "Structural properties and electronic structure of low-compressibility materials: β-C_3N_4 and hypothetical β-C_3N_4", *Phys. Rev. B* **1990**, *41*, 10727-10734.

[25] M. L. Cohen, "Calculation of bulk moduli of diamond and zinc-blende solids", *Phys. Rev. B* **1985**, *32*, 7988-7991.

[26] A. Y. Liu, R. M. Wentzcovitch, "Stability of carbon nitride solids", *Phys. Rev. B* **1994**, *50*, 10362-10365.

[27] T. Sekine, H. Kanda, Y. Bando, M. Yokoyama, K. Hojou, "A graphitic carbon nitride", *J. Mater. Sci. Lett.* **1990**, *9*, 1376-1378.

[28] L. Maya, D. R. Cole, E. W. Hagaman, "Carbon–Nitrogen Pyrolyzates: Attempted Preparation of Carbon Nitride", *J. Am. Ceram. Soc.* **1991**, *74*, 1686-1688.

[29] T. Komatsu, M. Samejima, "Preparation of carbon nitride C_2N by shock-wave compression of poly(aminomethineimine)", *J. Mater. Chem.* **1998**, *8*, 193-196.

[30] H.-X. Han, B. J. Feldman, "Structural and optical properties of amorphous carbon nitride", *Solid State Commun.* **1988**, *65*, 921-923.

[31] K. M. Yu, M. L. Cohen, E. E. Haller, W. L. Hansen, A. Y. Liu, I. C. Wu, "Observation of crystalline C_3N_4", *Phys. Rev. B* **1994**, *49*, 5034-5037.

[32] S. Muhl, J. M. Méndez, "A review of the preparation of carbon nitride films", *Diamond Relat. Mater.* **1999**, *8*, 1809-1830.

[33] S. Matsumoto, E. Q. Xie, F. Izumi, "On the validity of the formation of crystalline carbon nitrides, C_3N_4", *Diamond Relat. Mater.* **1999**, *8*, 1175-1182.

[34] D. M. Teter, R. J. Hemley, "Low-Compressibility Carbon Nitrides", *Science* **1996**, *271*, 53-55.

[35] E. Kroke, M. Schwarz, E. Horath-Bordon, P. Kroll, B. Noll, A. D. Norman, "Tri-s-triazine derivatives. Part I. From trichloro-tri-s-triazine to graphitic C_3N_4 structures", *New J. Chem.* **2002**, *26*, 508-512.

[36] T. Komatsu, "The First Synthesis and Characterization of Cyameluric High Polymers", *Macromol. Chem. Phys.* **2001**, *202*, 19-25.

[37] T. Komatsu, "Prototype carbon nitrides similar to the symmetric triangular form of melon", *J. Mater. Chem.* **2001**, *11*, 802-803.

[38] T. Komatsu, T. Nakamura, "Polycondensation/pyrolysis of tris-s-triazine derivatives leading to graphite-like carbon nitrides", *J. Mater. Chem.* **2001**, *11*, 474-478.

[39] T. Komatsu, "Attempted chemical synthesis of graphite-like carbon nitride", *J. Mater. Chem.* **2001**, *11*, 799-801.

[40] F. Goettmann, A. Fischer, M. Antonietti, A. Thomas, "Metal-free catalysis of sustainable Friedel-Crafts reactions: direct activation of benzene by carbon nitrides to avoid the use of metal chlorides and halogenated compounds", *Chem. Commun.* **2006**, 4530-4532.

[41] F. Goettmann, A. Fischer, M. Antonietti, A. Thomas, "Chemical Synthesis of Mesoporous Carbon Nitrides Using Hard Templates and Their Use as a Metal-Free Catalyst for Friedel–Crafts Reaction of Benzene", *Angew. Chem.* **2006**, *118*, 4579-4583; *Angew. Chem. Int. Ed.* **2006**, *45*, 4467-4471.

[42] F. Goettmann, A. Fischer, M. Antonietti, A. Thomas, "Mesoporous graphitic carbon nitride as a versatile, metal-free catalyst for the cyclisation of functional nitriles and alkynes", *New J. Chem.* **2007**, *31*, 1455-1460.

[43] F. Goettmann, A. Thomas, M. Antonietti, "Metal-Free Activation of CO_2 by Mesoporous Graphitic Carbon Nitride", *Angew. Chem.* **2007**, *119*, 2773-2776; *Angew. Chem. Int. Ed.* **2007**, *46*, 2717-2720.

[44] A. Thomas, A. Fischer, F. Goettmann, M. Antonietti, J. O. Müller, R. Schlögl, J. M. Carlsson, "Graphitic carbon nitride materials: variation of structure and morphology and their use as metal-free catalysts", *J. Mater. Chem.* **2008**, *18*, 4893-4908.

[45] X. Wang, K. Maeda, A. Thomas, K. Takanabe, G. Xin, J. M. Carlsson, K. Domen, M. Antonietti, "A metal-free polymeric photocatalyst for hydrogen production from water under visible light", *Nat. Mater.* **2009**, *8*, 76-80.

[46] M. Xiao, B. Luo, S. Wang, L. Wang, "Solar energy conversion on g-C_3N_4 photocatalyst: Light harvesting, charge separation, and surface kinetics", *J. Energy Chem.* **2018**, *27*, 1111-1123.

[47] I. F. Teixeira, E. C. M. Barbosa, S. C. E. Tsang, P. H. C. Camargo, "Carbon nitrides and metal nanoparticles: from controlled synthesis to design principles for improved photocatalysis", *Chem. Soc. Rev.* **2018**, *47*, 7783-7817.

[48] A. Sudhaik, P. Raizada, P. Shandilya, D.-Y. Jeong, J.-H. Lim, P. Singh, "Review on fabrication of graphitic carbon nitride based efficient nanocomposites for photodegradation of aqueous phase organic pollutants", *J. Ind. Eng. Chem.* **2018**, *67*, 28-51.

[49] Z. Zhou, Y. Zhang, Y. Shen, S. Liu, Y. Zhang, "Molecular engineering of polymeric carbon nitride: advancing applications from photocatalysis to biosensing and more", *Chem. Soc. Rev.* **2018**, *47*, 2298-2321.

[50] J. Fu, J. Yu, C. Jiang, B. Cheng, "g-C_3N_4-Based Heterostructured Photocatalysts", *Adv. Energy Mater.* **2018**, *8*, 1701503.

[51] W. Iqbal, B. Yang, X. Zhao, M. Rauf, M. Waqas, Y. Gong, J. Zhang, Y. Mao, "Controllable synthesis of graphitic carbon nitride nanomaterials for solar energy conversion and environmental remediation: the road travelled and the way forward", *Catal. Sci. Technol.* **2018**, *8*, 4576-4599.

[52] S. Kumar, S. Karthikeyan, A. Lee, "g-C_3N_4-Based Nanomaterials for Visible Light-Driven Photocatalysis", *Catalysts* **2018**, *8*, 74.

[53] B. Xu, M. B. Ahmed, J. L. Zhou, A. Altaee, G. Xu, M. Wu, "Graphitic carbon nitride based nanocomposites for the photocatalysis of organic contaminants under visible irradiation: Progress, limitations and future directions", *Sci. Total Environ.* **2018**, *633*, 546-559.

[54] J. H. Thurston, N. M. Hunter, L. J. Wayment, K. A. Cornell, "Urea-derived graphitic carbon nitride (u-g-C_3N_4) films with highly enhanced antimicrobial and sporicidal activity", *J. Colloid Interface Sci.* **2017**, *505*, 910-918.

[55] C. Merschjann, T. Tyborski, S. Orthmann, F. Yang, K. Schwarzburg, M. Lublow, M. C. Lux-Steiner, T. Schedel-Niedrig, "Photophysics of polymeric carbon nitride: An optical quasimonomer", *Phys. Rev. B* **2013**, *87*, 205204.

[56] C. Merschjann, S. Tschierlei, T. Tyborski, K. Kailasam, S. Orthmann, D. Hollmann, T. Schedel-Niedrig, A. Thomas, S. Lochbrunner, "Complementing Graphenes: 1D Interplanar Charge Transport in Polymeric Graphitic Carbon Nitrides", *Adv. Mater.* **2015**, *27*, 7993-7999.

[57] F. K. Kessler, Y. Zheng, D. Schwarz, C. Merschjann, W. Schnick, X. Wang, M. J. Bojdys, "Functional carbon nitride materials — design strategies for electrochemical devices", *Nat. Rev. Mater.* **2017**, *2*, 17030.

[58] H. May, "Pyrolysis of melamine", *J. Appl. Chem.* **1959**, *9*, 340-344.

[59] A. Sattler, S. Pagano, M. Zeuner, A. Zurawski, D. Gunzelmann, J. Senker, K. Müller-Buschbaum, W. Schnick, "Melamine–Melem Adduct Phases: Investigating the Thermal Condensation of Melamine", *Chem. Eur. J.* **2009**, *15*, 13161-13170.

[60] V. W.-h. Lau, M. B. Mesch, V. Duppel, V. Blum, J. Senker, B. V. Lotsch, "Low-Molecular-Weight Carbon Nitrides for Solar Hydrogen Evolution", *J. Am. Chem. Soc.* **2015**, *137*, 1064-1072.

[61] M. Döblinger, B. V. Lotsch, J. Wack, J. Thun, J. Senker, W. Schnick, "Structure elucidation of polyheptazine imide by electron diffraction-a templated 2D carbon nitride network", *Chem. Commun.* **2009**, 1541-1543.

[62] G. M. Crews, W. Ripperger, J. Seeholzer, "Melamine and Guanamines" in *Ullmann's encyclopedia of industrial chemistry, Vol. A16*, 5 ed. (Ed.: W. Gerhartz), VCH, Weinheim, **1990**, 171-185.

[63] The Market Publishers Ltd., "World Melamine Supply to Exceed 2 Mln Tonnes in 2018, According to In-demand Report by Merchant Research & Consulting", **2014**. Available at: http://www.prweb.com/releases/2014/02/prweb11582781.htm, accessed January 31, 2018.

[64] W. H. Binder, M. Dunky, "Melamine–Formaldehyde Resins", in *Encyclopedia of Polymer Science and Technology*, 4th ed. (Ed.: H. F. Mark), Wiley, New York, **2004**.

[65] W. H. Binder, M. Dunky, S. Jahromi, "Melamine Resins", in *Kirk-Othmer Encyclopedia of Chemical Technology*, Wiley, New York, **2005**.

[66] H. Diem, G. Matthias, "Amino Resins", in *Ullmann's Encyclopedia of Industrial Chemistry, Vol. A2*, 5 ed. (Ed.: W. Gerhartz), VCH, Weinheim, **1985**, 115-141.

[67] Y. Feng, J. Yao, "Design of Melamine Sponge-Based Three-Dimensional Porous Materials toward Applications", *Ind. Eng. Chem. Res.* **2018**, *57*, 7322-7330.

[68] M. Klatt, "Nitrogen-Based Flame Retardants", in *Non-Halogenated Flame Retardant Handbook* (Eds.: A. B. Morgan, C. A. Wilkie), Scrivener Publishing, Beverly, **2014**, 143-168.

[69] E. D. Weil, S. V. Levchik, "Flame Retardants in Commercial Use or Development for Textiles", *J. Fire Sci.* **2009**, *26*, 243-281.

[70] E. D. Weil, "Fire-Protective and Flame-Retardant Coatings – A State-of-the-Art Review", *J. Fire Sci.* **2011**, *29*, 259-296.

[71] E. W. Hughes, "The Crystal Structure of Melamine", *J. Am. Chem. Soc.* **1941**, *63*, 1737-1752.

[72] E. Wirnhier, M. B. Mesch, J. Senker, W. Schnick, "Formation and Characterization of Melam, Melam Hydrate, and a Melam–Melem Adduct", *Chem. Eur. J.* **2013**, *19*, 2041-2049.

[73] N. E. Braml, A. Sattler, W. Schnick, "Formation of Melamium Adducts by Pyrolysis of Thiourea or Melamine/NH_4Cl Mixtures", *Chem. Eur. J.* **2012**, *18*, 1811-1819.

[74] B. V. Lotsch, W. Schnick, "New Light on an Old Story: Formation of Melam during Thermal Condensation of Melamine", *Chem. Eur. J.* **2007**, *13*, 4956-4968.

[75] A. Schwarzer, T. Saplinova, E. Kroke, "Tri-s-triazines (s-heptazines)—From a "mystery molecule" to industrially relevant carbon nitride materials", *Coord. Chem. Rev.* **2013**, *257*, 2032-2062.

[76] M. Shahbaz, S. Urano, P. R. LeBreton, M. A. Rossman, R. S. Hosmane, N. J. Leonard, "Tri-s-triazine: synthesis, chemical behavior, and spectroscopic and theoretical probes of valence orbital structure", *J. Am. Chem. Soc.* **1984**, *106*, 2805-2811.

[77] B. Jürgens, E. Irran, J. Senker, P. Kroll, H. Müller, W. Schnick, "Melem (2,5,8-Triamino-tri-s-triazine), an Important Intermediate during Condensation of Melamine Rings to Graphitic Carbon Nitride: Synthesis, Structure Determination by X-ray Powder Diffractometry, Solid-State NMR, and Theoretical Studies", *J. Am. Chem. Soc.* **2003**, *125*, 10288-10300.

[78] A. Sattler, W. Schnick, "Zur Kenntnis der Kristallstruktur von Melem $C_6N_7(NH_2)_3$", *Z. Anorg. Allg. Chem.* **2006**, *632*, 238-242.

[79] B. V. Lotsch, M. Döblinger, J. Sehnert, L. Seyfarth, J. Senker, O. Oeckler, W. Schnick, "Unmasking Melon by a Complementary Approach Employing Electron Diffraction, Solid-State NMR Spectroscopy, and Theoretical Calculations—Structural Characterization of a Carbon Nitride Polymer", *Chem. Eur. J.* **2007**, *13*, 4969-4980.

[80] L. Seyfarth, J. Seyfarth, B. V. Lotsch, W. Schnick, J. Senker, "Tackling the stacking disorder of melon—structure elucidation in a semicrystalline material", *Phys. Chem. Chem. Phys.* **2010**, *12*, 2227-2237.

[81] D. Dontsova, S. Pronkin, M. Wehle, Z. Chen, C. Fettkenhauer, G. Clavel, M. Antonietti, "Triazoles: A New Class of Precursors for the Synthesis of Negatively Charged Carbon Nitride Derivatives", *Chem. Mater.* **2015**, *27*, 5170-5179.

[82] A. Savateev, S. Pronkin, J. D. Epping, M. G. Willinger, C. Wolff, D. Neher, M. Antonietti, D. Dontsova, "Potassium Poly(heptazine imides) from Aminotetrazoles: Shifting Band Gaps of Carbon Nitride-like Materials for More Efficient Solar Hydrogen and Oxygen Evolution", *ChemCatChem* **2017**, *9*, 167-174.

[83] A. Savateev, S. Pronkin, M. G. Willinger, M. Antonietti, D. Dontsova, "Towards Organic Zeolites and Inclusion Catalysts: Heptazine Imide Salts Can Exchange Metal Cations in the Solid State", *Chem. - Asian J.* **2017**, *12*, 1517-1522.

[84] A. Savateev, D. Dontsova, B. Kurpil, M. Antonietti, "Highly crystalline poly(heptazine imides) by mechanochemical synthesis for photooxidation of various organic substrates using an intriguing electron acceptor – Elemental sulfur", *J. Catal.* **2017**, *350*, 203-211.

[85] V. W.-h. Lau, I. Moudrakovski, T. Botari, S. Weinberger, M. B. Mesch, V. Duppel, J. Senker, V. Blum, B. V. Lotsch, "Rational design of carbon nitride photocatalysts by identification of cyanamide defects as catalytically relevant sites", *Nat. Commun.* **2016**, *7*, 12165.

[86] V. W.-h. Lau, D. Klose, H. Kasap, F. Podjaski, M.-C. Pignié, E. Reisner, G. Jeschke, B. V. Lotsch, "Dark Photocatalysis: Storage of Solar Energy in Carbon Nitride for Time-Delayed Hydrogen Generation", *Angew. Chem.* **2017**, *129*, 525-529; *Angew. Chem. Int. Ed.* **2017**, *56*, 510-514.

[87] A. Savateev, B. Kurpil, A. Mishchenko, G. Zhang, M. Antonietti, "A “waiting” carbon nitride radical anion: a charge storage material and key intermediate in direct C–H thiolation of methylarenes using elemental sulfur as the “S”-source", *Chem. Sci.* **2018**, *9*, 3584-3591.

[88] Z. Zhang, K. Leinenweber, M. Bauer, L. A. J. Garvie, P. F. McMillan, G. H. Wolf, "High-Pressure Bulk Synthesis of Crystalline $C_6N_9H_3$·HCl: A Novel C_3N_4 Graphitic Derivative", *J. Am. Chem. Soc.* **2001**, *123*, 7788-7796.

[89] M. J. Bojdys, J. O. Müller, M. Antonietti, A. Thomas, "Ionothermal Synthesis of Crystalline, Condensed, Graphitic Carbon Nitride", *Chem. Eur. J.* **2008**, *14*, 8177-8182.

[90] E. Wirnhier, M. Döblinger, D. Gunzelmann, J. Senker, B. V. Lotsch, W. Schnick, "Poly(triazine imide) with Intercalation of Lithium and Chloride Ions $[(C_3N_3)_2(NH_xLi_{1-x})_3$·LiCl]: A Crystalline 2D Carbon Nitride Network", *Chem. Eur. J.* **2011**, *17*, 3213-3221.

[91] M. B. Mesch, K. Bärwinkel, Y. Krysiak, C. Martineau, F. Taulelle, R. B. Neder, U. Kolb, J. Senker, "Solving the Hydrogen and Lithium Substructure of Poly(triazine imide)/LiCl Using NMR Crystallography", *Chem. Eur. J.* **2016**, *22*, 16878-16890.

[92] S. Y. Chong, J. T. A. Jones, Y. Z. Khimyak, A. I. Cooper, A. Thomas, M. Antonietti, M. J. Bojdys, "Tuning of gallery heights in a crystalline 2D carbon nitride network", *J. Mater. Chem. A* **2013**, *1*, 1102-1107.

[93] K. Schwinghammer, B. Tuffy, M. B. Mesch, E. Wirnhier, C. Martineau, F. Taulelle, W. Schnick, J. Senker, B. V. Lotsch, "Triazine-based Carbon Nitrides for Visible-Light-Driven Hydrogen Evolution", *Angew. Chem.* **2013**, *125*, 2495-2499; *Angew. Chem. Int. Ed.* **2013,** *52*, 2435-2439.

[94] K. Schwinghammer, M. B. Mesch, V. Duppel, C. Ziegler, J. Senker, B. V. Lotsch, "Crystalline Carbon Nitride Nanosheets for Improved Visible-Light Hydrogen Evolution", *J. Am. Chem. Soc.* **2014**, *136*, 1730-1733.

[95] E. J. McDermott, E. Wirnhier, W. Schnick, K. S. Virdi, C. Scheu, Y. Kauffmann, W. D. Kaplan, E. Z. Kurmaev, A. Moewes, "Band Gap Tuning in Poly(triazine imide), a Nonmetallic Photocatalyst", *J. Phys. Chem. C* **2013**, *117*, 8806-8812.

[96] G. Algara-Siller, N. Severin, S. Y. Chong, T. Björkman, R. G. Palgrave, A. Laybourn, M. Antonietti, Y. Z. Khimyak, A. V. Krasheninnikov, J. P. Rabe, U. Kaiser, A. I. Cooper, A. Thomas, M. J. Bojdys, "Triazine-Based Graphitic Carbon Nitride: a Two-Dimensional Semiconductor", *Angew. Chem.* **2014**, *126*, 7580-7585; *Angew. Chem. Int. Ed.* **2014**, *53*, 7450-7455.

[97] E. Bamberger, "Synthesen des Ammelins und der Cyanursäure", *Ber. Dtsch. Chem. Ges.* **1890**, *23*, 1856-1869.

[98] A. Smolka, A. Friedreich, "Zur Kenntniss des Ammelins", *Monatsh. Chem.* **1890**, *11*, 42-60.

[99] Y. Wang, C. U. Pittman, S. Saebo, "Investigation of the structure and properties of ammeline, melamine, and 2,4-diamino-1,3,5-triazine by ab initio calculations", *J. Org. Chem.* **1993**, *58*, 3085-3090.

[100] M. Hatanaka, "Some structural aspects of ammeline — Keto preference and dimerization", *Spectrochim. Acta, Part A* **2018**, *202*, 87-92.

[101] E. A. Werner, "CCXXXVII.—Mechanism of the decomposition of carbamide and biuret by heat, and of the formation of ammelide", *J. Chem. Soc., Trans.* **1913**, *103*, 2275-2282.

[102] R. Tyka, L. Syper, "Preparation of pure ammelide and ammeline", *Chem. Stosow., Ser. A* **1970**, *14*, 339-342.

[103] V. Pichon, L. Chen, S. Guenu, M. C. Hennion, "Comparison of sorbents for the solid-phase extraction of the highly polar degradation products of atrazine (including ammeline, ammelide and cyanuric acid)", *J. Chromatogr. A* **1995**, *711*, 257-267.

[104] S. Nélieu, L. Kerhoas, J. Einhorn, "Degradation of Atrazine into Ammeline by Combined Ozone/Hydrogen Peroxide Treatment in Water", *Environ. Sci. Technol.* **2000**, *34*, 430-437.

[105] H. Miao, S. Fan, Y.-N. Wu, L. Zhang, P.-P. Zhou, H.-J. Chen, Y.-F. Zhao, J.-G. Li, "Simultaneous Determination of Melamine, Ammelide, Ammeline, and Cyanuric Acid in Milk and Milk Products by Gas Chromatography-tandem Mass Spectrometry", *Biomed. Environ. Sci.* **2009**, *22*, 87-94.

[106] L. E. Wise, E. H. Walter, "Isolation of cyanuric acid from soil", *J. Agric. Res.* **1917**, *10*, 85-92.

[107] J. L. Seffernick, L. P. Wackett, "Ancient Evolution and Recent Evolution Converge for the Biodegradation of Cyanuric Acid and Related Triazines", *Appl. Environ. Microbiol.* **2016**, *82*, 1638.

[108] F. Wöhler, "Ueber die Zersetzung des Harnstoffs und der Harnsäure durch höhere Temperatur", *Ann. Phys. Chem.* **1829**, *15*, 619-630.

[109] K. Huthmacher, D. Most, "Cyanuric Acid and Cyanuric Chloride", in *Ullmann's Encyclopedia of Industrial Chemistry*, **2005**.

[110] E. H. Wiebenga, N. F. Moerman, "Crystal Structure of Cyanuric Acid", *Nature* **1938**, *141*, 122.

[111] E. H. Wiebenga, N. F. Moerman, "Die Kristallstruktur der Cyanursäure $(HCNO)_3$", *Z. Kristallogr.* **1938**, *99*, 217-229.

[112] E. H. Wiebenga, "Crystal structure of cyanuric acid", *J. Am. Chem. Soc.* **1952**, *74*, 6156-6157.

[113] R. Newman, R. M. Badger, "Infrared Spectra of Cyanuric Acid and Deutero Cyanuric Acid", *J. Am. Chem. Soc.* **1952**, *74*, 3545-3548.

[114] F. W. Linda, R. C. Hollenbach, "The bactericidal efficacy of cyanurates - a review", *J. Environ. Health* **1978**, *40*, 324-329.

[115] A. Hantzsch, H. Bauer, "Ueber Cyanursäure-derivate", *Ber. Dtsch. Chem. Ges.* **1905**, *38*, 1005-1013.

[116] A. Hantzsch, "Ueber das Cyamelid", *Ber. Dtsch. Chem. Ges.* **1905**, *38*, 1013-1021.

[117] G. B. Seifer, "Cyanuric Acid and Cyanurates", *Russ. J. Coord. Chem.* **2002**, *28*, 301-324.

[118] M. Sérullas, "Perchlorure de cyanogène", *Ann. Chim. Phys.* **1828**, *37*, 370-393.

[119] P. Puthiaraj, Y.-R. Lee, S. Zhang, W.-S. Ahn, "Triazine-based covalent organic polymers: design, synthesis and applications in heterogeneous catalysis", *J. Mater. Chem. A* **2016**, *4*, 16288-16311.

[120] J. Artz, "Covalent Triazine-based Frameworks—Tailor-made Catalysts and Catalyst Supports for Molecular and Nanoparticulate Species", *ChemCatChem* **2018**, *10*, 1753-1771.

[121] X. Liang, W. Zheng, N.-B. Wong, J. Li, A. Tian, "Theoretical study on the mechanism of keto–enol isomerization for cyanuric acid and cyameluric acid", *J. Mol. Struct.: THEOCHEM* **2004**, *672*, 151-159.

[122] I. Alkorta, N. Jagerovic, J. Elguero, "Theoretical study of cyameluric acid and related compounds", *ARKIVOC* **2004**, *4*, 130-136.

[123] J. Wagler, E. A. El-Gamel Nadia, E. Kroke, "The Structure And Tautomerism Of Cyameluric Acid", *Z. Naturforsch. B* **2006**, *61*, 975-978.

[124] L. Seyfarth, J. Sehnert, N. E. A. El-Gamel, W. Milius, E. Kroke, J. Breu, J. Senker, "Structure elucidation of cyameluric acid by combining solid-state NMR spectroscopy, molecular modeling and direct-space methods", *J. Mol. Struct.* **2008**, *889*, 217-228.

[125] A. Sattler, W. Schnick, "Zur Frage der Tautomerie von Cyamelursäure im Kristall", *Z. Anorg. Allg. Chem.* **2006**, *632*, 1518-1523.

[126] S. Tragl, H.-J. Meyer, "Die Schichtstruktur von Cyamelurchlorid $C_6N_7Cl_3$", *Z. Anorg. Allg. Chem.* **2005**, *631*, 2300-2302.

[127] H. Schroeder, E. Kober, "Some Reactions of Cyameluric Chloride", *J. Org. Chem.* **1962**, *27*, 4262-4266.

[128] E. Horvath-Bordon, E. Kroke, I. Svoboda, H. Fuess, R. Riedel, "Potassium melonate, $K_3[C_6N_7(NCN)_3]\cdot 5H_2O$, and its potential use for the synthesis of graphite-like C_3N_4 materials", *New J. Chem.* **2005**, *29*, 693-699.

[129] S. G. Fedoruk, A. I. Finkel'shtein, N. V. Spiridonova, "Hydrolytic transformations of hydromelonic acid salts", *Zh. Obshch. Khim.* **1972**, *42*, 419-420.

[130] C. Clauss, J. Wagler, M. Schwarz, A. Schwarzer, E. Kroke, "Lithium Melonate, $Li_3[C_6N_7(NCN)_3]\cdot 6H_2O$ – Synthesis, Crystal Structure and Thermal Properties of a Novel Precursor for Graphitic Carbon Nitrides", *Z. Anorg. Allg. Chem.* **2010**, *636*, 196-200.

[131] C. Clauss, U. Böhme, A. Schwarzer, E. Kroke, "Silver Melonates and Coordination Modes of the Multidentate $[C_6N_7(NCN)_3]_3^-$ Anion", *Eur. J. Inorg. Chem.* **2012**, *2012*, 978-986.

[132] S. J. Makowski, D. Gunzelmann, J. Senker, W. Schnick, "Protonated Melonate $Ca[HC_6N_7(NCN)_3]\cdot 7H_2O$ – Synthesis, Crystal Structure, and Thermal Properties ", *Z. Anorg. Allg. Chem.* **2009**, *635*, 2434-2439.

[133] S. J. Makowski, W. Schnick, "$Rb_3[C_6N_7(NCN)_3]\cdot 3H_2O$ and $Cs_3[C_6N_7(NCN)_3]\cdot 3H_2O$ – Synthesis, Crystal Structure and Thermal Behavior of Two Novel Alkali Melonates", *Z. Anorg. Allg. Chem.* **2009**, *635*, 2197-2202.

[134] S. J. Makowski, A. Schwarze, P. J. Schmidt, W. Schnick, "Rare-Earth Melonates $LnC_6N_7(NCN)_3\cdot xH_2O$ (Ln = La, Ce, Pr, Nd, Sm, Eu, Tb; x = 8–12): Synthesis, Crystal Structures, Thermal Behavior, and Photoluminescence Properties of Heptazine Salts with Trivalent Cations", *Eur. J. Inorg. Chem.* **2012**, 1832-1839.

[135] W. Madelung, E. Kern, "Über Tricyanmelamin", *Justus Liebigs Ann. Chem.* **1922**, *427*, 26-34.

[136] J. L. Hoard, "The Structure of Trisodium Tricyanmelamine Trihydrate", *J. Am. Chem. Soc.* **1938**, *60*, 1194-1198.

[137] B. Jürgens, W. Milius, P. Morys, W. Schnick, "Trimerisierung von Dicyanamid-Ionen $C_2N_3^-$ im Festkörper – Synthesen, Kristallstrukturen und Eigenschaften von $NaCs_2(C_2N_3)_3$ und $Na_3C_6N_9{\cdot}3H_2O$", *Z. Anorg. Allg. Chem.* **1998**, *624*, 91-97.

[138] B. Jürgens, E. Irran, J. Schneider, W. Schnick, "Trimerization of NaC_2N_3 to $Na_3C_6N_9$ in the Solid: Ab Initio Crystal Structure Determination of Two Polymorphs of NaC_2N_3 and of $Na_3C_6N_9$ from X-ray Powder Diffractometry", *Inorg. Chem.* **2000**, *39*, 665-670.

[139] E. Irran, B. Jürgens, W. Schnick, "Synthesis, crystal structure determination from X-ray powder diffractometry and vibrational spectroscopy of the tricyanomelaminate monohydrates $M_3[C_6N_9]{\cdot}H_2O$ (M=K, Rb)", *Solid State Sci.* **2002**, *4*, 1305-1311.

[140] B. F. Abrahams, S. J. Egan, B. F. Hoskins, R. Robson, "Three-dimensional coordination networks from tricyanomelamine and Co, Ni, Cu and Cd", *Chem. Commun.* **1996**, 1099-1100.

[141] E. Irran, B. Jürgens, W. Schnick, "Trimerization of Alkali Dicyanamides $M[N(CN)_2]$ and Formation of Tricyanomelaminates $M_3[C_6N_9]$ (M=K, Rb) in the Melt: Crystal Structure Determination of Three Polymorphs of $K[N(CN)_2]$, Two of $Rb[N(CN)_2]$, and One of $K_3[C_6N_9]$ and $Rb_3[C_6N_9]$ from X-ray Powder Diffractometry", *Chem. Eur. J.* **2001**, *7*, 5372-5381.

[142] B. V. Lotsch, W. Schnick, "From Triazines to Heptazines: Novel Nonmetal Tricyanomelaminates as Precursors for Graphitic Carbon Nitride Materials", *Chem. Mater.* **2006**, *18*, 1891-1900.

[143] F. Wöhler, "Ueber die Constitution der Cyanursäure", *Justus Liebigs Ann. Chem.* **1847**, *62*, 241-253.

[144] A. Claus, O. J. Putensen, "XI. Beiträge zur Kenntniss der cyanursauren Salze", *J. Prakt. Chem.* **1888**, *38*, 208-229.

[145] M. Kalmutzki, M. Ströbele, H. F. Bettinger, H.-J. Meyer, "Development of Metal Cyanurates: The Example of Barium Cyanurate (BCY)", *Eur. J. Inorg. Chem.* **2014**, 2536-2543.

[146] M. Kalmutzki, M. Ströbele, D. Enseling, T. Jüstel, H.-J. Meyer, "Synthesis, Structure, and Luminescence of Rare Earth Cyanurates", *Eur. J. Inorg. Chem.* **2015**, 134-140.

[147] M. Kalmutzki, X. Wang, A. J. Meixner, H.-J. Meyer, "Second harmonic generation properties of $Ca_3(O_3C_3N_3)_2$ -$Sr_3(O_3C_3N_3)_2$ solid solutions", *Cryst. Res. Technol.* **2016**, *51*, 460-465.

[148] N. I. Zhagrova, N. V. Spiridonova, A. I. Finkel'shtein, " Vibrational spectra and molecular structure of cyameluric acid salts", *Zh. Prikl. Spektrosk.* **1973**, *19*, 153-154.

[149] N. I. Zhagrova, N. V. Spiridonova, A. I. Finkel'shtein, "Thermal decomposition of cyameluric acid salts with some mono- and bivalent metals", *Zh. Prikl. Khim.* **1975**, *48*, 452-453.

[150] E. Horvath-Bordon, E. Kroke, I. Svoboda, H. Fueß, R. Riedel, S. Neeraj, A. K. Cheetham, "Alkalicyamelurates, $M_3[C_6N_7O_3]{\cdot}xH_2O$, M = Li, Na, K, Rb, Cs: UV-luminescent and thermally very stable ionic tri-s-triazine derivatives", *Dalton Trans.* **2004**, 3900-3908.

[151] N. E. A. El-Gamel, L. Seyfarth, J. Wagler, H. Ehrenberg, M. Schwarz, J. Senker, E. Kroke, "The Tautomeric Forms of Cyameluric Acid Derivatives", *Chem. Eur J.* **2007**, *13*, 1158-1173.

[152] J. Janczak, G. J. Perpetuo, "Melaminium chloride hemihydrate", *Acta Crystallogr., Sect. C* **2001**, *57*, 1120-1122.

[153] H. Jing, M. Ströbele, M. Weisser, H.-J. Meyer, "Die Kristallstruktur von wasserfreiem Melaminiumchlorid", *Z. Anorg. Allg. Chem.* **2003**, *629*, 368-370.

[154] A. Martin, A. A. Pinkerton, "Melaminium Diperchlorate Hydrate", *Acta Crystallogr., Sect. C* **1995**, *51*, 2174-2177.

[155] R. Tanbug, K. Kirschbaum, A. A. Pinkerton, "Energetic materials: The preparation and structural characterization of melaminium dinitramide and melaminium nitrate", *J. Chem. Crystallogr.* **1999**, *29*, 45-55.

[156] J. Janczak, G. J. Perpetuo, "Bis(melaminium) sulfate dihydrate", *Acta Crystallogr., Sect. C* **2001**, *57*, 1431-1433.

[157] J. Janczak, G. J. Perpetuo, "Melaminium phthalate", *Acta Crystallogr., Sect. C* **2001**, *57*, 123-125.

[158] M. K. Marchewka, A. Pietraszko, "Structure and spectra of melaminium citrate", *J. Phys. Chem. Solids* **2003**, *64*, 2169-2181.

[159] A. Colombo, L. Menabue, A. Motori, G. C. Pellacani, W. Porzio, F. Sandrolini, R. D. Willet, "Crystal Structure and Spectroscopic, Magnetic, and Electrical Properties of a Copper(II) Dimer, Melaminium Hexachlorodicuprate(II), Exhibiting a New Stacking Interaction", *Inorg. Chem.* **1985**, *24*, 2900-2905.

[160] W. J. Kroenke, J. P. Fackler Jr., A. M. Mazany, "Structure and Bonding of Melaminium beta-Octamolybdate", *Inorg. Chem.* **1983**, *22*, 2412-2416.

[161] M. Göbel, T. M. Klapötke, "Potassium-, Ammonium-, Hydrazinium-, Guanidinium-, Aminoguanidinium-, Diaminoguanidinium-, Triaminoguanidinium- and Melaminiumnitroformate – Synthesis, Characterization and Energetic Properties", *Z. Anorg. Allg. Chem.* **2007**, *633*, 1006-1017.

[162] F. C. Wu, "Flame Retardant Epoxy Resins Containing Microcapsules", *Adv. Mater. Res.* **2011**, *197-198*, 1346-1349.

[163] W. J. Kroenke, "Melaminium molybdate smoke and fire retarders for poly(vinyl chloride)", *J. Appl. Polym. Sci.* **1986**, *32*, 4155-4168.

[164] M. Drozd, M. K. Marchewka, "The structure, vibrational spectra and nonlinear optical properties of neutral melamine and singly, doubly and triply protonated melaminium cations—theoretical studies", *J. Mol. Struct.: THEOCHEM* **2005**, *716*, 175-192.

[165] R. Thomas, S. Pal, A. Datta, M. K. Marchewka, H. Ratajczak, S. K. Pati, G. U. Kulkarni, "Charge density analysis of two proton transfer complexes: Understanding hydrogen bonding and determination of in-crystal dipole moments", *J. Chem. Sci.* **2008**, *120*, 613-620.

[166] N. K. Gavrilova, V. A. Gal'perin, A. I. Finkel'shtein, A. G. Koryakin, "Synthesis of Melam and its Salts with Mineral Acids", *Zh. Org. Khim.* **1977**, *13*, 669-670.

[167] B. V. Lotsch, W. Schnick, "Synthesis and Structural Characterization of the Ammelinium Salts $[C_3H_6N_5O]Cl$, $[C_3H_6N_5O]Br$, and $[C_3H_6N_5O]NO_3$", *Z. Anorg. Allg. Chem.* **2006**, *632*, 1457-1464.

[168] A. Sattler, L. Seyfarth, J. Senker, W. Schnick, "Synthesen, Kristallstrukturen und spektroskopische Eigenschaften des Melem-Adduktes $C_6N_7(NH_2)_3 \cdot H_3PO_4$ sowie der Melemium-Salze $(H_2C_6N_7(NH_2)_3)SO_4 \cdot 2\ H_2O$ und $(HC_6N_7(NH_2)_3)ClO_4 \cdot H_2O$", *Z. Anorg. Allg. Chem.* **2005**, *631*, 2545-2554.

[169] A. Sattler, W. Schnick, "Melemium Hydrogensulfate $H_3C_6N_7(NH_2)_3(HSO_4)_3$ – the First Triple Protonation of Melem", *Z. Anorg. Allg. Chem.* **2010**, *636*, 2589-2594.

[170] A. Sattler, S. Schönberger, W. Schnick, "Melemium Methylsulfonates $HC_6N_7(NH_2)_3H_2C_6N_7(NH_2)_3(SO_3Me)_3{\cdot}H_2O$ and $H_2C_6N_7(NH_2)_3(SO_3Me)_2{\cdot}H_2O$ ", *Z. Anorg. Allg. Chem.* **2010**, *636*, 476-482.

[171] W. Liu, Q.-H. Lin, Y.-Z. Yang, X.-J. Zhang, Y.-C. Li, Z.-H. Lin, S.-P. Pang, "Energetic Salts Based on an Oxygen-Containing Cation: 2,4-Diamino-1,3,5-triazine-6-one", *Chem. - Asian J.* **2014**, *9*, 479-486.

2. Summary

This thesis is dedicated to the investigation of synthesis parameters that lead to the formation of triazine-based C/N/H compounds or stabilization of such against further condensation reactions. In particular, the influence of inorganic salts that act as reaction media or as additional reactants beside C/N/H starting materials is investigated and underlying mechanisms of these reactions are elucidated. Aspects that prevent, promote or reverse the condensation of triazines to heptazines are of particular interest herein. Furthermore, structural features of said compounds and relevance of different types of inter- and intramolecular interactions—namely hydrogen bridge interactions, π-stacking and ionic interactions—for their formation are examined in detail. To this end, a number of novel triazine-based compounds were synthesized by various different methods and characterized structurally and spectroscopically, as well as compared to the existing range of compounds.

The compounds investigated in these studies can be divided into three subgroups, to each of which a chapter of this thesis is dedicated: ionic compounds based on protonated C/N/H molecules, molecular adducts, and polymeric materials obtained from reactions in salt melts, with the former two categories showing a certain degree of overlap. Furthermore, while different subgroups of compounds have been investigated with different questions in mind, due to the close relation between the respective compounds—all of which in the end are C/N/H compounds and exhibit the characteristic behavior of this compound class—various studied aspects continuously reoccur throughout these chapters.

In the following, the different subgroups, the compounds investigated for the respective chapter as well as the questions addressed by each study are presented in short.

2.1 Ionic Compounds—Melamium and Ammelinium Salts

A plethora of salts containing C/N/H-based cations has been investigated in recent years, among those a broad range of melaminium and melemium salts. However, only a few representatives of the group of melamium salts are known at all. Ionic compounds containing the melamium cation have the potential to yield valuable insights into the condensation process of C/N/H materials, since they are readily obtained and are stable over a large temperature range, whereas pure melam is difficult to isolate and is supposedly only formed as a reactive intermediate during the formation of melem. To elucidate the reason for the inhibition of melem formation in ionic melamium compounds, several of these salts have been prepared and structurally characterized.

Ammelinium salts are closely related to melamium salts in that ammelinium is the product of acidic hydrolysis of melam. For several poorly characterized 'melamium' salts of strong mineral acids that have been reported on in literature, it has to be assumed—and in some cases has been proven—that in fact they rather represent salts of the ammelinium cation. While they are not strictly part of the condensation cascade or the transformation reactions in question, they do exhibit the same structure directing interactions as other triazine-based compounds and thus add to the understanding of the compound class in general.

Melamium Bromide, Iodide and Melamium Thiocyanate Melam (1:1)

(Chapter 3, published in a) *Z. Anorg. Allg. Chem.* **2018**, *644*, 186-192; b) *Z. Anorg. Allg. Chem.* **2019**, *645*, 840-847.)

Only three representatives of the group of melamium salts have been reported on and structurally characterized prior to this thesis: melamium perchlorate, $C_6N_{11}H_{11}(ClO_4)_2{\cdot}2H_2O$, as well as the adduct compounds melamium chloride ammonium chloride, $C_6N_{11}H_{10}Cl{\cdot}0.5NH_4Cl$, and melamium thiocyanate melamine, $C_6N_{11}H_{10}SCN{\cdot}2C_3N_6H_6$. However, a bromide adduct compound analogous to melamium chloride ammonium chloride has been postulated by *Jürgens*. In chapter 3, three new salts containing the melamium cation—melamium bromide, $C_6N_{11}H_{10}Br$, melamium iodide, $C_6N_{11}H_{10}I$, and a melamium thiocyanate melam (1:1) adduct, $C_6N_{11}H_{10}SCN{\cdot}C_6N_{11}H_9$—are presented, which were obtained through synthesis in sealed glass ampoules starting from C/N/H precursor material dicyandiamide and the respective ammonium salt. Explorative optimization of synthesis parameters yielded single-crystals of all three compounds that allowed for structure elucidation via single-crystal X-ray diffractometry. None of the structures is isostructural to any other melamium salt.

Melamium bromide is comprised of corrugated layers, which are stacked in a staggered arrangement. Bromide ions are located within as well as between the layers. Two crystallographically independent melamium ions exist within the structure, one of which is planar—as is expected for melamium—while the other exhibits a moderate torsion angle between the planes of the two triazine rings—a phenomenon, which has also been observed for non-protonated melam. In contrast, melamium iodide

forms a very orderly structure comprised of planar layers with melamium ions forming a porous network with infinitely extended channels along *c*, in which the iodide anions are located. In melamium thiocyanate melam, layers are slightly corrugated, however, molecules are arranged in an analogous channel-forming arrangement as observed in melamium iodide. Thiocyanate counter ions occupy the same sites within the cavities that are occupied by iodide in melamium iodide, however, are heavily disordered and could not be assigned to fixed sites within the structure. Instead of distinct atom positions, continuous, homogeneous columns of electron density spanning through the layers were observed. All of these structures exhibit dense networks of hydrogen bridge interactions between melamium ions as well as between melamium and the respective counter ions.
Melamium bromide, melamium iodide and melamium thiocyanate melam were obtained phase pure with no side phases detectable by crystallographic nor spectroscopic methods. All three compounds were characterized by FT-IR spectroscopy. Melamium thiocyanate melam was further studied by solid-state MAS NMR spectroscopy and thermoanalytic measurements.

Ammelinium Sulfate Cyanuric Acid (3:1) and Ammelinium Sulfate Monohydrate

(Chapter 3, published in *Z. Anorg. Allg. Chem.* **2019**, *645*, 848-856.)
Ammelinium, $C_3N_5H_5O$, is formed through acidic hydrolysis of melam as has already been stated by *Liebig* in 1834, thus complicating the synthesis of melamium salts of strong mineral acids such as melamium chloride, nitrate or sulfate. Two novel ammelinium-based compounds were obtained from attempted syntheses of melamium sulfate in diluted sulfuric acid. For these, melam was suspended in boiling water and diluted H_2SO_4 was added dropwise over an extended period of time. Afterwards, the resulting solution was cooled for several days to enable crystal growth through precipitation. Ammelinium sulfate cyanuric acid (3:1), $6C_3N_5H_6O^+ \cdot 3SO_4^{2-} \cdot 1⅔C_3N_3H_3O_3 \cdot H_2O$, was obtained in the form of millimeter-wide hexagonal pyramids as well as tapered rods. The structure is comprised of more or less planar layers of ring systems stacked along *c* with sulfate anions extending into the layer planes. Within the layers, triazine units are arranged in isolated clusters, in which one cyanuric acid molecule is coordinated by three ammelinium cations. These clusters form cavities, into which sulfate ions extend. A threefold superstructure was observed, in which cyanuric acid units are replaced by water of crystallization and sulfate tetrahedra can point either upwards or downwards. The adduct compound was further investigated by FT-IR and solid-state MAS NMR spectroscopy.
A second ammelinium salt, ammelinium sulfate monohydrate, $2C_3N_5H_6O^+ \cdot SO_4^{2-} \cdot H_2O$, was obtained through analogous synthesis, however, only as a minor side phase that formed small, translucent crystals in an otherwise unidentifiable sample. No phase pure sample of ammelinium sulfate monohydrate could be obtained. Characterization of this compound was thus limited to crystallographic structure elucidation. Like ammelinium sulfate cyanuric acid (3:1), ammelinium

sulfate monohydrate exhibits a layered structure with either a face or vertex of each sulfate tetrahedron embedded within the layer. Only a very limited amount of hydrogen bridge interactions exists between the respective ammelinium units. Instead, interactions between ammelinium and sulfate ions appear to dominate the structure. It is noteworthy, that for one of two ammelinium units disorder within the terminal groups was observed, which allows for the formation of additional hydrogen bridge interactions between keto and amino groups, which would otherwise lack an opposite donor or acceptor, respectively.

2.2 Molecular Adduct Compounds: Melam-Melem (1:1)

(Chapter 4, published in *Chem. Eur. J.* **2019**, *25*, 8415-8424.)

Adduct compounds in general are comprised of two or more components that coexist in a non-ionic arrangement. When these components are formed from the same starting material(s)—as is typically the case in C/N/H chemistry—this coexistence raises the question for the reason of this disproportionation and the apparently equal (meta)stability of those components. A very prominent example of adduct compounds in C/N/H chemistry is a series of melamine-melem adducts described by *Sattler et al.*, which were interpreted as intermediates in and indication for the direct transformation reaction of melamine to melem.

In chapter 4, an adduct compound between melam and melem is described that can be interpreted as evidence for another reaction pathway, which involves melam as an intermediate between melamine and melem. Thus, this compound might clarify the role of melam in the condensation cascade of C/N/H compounds. The adduct melam-melem (1:1), $C_6N_{11}H_9 \cdot C_6N_{10}H_6$, was obtained from autoclave syntheses under elevated ammonia pressure. While under atmospheric conditions no such intermediate of the condensation process could be isolated, elevated ammonia pressure inhibits or slows down C/N/H condensation reactions according to *Le Chatelier's* principle. The compound is formed as a microcrystalline material, which necessitated synchrotron microfocus measurements to obtain structural data. The herein described structure was initially solved from these data and afterwards optimized by quantum-chemical calculations on the PBE-D3/pob-TZVP level of theory to account for mediocre precision of experimental data and to determine hydrogen atom sites that could not be refined from microfocus measurements.

The structure is best described in terms of a melam substructure and a melem substructure that are arranged in alternating ribbons and connected via a dense network of hydrogen bridge interactions. Within the melem substructure, zigzag chains of melem are formed, while melam forms double strands of hydrogen bridge connected dimers. Melam molecules show an exceptionally large dihedral angle of 48° between the triazine ring planes, allowing them to span between melem molecules located in different layers of the melem substructure.

Further characterization of the melam-melem adduct was conducted using FT-IR and solid-state NMR spectroscopy. Rietveld refinement of bulk samples showed the presence of moderate amounts of pure melam and pure melem as side phases, further verifying the parallel existence of the two C/N/H molecules.

2.3 Polymeric Compounds

From the point of view of application, polymeric C/N/H compounds are by far the most interesting subgroup of this material class. The semiconducting properties and appropriate band edge positions required for (photo-)catalytic applications are typically found in these polymeric materials, while molecular C/N/H compounds—apart from melamine—are predominantly of interest as potential precursors for these. However, except for melon, $[C_6N_9H_3]_n$, which is obtained from simple thermal condensation of C/N/H precursors, the availability of such polymeric materials was limited for a long time. The discovery of poly(triazine imide) (PTI) obtained via an ionothermal synthesis route can thus be seen as a breakthrough in C/N/H chemistry. The application of molten salts as reaction media opened up a multitude of possibilities, not only by making this novel, 2D extended material accessible, but also, since the plethora of suitable inorganic salts and combinations thereof and the dependence of the reaction behavior of the C/N/H precursors on the respectively chosen salt(s), opens up a wide field of further possibilities in explorative C/N/H synthesis. As representatives of this range, syntheses in molten zinc(II) chloride, $ZnCl_2$, and other lewis-acidic salts, were studied in this thesis and the results—although preliminary—are presented in chapter 5. Furthermore, investigations into the formation mechanism of PTI were conducted.

On the Formation Mechanism of Poly(triazine imide) (PTI)

(Chapter 5, published in *Z. Anorg. Allg. Chem.* **2019**, *645*, 857-862.)

Poly(triazine imide) with intercalated lithium and halide ions, $C_6N_9H_3{\cdot}LiX$ (X = Cl, Br), is a fascinating material that not only exhibits promising properties for application, but also represents the first 2D extended C/N/H material that could be synthesized phase pure and in quantitative amounts. Little, however, is known about the formation process of PTI and the crucial role of the salt melt reaction medium in this. Furthermore, the material is intriguing in that on the one hand, it is highly condensed and obtained at rather high temperatures, on the other hand, however, is comprised of triazine units, which typically occur only in 'low temperature' C/N/H compounds. The process of PTI formation was thus studied in several series of experiments, in which the reaction parameters temperature, reaction time, chosen precursor material and chosen salt melt were varied and the thus obtained products analyzed by FT-IR spectroscopy and powder X-ray diffractometry. It is shown that independent of chosen precursor material, the reaction always proceeds via a pathway analogous to the condensation

cascade, with melem being the imminent intermediate before the formation of PTI. This is also true when using melon as a starting material, which necessitates depolymerization. Thus, the reaction requires the formation of triazines from heptazines, which stands in stark contrast to the reaction behavior these compounds exhibit during the thermal condensation in the absence of a salt melt. A mechanism for this reversed reaction is proposed and the influence of the respective reaction conditions discussed.

Synthesis of C/N/H compounds in lewis-acidic salt melts

(Chapter 5, unpublished)

$ZnCl_2$, a strong Lewis acid, is known to catalyze the trimerization of cyanido groups to triazine rings and has thus found successful application in the synthesis of covalent triazine frameworks. Furthermore, it possesses a low melting point and large thermal stability range, which makes it suitable as a salt melt in ionothermal syntheses. These two properties made $ZnCl_2$ particularly suitable for investigating the influence of the salt melt as a liquid reaction medium in ionothermal syntheses—as opposed to the influence other properties of the salt might exert on the reaction. To this end, experiments where performed in which a C/N/H precursor compound was mixed with different amounts of inorganic salts and brought to reaction. $ZnCl_2$ was either added in quantities that would allow the salt to act as a solvent or only in catalytic amounts. Similar experiments were conducted in $CdCl_2$/KCl and various other salt melts. Throughout this chapter, three novel compounds obtained in these experiments are presented. None of them could be structurally elucidated through diffraction methods, however, compounds were investigated spectroscopically and structure models deduced from these measurements.

Compound **(1)**, which was obtained from syntheses in excess $ZnCl_2$ salt melt, shows great resemblance to poly(triazine imide). It was deduced that the product is a highly symmetric polymeric compound based on triazine nuclei interconnected by imide bridges. Deviations from PTI are slight but noticeable and are discussed on the basis of intercalated ions and protonation patterns. Analogous reactions in excess $CdCl_2$/KCl melt, on the other hand, yielded compound **(2)**, which appears to be based on the melem building block $C_6N_{10}H_6$. The compound is very sensitive to hydrolysis and yields melem on aqueous workup, however, both FT-IR and PXRD patters differ completely from the pure compound. Spectroscopic experiments identified **(2)** as a molecular compound comprising heptazine nuclei, however, no crystallographic structure could be established. As for all the compounds presented in this chapter, it was not possible to unambiguously determine whether ions of the salt melt are incorporated in the structure and which structural role they play. Finally, compound **(3)** could be obtained from heating dicyandiamide in the presence of very minor amounts of $ZnCl_2$, $CdCl_2$ or various other salts. This compound closely resembles melon—the C/N/H compound expected to form under such conditions in the absence of salts—in FT-IR as well as NMR spectroscopy, however, exhibits good crystallinity and shows signs of a highly ordered material, which is completely atypical

for melon. It is thus argued that the presence of lewis-acidic salts might possess a structure directing effect that leads to the formation of a ‘crystalline melon’ without the usually expressed stacking disorder of this material.

3. Ionic Compounds—Melamium and Ammelinium Salts

3.1 Melamium Bromide and Melamium Iodide

Synthesis and Structure of Melamium Bromide $C_6N_{11}H_{10}Br$ and Melamium Iodide $C_6N_{11}H_{10}I$

Fabian K. Kessler, Thaddäus J. Koller, and Wolfgang Schnick

Published in: *Z. Anorg. Allg. Chem.* **2018**, *644*, 186-192.

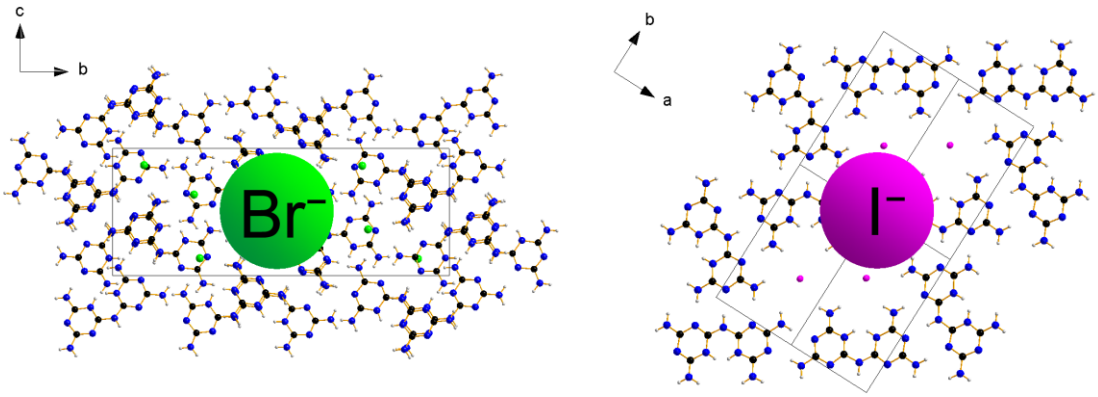

Abstract

Melamium bromide and melamium iodide were synthesized from dicyandiamide in the presence of ammonium halides in evacuated Duran glass ampoules at temperatures of 450 °C. The crystal structures of both compounds were obtained from single-crystal X-ray diffraction. Melamium bromide $C_6N_{11}H_{10}Br$ crystallizes in space group $P2_1/n$ [no. 14, a = 7.0500(5), b = 28.7096(18), c = 10.8783(8) Å, β = 96.060(2)°, Z = 8, $wR2$ = 0.2231] and exhibits a layer-like arrangement of melamium ions, wherein both planar as well as twisted molecular structures of the cations occur. Melamium iodide $C_6N_{11}H_{10}I$ crystallizes in space group $P2_1/c$ [no. 14, a = 6.8569(3), b = 11.9949(6), c = 14.0932(6) Å, β = 97.613(2)°,

$Z = 4$, $wR2 = 0.0654$], however in a structure completely different from the one of melamium bromide. The melamium iodide structure is comprised of stacks of planar melamium ions that form complex, hydrogen-bonded network layers with iodide ions within the layers. Both compounds were further characterized by FT-IR spectroscopy, mass spectrometry, and elemental analyses. Melamium bromide and melamium iodide could be obtained as air stable and colorless crystals. Samples are crystallographically phase pure as shown by Rietveld refinement.

3.1.1 Introduction

Melam, $C_6N_{11}H_9$, often denoted as $(C_3N_3(NH_2)_2)NH$ to better account for its constitution, is an inorganic nitrogen-rich heterocycle consisting of two imide-bridged triazine rings terminated by amine groups.[1] It is one of several C/N/H compounds described by 19th century chemist *Justus Liebig* in his initial publication on carbon nitride compounds in 1834.[2] This group of compounds comprises a variety of inorganic substances, then arbitrarily named as melamine, melam, melem, and melon, that are all based on either the triazine or heptazine building unit (Figure 3.1.1). Despite this early discovery, efforts to characterize these compounds longtime were scarce. Propositions for their molecular structures were only made in the late first half of the 20th century with the prediction of the cyameluric nucleus by *Pauling et al.* and the constitution of melon as well as melam by *Redemann et al.*[3,4] Crystal structures of these compounds were not established until recently.[5-7]

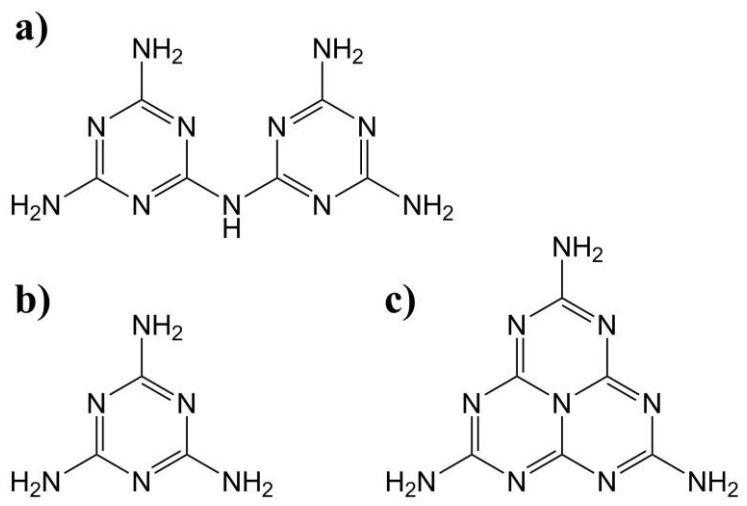

Figure 3.1.1 Molecular structures of (a) melam, (b) melamine, and (c) melem.

While *Liebig* conducted his initial syntheses starting from various thiocyanate salts with or without ammonium chloride, a more straightforward approach towards these substances has been found in the thermal condensation of melamine.[8] By heating this triamino-triazine, a cascade of condensation reactions with elimination of several formula units of ammonia is initiated. Melam, the condensation product of two melamine molecules, is formed at about 320 to 380 °C. However, it is rather difficult to isolate since it readily undergoes further condensation towards melem at these temperatures with release of one additional formula unit of ammonia. Melem is stable up towards temperatures of around 450 °C, at which it starts to polymerize to melon $[C_6N_7(NH_2)(NH)]_n$.[6]

Of the C/N/H compounds described by *Liebig* melam has received the least attention in scientific literature. While melamine has become an important industrial product with application in melamine-formaldehyde resins as well as flame retardants[9-11] and the polymer melon was intensely studied in recent years due to its properties as a photocatalyst suitable for water splitting[12-14] there are scant mentions of melam. This is most likely due to the intermediate role melam takes up in the condensation pathway, resulting in difficulties to obtain the compound phase pure and thus making it unattractive for potential applications.[15] Certain synthesis routes starting from melamine or its chloro-substituted derivatives in the presence of Lewis acidic salts have been proposed,[16,17] however, a route to obtain larger quantities of phase pure melam has first been published in 2013.[18] In this, melam could be obtained from dicyandiamide in autoclaves under ammonia pressure, thus preventing further condensation towards melem by impeding ammonia eliminating reactions through an already high ammonia partial pressure.

There have been some reports on the investigation of optical and spectroscopic properties of melam[17,19,20] as well as theoretical calculation of such properties and the according spectra,[21] a complete crystal structure determination, however, could not be performed until 2007.[7]

Salts of melamium (i.e. monoprotonated melam) have been even less investigated. While there are plenty of reports on melemium salts[22-25] there is extremely little work on salts containing the melamium ion. A rather simple route has been proposed for synthesis of melamium salts of inorganic acids starting from melam and either a solution of the respective acid, or its ammonium salt as a compound able to liberate the acid. It has been reported that the chloride, sulfate, nitrate, perchlorate, and phosphate salt of melamium could be obtained via this route.[26] The respective structures as well as properties, however, could not be elucidated. The structure of melamium perchlorate hydrate was obtained from single-crystal X-ray diffractometry in a recent work using a mostly analogous synthesis process.[7] Reactions of melamine with ammonium chloride in fused glass ampoules have been shown to yield a melamium chloride ammonium chloride adduct phase, whose structure could be elucidated from single-crystal X-ray diffraction.[27] This appears to be contradictory to the before mentioned route, which would predict melamium chloride as the expected product for the reaction of melamine and ammonium chloride.

We therefore investigated the reaction behavior of C/N/H materials in the presence of ammonium halide salts. We were able to obtain two melamium salts, which have not been mentioned in literature so far. It could be shown that instead of yielding an adduct phase as the analogous reaction with ammonium chloride, the reaction of dicyandiamide with ammonium bromide or ammonium iodide leads to the respective halide salts. We were able to elucidate the structures of both melamium bromide and melamium iodide from single-crystal X-ray diffraction data.

3.1.2 Results and Discussion

Preparation

The synthesis of melamium bromide and melamium iodide was conducted vastly analogous to the synthesis of the melamium chloride ammonium chloride adduct phase described by *Braml et al.*[27] Dicyandiamide, $C_2N_4H_4$, was chosen as a C/N/H precursor compound and pyrolyzed in sealed and evacuated glass ampoules in the presence of ammonium bromide and ammonium iodide, respectively. Due to the known tendency towards decomposition on moist air and hygroscopicity of both ammonium halide salts all chemicals were handled in a glove box in a protective argon atmosphere. Ampoules were placed in a vertical tube furnace that allowed for sublimation to take place. For both ammonium halide salts, different products could be obtained from both ends of the ampoule. A temperature gradient of 40 °C was measured along the length of the ampoule.

For ammonium bromide, a pale beige substance was obtained from the lower, hotter end of the ampoule that could be identified as melon ($[C_6N_9H_3]_n$) by FT-IR spectroscopy and powder X-ray diffraction. From the top end melamium bromide $C_6N_{11}H_{10}Br$ was isolated as colorless crystals. Synthesis with ammonium iodide yielded a grey to brown substance at the bottom of the ampoule and colorless, well-defined crystals at the top end. Both, however, showed to be melamium iodide in FT-IR spectroscopy and powder X-ray diffraction. It is assumed that the bottom product was contaminated by a minor side phase that lead to the divergence in optical appearance but could not be identified by X-ray diffraction due to its amorphous character and/or low content.

Elemental composition of both melamium salts was determined by combustion analysis and potentiometric titration. Melamium bromide showed good agreement with calculated values for the formula $C_6N_{11}H_{10}Br$. For melamium iodide the obtained iodine value was slightly less than expected (33.60 % found as opposed to 34.95 % expected), indicating minor impurities by iodine-free C/N/H compounds.

Both melamium salts were further examined by mass spectrometry. While no signals could be observed for *m/z* equal the respective molecular weight of 316.16 (melamium bromide) and 363.15 (melamium iodide), all investigated samples showed signals at *m/z* = 235.1 that could be assigned to the melamium ion. Furthermore, signals for Br^- at *m/z* = 80.1 and for I^- at *m/z* = 127.9 as well as for I_2 at *m/z* = 253.8 were observed.

Single-Crystal X-ray Analysis of Melamium Bromide

The structure of the bromide salt could be refined in the monoclinic space group $P2_1/n$ with a rather large unit cell containing eight formula units. Crystallographic data are summarized in Table 3.1.1. Poor *R* indices for the structure refinement are attributed to the poor quality of the small, platelet-like crystals as also indicated by a high R_σ value (significance of measured data) of 0.2253.

Table 3.1.1 Crystallographic data and details of the structure refinement for melamium bromide and melamium iodide.

	Melamium bromide	**Melamium iodide**
Empirical formula	$C_6N_{11}H_{10}Br$	$C_6N_{11}H_{10}I$
Formula weight [g mol^{-1}]	316.16	363.15
Crystal system	Monoclinic	Monoclinic
Space group	$P2_1/n$ (no. 14)	$P2_1/c$ (no. 14)
Radiation, λ [ppm]	Mo-K$_\alpha$, 0.71073	Mo-K$_\alpha$, 0.71073
a [Å]	7.0500(5)	6.8569(3)
b [Å]	28.7096(2)	11.9949(6)
c [Å]	10.8783(8)	14.0932(6)
β [°]	96.060(2)	97.613(2)
V [Å^3]	2189.5(3)	1148.92(9)
Z	8	4
Density (calcd.) [g cm^{-1}]	1.918	2.099
Temperature [K]	100(2)	100(2)
Absorption coefficient [mm^{-1}]	3.760	2.792
Diffraction range [°]	$2.991 \leq \theta \leq 24.989$	$2.238 \leq \theta \leq 24.991$
F(000)	1264	704
Index range	$-8 \leq h \leq 8$	$-8 \leq h \leq 8$
	$0 \leq k \leq 34$	$-14 \leq k \leq 14$
	$0 \leq l \leq 12$	$-16 \leq l \leq 16$
Absorption correction	numerical	multiscan
Parameters	326	169
No. of independent reflections	2951	2023
No. of independent reflections ($I \leq 2\sigma$)	1908	1825
GooF	1.310	1.242
R indices ($I \leq 2\sigma$)	$R1 = 0.0907$, $wR2 = 0.2231$	$R1 = 0.0239$, $wR2 = 0.0654$
R indices (all data)	$R1 = 0.1389$, $wR2 = 0.2301$	$R1 = 0.0347$, $wR2 = 0.0970$

The asymmetric unit contains two individual melamium ions. Both of these show significant distortion from regular hexagonal ring symmetry with C–N distances varying from 1.317 to 1.385 Å for molecule 1 (centered around bridging nitrogen atom N4) and from 1.295 to 1.398 Å for molecule 2 (centered around bridging nitrogen atom N15). Angles deviate in a similarly broad range, with values from 111° to 120° for CNC and 120° to 129° for NCN. The imide bridges show widened CNC angles of 128° (molecule 1) and 129° (molecule 2), respectively, as expected from related compounds (128° for the melamium chloride ammonium chloride adduct, 129° to 132° for pure melam). Interestingly, while molecule 1 shows almost no twist around the central bridging imide group as expected from comparison with known melamium compounds, a dihedral angle of 6.8° can be found between the

planes of the two triazine rings in molecule 2, resulting in a notable twist, which is, however, still smaller than in pure melam (11° to 14°).[7]

Melamium ions do not form planar layers, but instead are arranged in a "wave-like" pattern along the *b* axis with stacks of downwards tilted molecules followed by stacks of upwards tilted melamium units (see Figure 3.1.2). In the transition zone between these two kinds of stacks, triazine units of molecule 2, which are twisted out of the "stacking plane" are aligned along the *a* axis and completely overlapping with further triazine rings from the respective other stack. There are, however, no melamium units in the structure that show complete overlap with other molecules, but only overlap of single triazine rings.

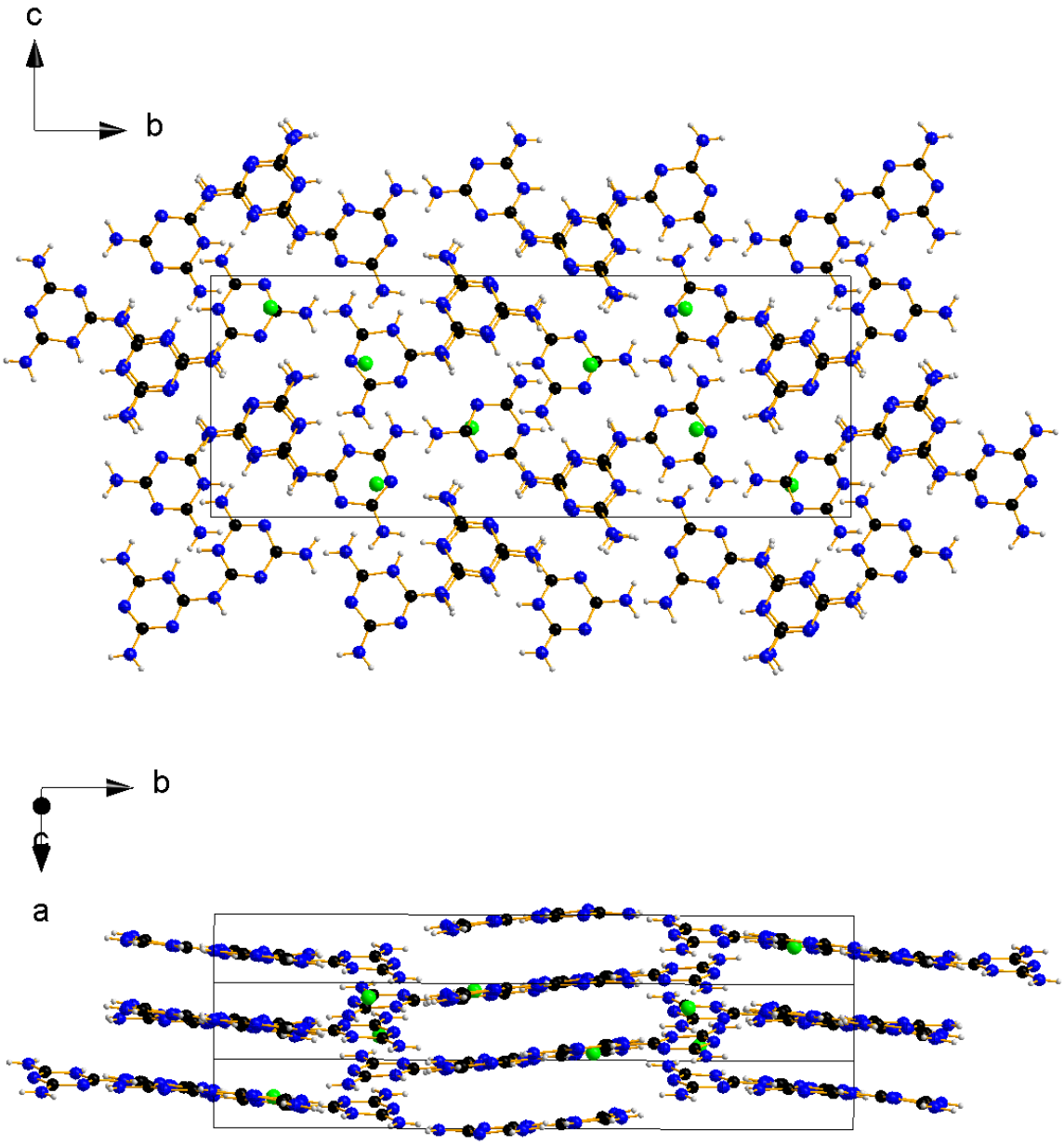

Figure 3.1.2 Crystal structure of melamium bromide. C atoms are displayed in black, N atoms in blue, Br atoms in green, and H atoms in light gray. Top: projection along the *a* axis on top of the melamium layers. Bottom: corrugated layers of melamium bromide.

Hydrogen atom positions could not be freely refined but are assumed from geometrical calculations. The protonation of melamium is assumed to take place at the inwards directed ring nitrogen atoms N3, N5, N14, and N16 based on similar protonation patterns found in other melamium compounds.[7,27] However, the twist in molecule 2 might as well indicate a non-protonated melam molecule, resulting in a doubly protonated molecule 1 to obtain electroneutrality.

Two independent bromide positions can be found in the structure. They are located in cavities within the melamium structure with Br1 in between the stacks of melamium ions and Br2 in the transition zone surrounded by out-of-plane twisted triazine rings.

Five amine groups are oriented towards Br1, allowing for hydrogen bridge formation. However, donor-acceptor distances are found to be between 3.32 and 3.75 Å and thus rather large, resulting in weak bonds that are not expected to play a major role in the formation of the structure. Similarly, five potential hydrogen bonds could be identified for Br2 with donor-acceptor distances of 3.35 to 3.52 Å.

The orientation of amine groups towards the bromide ions offers an explanation for the different dihedral angles found for melamium molecules 1 and 2: twisting one of the triazine units of molecule 2 out of plane allows for orientation of two amine groups towards the anion. In contrast, no such constellation can be found for molecule 1, thus the intramolecular hydrogen bond enabled by planarity makes this conformation energetically favorable.

Further hydrogen bonds can be found between melamium ions with N–N donor-acceptor lengths between 2.81 and 3.02 Å. Two different bonding motifs can be observed, as shown in Figure 3.1.3: there are “end-on-end” arrangements between melamium molecules allowing for two hydrogen bridges as well as “side-on-end” arrangements resulting in three such bonds. The latter of those is unknown from previously described melamium salts[7,27], however can be found in melam hydrate.[18]

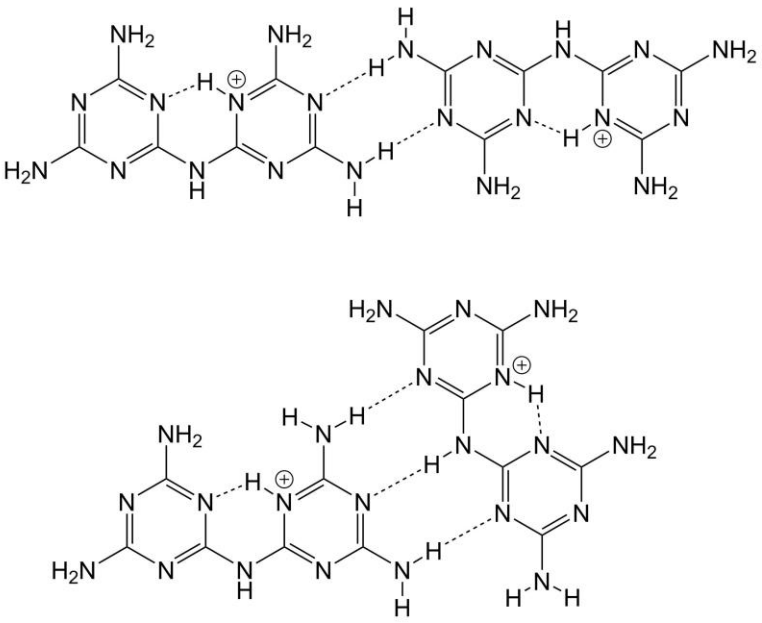

Figure 3.1.3 Hydrogen bonding motifs: end-on-end (top) and side-on-end (bottom).

Single-Crystal X-ray Analysis of Melamium Iodide

Melamium iodide crystallizes in the monoclinic space group $P2_1/c$. In contrast to melamium bromide it contains but four formula units per unit cell. Crystallographic data can be found in Table 3.1.1. The structure of melamium iodide is comprised of layers of melamium ions that are stacked roughly along the *ac* face diagonal with four layers of melamium ions per unit cell and a stacking distance of 3.3 Å (see Figure 3.1.4). This is significantly shorter than in melamium chloride ammonium chloride, exhibiting a stacking distance of about 3.4 Å.[27] This is surprising considering the rather similar structure of both compounds and the larger ionic radius for iodide compared to chloride as well as ammonium.[28] It is assumed that the shorter stacking distance in melamium iodide is due to reduced repulsive interactions.

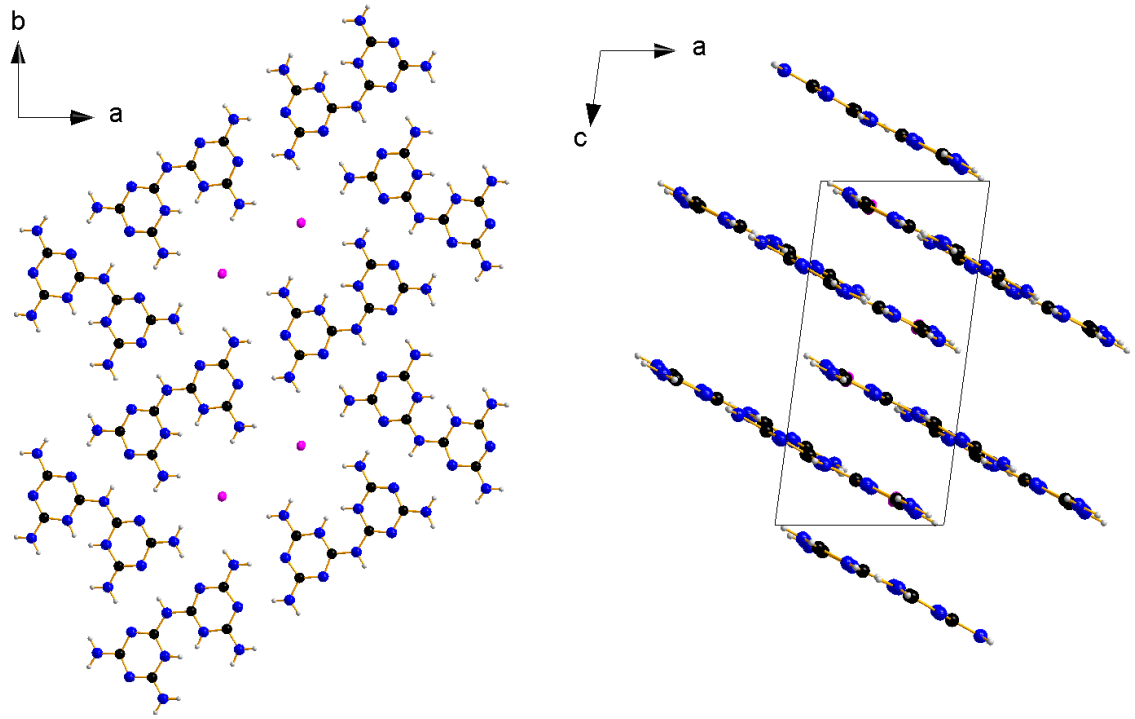

Figure 3.1.4 Crystal structure of melamium iodide. C atoms are displayed in black, N atoms in blue, I atoms in pink and H atoms in light gray. Left: projection along *c* axis on a single layer of melamium iodide. Right: projection along the *b* axis with a viewpoint orthogonal to the stacking direction.

Iodide ions are found within the melamium planes in elongated cavities comprised of six melamium molecules, with two iodide ions per cavity. Melamium ions in melamium iodide are mostly planar with a torsion angle of only 0.96°—as opposed to a twist of 11 to 14° in pure melam but well in line with other melamium salts such as the melamium chloride ammonium chloride adduct or melamium perchlorate.[7,27] Triazine rings in the melamium ions show certain deviations from regular hexagonal symmetry with C–N bond lengths varying from 1.319 to 1.373 Å. NCN angles are slightly widened, ranging from 121 to 127°, whereas CNC angles are narrowed to 114 to 119°. Bond lengths for the bridging imide group are 1.360 and 1.394 Å, respectively, and therefore slightly longer than the average

C–N distance within the rings, indicating a stronger single bond character. The CNC angle of the imide group is 127° and therefore significantly widened, however still narrower than found for non-protonated melam (129° to 132°).

As for melamium bromide, no free refinement of hydrogen atom positions was possible. Protonation of the ring at N9 or N11 is in accordance with structures presented in previous work. This would allow for intramolecular hydrogen bridging between the respective N atoms. Intermolecular hydrogen bonding within the melamium planes occurs in the same two motifs described for melamium bromide. Donor-acceptor distances range from 2.84 to 3.00 Å for "side-on-end" and 3.02 Å for "end-on-end" arrangements, indicating medium strength bonds.

The N–I distances range from 3.53 to 3.73 Å and are thus comparable to donor–acceptor distances found in melamium bromide, indicating interactions of about the same strength.

Powder X-ray Diffraction and Rietveld Refinement

Samples of both melamium salts were investigated by powder diffraction to confirm phase purity of the bulk samples. Since single-crystal X-ray experiments were conducted at temperatures of 100 K, Rietveld refinement of powder diffractograms obtained at 298 K was used to elucidate room temperature lattice parameters and deviations from low temperature measurements.

The Rietveld refinement for melamium bromide is displayed in Figure 3.1.5. Some small reflections at 2θ = 14.8, 17.7, and 19.2° indicate the presence of a not yet identified, however very minor side phase. Certain remaining problems in the refinement of the intensities are attributed partly to the different recording temperatures for the powder diffractogram and the single-crystal measurement, partly to diffractometer artifacts. A minor amorphous side phase is observed.

The refined lattice parameters of a = 7.1483(2), b = 28.7256(6), c = 10.8808(3) Å, and β = 95.822(3)° show an elongation of the cell primarily along the a axis. This can be rationalized as a widening of the spacing between the corrugated layers with increasing temperature, whereas the molecular structures themselves remain relatively rigid, resulting in only minor increases along the respective lattice directions.

As for melamium bromide, Rietveld refinement could be used for melamium iodide to establish this compound as the only crystalline phase in the respective sample. All reflections were assigned to melamium iodide as obtained from single-crystal X-ray analysis. However, rather pronounced hill-like background shape between 2θ = 13 and 35° indicates the presence of an amorphous side phase.

As is the case with melamium bromide, no satisfying refinement of reflection intensities was possible. We again assign this problem to the different recording temperatures for the powder and single-crystal data.

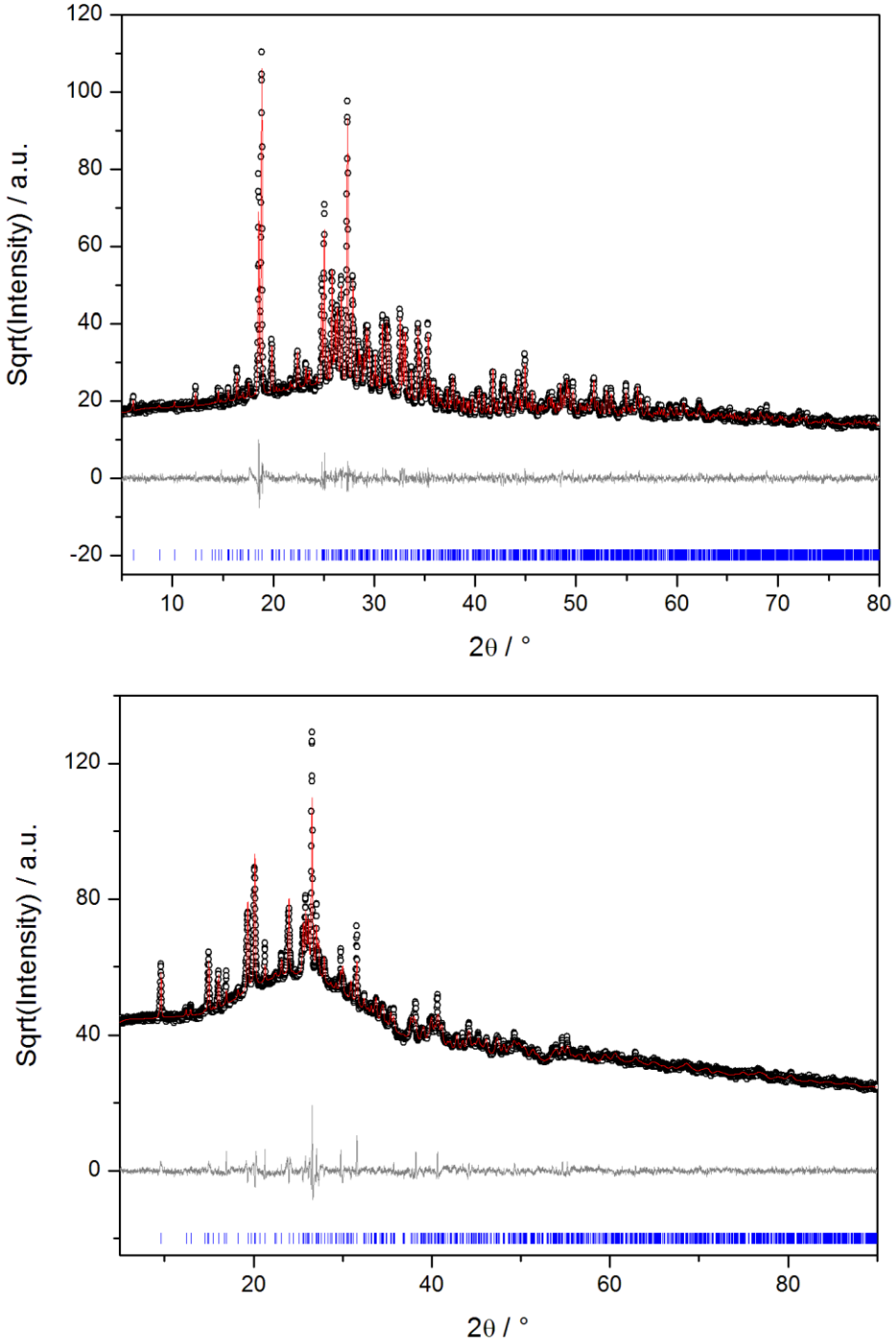

Figure 3.1.5 Results of the Rietveld refinement of melamium bromide (top) and melamium iodide (bottom). Measured data are displayed as black circles, the calculated model from the fitted pattern is plotted in red. The difference plot is displayed in gray below. Blue tickmarks indicate theoretical Bragg positions.

Lattice parameters as obtained from Rietveld refinement account to a = 6.8928(7), b = 11.987(2), c = 14.353(2) Å, and β = 98.380(5)°. Here, the cell primarily elongates along c and slightly along the a axis. This again is consistent with an increased spacing between the layers but hardly any change in the molecular structure.

In both cases we conclude that broad signals in the diffractograms originating from amorphous side phases are due to less crystalline phases of the same compound since neither elemental analysis nor FT-IR spectroscopy or mass spectrometry indicate any other present species. This allows us to conclude that the samples were obtained almost (in the case of melamium bromide) or entirely (in the case of melamium iodide) phase pure.

FT-IR Spectroscopy

Infrared spectra for both compounds were recorded in a range from 4000 to 650 cm^{-1} as displayed in Figure 3.1.6. Relatively well defined bands indicate a high degree of order. As expected, both compounds exhibit rather similar spectra, particularly in the region between 1600 and 950 cm^{-1} that can be assigned to stretching vibrations of the C/N framework in analogy with related C/N/H compounds.[5,7,15] Differences can be seen in the regions between 3400 to 3000 cm^{-1} and 1660 to 1600 cm^{-1} attributed to NH stretching and bending vibrations, respectively.[7] These can be explained by the structural differences in hydrogen bonding interactions towards the halide ions. The characteristic out-of-plane breathing mode typically found for triazine and heptazine ring based compounds appears at 797 in the bromide salt and at 804 cm^{-1} in the iodide salt.

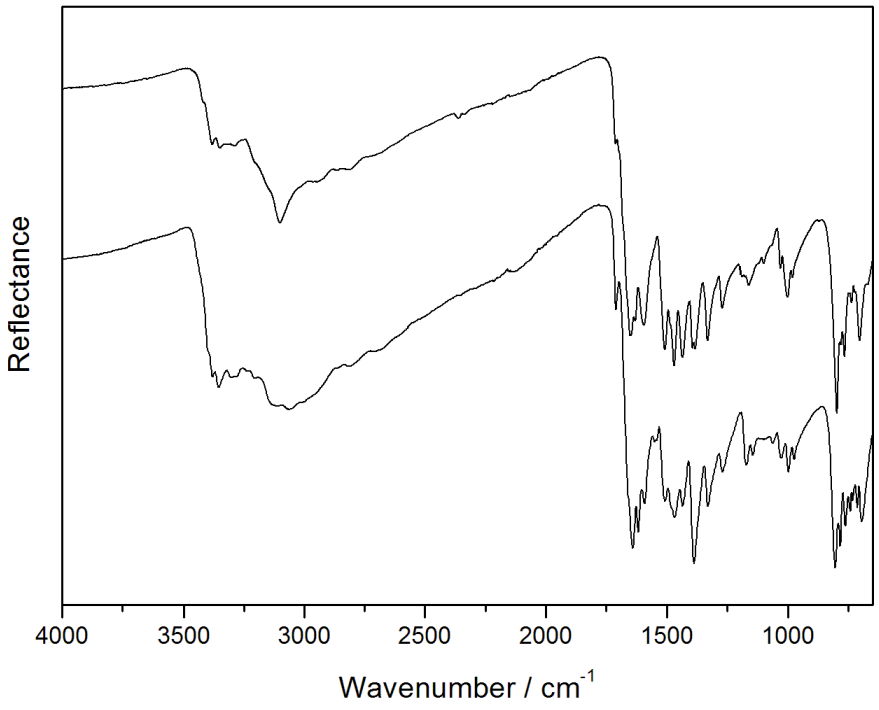

Figure 3.1.6 FT-IR spectra of melamium bromide (top) and melamium iodide (bottom).

Signals appearing at 1269 cm^{-1} in both compounds can be assigned to the stretching vibration of the bridging C–NH–C unit of the melamium ion, which can be found as well in melon[6] and pure melam.[7] Furthermore, a comparison of the FT-IR spectra of melamium bromide and melamium iodide with the melamium chloride ammonium chloride adduct phase reveals hardly any differences, in contrast to pure melam, whose spectrum does show significant divergences. We assign this to the twist between triazine rings in melam, whereas melaminium salts show almost planar conformation.

3.1.3 Conclusions

Melamium bromide and melamium iodide were prepared by thermal condensation of dicyandiamide in closed glass ampoules in the presence of ammonium bromide or ammonium iodide, which acted as a source for the respective hydrogen halide. Both products sublimated on the top end of the ampoule as colorless crystals. The structures of both compounds could be obtained from single-crystal X-ray diffraction.

Melamium bromide and melamium iodide crystallize in different structures. Melamium bromide contains two melamium ions in its asymmetric unit, one of which is planar as in melamium chloride ammonium chloride or melamium perchlorate while the other one shows a twist around the imide bridge as is also found for pure melam. We argue that these different conformations occur due to the molecules' orientation towards the bromide ions, with one molecule coordinating an anion twofold with its amide groups and the other molecule lacking such stabilization.

Melamium iodide is exclusively comprised of planar melamium ions that form layered arrangements with a dense network of hydrogen bonds comprised of two distinct coordination motifs. Iodide is found in large cavities within this network with two ions per cavity.

Rietveld refinement for both melamium salts showed the examined samples to be crystallographically phase pure (for melamium iodide) or only very weakly contaminated (for melamium bromide). Refined lattice parameters at room temperature in contrast to single-crystal measurements at 100 K indicate an elongation along the respective stacking direction with increasing temperature.

Both salts were further characterized by elemental analysis and FT-IR spectroscopy.

The facile synthesis route for well crystalline melamium bromide and melamium iodide allows for the investigation of various other melamium salts or – in general – salts of C/N/H compounds that could prove to be valuable precursor materials for polymeric carbon nitride materials. We expect to be able to synthesize and structurally elucidate several other postulated melamium compounds either via an analogous synthesis route in evacuated glass ampoules or by ion exchange starting from the now readily available bromide and iodide.

3.1.4 Experimental Section

Melamium Bromide: A dried glass ampoule was charged with dicyandiamide $C_2N_4H_4$ (329.5 mg, 3.92 mmol, Acros Organics, 99.5 %) and ammonium bromide NH_4Br (170.5 mg, 1.74 mmol, Grüssing, 99.5 %) ground together in a glove box and sealed at a length of about 120 mm under vacuum. The ampoule was heated in a vertical tube furnace to 450 °C at a rate of 2 K·min^{-1}, held at this temperature for 24 h and afterwards cooled to room temperature with a rate of 1 K·min^{-1}. A pale beige solid was obtained from the bottom end of the ampoule and identified as melon $[C_6N_9H_3]_n$. Melamium bromide could be isolated from the top end of the ampoule as fine colorless crystals. $C_6N_{11}H_{10}Br$: calcd. C 22.80, N 48.74, H 3.19, Br 25.28 %; found C 22.86, N 48.49, H 3.29, Br 25.35 %.

Melamium Iodide: A dried glass ampoule was charged with dicyandiamide $C_2N_4H_4$ (280.6 mg, 3.34 mmol, Acros Organics, 99.5 %) and ammonium iodide NH_4I (219.4 mg, 1.51 mmol, Alfa Aesar, 99 %) ground together in a glove box and sealed at a length of about 120 mm under vacuum. The ampoule was heated in a vertical tube furnace to 450 °C at a rate of 0.2 K·min^{-1}, held at this temperature for 24 h and afterwards cooled to room temperature with a rate of 2 K·min^{-1}. Melamium iodide was obtained from the bottom end of the ampoule as a gray-brown, moist solid that was dried at 100 °C for 30 min, as well as from the top end of the ampoule in the form of large colorless crystals. $C_6N_{11}H_{10}I$: calcd. C 19.85, N 42.34, H 2.78, I 34.95 %; found C 20.10, N 42.36, H 2.72, I 33.60 %.

Single-Crystal X-ray Diffraction: Single-crystal X-ray diffraction data were measured with a Bruker D8 Venture diffractometer (Bruker, Billerica MA, USA) at a temperature of 100 K using Mo-K_α radiation (λ = 0.71073 Å). The obtained data were corrected for absorption and the structure solved by direct methods implemented in the program APEX 3.[29] For structure refinement the program package WinGX (Shelxl-97, PLATON) was used.[30,31] All atoms apart from hydrogen atoms were refined anisotropically. Visualization of crystal structures was conducted using Diamond3.[32]

Further details of the crystal structures investigations may be obtained from the Fachinformationszentrum Karlsruhe, 76344 Eggenstein-Leopoldshafen, Germany (Fax: +49-7247-808-666; E-Mail: crysdata@fiz-karlsruhe.de, http://www.fiz-karlsruhe.de/request for deposited data.html) on quoting the depository numbers CSD-433426 for $C_6N_{11}H_{10}Br$ and CSD-433427 for $C_6N_{11}H_{10}I$.

Powder X-ray Diffraction: Powder samples were carried out with a Stoe Stadi P powder diffractometer (Stoe, Darmstadt, Germany) equipped with a Mythen 1 K silicon strip detector (Dectris, Baden, Switzerland) in Debye-Scherrer geometry applying monochromated Cu-$K_{\alpha1}$ radiation (λ = 1.54056 Å). Samples were prepared in glass capillaries of an inner diameter of 0.5 mm and wall thicknesses of 0.01 mm. The obtained data were processed using the program Stoe WinXPOW Vers. 2.21.[33] Rietveld refinement was carried out using TOPAS-Academic V4.1.[34]

General Techniques: FT-IR spectra were recorded with a Perkin-Elmer BX II FT-IR spectrometer equipped with a DuraSampler Diamond ATR (attenuated total reflection) unit. Measurements were conducted at room temperature in air. Mass spectrometry was performed with a Joel JMS-700 MStation spectrometer using electron ionization. Elemental analyses were performed in the microanalytic

laboratory of the Department of Chemistry, LMU Munich. Element contents of C, N and H were determined by combustion analysis with a Vario EL elemental analyzer (Elementar Analysensysteme GmbH). Halide contents were determined by potentiometric titration with a Titrando 888 titrator (Metrohm, Filderstadt, Germany).

Acknowledgements

The authors would like to thank Dr. Peter Mayer (Department of Chemistry, LMU Munich) for single-crystal X-ray diffraction measurements. Financial support granted by the Fonds der Chemischen Industrie (FCI) and the Deutsche Forschungsgemeinschaft (DFG) is gratefully acknowledged.

3.1.5 References

[1] P. Klason, "Ueber Melamverbindungen", *J. Prakt. Chem.* **1886**, *33*, 285-289.

[2] J. Liebig, "Ueber einige Stickstoff-Verbindungen", *Ann. Pharm.* **1834**, *10*, 1-47.

[3] L. Pauling, J. H. Sturdivant, "The Structure of Cyameluric Acid, Hydromelonic Acid and Related Substances", *Proc. Natl. Acad. Sci. USA* **1937**, *23*, 615-620.

[4] C. E. Redemann, H. J. Lucas, "Some Derivatives of Cyameluric Acid and Probable Structures of Melam, Melem and Melon", *J. Am. Chem. Soc.* **1940**, *62*, 842-846.

[5] B. Jürgens, E. Irran, J. Senker, P. Kroll, H. Müller, W. Schnick, "Melem (2,5,8-Triamino-tri-s-triazine), an Important Intermediate during Condensation of Melamine Rings to Graphitic Carbon Nitride: Synthesis, Structure Determination by X-ray Powder Diffractometry, Solid-State NMR, and Theoretical Studies", *J. Am. Chem. Soc.* **2003**, *125*, 10288-10300.

[6] B. V. Lotsch, M. Döblinger, J. Sehnert, L. Seyfarth, J. Senker, O. Oeckler, W. Schnick, "Unmasking Melon by a Complementary Approach Employing Electron Diffraction, Solid-State NMR Spectroscopy, and Theoretical Calculations—Structural Characterization of a Carbon Nitride Polymer", *Chem. Eur. J.* **2007**, *13*, 4969-4980.

[7] B. V. Lotsch, W. Schnick, "New Light on an Old Story: Formation of Melam during Thermal Condensation of Melamine", *Chem. Eur. J.* **2007**, *13*, 4956-4968.

[8] H. May, "Pyrolysis of melamine", *J. Appl. Chem.* **1959**, *9*, 340-344.

[9] H. Diem, G. Matthias, "Amino Resins", in *Ullmann's Encyclopedia of Industrial Chemistry, Vol. A2*, 5 ed. (Ed.: W. Gerhartz), VCH, Weinheim, **1985**, pp. 115-141.

[10] E. D. Weil, "Fire-Protective and Flame-Retardant Coatings – A State-of-the-Art Review", *J. Fire Sci.* **2011**, *29*, 259-296.

[11] E. D. Weil, S. V. Levchik, "Flame Retardants in Commercial Use or Development for Textiles", *J. Fire Sci.* **2009**, *26*, 243-281.

[12] X. Wang, K. Maeda, A. Thomas, K. Takanabe, G. Xin, J. M. Carlsson, K. Domen, M. Antonietti, "A metal-free polymeric photocatalyst for hydrogen production from water under visible light", *Nat. Mater.* **2009**, *8*, 76-80.

[13] A. Thomas, A. Fischer, F. Goettmann, M. Antonietti, J. O. Müller, R. Schlögl, J. M. Carlsson, "Graphitic carbon nitride materials: variation of structure and morphology and their use as metal-free catalysts", *J. Mater. Chem.* **2008**, *18*, 4893-4908.

[14] F. K. Kessler, Y. Zheng, D. Schwarz, C. Merschjann, W. Schnick, X. Wang, M. J. Bojdys, "Functional carbon nitride materials — design strategies for electrochemical devices", *Nat. Rev. Mater.* **2017**, *2*, 17030.

[15] A. I. Finkel'shtein, N. V. Spiridonova, "Chemical Properties and Molecular Structure of Derivatives of sym-heptazine[1,3,4,6,7,9,9b-heptaazaphenalene, tri-1,3,5-triazine]", *Russ. Chem. Rev.* **1964**, *33*, 400-405.

[16] V. A. Gal'perin, A. I. Finkel'shtein, N. K. Gavrilova, "Synthesis of melam from melamine", *Zh. Org. Khim.* **1971**, *7*, 2431-2432.

[17] N. V. Spiridonova, A. I. Finkel'shtein, "Melam synthesis and its physical and chemical properties", *Khim. Geterotsikl. Soedin.* **1966**, 126-129.

[18] E. Wirnhier, M. B. Mesch, J. Senker, W. Schnick, "Formation and Characterization of Melam, Melam Hydrate, and a Melam–Melem Adduct", *Chem. Eur. J.* **2013**, *19*, 2041-2049.

[19] M. Takimoto, "Infrared absorption spectra and structure of cyanamide derivatives", *Nippon Kagaku Zasshi* **1964**, *85*, 168-176.

[20] M. Takimoto, "Ultraviolet absorption spectra and structure of cyanamide derivatives", *Nippon Kagaku Zasshi* **1964**, *85*, 159-168.

[21] E. M. Moncharzh, N. K. Gavrilova, V. A. Gal'perin, A. I. Finkel'shtein, "Calculation of the structure and electronic spectra of melam and its ions", *Zh. Strukt. Khim.* **1982**, *23*, 152-154.

[22] A. Sattler, W. Schnick, "Melemium Hydrogensulfate $H_3C_6N_7(NH_2)_3(HSO_4)_3$ – the First Triple Protonation of Melem", *Z. Anorg. Allg. Chem.* **2010**, *636*, 2589-2594.

[23] A. Sattler, W. Schnick, "Preparation and Structure of Melemium Melem Perchlorate $HC_6N_7(NH_2)_3ClO_4{\cdot}C_6N_7(NH_2)_3$", *Z. Anorg. Allg. Chem.* **2008**, *634*, 457-460.

[24] A. Sattler, S. Schönberger, W. Schnick, "Melemium Methylsulfonates $HC_6N_7(NH_2)_3H_2C_6N_7(NH_2)_3(SO_3Me)_3{\cdot}H_2O$ and $H_2C_6N_7(NH_2)_3(SO_3Me)_2{\cdot}H_2O$ ", *Z. Anorg. Allg. Chem.* **2010**, *636*, 476-482.

[25] A. Sattler, L. Seyfarth, J. Senker, W. Schnick, "Synthesen, Kristallstrukturen und spektroskopische Eigenschaften des Melem-Adduktes $C_6N_7(NH_2)_3 \cdot H_3PO_4$ sowie der Melemium-Salze $(H_2C_6N_7(NH_2)_3)SO_4 \cdot 2\ H_2O$ und $(HC_6N_7(NH_2)_3)ClO_4 \cdot H_2O$", *Z. Anorg. Allg. Chem.* **2005**, *631*, 2545-2554.

[26] N. K. Gavrilova, V. A. Gal'perin, A. I. Finkel'shtein, A. G. Koryakin, "Synthesis of Melam and its Salts with Mineral Acids", *Zh. Org. Khim.* **1977**, *13*, 669-670.

[27] N. E. Braml, A. Sattler, W. Schnick, "Formation of Melamium Adducts by Pyrolysis of Thiourea or Melamine/NH_4Cl Mixtures", *Chem. Eur. J.* **2012**, *18*, 1811-1819.

[28] R. D. Shannon, "Revised Effective Ionic Radii and Systematic Studies of Interatomic Distances in Halides and Chalcogenides", *Acta Crystallogr., Sect. A: Found. Adv.* **1976**, *32*, 751-767.

[29] *APEX 3,* Bruker AXS Inc., Madison WI, USA, **2016.**

[30] G. M. Sheldrick, *Acta Crystallogr., Sect. A: Found. Adv.* **2008**, *64*, 112-122.

[31] G. M. Sheldrick, *SHELX-97, Program Package for the Solution and Refinement of Crystal Structures, Release 97-2,* Universität Göttingen, **1997.**

[32] *Diamond, Program for X-ray structure analysis, v3.1f,* Crystal Impact GbR, Bonn, **2010.**

[33] *Win XPOW, v2.12,* STOE & Cie GmbH, Darmstadt, **2005.**

[34] A. A. Coelho, *TOPAS-Academic V4.1,* Coelho Software, Brisbane, **2007.**

3.2 Melamium Thiocyanate Melam

Melamium Thiocyanate Melam, a Melamium Salt with Disordered Anion Sites

Fabian K. Kessler, Alexander M. Schuhbeck, and Wolfgang Schnick

Published in: *Z. Anorg. Allg. Chem.* **2019**, *645*, 840-847.

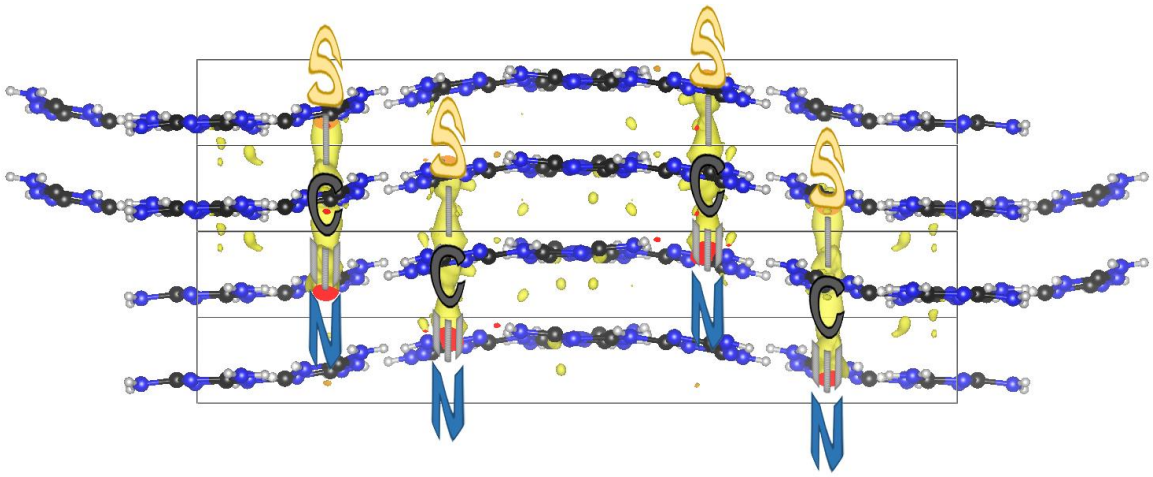

Abstract

Melamium salts are a group of ionic carbon nitride type compounds that has been investigated only scarcely. We herein present a novel representative of this group. A melamium thiocyanate melam (1:1) adduct was synthesized from dicyandiamide and ammonium thiocyanate in sealed glass ampoules. The structure of the adduct was determined from single-crystal X-ray diffraction. Melamium thiocyanate melam crystallizes in monoclinic space group $P2_1/c$ (no. 14) with lattice parameters of a = 3.6041(11), b = 28.532(7), c = 10.937(4) Å, β = 99.051(14)°, and Z = 4. While the melamium ions form 2D extended hydrogen bridged networks, the thiocyanate ions are disordered and no distinct structural sites could be assigned to the respective atoms. Instead, continuous columns of electron density located in channels in the porous structure were identified as potential space for anion locations. The compound was further characterized by elemental analysis, FT-IR spectroscopy and solid-state MAS-NMR spectroscopy of the nuclei ^{1}H, ^{13}C and ^{15}N. Rietveld refinement of powder samples was performed for phase analysis. Furthermore, DSC-TG was used to investigate the thermal behavior of the compound.

3.2.1 Introduction

When it comes to carbon nitride type compounds, chances are high that the topic is on one of but two groups of materials. On the one hand, there are molecular compounds such as melamine [$(C_3N_3)(NH_2)_3$], melam [$(C_3N_3)(NH_2)_2NH(C_3N_3)(NH_2)_2$], or melem [$(C_6N_7)(NH_2)_3$] (Figure 3.2.1). These have been known for almost two centuries, their discovery going back to *Liebig, Berzelius*, und *Gmelin*.[1-3] Of these, melamine is the most prominent representative since it is by far of the greatest industrial relevance. In the form of melamine-formaldehyde resins, it finds application in surface coatings, laminates, tableware or dirt sponges.[4-7] Further applications for not only melamine but molecular carbon nitride compounds in general include agents in steel nitridation baths or, more recently, flame retardants.[8-10] For the latter application, these compounds are particularly apt since they possess a high thermal stability, which allows them to draw a significant amount of heat before decomposition, in which case they release fire suppressing nitrogen.

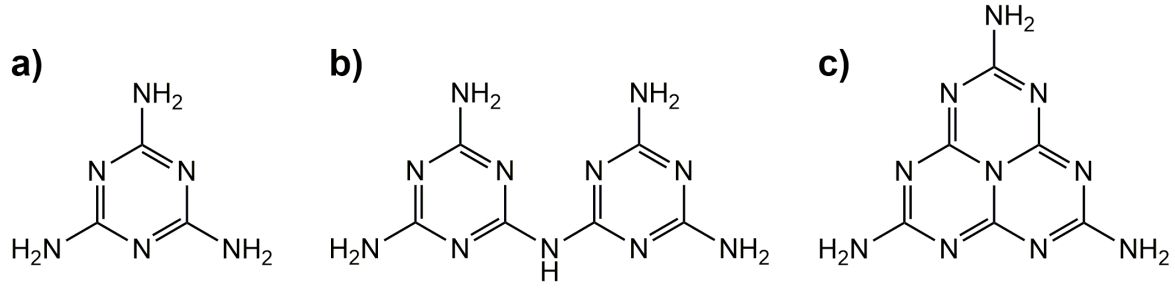

Figure 3.2.1 Molecular carbon nitride type compounds. (a) melamine, (b) melam, (c) melem.

On the other hand, polymeric carbon nitride compounds consisting of imide-bridged triazine (C_3N_3) or heptazine (C_6N_7) units have gained significant importance in recent years. These materials show semiconducting behavior due to an extended conjugated aromatic π-system and are thus valued for their electronic properties. Potential application primarily lies in photocatalysis, e.g. for degradation of organic pollutants, bactericides or fungicides, certain organic reactions such as CO_2 reduction or Friedel-Craft acylation and, most prominently, photocatalytic water splitting for hydrogen evolution.[11-18]

All of these compounds, however, are covalent in nature. Ionic carbon nitride type compounds, which are interesting rather for their structural properties than their potential application, receive significantly less attention. However, there are valuable insights to be gained from these compounds concerning the reactivity of carbon nitride type compounds – insights not only relevant for ionic, but also the more interesting-for-application covalent compounds.

Ionic carbon nitride type compounds exist for all of the molecules initially described by *Liebig* and various further derivatives. Both anionic and cationic carbon nitride type building blocks are known to occur in such salts. Anionic carbon nitride type building blocks usually carry deprotonated functional side chains. Melonate, $[C_6N_7(NCN)_3]^{3-}$, a melem derivative with all amino groups

substituted for cyanamide groups, forms salts with alkali metals, alkaline earth metals and lanthanides.[19-22] Tricyanomelaminates, the triazine-based equivalent of melonates, are known of alkali metals, lanthanides as well as several late transition metals.[23-26] Furthermore, various non-metal tricyanomelaminates have been reported.[27] Triazine tricarboxylate salts were successfully synthesized with alkali metals as well as Fe^{2+} as counterions.[28-30]

While in anionic carbon nitride type compounds the charge is usually localized on a functional group, in cationic building blocks the ring system itself is protonated and carries the charge. Accordingly, these compounds do not require any modification to their molecular structure, but consist of the protonated version of melamine, melam or melem, respectively, and a counter anion. Melaminium salts, which find application as flame retardants and have thus been extensively studied, are by far the largest group in this. Most notably, halides, phosphates and pyrophosphates, borates, nitrates and various organic salts such as oxalates or benzoates have been reported.[31-38] Melemium salts are scarcer: known compounds comprise melemium sulfate, perchlorate, hydrogen sulfate, two different methylsulfates as well as a melemium perchlorate melem adduct.[39-42] Likewise, only a few melamium salts have been characterized. Syntheses of the chloride, sulfate, nitrate, perchlorate and phosphate salts have been postulated in 1977,[43] however, it took until 2007 until the first of these—melamium perchlorate—was structurally elucidated.[44] Two melamium containing adducts, melamium thiocyanate melamine and melamium chloride ammonium chloride, were synthesized through ampoule syntheses.[45] Only recently, we managed to extend the range of known melamium salts by two additional halide salts, melamium bromide and melamium iodide.[46] However, compared to melaminium salts the number of melamium salts is still small and little is known about their properties and reactivity.

We have now discovered another member of this substance class in the form of a melamium thiocyanate melam (1:1) adduct. We herein report on the synthesis and characterization of this compound and its unusual structural disorder.

3.2.2 Results and Discussion

Melamium thiocyanate melam was synthesized in analogy to melamium bromide, melamium iodide, and the melamium chloride ammonium chloride adduct in sealed glass ampoules from dicyandiamide and ammonium thiocyanate.[45,46] The molar ratio of the starting materials was initially chosen to be 3:1 equivalents in order to obtain a melamium thiocyanate salt of composition $C_6N_{11}H_{10}SCN$, however, elemental analyses rather suggest a composition of $C_6N_{11}H_{10}SCN{\cdot}C_6N_{11}H_9$ (see Table 3.2.1), corresponding to an adduct compound, in which only every second melam unit is protonated. The reaction would thus proceed according to Equation 3.2.1:

$$6\,C_2N_4H_4 + NH_4SCN \rightarrow C_6N_{11}H_{10}SCN \cdot C_6N_{11}H_9 + 3\,NH_3 \qquad (3.2.1)$$

Table 3.2.1 Elemental analyses of melamium thiocyanate melam.

	C [w%]	N [w%]	H [w%]	S [w%]
Found	29.21	59.25	3.51	6.02
Calc. ($C_6N_{11}H_{10}SCN{\cdot}C_6N_{11}H_9$)	29.49	60.84	3.62	6.06
Calc. ($C_6N_{11}H_{10}SCN$)	28.54	57.11	3.42	10.90

The disposition of excess ammonium thiocyanate could not be unambiguously determined. However, powder X-ray diffraction indicated that none of the obtained samples was phase pure, but minor contaminations of unidentified side phases were always present (see below). Furthermore, small amounts of sublimate were found at the upper end of the ampoule. FT-IR spectroscopy showed a band pattern that indicated melamine as the primary component. However, the presence of a minor characteristic band at ca. 2060 cm^{-1} suggests additional cyano groups. We thus conclude that at least part of the ammonium thiocyanate underwent decomposition and reformed during cooling of the ampoule. Considering IR band intensities, however, it appears highly unlikely that this can account for the complete amount of excess ammonium thiocyanate.

Melamium thiocyanate melam was obtained as a colorless to pale beige material that appeared polycrystalline in optical microscope images (see Figure 7.1.1). Single-crystals appeared only in a fraction of the samples and even in those, they were sparsely distributed throughout the polycrystalline material. Single-crystals took the shape of small, transparent needles. Most of those, unfortunately, were of subpar quality. We were, however, able to obtain a single-crystal X-ray diffraction data set from one specimen, from which the structure was elucidated.

The structure of melamium thiocyanate melam was solved in space group $P2_1/c$ with lattice parameters of a = 3.6041(11), b = 28.532(7), c = 10.937(4) Å, and β = 99.051(14)°. Crystallographic data are summarized in Table 3.2.2. Rather high R_σ and R_{int} values result from the poor quality of the crystal and low intensities due to the composition of the adduct, which, apart from sulfur, is exclusively comprised of light atoms. Hydrogen atoms could not be refined freely, but had to be assigned through geometrical calculations.

The asymmetric unit of melamium thiocyanate melam contains only a single melamium unit. It was thus not possible to differentiate between protonated melamium and non-protonated melam within the structure. Neither, however, could the structure be plausibly refined in any space group of lower symmetry that would allow for the discrimination between different types of melam(ium) units, nor did the thus obtained models show any noticeable differences in the structure of independent melam(ium) units or any significant preference for protonation of any molecule or site. In related carbon nitride type compounds, melam and melamium tend to structurally deviate from each other in the torsion angle between the triazine ring planes.[44-46] While non-protonated melam shows a tendency to exhibit moderate torsion, planarity is expected for melamium since this arrangement allows for the formation of an additional intramolecular hydrogen bond. In melamium thiocyanate melam, exclusively planar melam(ium) units are observed, indicating the protonated form. However,

Table 3.2.2 Crystallographic data for $C_6N_{11}H_{10}SCN{\cdot}C_6N_{11}H_9$, excluding unrefinable thiocyanate anions.

Empirical formula	"$C_6N_{11}H_{9.5}$"
Formula weight [g mol^{-1}]	235.72
Crystal system	Monoclinic
Space group	$P2_1/c$ (no. 7)
Radiation, λ [ppm]	Mo-K_α, 0.71073
a [Å]	3.6041(11)
b [Å]	28.532(7)
c [Å]	10.937(4)
β [°]	99.051(14)
V [Å^3]	1110.7(6)
Z	4
Density (calcd.) [g cm^{-1}]	1.335
Temperature [K]	100(2)
Absorption coefficient [mm^{-1}]	0.098
Diffraction range [°]	$8.180 \leq \theta \leq 23.669$
F(000)	468
Index range	$-3 \leq h \leq 4$
	$-32 \leq k \leq 32$
	$-12 \leq l \leq 12$
Absorption correction	multiscan
Parameters	308
No. of independent reflections	1583
No. of independent reflections ($I \leq 2\sigma$)	1131
R_σ, R_{int}	0.1449, 0.0869
GooF	2.147
R indices ($I \leq 2\sigma$)	$R1$ = 0.1325, $wR2$ = 0.3127
R indices (all data)	$R1$ = 0.1587, $wR2$ = 0.3291

should the entirety of these units represent melamium cations, electroneutrality would demand for further counter-anions, which are neither accounted for by the observed elemental composition, nor does the structure possess any additional cavities to accommodate such. The peculiar coexistence of the protonated and non-protonated forms has thus to be assumed even without structural evidence.

We herein propose that the indistinguishability of melamium and melam within the structure is caused by proton disorder. Statistical disorder of protonated and non-protonated melam molecules, which would result in a positional average structure to be observed, as well as proton hopping between protonation sites of different melam units, resulting in a temporal average, is conceivable. However, impedance spectroscopy (see Figure 7.1.2) of the compound showed conductivity behavior typical for insulating materials, thus no evidence for noticeable proton mobility that would support a proton

hopping mechanism could be found. We thus tend towards the assumption of statistically disordered protonation.

This behavior stands in contrast to other melamium adduct compounds,[45,47] for neither of which a disordered protonation pattern has been reported. We attribute this to the presence of species of different basicity within these adducts, resulting in preferred protonation of melamium. To our best knowledge, no other adduct of melam and melamium is known to literature. Melamium thiocyanate melam might be compared to melemium melem perchlorate,[40] or melaminium thiocyanate melamine,[45] both of which, however, possesses multiple molecules per asymmetric unit that can be distinguished, so that localization of the proton was possible. In the following, all carbon nitride type molecules in the structure of melamium thiocyanate melam are assumed to be melamium for purpose of discussion and protonating hydrogen atom positions as only partially occupied.

The crystallographic structure of melamium thiocyanate melam is comprised of corrugated layers stacked along *a* formed by melamium units, which build up a hydrogen bridged network with elongated cavities within (see Figure 3.2.2). Groups of six melamium units surround each cavity and each melamium unit participates in three such groups. This allows for the formation of two different hydrogen bonding motifs: one, in which two melamium molecules are facing “end-on-end” with their outer sides oriented towards each other, resulting in two hydrogen bridges being formed; and one, in which the molecules are facing “side-on-end“, with the outer side of one molecule oriented towards the backbone of the other. This allows for the formation of three hydrogen bridges. A very similar arrangement can be found in melamium iodide, in which the same elongated cavities as well as hydrogen bonding motifs occur.[46] However, while the layers in melamium thiocyanate melam are corrugated, melamium iodide features plane layers.

Triazine rings as obtained from our model deviate only slightly from ideal triazine symmetry. C–N bond lengths within the rings range from 1.305 to 1.374 Å and are thus, although there is a certain spread, within the range expected for triazines. A similar spread can be found for C–N bond lengths towards the terminal amino groups, which range from 1.315 to 1.361 Å and are thus very comparable to ring bonds. In contrast, all angles within the triazine rings lie within a narrow range as well as within expectancy. C–N–C angles, that typically tend to be smaller than 120° in triazines, range from 113.3 to 115.3°. Likewise, the corresponding N–C–N angles show values between 125.0 and 127.0°. Imide bridges show bond lengths somewhat longer than found within the rings, ranging from 1.358 to 1.416 Å, and an angle of 130.3°. Again, these larger lengths and angles are consistent with expectancy for melamium compounds. A complete list of bond length and angles can be found in Tables 7.1.1 and 7.1.2; site coordinates are given in Table 7.1.3.

Despite the mediocre quality of the measured crystal, as indicated by rather large intrinsic *R* values, structural parameters as well as errors appear to be very reasonable.

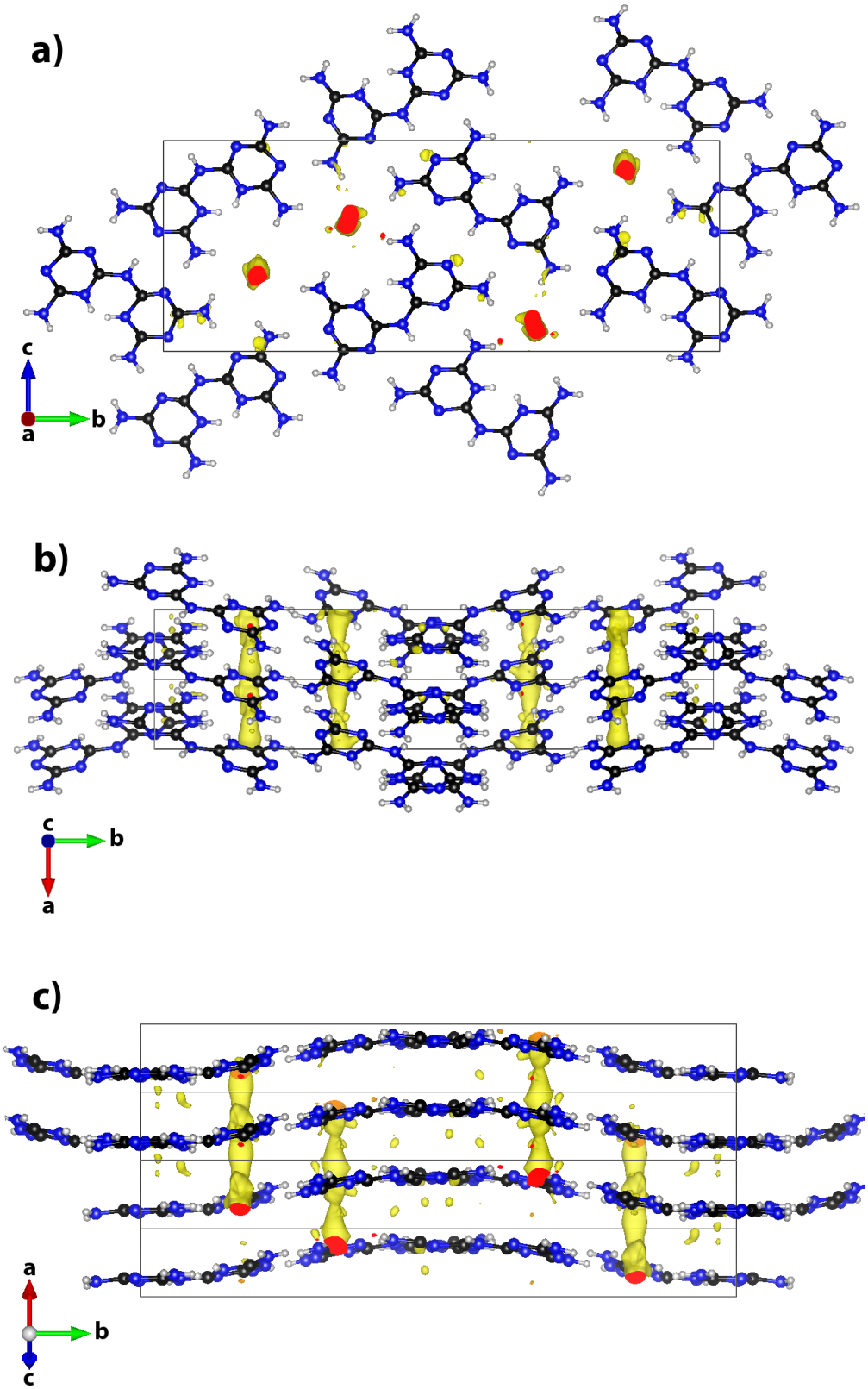

Figure 3.2.2 Crystallographic structure of melamium thiocyanate melam. C atoms in black, N atoms in blue, and H atoms in light gray. Electron density rendered at an isosurface level of 1.6 in yellow resp. red. (a) viewing directing along *a*; (b) viewing direction along *c*; (c) viewing direction along [5 0 27], perpendicular to the corrugated layers.

Structure refinement was impeded to a certain degree by disorder of the thiocyanate anions. In analogy to melamium iodide the anions are expected to be located within the cavities of the structure. However, it proved impossible to assign any fixed position to the atoms of SCN^- units. Electron density plots show more or less homogeneous, continuous strands of electron density located in the expected anion positions and spanning through the layers of melamium network with no apparent maxima (see Figure 2b–c). We interpret these continuous strands of electron density as an average over all possible atom sites for the thiocyanate anions. Additionally, it has to be mentioned that according to the sum formula obtained from elemental analysis, each strand could only contain one thiocyanate ion per two unit cells. For an ordered variant of the structure, a larger unit cell with the lattice parameter *a* doubled has to be assumed. It is expected that this disorder phenomenon correlates with the disorder of melamium protonation that has been discussed above, i.e. that the location of protons depends on the respective location of thiocyanate anions.

As a consequence of the impossibility to locate the anion atoms, we artificially removed the unassigned electron density from the cavities using a SQUEEZE algorithm implemented in the program package PLATON.[48,49] This allowed for the independent refinement of the melamium network. The obtained structure is shown in Figure 7.1.3. However, with sulfur as the heaviest atom species in the structure missing and ignoring interactions between the thiocyanate anions and the rest of the structure, ramifications on the refinement are still expected.

Since no unambiguous verification of thiocyanate as the anion was possible from structure elucidation alone, we performed qualitative chemical analysis. Thiocyanate was brought into solution by stirring melamium thiocyanate melam in an aqueous ammonia solution and removing the undissolved residue via filtration. A colorless solution was obtained, to which a few drops of $FeCl_3$ solution were added. The solution changed color to deep red, indicating the formation of $[Fe(SCN)(H_2O)_5]^{2+}$, thus proving the presence of thiocyanate. However, quantification of $[Fe(SCN)(H_2O)_5]^{2+}$ via UV/Vis spectroscopy showed that elution of thiocyanate from the compound is incomplete. The observed amount of thiocyanate equates to only 5.88 % of sample weight, when 11.0 % would have been expected from the supposed sum formula. Details on UV/Vis measurements are found in the chapter 7.1 in the appendix.

Further characterization of melamium thiocyanate melam was conducted through FT-IR spectroscopy. The IR spectrum (Figure 3.2.3) clearly shows a band with a maximum at 2056 cm^{-1} that can be identified as belonging to a δ(C≡N) vibration. While such bands are not exclusive to thiocyanate, comparison with related compounds, in which no C≡N groups are formed under comparable synthesis conditions, makes it highly unlikely for this band to be attributed to any other structural feature than the anion. Furthermore, the IR spectrum contains a medium strong band at 1254 cm^{-1}, which we attribute to group stretching vibrations of the imide bridge of melamium units, as well as an intense band at 801 cm^{-1} characteristic for the ring out-of-plane breathing mode of triazine or heptazine rings. Both of these features are expected for melamium and well known from related compounds.[44-46]

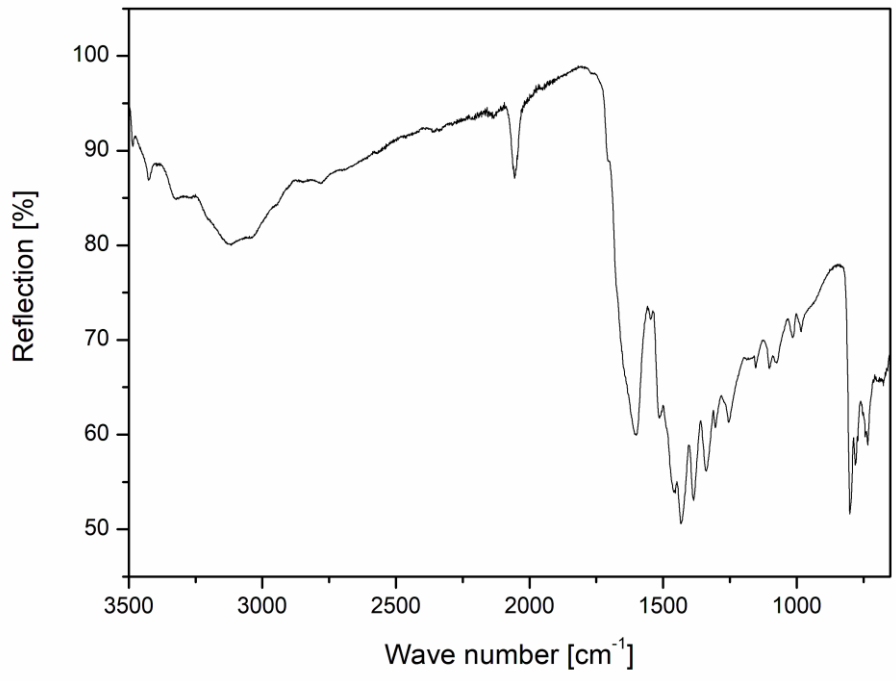

Figure 3.2.3 FT-IR spectrum of melamium thiocyanate melam.

Solid-state MAS NMR measurements were performed for ^{1}H, ^{13}C, and ^{15}N. Two resonances were obtained for ^{1}H, a narrow signal at δ = 4.56 ppm, which we attribute to terminal amino groups and a rather broad one with a maximum at δ = 9.25 ppm interpreted as bridging imide groups (see Figure 7.1.4). No unambiguous signal was found for the protonation of the triazine ring of melamium, however, the profile form of the broad signal shows a weak shoulder towards the low field, indicating an acidic proton. We presume that this shoulder results from protonation of melam to melamium. The ^{13}C spectrum of melamium thiocyanate melam shows a rather poor signal-to-noise ratio, making it difficult to discern several signals (see Figure 7.1.5). The most intense signal shows two peaks at 165.79 and 163.72 ppm. Three weaker signals, that are not unambiguously discernible, are found between δ = 160 and 155 ppm. These two groups of signals are well in line with expectations from comparison with other melamium salts.[45] We attribute the multitude of signals to the co-existence of differently protonated molecules in the structure, as different protonation patterns would influence the chemical shifts. No ^{13}C resonance was found in the range, in which thiocyanate C atoms would be expected. However, the measurements used a cross polarization pulse sequence, so low intensities for C atoms without H atoms in their immediate proximity are expected. The low content of thiocyanate in the compound in combination with the poor signal-to-noise ratio might thus lead to an undiscernible signal. In the ^{15}N spectrum, only a very broad signal with a maximum at −292.25 ppm (referenced to nitromethane) indicating terminal amino N atoms and a very small signal at −249.44 ppm that might result from imide N atoms could be discerned (see Figure 7.1.6). Both of these values are well in line with expectations for the respective functional group. However, the sample showed a long relaxation time, resulting in low signal intensities, especially for those atoms not amplified by cross-polarization.

Thus, no signals could be obtained for tertiary melamium ring N atoms and thiocyanate N atoms. Longer measurement times or ^{15}N enrichment of the samples would be required to obtain more significant spectra and NMR spectroscopic evidence for the assumed sample composition.

Phase analysis of bulk powder samples was performed by Rietveld refinement. Results are summarized in Table 7.1.2. Since an incomplete model without inclusion of any thiocyanate anions had to be used, the refinement was expected to show some significant discrepancies between measured intensities and the calculated model. As can be seen in Figure 3.2.4, a number of reflections could not be fitted properly. This applies primarily to three intense reflections at 18.6°, 18.9°, and 24.9°. All of these, however, correspond to Bragg reflection positions expected for melamium thiocyanate melam. We thus attribute these missing intensities to the incompleteness of the model.

Determination of thiocyanate atom positions from difference Fourier analysis of the Rietveld plot was attempted, however, mapping of residual electron density showed homogeneous, extended columns very similar to those observed in single-crystal XRD measurements (Figure 7.1.8).

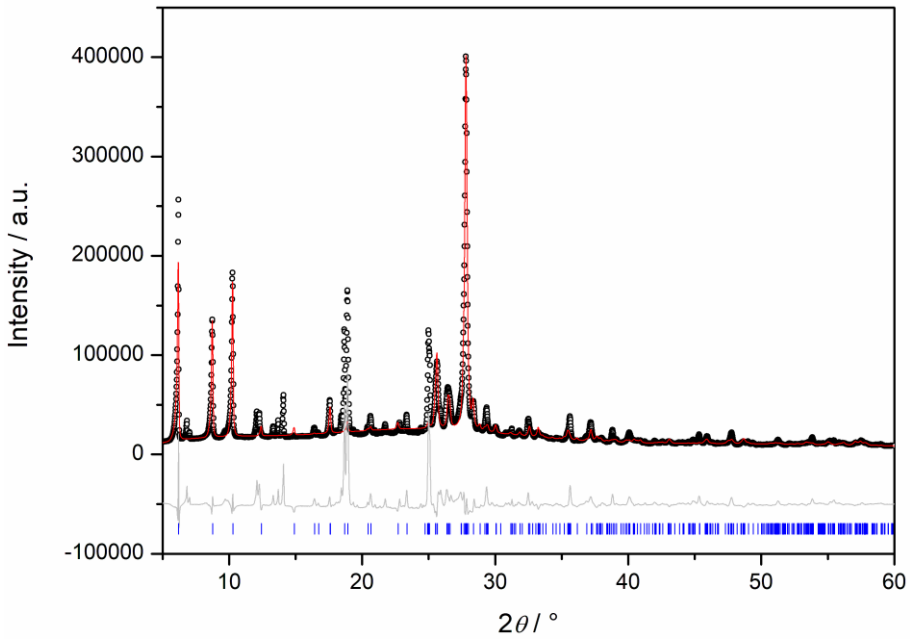

Figure 3.2.4 Rietveld plot of melamium thiocyanate melam. Measured data points are depicted as black circles, the calculated model is depicted in red, the difference plot $Y_{obs}–Y_{calc}$ in gray. Blue tick marks indicate theoretical Bragg reflection positions.

Likewise, attempts to refine atoms to these positions resulted in unreasonably short interatomic distances within thiocyanate ions and accounted for the observed electron density only poorly. Powder XRD thus confirms the observations from single-crystal measurements, but yields no further insights into the structure of the compound.

Some minor reflections, with the most prominent ones at 12.2° and 14.1°, could not be explained by the model of melamium thiocyanate melam, lacking not only intensity, but were also found at diffraction angles, at which no Bragg reflection is expected. However, we were unable to assign these

signals to any known carbon nitride type compound or starting materials species. For this reason, we were also unable to determine the percentage of side phase in the sample. Rather low intensities for the respective reflections, however, suggest minor phase content. No phase pure sample of melamium thiocyanate melam was obtained in any preparative attempt.

Room temperature lattice parameters for melamium thiocyanate melam were refined to a = 3.6401(6), b = 28.459(9), c = 10.903(3) Å, and β = 98.616(15)°. The by far greatest percentage increase is noted for a, which elongates by 1.0 % compared to the parameters found for single-crystal measurements at 100 K. This correlates to an extended spacing between the stacked layers with increasing temperature, while only a moderate expansion along the sheets is noted. This thermal behavior of lattice constants is well in line with observations made for related melamium compounds.[46]

Thermal behavior of the compound was further investigated by coupled differential scanning calorimetry and thermogravimetry. Upon heating to 1073 K two thermally induced processes could be observed. Starting around 673 K, an endothermic process takes place that results in a mass loss of about 21 %. In analogy to related carbon nitride type compounds, we attribute this signal to a thermal condensation reaction of melam, resulting in polymeric melon. For this process a theoretical mass loss of 24 % is expected, which diverges slightly from the observed value. However, as can be seen in Figure 3.2.5, the mass loss continues after the initial endothermic process. We interpret this as the condensation reaction being kinetically hindered and proceeding further with time. This is in agreement with standard synthesis procedures for melon, which is known to require heating to these temperatures for several hours until no remaining precursor phases are present.[50]

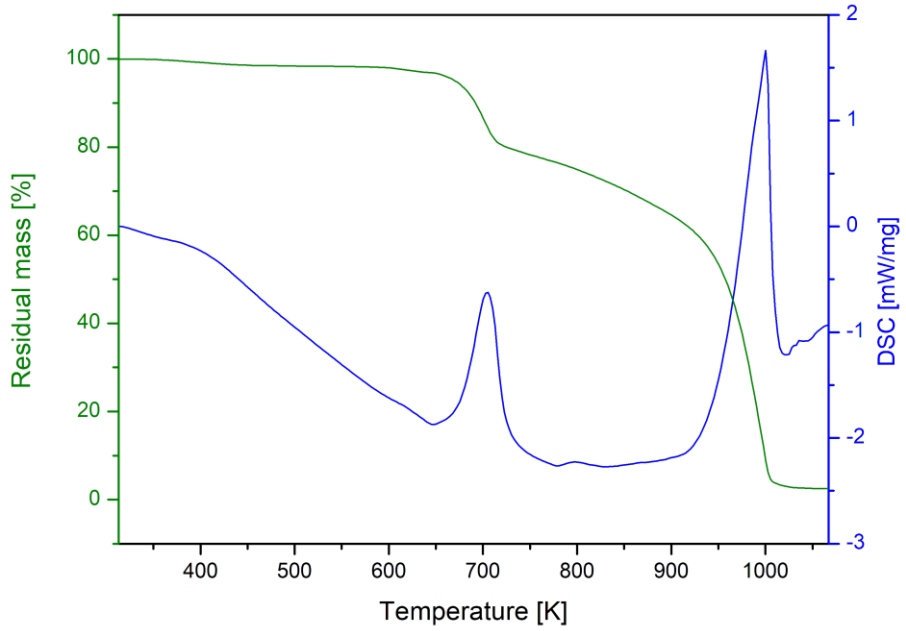

Figure 3.2.5 Thermal behavior of melamium thiocyanate melam. Thermogravimetry measurement curve in green, differential scanning calorimetry measurement curve in blue.

A second endothermic process is observable starting at a temperature of about 935 K. This process results in a massive mass loss of over 75 % and a residual mass of only 2.5 %. This process is identified as thermal decomposition of melon, which is known to take place at these temperatures. The residue is a black, carbonaceous compound consisting mainly of graphite. This behavior is well in line with expectations based on the behavior of related carbon nitride type compounds. No further thermally induced reaction processes could be detected. Side phases, whose presence was proven by powder X-ray diffraction, appear to show a thermal behavior similar to the primary compound and undergo the same condensation reaction towards melon. Thiocyanate is expected to decompose during the thermal condensation of melamium thiocyanate melam to melon and form gaseous side products.

3.2.3 Conclusions

The adduct compound melamium thiocyanate melam, $C_6N_{11}H_{10}SCN{\cdot}C_6N_{11}H_9$, was synthesized in sealed ampoules from ammonium thiocyanate and carbon nitride precursor dicyandiamide. The composition of the compound was determined from combustion analysis. Co-presence of melam and melamium was established depending on the amount of thiocyanate counterions that cannot account for protonation of every melamium unit; however, no crystallographic distinction of protonated and non-protonated building blocks was possible. The presence of thiocyanate was proven experimentally by formation of $[Fe(SCN)(H_2O)_5]^{2+}$ with Fe^{3+}. Single-crystals of melamium thiocyanate melam were found distributed throughout the otherwise polycrystalline sample and the structure elucidated from single-crystal X-ray diffraction data. Melamium thiocyanate melam forms a cation network very similar to the one observed for melamium iodide.[46] Continuous pores along *a* pass through stacked corrugated layers of network structure in which each cavity is surrounded by six melamium units and each melamium unit is adjacent to three such cavities. Each cavity is supposed to incorporate two thiocyanate anions; however, it proved impossible to assign fixed sites to the respective atoms. Instead, homogeneous und continuous columns of electron density were observed. We assign this to structural disorder of the anions, which are able to occupy any space in these columns. The melamium partial structure was refined independently from this unassigned electron density by applying a SQUEEZE algorithm.

Rietveld refinement was performed on a bulk sample applying the model obtained from single-crystal X-ray diffraction. Due to the incompleteness of the model, theoretical intensities diverge from observed ones. Some reflections were determined to belong to a side phase. However, identification of this phase was not possible. Further characterization of melamium thiocyanate melam was conducted by spectroscopic means. FT-IR spectroscopy showed a band pattern very similar to other melamium compounds, including all expected characteristic bands of functional groups. Furthermore, a distinct band of the C≡N group of thiocyanate was observed. Solid-state MAS-NMR spectroscopy was conducted for ^{1}H, ^{13}C and ^{15}N. Spectra verified the presence of protonated melamium units. No

signals of thiocyanate C or N atoms were observed, however. Thermal analysis shows thermal stability for the compound up to a temperature of 673 K, at which condensation towards melon takes place. The presence of thiocyanate appears to have no significant influence on this reaction behavior, which would be expected analogously for pure melam.

3.2.4 Experimental Section

Preparation of Melamium Thiocyanate Melam: Ammonium thiocyanate (46.4 mg, 0.61 mmol, 99 %, Grüssing GmbH) and dicyandiamide (153.6 mg, 1.83 mmol, 3 equiv., 99.5 %, Acros Organics) were ground together thoroughly, sealed in a glass ampoule (inner diameter 12 mm, wall thickness 1.5 mm) at a length of 130 mm and placed in a tube furnace. The ampoule was heated with 6 $K \cdot min^{-1}$ to 623 K, held at this temperature for 48 h and then cooled down to room temperature at 0.1 $K \cdot min^{-1}$. Melamium thiocyanate melam was obtained as a colorless to pale beige polycrystalline material. Transparent, colorless single-crystals of melamium thiocyanate melam were found scattered among the polycrystalline sample.

Thiocyanate Detection: Thiocyanate was detected as $[Fe(SCN)(H_2O)_5]^{2+}$. Melamium thiocyanate melam (50.0 mg) was suspended in 20 mL of aqueous ammonia solution (25 %) und stirred for 2 h to deprotonate melamium and flush out thiocyanate. Melam was removed from the suspension by filtration and the filtrate heated to boiling to strip the solution of ammonia. The obtained solution was clear and colorless. An aliquot of about 2 mL was taken and approximately the same amount of concentrated $FeCl_3$ solution added. Appearance of a deep red color indicated the presence of $[Fe(SCN)(H_2O)_5]^{2+}$.

General Techniques: FT-IR spectra were recorded with a Perkin–Elmer BX II FT-IR-ATR (attenuated total reflection) spectrometer equipped with a DuraSampler Diamond ATR unit at room temperature. UV/Vis spectroscopic measurements were performed with a Jasco V-650 spectrophotometer. CHNS elemental analyses were conducted by combustion analysis on a Vario EL elemental analyzer (Elementar Analysensysteme GmbH) at the microanalytic laboratory of the Department of Chemistry, LMU Munich. Electro-chemical impedance spectroscopy was performed with an Ivium CompactStat.h (24 bit instrument) in a two-electrode setup with the TSC battery cell and temperature control from rhd instruments at ambient conditions. The applied root mean square (rms) alternating current voltage was 100 mV. The analysis of the impedance spectrum was carried out with the RelaxIS3 software from rhd instruments. Before measuring, the samples were ground thoroughly and compacted to a pellet of about 0.3 mm thickness and 8 mm diameter by uniaxial cold pressing (800 MPa). The pellets were sandwiched between stainless steel electrodes. Additional measurements utilizing Nafion117 as a proton selective membrane were conducted but yielded no further insights since neither protons nor anionic species exhibited any significant conductivity. Solid-state MAS NMR spectra were recorded with a Bruker Avance III-500 spectrometer with an external magnetic field of 11.74 T. Measurements

were performed at room temperature. Samples were measured at spinning frequencies of 10 kHz in 4 mm double resonance probe heads. ^{13}C and ^{15}N spectra were recorded applying ^{1}H decoupling. Cross polarization (CP) pulse sequences were applied for ^{13}C and ^{15}N measurements to amplify signal intensities. All nuclei were referenced to 0.1 % TMS in $CDCl_3$. Differential scanning calorimetry and thermogravimetry were performed with a Netzsch STA F5 449fA Jupiter simultaneous thermoanalyzer. Samples were prepared in corundum crucibles and heated under continuous argon gas flow with a flow rate of 50 mL·min^{-1}.

Single-Crystal X-ray Diffraction: For single-crystal X-ray diffraction, a Bruker D8 Venture diffractometer (Bruker, Billerica MA, USA) was used. Measurements were performed at 100 K applying Mo-K_α radiation (λ = 0.71073 Å). Absorption correction, raw data integration and structure solution were performed using APEX 3.[51] Structure refinement used Shelxl-97.[52,53] Visualization of single-crystal structures was performed with VESTA 3.[54]

Crystallographic data (excluding structure factors) for the structure in this paper have been deposited with the Cambridge Crystallographic Data Centre, CCDC, 12 Union Road, Cambridge CB21EZ, UK. Copies of the data can be obtained free of charge on quoting the depository number CCDC-1898050 (Fax: +44-1223-336-033; E-Mail: deposit@ccdc.cam.ac.uk, http://www.ccdc.cam.ac.uk).

Powder X-ray Diffraction: Powder X-ray diffraction measurements were performed with a Stoe Stadi-P powder diffractometer (Stoe, Darmstadt, Germany) equipped with a Mythen 1 K silicon strip detector (Dectris, Baden, Switzerland) in Debye–Scherrer setup. Monochromated Cu-$K_{\alpha1}$ radiation (λ = 1.54056 Å) was applied. Samples were prepared in sealed glass capillaries (inner diameter 0.5 mm, wall thickness 0.01 mm). For data processing Stoe WinXPOW Vers. 3.06 was used.[55] Rietveld refinement was performed using TOPAS-Academic V4.1.[56]

Acknowledgements

The authors wish to express their gratitude to Dr. Peter Mayer for single-crystal X-ray diffraction measurements, Anna-Katharina Hatz for electro-chemical impedance spectroscopy measurements and to Sascha Harm (all at Department of Chemistry, LMU Munich) for thermoanalytic measurements. Financial support granted by the Fonds der Chemischen Industrie (FCI) and the Deutsche Forschungsgemeinschaft (DFG) is gratefully acknowledged.

3.2.5 References

[1] J. Liebig, "Ueber einige Stickstoff-Verbindungen", *Ann. Pharm.* **1834**, *10*, 1-47.

[2] L. Gmelin, "Ueber einige Verbindungen des Melon's", *Ann. Pharm.* **1835**, *15*, 252-258.

[3] J. Liebig, "Ueber einige Stickstoffverbindungen", *Ann. Phys.* **1835**, *110*, 570-612.

[4] W. H. Binder, M. Dunky, "Melamine–Formaldehyde Resins", in *Encyclopedia of Polymer Science and Technology*, 4th ed. (Ed.: H. F. Mark), Wiley, New York, **2004**.

[5] W. H. Binder, M. Dunky, S. Jahromi, "Melamine Resins", in *Kirk-Othmer Encyclopedia of Chemical Technology*, Wiley, New York, **2005**.

[6] H. Diem, G. Matthias, "Amino Resins", in *Ullmann's Encyclopedia of Industrial Chemistry, Vol. A2*, 5 ed. (Ed.: W. Gerhartz), VCH, Weinheim, **1985**, pp. 115-141.

[7] Y. Feng, J. Yao, "Design of Melamine Sponge-Based Three-Dimensional Porous Materials toward Applications", *Ind. Eng. Chem. Res.* **2018**, *57*, 7322-7330.

[8] E. D. Weil, S. V. Levchik, "Flame Retardants in Commercial Use or Development for Textiles", *J. Fire Sci.* **2009**, *26*, 243-281.

[9] E. D. Weil, "Fire-Protective and Flame-Retardant Coatings – A State-of-the-Art Review", *J. Fire Sci.* **2011**, *29*, 259-296.

[10] M. Klatt, "Nitrogen-Based Flame Retardants", in *Non-Halogenated Flame Retardant Handbook* (Eds.: A. B. Morgan, C. A. Wilkie), Scrivener Publishing, Beverly, **2014**, pp. 143-168.

[11] W. Iqbal, B. Yang, X. Zhao, M. Rauf, M. Waqas, Y. Gong, J. Zhang, Y. Mao, "Controllable synthesis of graphitic carbon nitride nanomaterials for solar energy conversion and environmental remediation: the road travelled and the way forward", *Catal. Sci. Technol.* **2018**, *8*, 4576-4599.

[12] Z. Zhou, Y. Zhang, Y. Shen, S. Liu, Y. Zhang, "Molecular engineering of polymeric carbon nitride: advancing applications from photocatalysis to biosensing and more", *Chem. Soc. Rev.* **2018**, *47*, 2298-2321.

[13] A. Sudhaik, P. Raizada, P. Shandilya, D.-Y. Jeong, J.-H. Lim, P. Singh, "Review on fabrication of graphitic carbon nitride based efficient nanocomposites for photodegradation of aqueous phase organic pollutants", *J. Ind. Eng. Chem.* **2018**, *67*, 28-51.

[14] J. Fu, J. Yu, C. Jiang, B. Cheng, "g-C_3N_4-Based Heterostructured Photocatalysts", *Adv. Energy Mater.* **2018**, *8*, 1701503.

[15] F. Goettmann, A. Fischer, M. Antonietti, A. Thomas, "Metal-free catalysis of sustainable Friedel-Crafts reactions: direct activation of benzene by carbon nitrides to avoid the use of metal chlorides and halogenated compounds", *Chem. Commun.* **2006**, 4530-4532.

[16] F. Goettmann, A. Fischer, M. Antonietti, A. Thomas, "Mesoporous graphitic carbon nitride as a versatile, metal-free catalyst for the cyclisation of functional nitriles and alkynes", *New J. Chem.* **2007**, *31*, 1455-1460.

[17] F. Goettmann, A. Thomas, M. Antonietti, "Metal-Free Activation of CO_2 by Mesoporous Graphitic Carbon Nitride", *Angew. Chem.* **2007**, *119*, 2773-2776; *Angew. Chem. Int. Ed.* **2007**, *46*, 2717-2720.

[18] X. Wang, K. Maeda, A. Thomas, K. Takanabe, G. Xin, J. M. Carlsson, K. Domen, M. Antonietti, "A metal-free polymeric photocatalyst for hydrogen production from water under visible light", *Nat. Mater.* **2009**, *8*, 76-80.

[19] S. J. Makowski, D. Gunzelmann, J. Senker, W. Schnick, "Protonated Melonate $Ca[HC_6N_7(NCN)_3]\cdot 7H_2O$ – Synthesis, Crystal Structure, and Thermal Properties ", *Z. Anorg. Allg. Chem.* **2009**, *635*, 2434-2439.

[20] S. J. Makowski, W. Schnick, "$Rb_3[C_6N_7(NCN)_3]\cdot 3H_2O$ and $Cs_3[C_6N_7(NCN)_3]\cdot 3H_2O$ – Synthesis, Crystal Structure and Thermal Behavior of Two Novel Alkali Melonates", *Z. Anorg. Allg. Chem.* **2009**, *635*, 2197-2202.

[21] S. J. Makowski, A. Schwarze, P. J. Schmidt, W. Schnick, "Rare-Earth Melonates $LnC_6N_7(NCN)_3\cdot xH_2O$ (Ln = La, Ce, Pr, Nd, Sm, Eu, Tb; x = 8–12): Synthesis, Crystal Structures, Thermal Behavior, and Photoluminescence Properties of Heptazine Salts with Trivalent Cations", *Eur. J. Inorg. Chem.* **2012**, 1832-1839.

[22] A. Sattler, W. Schnick, "On the Formation and Decomposition of the Melonate Ion in Cyanate and Thiocyanate Melts and the Crystal Structure of Potassium Melonate, $K_3[C_6N_7(NCN)_3]$", *Eur. J. Inorg. Chem.* **2009**, 4972-4981.

[23] B. Jürgens, W. Milius, P. Morys, W. Schnick, "Trimerisierung von Dicyanamid-Ionen $C_2N_3^-$ im Festkörper – Synthesen, Kristallstrukturen und Eigenschaften von $NaCs_2(C_2N_3)_3$ und $Na_3C_6N_9\cdot 3H_2O$", *Z. Anorg. Allg. Chem.* **1998**, *624*, 91-97.

[24] E. Irran, B. Jürgens, W. Schnick, "Trimerization of Alkali Dicyanamides $M[N(CN)_2]$ and Formation of Tricyanomelaminates $M_3[C_6N_9]$ (M=K, Rb) in the Melt: Crystal Structure Determination of Three Polymorphs of $K[N(CN)_2]$, Two of $Rb[N(CN)_2]$, and One of $K_3[C_6N_9]$ and $Rb_3[C_6N_9]$ from X-ray Powder Diffractometry", *Chem. Eur. J.* **2001**, *7*, 5372-5381.

[25] A. Nag, B. V. Lotsch, J. Schmedt auf der Günne, O. Oeckler, P. J. Schmidt, W. Schnick, "Rare-Earth Tricyanomelaminates $[NH_4]Ln[HC_6N_9]_2[H_2O]_7\cdot H_2O$ (Ln=La, Ce, Pr, Nd, Sm, Eu, Gd, Tb, Dy): Structural Investigation, Solid-State NMR Spectroscopy, and Photoluminescence", *Chem. Eur. J.* **2007**, *13*, 3512-3524.

[26] B. F. Abrahams, S. J. Egan, B. F. Hoskins, R. Robson, "Three-dimensional coordination networks from tricyanomelamine and Co, Ni, Cu and Cd", *Chem. Commun.* **1996**, 1099-1100.

[27] B. V. Lotsch, W. Schnick, "From Triazines to Heptazines: Novel Nonmetal Tricyanomelaminates as Precursors for Graphitic Carbon Nitride Materials", *Chem. Mater.* **2006**, *18*, 1891-1900.

[28] S. J. Makowski, M. Hörmannsdorfer, W. Schnick, "$K_3[C_3N_3(COO)_3]\cdot 2H_2O$ – Crystal Structure of a New Alkali Derivative of the Multidentate Ligand Triazine Tricarboxylate", *Z. Anorg. Allg. Chem.* **2010**, *636*, 2584-2588.

[29] S. J. Makowski, E. Calta, W. Schnick, "Novel Alkali Triazine Tricarboxylates $Li_3[C_3N_3(CO_2)_3]\cdot 4H_2O$, $Rb_3[C_3N_3(CO_2)_3]\cdot 2H_2O$ and $Cs_3[C_3N_3(CO_2)_3]\cdot 2H_2O$ – Synthesis, Crystal Structure and Thermal Behavior", *Z. Anorg. Allg. Chem.* **2011**, *637*, 2142-2147.

[30] J.-R. Galán-Mascarós, J.-M. Clemente-Juan, K. R. Dunbar, "Synthesis, structure and magnetic properties of the one-dimensional chain compound {K[Fe(1,3,5-triazine-2,4,6-tricarboxylate)(H_2O)$_2$]·2H_2O}$_\infty$", *J. Chem. Soc., Dalton Trans.* **2002**, 2710-2713.

[31] Y. L. Tan, L. Sun, S. C. Shao, J. P. Fu, Z. H. Peng, "Synthesis and Characterization of Melamine Halogen Acid Salts and its Application as Flame Retardant", *Adv. Mater. Res.* **2013**, *750-752*, 1087-1090.

[32] B. Schartel, A. Weiß, F. Mohr, M. Kleemeier, A. Hartwig, U. Braun, "Flame retarded epoxy resins by adding layered silicate in combination with the conventional protection-layer-building flame retardants melamine borate and ammonium polyphosphate", *J. Appl. Polym. Sci.* **2010**, *118*, 1134-1143.

[33] M. Scoponi, E. Polo, F. Pradella, V. Bertolasi, V. Carassiti, P. Goberti, "Crystal structure and spectroscopic analysis of melamine hydrobromide. Evidence for iso-melamine cations and charge–transfer complexes in the solid state", *J. Chem. Soc., Perkin Trans. 2* **1992**, 1127-1132.

[34] H. Yang, L. Song, Q. Tai, X. Wang, B. Yu, Y. Yuan, Y. Hu, R. K. K. Yuen, "Comparative study on the flame retarded efficiency of melamine phosphate, melamine phosphite and melamine hypophosphite on poly(butylene succinate) composites", *Polym. Degrad. Stab.* **2014**, *105*, 248-256.

[35] V. Brodski, R. Peschar, H. Schenk, A. Brinkmann, E. R. H. van Eck, A. P. M. Kentgens, B. Coussens, A. Braam, "Structure of Melaminium Dihydrogenpyrophosphate and Its Formation from Melaminium Dihydrogenphosphate Studied with Powder Diffraction Data, Solid-State NMR, and Theoretical Calculations", *J. Phys. Chem. B* **2004**, *108*, 15069-15076.

[36] S. I. Volfkovič, W. W. Feldmann, M. L. Kozmina, "Über Kondensierte Phosphate des Melamins", *Z. Anorg. Allg. Chem.* **1979**, *457*, 20-30.

[37] L. Vella-Zarb, D. Braga, A. Guy Orpen, U. Baisch, "The influence of hydrogen bonding on the planar arrangement of melamine in crystal structures of its solvates, cocrystals and salts", *CrystEngComm* **2014**, *16*, 8147-8159.

[38] A. I. Finkelshtein, T. N. Roginskaya, L. A. Simkina, "Spectra of melamine salts and complexes", *Izv. Vyssh. Uchebn. Zaved., Khim. Khim. Tekhnol.* **1994**, *37*, 51-56.

[39] A. Sattler, L. Seyfarth, J. Senker, W. Schnick, "Synthesen, Kristallstrukturen und spektroskopische Eigenschaften des Melem-Adduktes $C_6N_7(NH_2)_3 \cdot H_3PO_4$ sowie der Melemium-Salze $(H_2C_6N_7(NH_2)_3)SO_4 \cdot 2\ H_2O$ und $(HC_6N_7(NH_2)_3)ClO_4 \cdot H_2O$", *Z. Anorg. Allg. Chem.* **2005**, *631*, 2545-2554.

[40] A. Sattler, W. Schnick, "Preparation and Structure of Melemium Melem Perchlorate $HC_6N_7(NH_2)_3ClO_4 \cdot C_6N_7(NH_2)_3$", *Z. Anorg. Allg. Chem.* **2008**, *634*, 457-460.

[41] A. Sattler, W. Schnick, "Melemium Hydrogensulfate $H_3C_6N_7(NH_2)_3(HSO_4)_3$ – the First Triple Protonation of Melem", *Z. Anorg. Allg. Chem.* **2010**, *636*, 2589-2594.

[42] A. Sattler, S. Schönberger, W. Schnick, "Melemium Methylsulfonates $HC_6N_7(NH_2)_3H_2C_6N_7(NH_2)_3(SO_3Me)_3 \cdot H_2O$ and $H_2C_6N_7(NH_2)_3(SO_3Me)_2 \cdot H_2O$ ", *Z. Anorg. Allg. Chem.* **2010**, *636*, 476-482.

[43] N. K. Gavrilova, V. A. Gal'perin, A. I. Finkel'shtein, A. G. Koryakin, "Synthesis of Melam and its Salts with Mineral Acids", *Zh. Org. Khim.* **1977**, *13*, 669-670.

[44] B. V. Lotsch, W. Schnick, "New Light on an Old Story: Formation of Melam during Thermal Condensation of Melamine", *Chem. Eur. J.* **2007**, *13*, 4956-4968.

[45] N. E. Braml, A. Sattler, W. Schnick, "Formation of Melamium Adducts by Pyrolysis of Thiourea or Melamine/NH_4Cl Mixtures", *Chem. Eur. J.* **2012**, *18*, 1811-1819.

[46] F. K. Kessler, T. J. Koller, W. Schnick, "Synthesis and Structure of Melamium Bromide $C_6N_{11}H_{10}Br$ and Melamium Iodide $C_6N_{11}H_{10}I$", *Z. Anorg. Allg. Chem.* **2018**, *644*, 186-192.

[47] E. Wirnhier, M. B. Mesch, J. Senker, W. Schnick, "Formation and Characterization of Melam, Melam Hydrate, and a Melam–Melem Adduct", *Chem. Eur. J.* **2013**, *19*, 2041-2049.

[48] A. L. Spek, *PLATON A Multipurpose Crystallographic Tool,* V. 31017, Utrecht, **1980-2017.**

[49] A. L. Spek, "Structure validation in chemical crystallography", *Acta Crystallogr., Sect. D: Biol. Crystallogr.* **2009**, *65*, 148-155.

[50] B. V. Lotsch, M. Döblinger, J. Sehnert, L. Seyfarth, J. Senker, O. Oeckler, W. Schnick, "Unmasking Melon by a Complementary Approach Employing Electron Diffraction, Solid-State NMR Spectroscopy, and Theoretical Calculations—Structural Characterization of a Carbon Nitride Polymer", *Chem. Eur. J.* **2007**, *13*, 4969-4980.

[51] *APEX 3,* Bruker AXS Inc., Madison WI, USA, **2016.**

[52] G. M. Sheldrick, *SHELX-97, Program Package for the Solution and Refinement of Crystal Structures, Release 97-2,* Universität Göttingen, **1997.**

[53] G. M. Sheldrick, *Acta Crystallogr., Sect. A: Found. Adv.* **2008**, *64*, 112-122.

[54] K. Momma, F. Izumi, *VESTA,* 3.4.4, **2018.**

[55] *WinXPOW, v3.06,* STOE & Cie GmbH, Darmstadt, **2011.**

[56] A. A. Coelho, *TOPAS-Academic V4.1,* Coelho Software, Brisbane, **2007.**

3.3 Ammelinium Sulfate Cyanuric Acid and Ammelinium Sulfate Monohydrate

Ammelinium Sulfate Monohydrate and Ammelinium Sulfate Cyanuric Acid—Synthesis and Structural Characterization

Fabian K. Kessler, and Wolfgang Schnick

Published in: *Z. Anorg. Allg. Chem.* **2019**, *645*, 848-856.

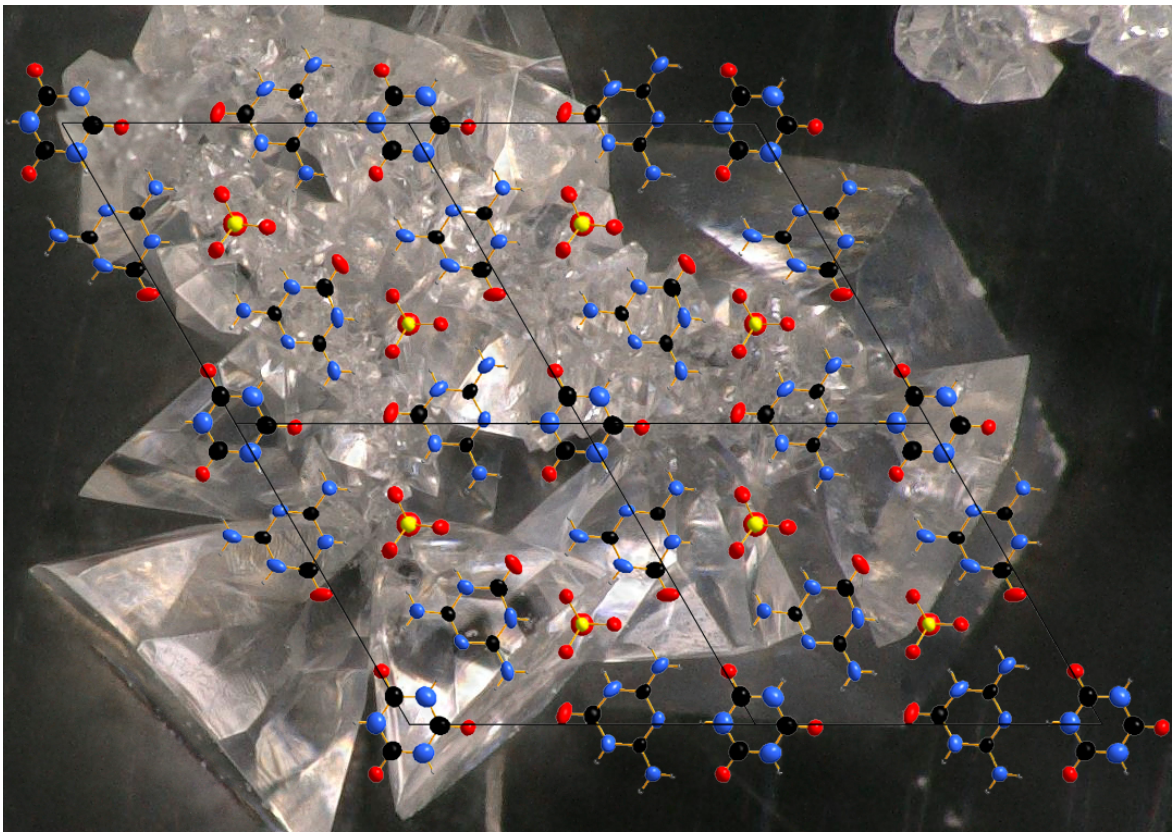

Abstract

Two ionic carbon nitride type compounds containing the ammelinium cation, ammelinium sulfate cyanuric acid ($6C_3N_5H_6O^+ \cdot 3SO_4^{2-} \cdot 1⅔C_3N_3H_3O_3 \cdot H_2O$) (**1**) and ammelinium sulfate monohydrate ($2C_3N_5H_6O^+ \cdot SO_4^{2-} \cdot H_2O$) (**2**) were synthesized through hydrolysis of melam ($C_6N_{11}H_9$) in diluted sulfuric acid. **1** crystallizes in hexagonal space group $P6_3$ (no. 173) with lattice parameters of a =

14.642(3), c = 13.113(4), and Z = 2. The structure is comprised of protonated ammelinium ions and neutral cyanuric acid molecules, which form a layered structure, as well as sulfate ions that span through these layers. **2** crystallizes in the triclinic space group $P\bar{1}$ with lattice parameters of a = 7.404(3), b = 9.673(4), c = 10.040(4), α = 91.098(15), β = 109.884(10), γ = 92.567(13), and Z = 2. As for **1**, the ammelinium rings form layers with the sulfate ions located in between. In both structures, no extended hydrogen bond networks between the respective triazine-based molecules are formed. Instead, single molecules or small building blocks occur isolated and interact primarily with sulfate anions. Compound **1**, which was obtained phase pure, was further investigated by FT-IR spectroscopy, solid-state NMR spectroscopy and powder X-ray diffractometry.

3.3.1 Introduction

In 1834, *Liebig* laid the foundations of carbon nitride chemistry with his extensive work on certain compounds that later proofed to be based on triazine and heptazine building units, respectively.[1] Some of these compounds—such as melamine, which finds various applications in the form of melamine-formaldehyde resins,[2-5] or melon, which recently has been intensively investigated as a photocatalyst material[6-12]—rose to great industrial and scientific relevance. Almost two centuries after their initial discovery, these compounds and their derivatives are still subject to scientific investigations and continue to raise interest.

Less attention has been shed on ammeline and ammelide. These triazine based compounds with compositions of $(C_3N_3)(NH_2)_2(OH)$ and $(C_3N_3)(NH_2)(OH)_2$ represent the partial hydrolysis products of melamine, whose final hydrolysis product would be cyanuric acid; or the partial ammonolysis products of cyanuric acid, vice versa (Figure 3.3.1).[13-15] All four of these closely related molecules came to unfortunate fame through two major food adulteration scandals in 2007 and 2008, in which melamine and cyanuric acid were added to infant formula and pet food to increase the apparent protein contents.[16,17] Since protein content in foods is often indirectly measured by the Kjeldahl method, which unspecifically quantifies nitrogen, certain manufacturers added inexpensive nitrogen-rich materials to increase their economic profits.[18] However, partial hydrolysis of melamine led to the formation of insoluble compounds, primarily adducts of melamine and cyanuric acid, which lead to renal failure by blocking of kidney tubules.[19] These melamine cyanurate (1:1) complexes have become famous before as an example of non-covalent synthesis of nanostructured materials via self-assembly and a prototype for the arrays of hydrogen bonds that can be found between the base pairs in DNA and RNA.[20-22]

In the 2008 incident, more than 50.000 infants were affected, with six confirmed deaths caused by contaminated milk powder. As a result, the majority of recent research concerned with ammeline, ammelide and cyanuric acid revolves around the simultaneous detection and quantification of these

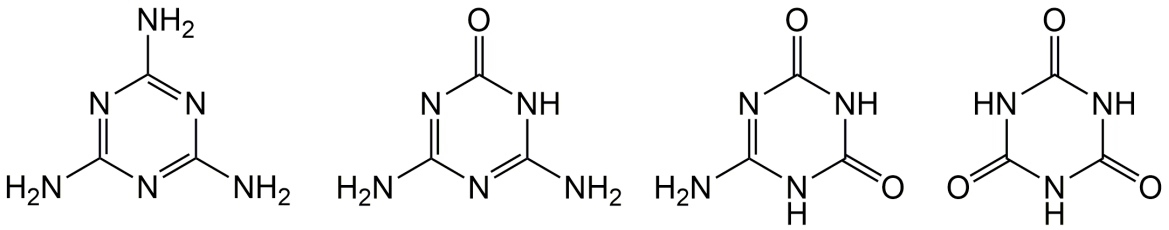

Figure 3.3.1 Triazine compounds, from left to right: melamine, ammeline, ammelide, cyanuric acid.

molecules through a plethora of analytical methods.[23] However, very little research is conducted towards their properties, characterization, and reactivity.

In recent years, the deamination of ammeline has been studied in detail by means of DFT calculations.[24,25] Understanding of this reaction is of great interest in view of the aforementioned hydrolysis of melamine, which is thought to be the cause for the formation of melamine cyanurate complexes from melamine contaminated foodstuff.

Another subject that has been intensely discussed is tautomerism of ammeline and the preference of either the keto or hydroxy form of the ring bound oxygen atom (Figure 3.3.2). Ab initio calculations predicted the hydroxy tautomer to be the most stable form in the gas phase.[26] However, the keto form appears to be more prevalent in solid-state structures, in which keto dimers are formed. Hydrated keto molecules are predicted to be the most stable species in aqueous solution.[27] Independent of state, the quinoid carbonyl tautomer is predicted to be the least stable form and no experimental evidence of this tautomer has been reported.

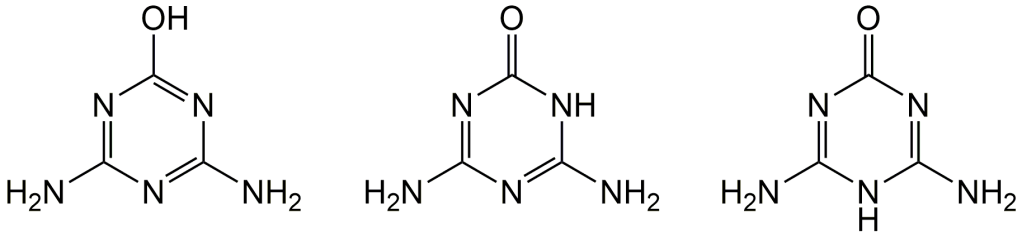

Figure 3.3.2 Different tautomers of ammeline, from left to right: hydroxy form, keto form, quinoid carbonyl form.

As in pure ammeline, the keto form is present in various ammelinium salts. Ammelinium chloride, bromide, and nitrate can be obtained from acidic hydrolysis of melam, $C_6N_{11}H_9$.[28] The structure of all three salts was established from single-crystal X-ray diffractometry. C–O bond lengths of 1.22 Å are indicative for carbonyl C=O bonds. A range of further ammelinium salts, namely the nitrate, sulfate, perchlorate, and 5-tetrazolate, have been discussed as insensitive energetic materials.[29] C–O bond lengths in these compounds are comparable to those in the abovementioned salts, so a trend is evident. However, ammelinium salts are structurally interesting beyond the preference for keto, hydroxy, or quinoid carbonyl tautomers. As is not uncommon for crystalline triazine or heptazine compounds, none of their structures are isotypic. Crystal structures are composed of different arrays of strands or layers, which can be stacked in several different patterns. Hydrogen bridge networks between the

ammelinium rings themselves as well as their respective anions appear to be the dominating structure directing factor, leading to a vast range of possible bonding motifs.

Herein, we expand the group of ammelinium salts by two new representatives, both containing the sulfate anion. Ammelinium sulfate monohydrate is a sulfate salt, which, however, is structurally independent from the known ammelinium sulfate.[29] Ammelinium sulfate cyanuric acid is an adduct between ammelinium sulfate and non-protonated cyanuric acid that emphasizes the partial hydrolysis process of melamine and its derivatives. Both of these salts have been structurally elucidated by single-crystal X-ray diffractometry. Further spectroscopic characterization was performed for the adduct compound.

3.3.2 Results and Discussion

The initial scope of this work was not the synthesis of ammelinium salts, but to synthesize and structurally elucidate a related triazine-based salt, melamium sulfate, "$(C_6N_{11}H_9)_2{\cdot}H_2SO_4$". *Gavrilova et al.* reported on the synthesis of this compound and a range of other melamium salts by dissolving melam, $[C_3N_3(NH_2)_2]NH$, in diluted mineral acids, however, provided little characterization and no structural data.[30] Later, *Lotsch et al.* described the crystal structure of melamium perchlorate hydrate that has been obtained by the same synthesis route.[31]

Trying to reproduce the synthesis of melamium sulfate yielded no product at all. We thus varied the concentration of sulfuric acid as well as the reaction and crystallization times. Given sufficient time to crystallize, a large volume of colorless crystals was obtained. However, none of the prepared samples proved to be the target compound. Instead, a combined approach of elemental analysis, single-crystal XRD, FT-IR spectroscopy, and solid-state NMR spectroscopy identified two different yet undescribed ammelinium salts.

The ammelinium sulfate cyanuric acid adduct (**1**) was initially assumed to possess the sum formula $6C_3N_5H_6O^+{\cdot}3SO_4^{2-}{\cdot}2C_3N_3H_3O_3$ based on elemental analysis and single-crystal XRD. However, one cyanuric acid molecule exhibits only partial site occupation, resulting in the sum formula $6C_3N_5H_6O^+{\cdot}3SO_4^{2-}{\cdot}1⅔C_3N_3H_3O_3{\cdot}H_2O$ instead. The compound was obtained as either tapering needle-shaped crystals, with bushels of smaller needles often growing on larger ones (Figure 7.2.1a); or in the form of large, hexagonal pyramids that showed a high degree of intergrowth (Figure 7.2.1b). However, neither single-crystal nor powder X-ray diffraction data show any difference between the different appearances. It is thus assumed that these differences do not result from different polymorphs, but are due to external influences. Since the reaction conditions for both samples were chosen identically, however, we are not able to name the respective parameter.

A less well-defined sample could be obtained by the same synthesis route. Optical microscopy showed spheroid agglomerates of colorless, polycrystalline material that showed no resemblance to the characteristically shaped single-crystals of **1**. However, a single-crystalline side phase of translucent

platelets could be detected within this sample. A specimen was isolated and identified as an unknown polymorph of ammelinium sulfate monohydrate $2C_3N_5H_6O^+ \cdot SO_4^{2-} \cdot H_2O$ (**2**).

The composition of **1** was investigated by combustion analysis. Results are listed in Table 3.3.1. It can be seen that observed values fit reasonably well to the calculated sum formula. Deviations are attributed to disorder phenomena, which are discussed below.

Table 3.3.1 Elemental composition of **(1)**. All values in w%. For observed values, Δ is the difference to 100 %, which is supposed to be oxygen.

	N	C	H	S	Δ / O
(1), obs.	37.94	21.10	3.47	7.63	29.86
$6C_3N_5H_6O^+ \cdot 3SO_4^{2-} \cdot 2C_3N_3H_3O_3$, calc.	38.35	21.92	3.22	7.32	29.20
$6C_3N_5H_6O^+ \cdot 3SO_4^{2-} \cdot 1⅔C_3N_3H_3O_3 \cdot H_2O$, calc.	37.65	20.89	3.51	7.60	30.35

The identified composition is in good agreement with the crystal structure as established from single-crystal XRD data (see below). It assumes the coexistence of ammeline and cyanuric acid within the structure. The formation of these from melam is readily explained. As has been shown for ammelinium chloride, bromide, and nitrate, strong mineral acids catalyze the hydrolysis of melam to ammelinium (Figure 3.3.3). In contrast, weak acids such as perchloric acid only protonate the molecule.[28, 31] Since sulfuric acid is a strong and oxidizing acid, even a diluted solution appears to be able to not only hydrolyze melam to ammelinium, but to continue the hydrolysis along the path described in Figure 3.3.3. This is not surprising, considering that this reaction is well known. However, it is remarkable to find ammeline next to cyanuric acid with no traces of the intermediate ammelide. We propose two possible explanations for this: either, the hydrolysis of ammeline is significantly slower than the hydrolysis of ammelide, resulting in all the formed ammelide to hydrolyze further to the final hydrolysis product; or, the solubility of ammelide in the chosen reaction medium significantly exceeds that of ammeline and cyanuric acid, so that ammelide remains in solution while ammeline and cyanuric acid precipitate via adduct formation.

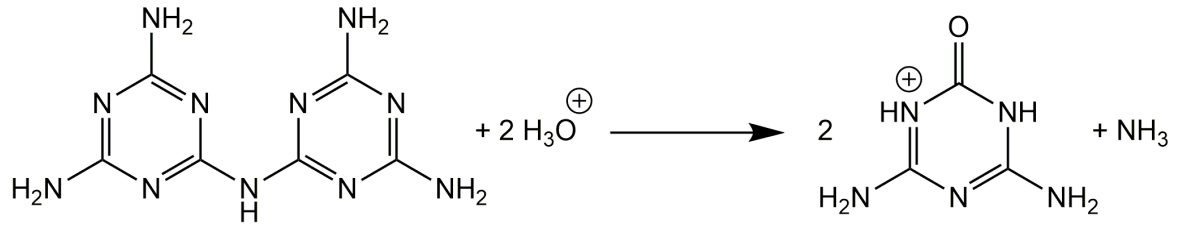

Figure 3.3.3 Hydrolysis of melam towards ammelinium.

Single-crystal X-ray diffraction played a major part in not only structure elucidation of **1** but also in the determination of its composition. Data were obtained from a needle-shaped specimen, which was

Table 3.3.2 Crystallographic data for Ammelinium Sulfate Cyanuric Acid (**1**) and Ammelinium Sulfate Monohydrate (**2**).

	Ammelinium Sulfate Cyanuric Acid (1)	**Ammelinium Sulfate Monohydrate (2)**
Empirical formula	$C_{22}N_{34}H_{44}S_3O_{24}$	$C_6N_{10}H_{14}SO_7$
Formula weight [g mol^{-1}]	1265.09	370.30
Crystal system	hexagonal	triclinic
Space group	$P6_3$ (no. 173)	$P\bar{1}$ (no. 2)
Radiation, λ [ppm]	Mo-K$_\alpha$, 0.71073	Mo-K$_\alpha$, 0.71073
a [Å]	14.642(3)	7.404(3)
b [Å]	14.642	9.673(4)
c [Å]	13.113(4)	10.040(4)
α [°]	90	91.098(15)
β [°]	90	109.884(10)
γ [°]	120	92.567(13)
V [Å^3]	2434.6(13)	675.0(4)
Z	2	2
Density (calcd.) [g cm^{-1}]	1.726	1.822
Temperature [K]	100(2)	100(2)
Absorption coefficient [mm^{-1}]	0.273	0.306
Diffraction range [°]	2.234 ≤ θ ≤ 27.220	2.930 ≤ θ ≤ 25.000
F(000)	1308	384
Index range	-18 ≤ h ≤ 18	-8 ≤ h ≤ 8
	-18 ≤ k ≤ 18	-11 ≤ k ≤ 11
	-16 ≤ l ≤ 16	-11 ≤ l ≤ 11
Absorption correction	multiscan	multiscan
No. of parameters	398	288
No. of independent reflections	3622	2383
No. of independent reflections ($I \leq 2\sigma$)	3410	2013
R_σ, R_{int}	0.0134, 0.0323	0.408, 0.405
GooF	1.105	1.146
R indices ($I \leq 2\sigma$)	$R1$ = 0.0522, $wR2$ = 0.1523	$R1$ = 0.0472, $wR2$ = 0.1108
R indices (all data)	$R1$ = 0.0560, $wR2$ = 0.1551	$R1$ = 0.0590, $wR2$ = 0.1148

refined as a merohedral twin, although with a rather small twin population. Details of measurement as well as structure solution and refinement can be found in Table 3.3.2. **1** crystallizes in hexagonal space group $P6_3$ (no. 173) with two formula units of $6C_3N_5H_6O^+ \cdot 3SO_4^{2-} \cdot 1⅔C_3N_3H_3O_3 \cdot H_2O$ in the unit cell. This results in a total of 16 triazine derivatives per unit cell. These ring molecules form layers stacked along c, which are very slightly corrugated along a as well as b axes (Figure 3.3.4).

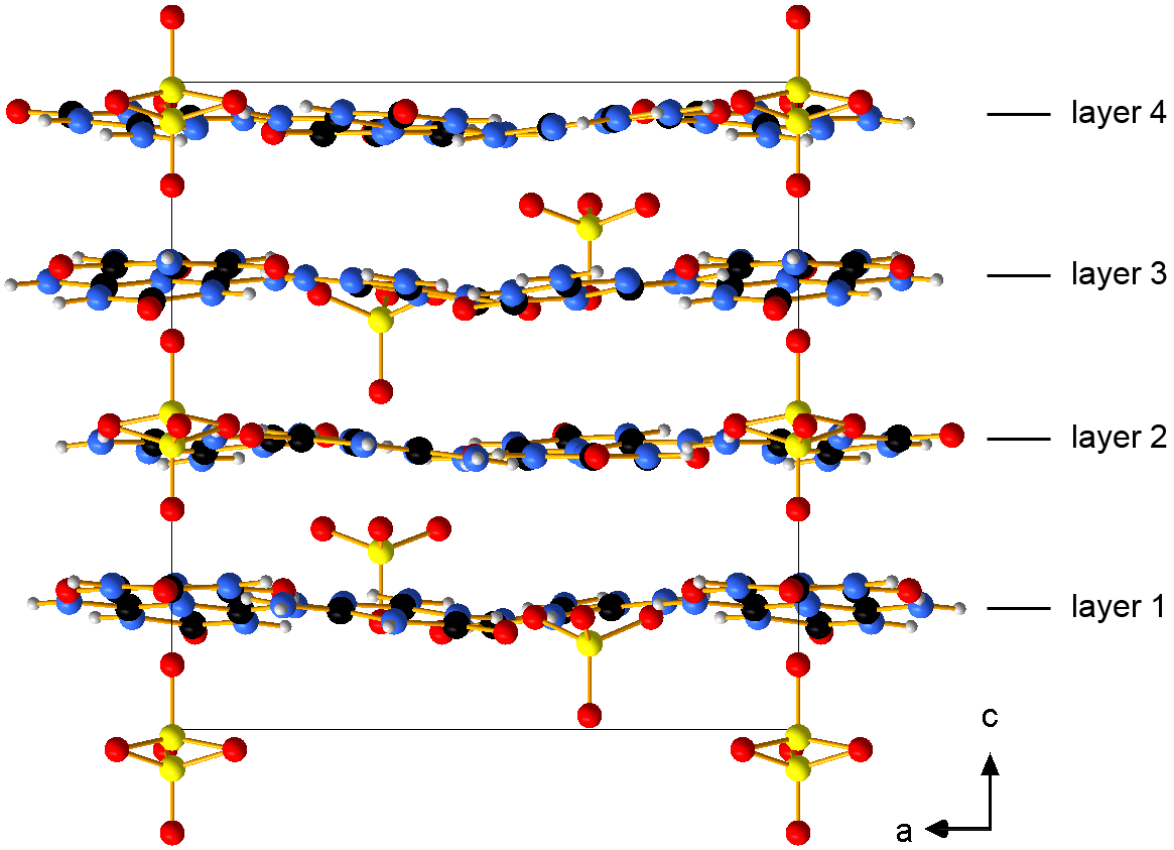

Figure 3.3.4 Crystallographic structure of **1**, viewing direction along *b*. C atoms in black, N atoms in blue, H atoms in gray, O atoms in red, S atoms in yellow. Disorder for sulfate anions and cyanuric acid molecules omitted for reasons of visibility.

Each unit cell contains four independent layers that show no particular stacking order towards each other. However, the first and third layers as well as the second and forth layer are connected by a twofold screw axis, respectively, resulting in two different types of layers. Exemplarily, a layer of type 2 is depicted in Figure 3.3.5. The two different types of layers are more or less identical apart from a shift of origin, however, type 1—represented by the first and third layer of each unit cell, respectively—is affected by structural disorder, which is discussed below. A comparison of the different types of layers can be found in Figure 7.2.2.

In each of these layers, the structure is comprised of triangular motifs, in which three ammelinium units are arranged around one cyanuric acid molecule. In this, the protonation pattern allows for the formation of three hydrogen bridges per ammelinium unit: twice between amino N–H groups and cyanuric acid keto O atoms and once between protonated cyanuric acid ring N atoms and non-protonated ring N atoms of ammelinium. Donor-acceptor distances range from 2.89 to 2.98 Å for the former and 2.79 to 2.88 Å for the latter. Every ammelinium unit is exclusive to one such triangular motif. These groups are isolated from each other with no hydrogen bridges or other interactions between them. However, ammelinium units from three adjacent triangular motifs form cavities that accommodate sulfate anions in two different fashions.

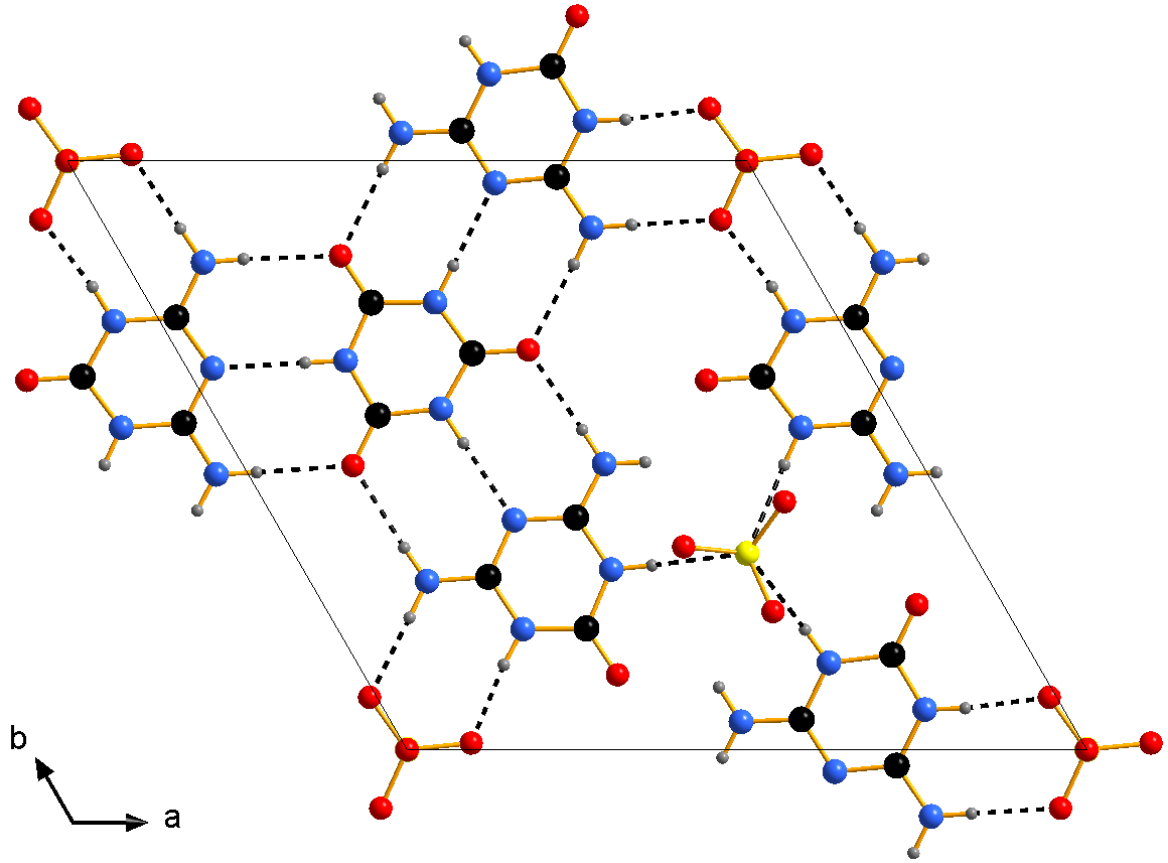

Figure 3.3.5 Single layer (type 2) of **1**, viewing direction along *c*. C atoms in black, N atoms in blue, H atoms in gray, O atoms in red, S atoms in yellow. Dashed black bonds indicate hydrogen bridge interactions. Half of the sulfate anions is located above the layer plane. Disorder for sulfate anions omitted for reasons of visibility.

For half of the cavities, the tip of a sulfate tetrahedron is oriented towards its center. In type 1 layers, this oxygen atom is located within the layer plane. This allows for the formation of three additional hydrogen bridges towards protonated ring N atoms. Here, donor-acceptor distances of 2.93 Å were found. In contrast, in type 2 layers the respective oxygen atom is found considerably above the layer plane, resulting in donor-acceptor distances of 2.98 Å for potential hydrogen bridges, as well as hydrogen atoms forming a rather steep 20.3° angle towards the triazine ring plane. This orientation makes any kind of strong interactions unlikely. In the other half of the cavities, three oxygen atoms forming one face of a sulfate tetrahedron are located in a fashion that allows for the formation of six hydrogen bridges—three towards protonated ring N atoms and towards amino groups, respectively. Rather short donor-acceptor distances of 2.67 to 2.88 Å were found. In type 1 layers, the tips of these tetrahedra are oriented in the same direction as for the tetrahedra whose tips occupy the other half of the cavities. In type 2 layers, however, sulfur and tip oxygen atom of this sulfate tetrahedron can be oriented above as well as below the layer plane—i.e. pointing in either direction—due to disorder affecting these sulfate anions.

Diffraction images of **1** show very weak additional reflections that indicate a threefold superstructure along *c* (Figure 7.2.3). However, it proved impossible to incorporate these in the refinement through use of a unit cell with tripled *c* axis, possibly due to the very low intensities of the superstructure reflections. Within the structure, this disorder is manifested in the cyanuric acid molecules of type 1 layers. Initially, disorder was only assumed for the sulfate tetrahedra located between these molecules and cyanuric acid itself was refined as fully occupied. However, this yielded anisotropic displacement ellipsoids that were rather inconsistent with the rest of the structure. A more consistent model could be obtained by partially replacing cyanuric acid molecules by three water molecules located in the sites of cyanuric acid keto oxygen atoms. This not only significantly improved refinement parameters but also removed an improbably short distance between a sulfate tetrahedron tip and the cyanuric acid triazine nucleus for the case of the tetrahedron pointing towards this molecule. Freely refining the occupancy of cyanuric acid against water, coupled to the respective orientation of the sulfate tetrahedron, yields a ratio close to 1:1. However, the diffraction pattern shows no indication of such a twofold superstructure. Neither would the resulting sum formula agree with the experimentally observed elemental composition. The occupancy was thus restrained to 0.6667 for cyanuric acid atoms and 0.3333 for water to better fit those observations, which yields only marginally poorer figures of merit. Structurally, this translates to the cyanuric acid molecule being replaced by three water molecules in every third layer of type 1. The disordered sulfate tetrahedra between the cyanuric acid units point away from the ring when the site is occupied by cyanuric acid to thus avoid short interatomic separations and point towards the respective site when it is instead occupied by water molecules. Hydrogen atoms found for these water molecules as established from residual electron density are oriented to allow hydrogen bridge interactions towards these sulfate oxygen atoms.

It has to be noted, however, that other interpretations of the observed disorder phenomena are conceivable as well. The threefold superstructure might exclusively result from partial ordering of the mentioned sulfate group, while the deviations in elemental composition might be explained by coexistence of crystals that do or do not show disorder of the cyanuric acid / water molecules. We propose the herein described disorder model since it deems us to best explain the entirety of observations.

Cyanuric acid molecules in the adduct structure show rather uniform C–N bond lengths of 1.36 to 1.38 Å, which are well in line with expected distances for triazine derivatives. The C–O bond lengths of 1.20 to 1.23 Å clearly indicate a double bond and thus a keto tautomer, as is expected for cyanuric acid. Triazine rings moderately deviate from ideal arrangement as the angles range from 115.4 to 124.6°. In ammelinium, a larger range of C–N bond lengths within the rings was observed, ranging from 1.32 to 1.37 Å. C–N bond lengths towards the amino groups are a bit shorter (1.29 to 1.31 Å). This phenomenon has been reported for ammelinium chloride, bromide, and nitrate as well[28] and can be explained as a result of the mixed functionalization of the triazine ring. The electronegative oxygen atom of the keto group possesses an electron withdrawing inductive effect on the conjugated aromatic

system of the triazine nucleus. This electron depletion increases the pull on electrons located at the amino groups, resulting in a partial double-bond character for the C–N_{amino} bond under participation of the nitrogen free electron pair and thus reducing the distance. Calculations of molecular orbitals for ammeline or ammelinium might be a suitable way to test this hypothesis but are beyond the scope of this work.

As for cyanuric acid, C–O distances of 1.20 to 1.21 Å indicate the keto tautomer. Deviations from ideal hexagonal symmetry in ammelinium can be explained by the mixed substitution of the terminal groups. N–C–N angles found at the O atom range from 113.4 to 113.8°, while remaining N–C–N angles span 120.6 to 121.8°. Contrary, C–N–C angles between 122.5 and 123.9° were found, except for those opposite the keto group, which showed angles of only 117.5 to 117.6°. All of these values are well in line with related triazine-based compounds and thus meet the expectations. Atomic coordinates as well as further bond lengths can be found in Tables 7.2.1 and 7.2.2 (Supporting Information).

All three independent sulfate anions are located on threefold screw axes. Tetrahedra are thus generated by cell symmetry. However, it was shown that better refinement parameters as well as more fitting hydrogen bridge donor acceptor distances were obtained when modeling a complete tetrahedron through restraints and refining it with occupancy of ⅓.

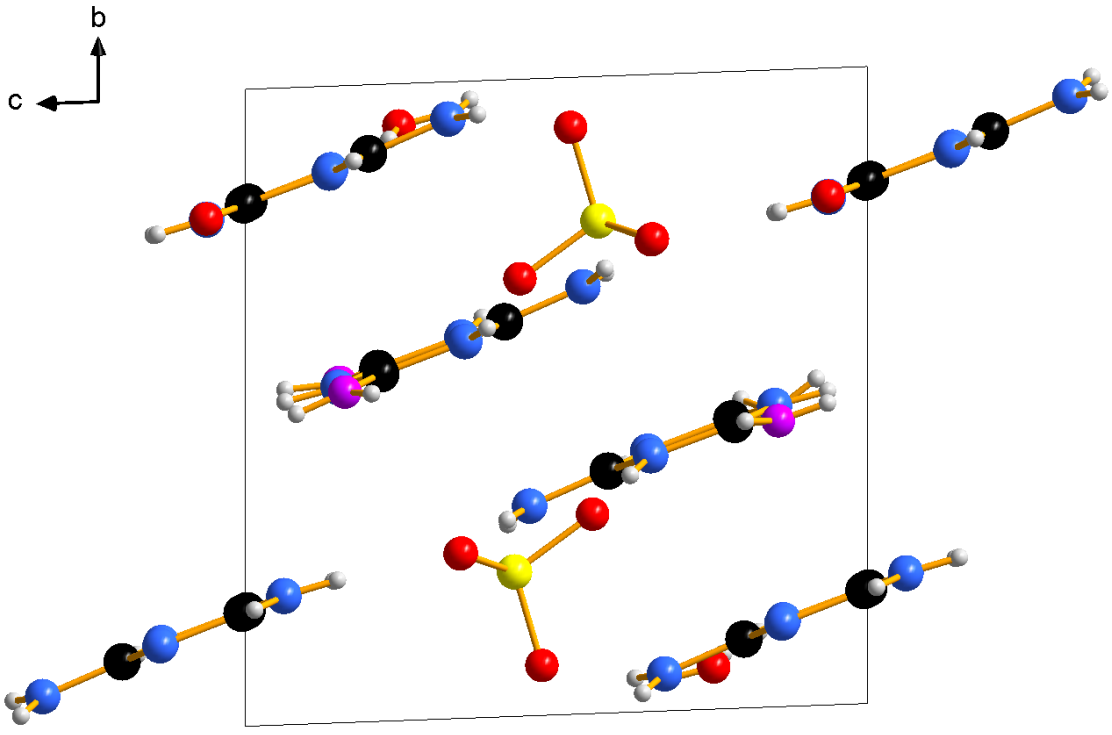

Figure 3.3.6 Crystallographic structure of **2**, viewing direction along *a*. C atoms in black, N atoms in blue, H atoms in gray, O atoms in red, S atoms in yellow, sites with mixed O/N occupation in purple.

For $2C_3N_5H_6O^+ \cdot SO_4^{2-} \cdot H_2O$ a crystal structure has already been published.[29] However, the structure established from single-crystal measurement of **2** is completely unrelated and appears to represent a different polymorph of this compound. **2** crystallizes in triclinic space group $P\bar{1}$ with two formula

units per unit cell, whereas for the polymorph established in literature monoclinic space group $P2_1/c$ has been reported. A summary of crystallographic data is presented in Table 3.3.2. The structure is layered, with ammelinium ions forming planar sheets and sulfate tetrahedra located between these (Figure 3.3.6). Layers are arranged in an abc-stacking pattern. Consequently, the repetition unit within one layer equals three unit cells (Figure 3.3.7).

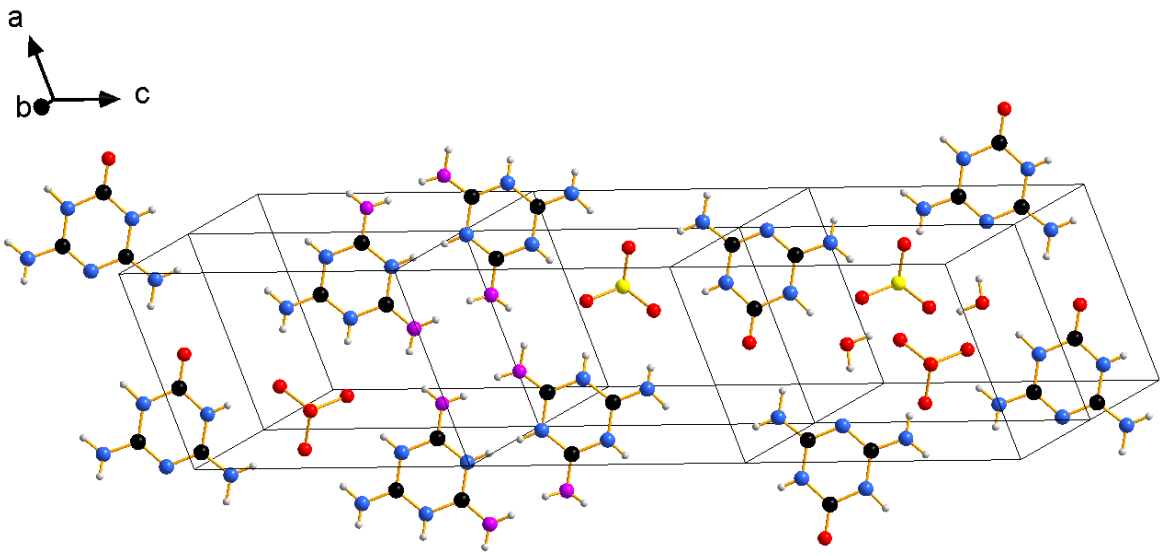

Figure 3.3.7 Complete repetition unit of a layer of **2**, viewing direction perpendicular to the layer plane. C atoms in black, N atoms in blue, H atoms in gray, O atoms in red, S atoms in yellow, sites with mixed O/N occupation in purple. 2 × 3 unit cells plotted.

Each layer is constructed from strands of ammelinium ions, which are mostly isolated. In only one single pair of adjacent strands, molecules are arranged in a way to allow the formation of hydrogen bridges. In these, two crystallographically equivalent molecules form three hydrogen bridges with donor-acceptor distances of 2.88 and 2.93 Å, respectively. The participating keto and amino group in this ammelinium unit are disordered and share a crystallographic site with a distribution of 0.59 to 0.41, which is attributed to these hydrogen bridge interactions. The local arrangement necessitates an amino donor group opposite to a keto acceptor group, elsewise, however, the two respective sites are absolutely equivalent, thus allowing for both functionalities. Furthermore, the ring N atom of one ammelinium unit is required to be protonated while the other must be un-protonated. To achieve this pattern, every second ammelinium unit has to be protonated not in the preferred *ortho* position, but instead in the usually un-protonated *para* position.

No network formation could be observed for the remaining ammelinium units. Instead, the ammelinium ions interact with sulfate groups and water located in two different types of cavities. Type one is formed by three ammelinium ions and contains three oxygen atoms forming the face of a sulfate tetrahedron in an analogous way to the one described for **1**. Six hydrogen bridges per cavity are formed, with donor-acceptor distances ranging from 2.75 to 2.85 Å. Each repetition unit contains two of these cavities with the sulfate tetrahedron pointing upwards in one and downwards in the other. The tip oxygen atoms of these tetrahedra are located in the second type of cavity. These are

formed by four ammelinium ions and contain two oxygen atoms from sulfate anions (one pointing upwards and one downwards, respectively) as well as two water molecules. Two ammelinium amino groups form hydrogen bridges towards each sulfate oxygen atom with donor-acceptor distances of 2.88 and 2.90 Å. However, the acceptor is located slightly above the layer plane, resulting in O–N–H angles of 16.3 to 19.1°, thus weakening the hydrogen bonds. Furthermore, two hydrogen bridges are formed towards each water molecule with ammelinium acting as donor in one case and as acceptor in the other. Here, distances of 2.73 and 2.90 Å were found, indicating medium to strong bonds. No hydrogen bonds appear to occur between water and sulfate since neither of the water protons is oriented towards the sulfate ion. These intense interactions between ammelinium and sulfate ions are in stark contrast to the monoclinic polymorph, in which significantly less hydrogen bridges are formed between different ions and whose structure appears to be much more dominated by ammelinium-ammelinium interactions.

Hydrogen bridge interactions in **2** are depicted in Figure 7.2.4.

The two ammelinium ions making up the structure differ slightly. Molecule 1 shows bond lengths and angles that are very characteristic for ammelinium. Ring C–N bonds range in their lengths from 1.33 to 1.38 Å with the longest bonds adjacent to the keto group and the shortest bonds opposite this group. Amino N atoms show bond lengths of 1.31 to 1.32 Å towards the ring and are thus slightly shorter than the ring bonds themselves, as already discussed for **1**. The C–O bond length was found to be 1.21 Å, unambiguously identifying a keto group. The ring is slightly compressed with angles of 113.7 and 116.7° at the keto group and the opposite N atom and angles of 121.5 to 123.5° for all other angles with no significant differentiation between C–N–C and N–C–N angles. All of these values are well in line with those found in other ammelinium compounds—including **1** and the monoclinic polymorph of ammelinium sulfate monohydrate—which show the same trends and peculiarities. Molecule 2, as already mentioned above, shows disorder in two of its three functionalities. The respective sites could be refined as partially occupied by a keto as well as an amino group. Accordingly, the remaining structure is most likely an average of two molecules in these two orientations. The triazine ring is an almost perfect hexagon with rather even ring C–N bond lengths of 1.35 to 1.36 Å. Likewise, all angles are found in the narrow range between 119.2 and 120.9°. For the fully occupied amino group position, a C–N bond length of 1.30 Å was observed, while for sites of mixed occupancy, lengths of 1.31 Å were found. A C–O bond length of 1.24 Å was obtained for the keto groups. This is slightly larger than expected, however, might be interpreted as an artefact of the refinement of the mixed occupancy. Keto and amino groups, respectively, show no significant divergences for the two sites. Atomic coordinates and bond lengths for **2** can be found in Tables 7.2.3 and 7.2.4.

FT-IR spectroscopy of **1** was performed in reflection geometry using the pure substance (Figure 3.3.8). The spectrum possesses certain noteworthy characteristics that have also been reported for ammelinium chloride, bromide, and nitrate and thus seem to be common to salts of protonated ammeline.[28] ν(C=O) vibration bands are found at 1754 and 1722 cm^{-1}. For ammelinium salts, values

between 1737 and 1757 cm^{-1} have been reported, which are blue-shifted compared to pure ammeline (1718 cm^{-1}). The observed values appear to be well in line with both of these. We attribute the band at 1722 cm^{-1} to cyanuric acid, for which a vibration band at 1720 cm^{-1} has been reported.[32] The ammelinium keto band would thus be shifted in respect to ammeline and well in line with other ammelinium salts.[28,29] Likewise, the band attributed to triazine ring stretching vibrations by *Lotsch et al.* is found at 1661 cm^{-1}, shifted in respect to ammeline. The characteristic triazine out-of-plane breathing mode, typically located around 800 cm^{-1}, is found at 764 cm^{-1}. This red-shift is typical for protonated triazine rings and vibration bands for other ammelinium salts occur between 780 and 765 cm^{-1}.[28,29] Again, the respective band of cyanuric acid would be expected in a comparable spectral region (772 cm^{-1}), so an unambiguous assignment is not possible.[32] We attribute the intense band at 1080 cm^{-1} to sulfate S–O vibrations. A similar band is found in 2,4-diamino-1,3,5-triazinate-6-one sulfate centered at 1105 cm^{-1} and various inorganic sulfates show vibrations in a comparable range.[29,33] The spectrum appears consistent with the structure established from single-crystal XRD.

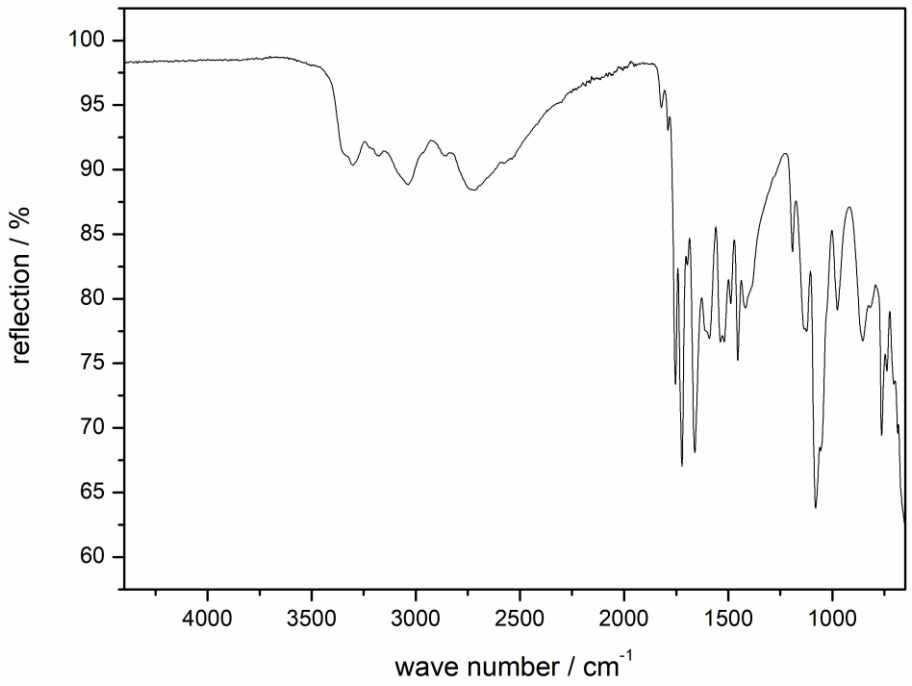

Figure 3.3.8 FT-IR spectrum of **1**.

The sample, from which **2** was obtained was investigated by FT-IR spectroscopy and powder X-ray diffractometry. The polycrystalline material making up the bulk of the sample was shown to differ from **2** but could not be identified from its diffractogram. Spectroscopic measurements yielded only very limited information about its nature. However, two IR bands at 1767 and 1728 cm^{-1} were both assigned to ν(C=O) vibrations of keto groups deviating in their structural environment and a very intense band originating from sulfate groups could be found at 1089 cm^{-1}. We thus assume the unknown bulk phase to be similar in composition to **1** and **2**. However, available methods allowed no further characterization of the minor side phase **2**.

Solid-state MAS NMR spectra of the nuclei ^{1}H, ^{13}C and ^{15}N were recorded for compound **1** to verify the parallel presence of ammelinium and cyanuric acid within the structure. Spectra for ^{13}C and ^{15}N NMR are depicted in Figure 3.3.9. The ^{1}H NMR spectrum shows a rather broad main signal at δ = 12.21 ppm as well as a smaller signal at δ = 6.17 ppm that is partially obscured by the main resonance (Figure 7.2.5). The main signal is attributed to protonated triazine ring N atoms of ammelinium as well as cyanuric acid. The signal at a chemical shift of 6.17 ppm represents amino groups of ammelinium.

Four different signals could be observed in the ^{13}C NMR spectrum, the most intense one at δ = 157.4 ppm. Two additional signals of lower intensity were found at δ = 153.9 and 147.2 ppm and a small shoulder at δ = 148.6 ppm. A database search yielded reported shifts of 154.5 and 159.5 ppm for ammeline and of 150 ppm for cyanuric acid. We thus interpret the signals at δ = 157.4 and 153.9 ppm as belonging to ammeline and the two close signals at δ = 148.6 and 147.2 ppm as resulting from two cyanuric acid molecules of different chemical environment. These different environments have been found in the crystal structure. Furthermore, the observed chemical shifts clearly identify the triazine derivatives that make up **1** as ammelinium and cyanuric acid since neither melamine nor ammelide could explain the number and shifts of the observed resonances.

Three signals were observed in the ^{15}N spectrum of **1**, showing chemical shifts of −243.45, −253.81, and −287.09 ppm, respectively. The signal at −287.09 ppm, which is also the most intense, thus indicating the vicinity of several protons, is interpreted as ammelinium amino groups. The shifts of the two remaining signals indicate monoprotonated N atoms of triazine rings. We assign these to ammelinium and cyanuric acid rings, respectively. However, no reference data could be obtained, thus making separate assignments difficult. No signals were found in the spectral region around −200 ppm in which tertiary N atoms would be expected. This, however, does not indicate a complete protonation of the triazine rings, but can rather be explained as an artefact of the applied cross-polarization pulse sequence, which amplifies signals according to their proximity to protons, resulting in poor intensities for tertiary N atoms, so that potential signals might simply be too weak to be resolved.

Rietveld refinement for **1** was performed to verify phase purity and establish room temperature cell parameters. The results are summarized in Figure 3.3.10 and Table 7.2.5. No reflections that could not be explained by Bragg reflections of ammelinium sulfate cyanuric acid as established from single-crystal XRD could be observed in the powder X-ray diffractogram. We thus conclude that the sample is phase pure and no other compounds—such as compound **2**—formed during the precipitation of the adduct. However, as seen in Figure 3.3.10, not all reflections could be refined with proper intensities. We attribute this to the superstructure, which has not been taken into account, as well as the difference in temperature between the single-crystal and powder XRD measurement.

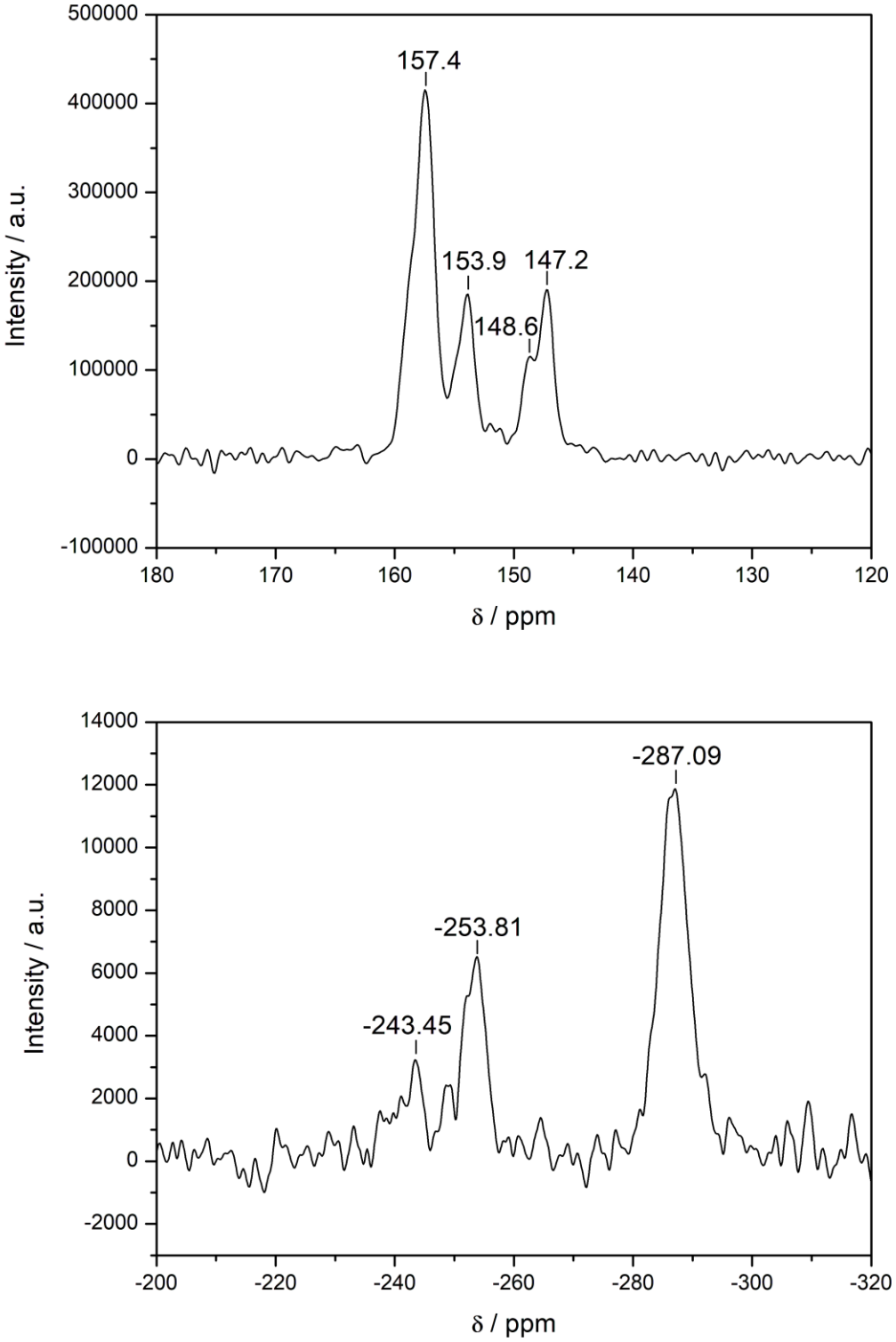

Figure 3.3.9 ^{13}C (top) and ^{15}N (bottom) solid-state MAS NMR spectra of **1**.

Room temperature cell parameters have been determined to a = 14.64540(39) Å and c = 13.12999(35) Å. As is often the case for layered carbon nitride type compounds,[34] the elongation along the stacking direction—here c—is significantly larger than along the other directions. This can be explained as an expansion of the interlayer distance, which is determined by van-der-Waals interactions, whereas the distances within the network layers (determined by hydrogen bonds) hardly elongate at all.

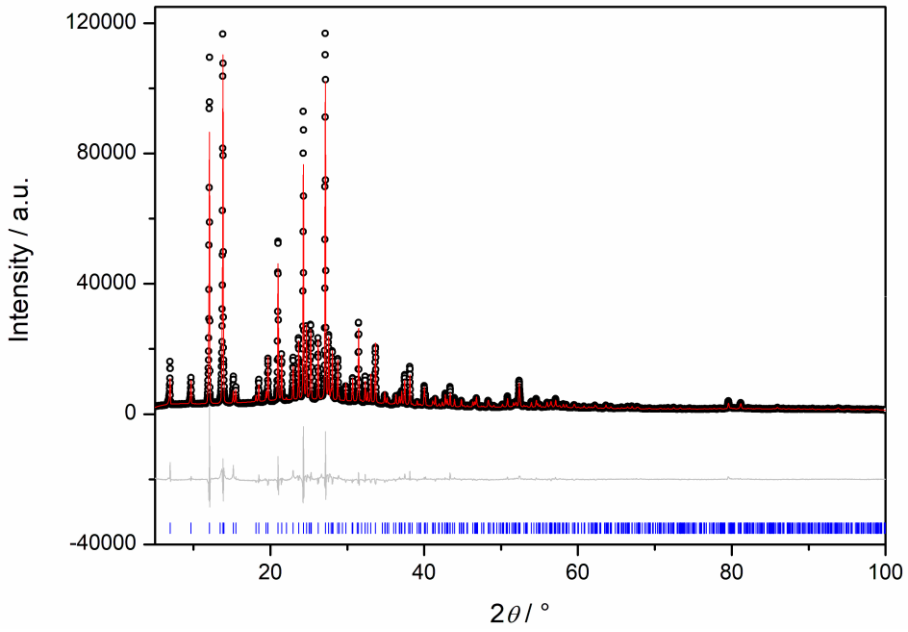

Figure 3.3.10 Rietveld plot of **1**. Measured data points are depicted as black circles, the calculated model is depicted in red, the difference plot Y_{obs}–Y_{calc} in gray. Blue tick marks indicate theoretical Bragg reflection positions.

3.3.3 Conclusions

The ammelinium salts ammelinium sulfate cyanuric acid (**1**) and ammelinium sulfate monohydrate (**2**) were synthesized through a synthesis route that has been described for the synthesis of melamium sulfate.[30] As has been reported before for nitric acid, hydrochloric acid and hydrobromic acid,[28] we observed the hydrolysis of melam in the presence of sulfuric acid, resulting in the formation of two structurally interesting species. **1** represents the first adduct compound between ammeline and cyanuric acid. While adduct formation between melamine and cyanuric acid is well known, no such behavior has been reported for the partial hydrolysis/ammonolysis products ammeline and ammelide.[20,21] In the structure of **1**, ammeline occurs as a protonated species, while cyanuric acid remains uncharged. Single-crystal X-ray diffractometry elucidated a layered structure, in which isolated triangular motifs of three ammelinium ions surrounding one cyanuric acid molecule form cavities that contain the sulfate anions. A superstructure caused by partial occupation of cyanuric acid sites, shared with three water molecules, as well as different orientations of one sulfate tetrahedron could be observed, however, not refined from the available data.

The compound, whose phase purity was shown by powder X-ray diffractometry and Rietveld refinement, was further characterized spectroscopically. FT-IR spectroscopy showed bands shifted in a characteristic way that has also been described for other ammelinium salts.[28] Two independent keto vibration bands could be assigned to ammelinium and cyanuric acid, respectively. A ^{13}C NMR spectrum showed four different resonances, two for ammelinium and cyanuric acid each. Chemical shifts are well in line with related compounds. The ^{15}N spectrum consists of one resonance attributed to terminal amino groups as well as two signals in a shift range expected for NH groups. We assign these to protonated ring N atoms of ammelinium and cyanuric acid.

Compound **2** was obtained as a minor side phase to a polycrystalline, as yet unidentified material. A crystal structure for ammelinium sulfate monohydrate has already been published by *Liu et al.*,[29] however, **2** appears to represent a different polymorph. The structure obtained from single-crystal X-ray diffractometry is layered with an abc stacking order. Mostly isolated ammelinium ions form cavities, in which sulfate and water are located. Hydrogen bridges occur primarily between ammelinium and sulfate ions. One of two crystallographically independent ammelinium ions shows structural disorder over two of three functional groups, which are partially occupied by an amino as well as a keto group. This disorder is caused by hydrogen bridge interactions, which only find fitting donors and acceptors through mixed occupation of these sites. This might indicate a lower symmetry than found from single-crystal X-ray diffractometry. Both compounds show several common structural features and appear to be closely related. We were, however, not able to determine the factors leading to the formation of one or the other.

3.3.4 Experimental Section

Synthesis of Ammelinium Sulfate Hydrate and Ammelinium Sulfate Cyanuric Acid: Syntheses for both compounds were identical. Melam was used as a carbon nitride precursor. It was obtained from stirring melamium bromide, which was prepared according to literature,[34] in a 25 % aqueous solution of ammonia for 2 h, filtrating and drying the residue at 105 °C for 12 h.

Melam (250 mg) was suspended in 12.5 mL of deionized water in a two-neck flask equipped with a reflux condenser and heated to boiling of the solvent. H_2SO_4 (25 mL of 10 %) was added dropwise. Heating was continued until the suspended colorless solid completely dissolved. The flask was closed with a stopper and placed in a refrigerator for 15 d. The colorless precipitate was isolated by filtration.

Single-Crystal X-ray Diffraction: Single-crystal X-ray diffraction data sets were measured with either a Bruker D8 Venture or a Bruker D8 Quest diffractometer (both Bruker, Billerica MA, USA). Measurements were performed at 100 K applying Mo-K_α radiation (λ = 0.71073 Å). For absorption correction, raw data integration and structure solution the program APEX 3 was used.[35] Structure refinement was performed using Shelxl-97.[36,37] Diamond3 was used for visualization of single-crystal structures.[38]

Crystallographic data (excluding structure factors) for the structures in this paper have been deposited with the Cambridge Crystallographic Data Centre, CCDC, 12 Union Road, Cambridge CB21EZ, UK. Copies of the data can be obtained free of charge on quoting the depository numbers CCDC-1898048 for **1** and CCDC-1898049 for **2** (Fax: +44-1223-336-033; E-Mail: deposit@ccdc.cam.ac.uk, http://www.ccdc.cam.ac.uk).

Powder X-ray Diffraction: Powder X-ray diffraction measurements were performed with a Stoe Stadi-P powder diffractometer (Stoe, Darmstadt, Germany) equipped with a Mythen 1 K silicon strip detector (Dectris, Baden, Switzerland) in Debye–Scherrer set-up. Monochromated Cu-$K_{\alpha1}$ radiation (λ = 1.54056 Å) was applied. Samples were prepared in sealed glass capillaries (inner diameter 0.5 mm, wall thickness 0.01 mm). For data processing Stoe WinXPOW Vers. 3.06 was used.[39] Rietveld refinement was performed using TOPAS-Academic V4.1.[40]

General Techniques: FT-IR spectra of all samples were recorded with a Perkin–Elmer BX II spectrometer equipped with a DuraSampler Diamond ATR (attenuated total reflection) unit at room temperature. Elemental analyses of C, N, H and S were conducted by combustion analysis with a Vario EL elemental analyzer (Elementar Analysensysteme GmbH) at the microanalytic laboratory of the Department of Chemistry, LMU Munich. Solid-state MAS NMR spectra were recorded with a Bruker Avance III-500 spectrometer with an external magnetic field of 11.74 T. Measurements were performed at room temperature. Samples were measured at spinning frequencies of 10 kHz in 4 mm double resonance probe heads. ^{13}C and ^{15}N spectra were recorded applying cross polarization (CP) pulse sequences to amplify signal intensities and ^{1}H decoupled. 0.1 % TMS in $CDCl_3$ was used as a reference for all nuclei.

Acknowledgements

The authors wish to express their gratitude to Arthur Haffner and Dr. Peter Mayer (both at Department of Chemistry, LMU Munich) for single-crystal X-ray diffraction measurements. Furthermore, the authors are very grateful for valuable input on crystallographic problems during the revision process. Financial support granted by the Fonds der Chemischen Industrie (FCI) and the Deutsche Forschungsgemeinschaft (DFG) is gratefully acknowledged.

3.3.4 References

[1] J. Liebig, "Ueber einige Stickstoff-Verbindungen", *Ann. Pharm.* **1834**, *10*, 1-47.

[2] W. H. Binder, M. Dunky, "Melamine–Formaldehyde Resins", in *Encyclopedia of Polymer Science and Technology*, 4th ed. (Ed.: H. F. Mark), Wiley, New York, **2004**.

[3] W. H. Binder, M. Dunky, S. Jahromi, "Melamine Resins", in *Kirk-Othmer Encyclopedia of Chemical Technology*, Wiley, New York, **2005**.

[4] H. Diem, G. Matthias, "Amino Resins", in *Ullmann's Encyclopedia of Industrial Chemistry, Vol. A2*, 5 ed. (Ed.: W. Gerhartz), VCH, Weinheim, **1985**, pp. 115-141.

[5] Y. Feng, J. Yao, "Design of Melamine Sponge-Based Three-Dimensional Porous Materials toward Applications", *Ind. Eng. Chem. Res.* **2018**, *57*, 7322-7330.

[6] X. Wang, K. Maeda, A. Thomas, K. Takanabe, G. Xin, J. M. Carlsson, K. Domen, M. Antonietti, "A metal-free polymeric photocatalyst for hydrogen production from water under visible light", *Nat. Mater.* **2009**, *8*, 76-80.

[7] W. Iqbal, B. Yang, X. Zhao, M. Rauf, M. Waqas, Y. Gong, J. Zhang, Y. Mao, "Controllable synthesis of graphitic carbon nitride nanomaterials for solar energy conversion and environmental remediation: the road travelled and the way forward", *Catal. Sci. Technol.* **2018**, *8*, 4576-4599.

[8] A. Thomas, A. Fischer, F. Goettmann, M. Antonietti, J. O. Müller, R. Schlögl, J. M. Carlsson, "Graphitic carbon nitride materials: variation of structure and morphology and their use as metal-free catalysts", *J. Mater. Chem.* **2008**, *18*, 4893-4908.

[9] Z. Zhou, Y. Zhang, Y. Shen, S. Liu, Y. Zhang, "Molecular engineering of polymeric carbon nitride: advancing applications from photocatalysis to biosensing and more", *Chem. Soc. Rev.* **2018**, *47*, 2298-2321.

[10] A. Sudhaik, P. Raizada, P. Shandilya, D.-Y. Jeong, J.-H. Lim, P. Singh, "Review on fabrication of graphitic carbon nitride based efficient nanocomposites for photodegradation of aqueous phase organic pollutants", *J. Ind. Eng. Chem.* **2018**, *67*, 28-51.

[11] J. Fu, J. Yu, C. Jiang, B. Cheng, "g-C_3N_4-Based Heterostructured Photocatalysts", *Adv. Energy Mater.* **2018**, *8*, 1701503.

[12] F. K. Kessler, Y. Zheng, D. Schwarz, C. Merschjann, W. Schnick, X. Wang, M. J. Bojdys, "Functional carbon nitride materials — design strategies for electrochemical devices", *Nat. Rev. Mater.* **2017**, *2*, 17030.

[13] F. Wöhler, J. Liebig, "Ueber ein neues Zersetzungsproduct des Harnstoffs", *Justus Liebigs Ann. Chem.* **1845**, *54*, 371-371.

[14] G. B. Seifer, "Cyanuric Acid and Cyanurates", *Russ. J. Coord. Chem.* **2002**, *28*, 301-324.

[15] A. Hantzsch, "Ueber das Cyamelid", *Ber. Dtsch. Chem. Ges.* **1905**, *38*, 1013-1021.

[16] S. A. Tittlemier, "Methods for the analysis of melamine and related compounds in foods: a review", *Food Addit. Contam. Part A* **2010**, *27*, 129-145.

[17] E. Braekevelt, B. P. Y. Lau, S. Feng, C. Ménard, S. A. Tittlemier, "Determination of melamine, ammeline, ammelide and cyanuric acid in infant formula purchased in Canada by liquid chromatography-tandem mass spectrometry", *Food Addit. Contam. Part A* **2011**, *28*, 698-704.

[18] Y.-N. Wu, Y.-F. Zhao, J.-G. Li, "A Survey on Occurrence of Melamine and Its Analogues in Tainted Infant Formula in China", *Biomed. Environ. Sci.* **2009**, *22*, 95-99.

[19] R. L. M. Dobson, S. Motlagh, M. Quijano, R. T. Cambron, T. R. Baker, A. M. Pullen, B. T. Regg, A. S. Bigalow-Kern, T. Vennard, A. Fix, R. Reimschuessel, G. Overmann, Y. Shan, G. P. Daston,

"Identification and Characterization of Toxicity of Contaminants in Pet Food Leading to an Outbreak of Renal Toxicity in Cats and Dogs", *Toxicol. Sci.* **2008**, *106*, 251-262.

[20] G. Whitesides, J. Mathias, C. Seto, "Molecular self-assembly and nanochemistry: a chemical strategy for the synthesis of nanostructures", *Science* **1991**, *254*, 1312-1319.

[21] G. M. Whitesides, E. E. Simanek, J. P. Mathias, C. T. Seto, D. Chin, M. Mammen, D. M. Gordon, "Noncovalent Synthesis: Using Physical-Organic Chemistry To Make Aggregates", *Acc. Chem. Res.* **1995**, *28*, 37-44.

[22] A. Ranganathan, V. R. Pedireddi, C. N. R. Rao, "Hydrothermal Synthesis of Organic Channel Structures: 1:1 Hydrogen-Bonded Adducts of Melamine with Cyanuric and Trithiocyanuric Acids", *J. Am. Chem. Soc.* **1999**, *121*, 1752-1753.

[23] H. Miao, S. Fan, Y.-N. Wu, L. Zhang, P.-P. Zhou, H.-J. Chen, Y.-F. Zhao, J.-G. Li, "Simultaneous Determination of Melamine, Ammelide, Ammeline, and Cyanuric Acid in Milk and Milk Products by Gas Chromatography-tandem Mass Spectrometry", *Biomed. Environ. Sci.* **2009**, *22*, 87-94.

[24] K. M. Uddin, D. J. Henry, A. I. Alrawashdeh, P. L. Warburton, R. A. Poirier, "Mechanism for the deamination of ammeline, guanine, and their analogues", *Struct. Chem.* **2017**, *28*, 1467-1477.

[25] M. H. Almatarneh, A. A.-A. A. Abu-Saleh, I. A. Elayan, "Mechanistic and spectral investigation on the deamination of ammeline and ammelide", *Comput. Theor. Chem.* **2017**, *1117*, 92-99.

[26] Y. Wang, C. U. Pittman, S. Saebo, "Investigation of the structure and properties of ammeline, melamine, and 2,4-diamino-1,3,5-triazine by ab initio calculations", *J. Org. Chem.* **1993**, *58*, 3085-3090.

[27] M. Hatanaka, "Some structural aspects of ammeline — Keto preference and dimerization", *Spectrochim. Acta, Part A* **2018**, *202*, 87-92.

[28] B. V. Lotsch, W. Schnick, "Synthesis and Structural Characterization of the Ammelinium Salts $[C_3H_6N_5O]Cl$, $[C_3H_6N_5O]Br$, and $[C_3H_6N_5O]NO_3$", *Z. Anorg. Allg. Chem.* **2006**, *632*, 1457-1464.

[29] W. Liu, Q.-H. Lin, Y.-Z. Yang, X.-J. Zhang, Y.-C. Li, Z.-H. Lin, S.-P. Pang, "Energetic Salts Based on an Oxygen-Containing Cation: 2,4-Diamino-1,3,5-triazine-6-one", *Chem. - Asian J.* **2014**, *9*, 479-486.

[30] N. K. Gavrilova, V. A. Gal'perin, A. I. Finkel'shtein, A. G. Koryakin, "Synthesis of Melam and its Salts with Mineral Acids", *Zh. Org. Khim.* **1977**, *13*, 669-670.

[31] B. V. Lotsch, W. Schnick, "New Light on an Old Story: Formation of Melam during Thermal Condensation of Melamine", *Chem. Eur. J.* **2007**, *13*, 4956-4968.

[32] SDBSWeb, https://sdbs.db.aist.go.jp, *National Institute of Advanced Industrial Science and Technology*, (15.01.2019), SDBS No.: 2043.

[33] D. E. Chasan, G. Norwitz, "Infrared Determination of Inorganic Sulfates and Carbonates by the Pellet Technique", *Army Materials Research Agency, Philadelphia*, **1969.**

[34] F. K. Kessler, T. J. Koller, W. Schnick, "Synthesis and Structure of Melamium Bromide $C_6N_{11}H_{10}Br$ and Melamium Iodide $C_6N_{11}H_{10}I$", *Z. Anorg. Allg. Chem.* **2018**, *644*, 186-192.

[35] *APEX 3,* Bruker AXS Inc., Madison WI, USA, **2016.**

[36] G. M. Sheldrick, *SHELX-97, Program Package for the Solution and Refinement of Crystal Structures, Release 97-2,* Universität Göttingen, **1997.**

[37] G. M. Sheldrick, *Acta Crystallogr., Sect. A: Found. Adv.* **2008**, *64*, 112-122.

[38] *Diamond, Program for X-ray structure analysis, v3.1f,* Crystal Impact GbR, Bonn, **2010.**

[39] *WinXPOW, v3.06,* STOE & Cie GmbH, Darmstadt, **2011.**

[40] A. A. Coelho, *TOPAS-Academic V4.1,* Coelho Software, Brisbane, **2007.**

4. Molecular Adduct Compounds: Melam-Melem (1:1)

Structure Elucidation of a Melam–Melem Adduct by a Combined Approach of Synchrotron X-ray Diffraction and DFT Calculations

Fabian K. Kessler, Asbjörn M. Burow, Gökcen Savasci, Tobias Rosenthal, Peter Schultz, Eva Wirnhier, Oliver Oeckler, Christian Ochsenfeld, and Wolfgang Schnick

Published in: *Chem. Eur. J.* **2019**, *25*, 8415-8424.

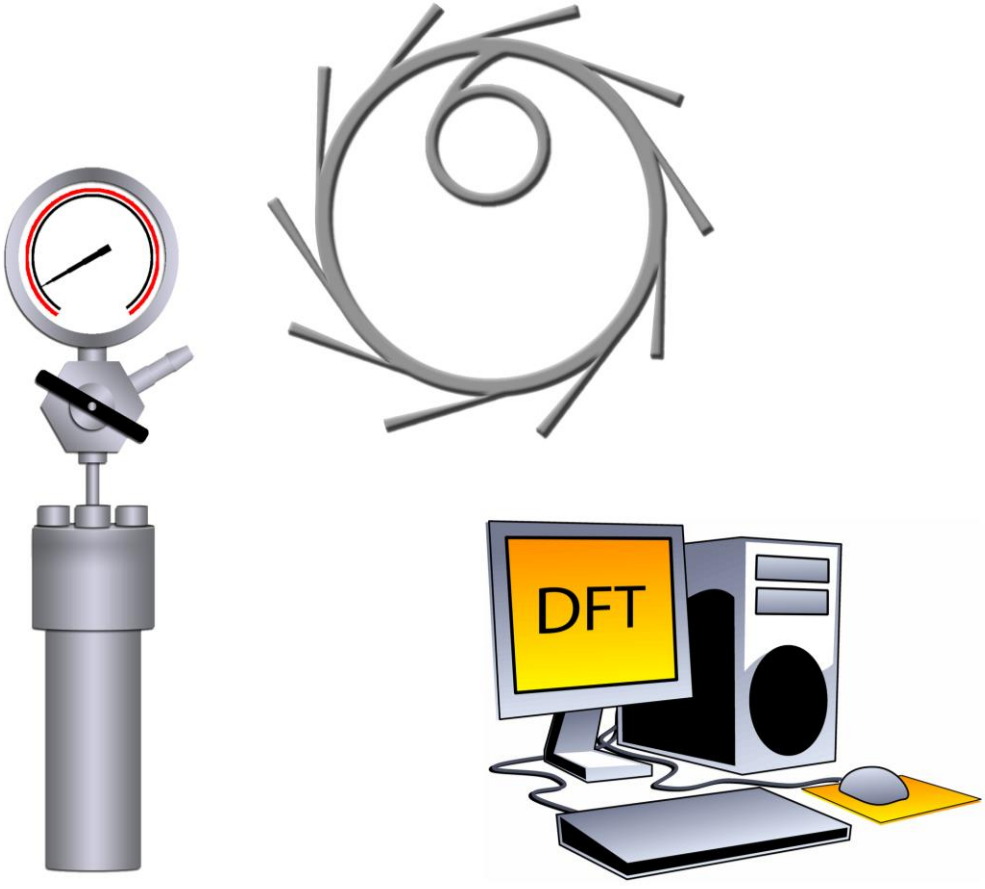

Abstract

Melam-melem (1:1), an adduct compound that can be obtained from dicyandiamide in autoclave reactions at 450 °C and elevated ammonia pressure, had previously been described based on mass spectrometry and NMR spectroscopy, but only incompletely characterized. The crystal structure of this compound has now been elucidated by means of synchrotron microfocus diffraction and subsequent quantum-chemical structure optimization applying DFT methods. The structure was refined in triclinic space group $P\bar{1}$ based on X-ray data. Cell parameters of a=4.56(2), b=19.34(8), c=21.58(11) Å, α=73.34(11)°, β=89.1(2)°, and γ=88.4(2)° were experimentally obtained. The resulting cell volumes agree with the DFT optimized value to within 7 %. Molecular units in the structure form stacks that are interconnected by a vast array of hydrogen bridge interactions. Remarkably large melam dihedral angles of 48.4° were found that allow melam to interact with melem molecules from different stack layers, thus forming a 3D network. π-stacking interactions appear to play no major role in this structure.

4.1 Introduction

Carbon nitride type materials—inorganic ring-compounds based on the triazine or heptazine building unit—are an extensively studied class of materials. While they have been known for almost two centuries, they only came to greater attention in the scientific community during the last thirty years.[1-6] A major part of this newly sparked interest emerged around the synthesis of sp^3-C_3N_4, for which extreme incompressibility comparable to diamond had been predicted in theoretical studies.[7-9] More recent investigations, however, primarily focus on properties and application of these materials.[10-18] For a long time, the application of carbon nitride type materials was mostly limited to the use of the molecular compound melamine in melamine foams, flame retardants, and mostly in melamine-formaldehyde resins which find broad application as coating materials, tableware or laminate flooring.[19] These products are well established. Recent investigations, however, mainly concern polymeric carbon nitride compounds of which melon (i.e., poly(aminoimino)heptazine) is the most prominent representative. This 1D polymer has been found to be a semiconductor, with a band gap of appropriate width and position for application in various photocatalyzed reactions such as water splitting or pollutant degradation.[4,20] These materials are promising photocatalysts since they are inexpensive, non-toxic, and lightweight due to the lack of rare earth or heavy metals. In addition, they are chemically and thermally stable up to 630 °C.[21]

Melon is easily obtained from melamine, which is readily available with a global annual production estimated to surpass 2 million tons in 2018.[22] This conversion proceeds along a condensation cascade through elimination of several formula units of ammonia.[23] While the constituents of this cascade and the general pathway are well established, the exact course of reactions in this is still under

discussion. Particularly, the formation mechanism of heptazine rings from triazine-based precursor compounds has not yet been unambiguously elucidated.

As can be seen in Figure 4.1, the heptazine nucleus is formed during the formation of melem, that is, triamino-*s*-heptazine. It has been suggested that this reaction proceeds either directly from melamine or via a highly reactive intermediate form of melam, a triaminotriazine dimer.[3,24,25] Several mechanisms have been proposed for either option. Mechanisms starting from melamine are thought to include a decomposition step of melamine to either cyanamide[23] or dicyandiamide.[3,21,26] The respective fragments bind to still undecomposed melamine in a series of nucleophilic addition reactions, and finally form melem through further ring closure reactions. In the case of a reaction via a melam intermediate, a ring opening process for one of the triazine rings of melam, followed by a ring closure, has been proposed. The theory of a direct condensation of melamine is supported by the discovery of three defined melamine-melem adducts with compositions $2\,C_3N_6H_6{\cdot}C_6N_{10}H_6$, $C_3N_6H_6{\cdot}C_6N_{10}H_6$, and $C_3N_6H_6{\cdot}3\,C_6N_{10}H_6$.[27] These clearly show a coexistence of these two molecules without any further molecular intermediate, and therefore strongly hint at the existence of a direct reaction pathway.

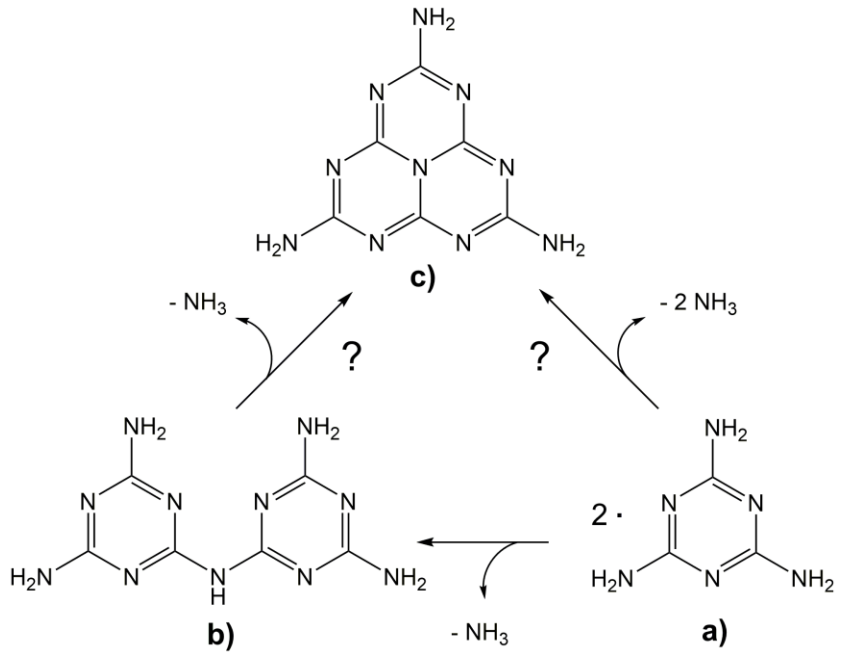

Figure 4.1 Molecular carbon nitride compounds a) melamine, b) melam and c) melem and possible pathways for thermally induced condensation reactions.

However, contrary evidence was provided by our group in 2013 with the discovery of an adduct compound comprised of melam and melem, which hints at an additional reaction pathway that does include the melam intermediate.[28] We were, however, unable to determine the ratio of the adduct components from composition alone, and structure elucidation of this compound could not be conducted, since no single-crystals large enough for single-crystal X-ray diffraction could be grown and it proved impossible to solve the structure from powder diffraction data. Nevertheless, this compound is of considerable interest as it grants valuable insights in the still unresolved triazine-to-heptazine conversion mechanism, and the potentially many pathways on which this reaction can proceed. In this contribution, we now present the crystal structure of this melam-melem adduct compound as

obtained from microfocused synchrotron radiation diffraction data, and quantum-chemical calculations using DFT methods.

4.2 Results and Discussion

Synchrotron X-ray diffraction

The melam-melem adduct compound was obtained from autoclave reactions as described previously,[28] as a colorless, polycrystalline powder. Since no single-crystals suitably large for conventional single-crystal X-ray diffraction could be obtained, the compound was investigated by transmission electron microscopy (TEM). However, crystallites proved to be very beam sensitive, so that approximate unit cell dimensions could be obtained, but data collection for electron crystallography was not successful. Single-particle X-ray data collection for this study was thus conducted at the European Synchrotron Radiation Facility (ESRF) in Grenoble, France, on a suitable crystallite pre-selected by TEM.

Diffraction data enabled an unambiguous structure solution, as well as determination of the composition of the adduct, which had been impossible from elemental analyses due to the very similar compositions of melam and melem. The compound proved to be a 1:1 adduct of melam und melem that crystallizes in triclinic space group $P\bar{1}$. Crystallographic data are given in Table 4.1. The unit cell contains four formula units, with the asymmetric unit containing two melam and two melem molecules. Due to the very limited range of rotation for a TEM grid in a synchrotron beam, and the low scattering power, the data set exhibits a completeness of only 47.2 % and rather weak intensities. Its quality is comparable to typical data from electron diffraction tomography.[29,30] *R* factors obtained for the refinement are accordingly rather poor. Structural parameters should thus be regarded as preliminary. H atom positions were geometrically constructed and fixed at a distance of 0.86 Å and angles of 120° with respect to the atoms that they ride on.

The structure of the melam-melem adduct is best described in terms of a melam substructure and a melem substructure (see Figures 4.1 and 4.2). For both of these, molecules are stacked along [1 0 0] so that the stacking distance equals the *a* lattice parameter of 4.56 Å. Since this is significantly larger than the van-der-Waals distance usually found for triazine- or heptazine-based compounds of about 3.2 to 3.4 Å,[21,24,31] it is assumed that—similar to the situation in pure melam—π-stacking interactions play no major role in this structure.[25]

Melem molecules in this structure are not planar, but exhibit slight corrugation of the ring systems as well as tilting of terminal amino groups out of the ring plane. Refined atomic positions are, however, not very precise. This leads to C–N bond lengths of great variance, ranging from 1.24 to 1.52 Å (standard deviations ca. 0.03 Å), showing rather large differences in length even for comparable bonds.

Table 4.1 Crystallographic data and details of structure refinement for the melam-melem adduct; structure solution and refinement performed on synchrotron XRD data.

Empirical formula	$C_6N_{11}H_9 \cdot C_6N_{10}H_6$
Formula weight (in g mol-1)	453.45
Crystal system	Triclinic
Space group	$P\ \bar{1}$ (no. 2)
Temperature	293(2) K
Radiation	synchrotron, ESRF ID 11;
	λ = 0.29464 Å
Lattice parameters	
a	4.56(2) Å
b	19.34(8) Å
c	21.58(11) Å
α	73.34(11)°
β	89.1(2)°
γ	88.4(2)°
Z	4
Cell volume	1823(15) Å^3
Calculated density	1.652 g cm-3
F(000)	936
Diffraction range	$0.82° \leq \theta \leq 9.98°$
Index range	$-5 \leq h \leq 5$
	$-21 \leq k \leq 22$
	$-23 \leq l \leq 25$
No. of parameters	265
No. of independent reflections	2947, thereof 2135 with $I > 2\ \sigma(I)$
GooF	2.199
$R1$	0.2380 ($I > 2\ \sigma(I)$), 0.2731 (all data)

A similar situation is encountered with bond angles within the molecules. Therefore, numerical values of interatomic distances and angles are not further discussed for the XRD model. Melem molecules in the adduct structure form dimers consisting of two symmetrically inequivalent molecules that are linked through two hydrogen bridges each, with one amino group per molecule participating in dimer formation. One molecule in each dimer is oriented towards a neighboring melem dimer to allow the formation of two further hydrogen bridges, which are only marginally longer than those within the dimer. At first glance, the other molecule in the dimer shows a similar alignment, which ultimately would lead to the formation of infinite zigzag chains that extend diagonally through the melem columns stacked along [1 0 0]. However, these two melem molecules exhibit a significantly larger distance than found elsewhere and the orientation of terminal amino groups indicates an absence of

hydrogen bridge interactions. Furthermore, while melem molecules that form a dimer lie in the same marginally corrugated plane, different melem dimers—those forming hydrogen bridge interactions as well as those that do not—are slightly displaced in height towards each other (Figure 4.2).

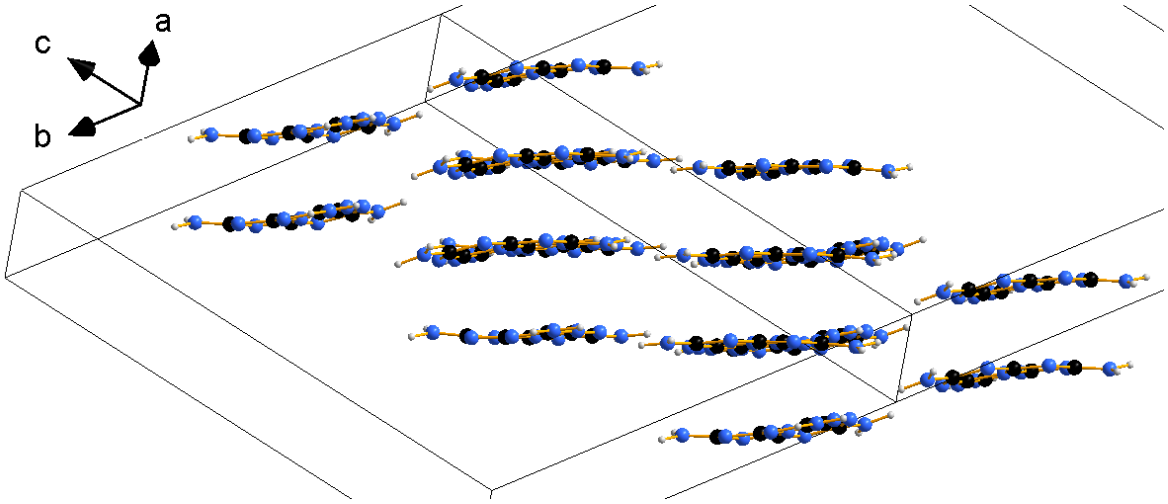

Figure 4.2 Melem cutout structure of the DFT-optimized structure of the melam-melem adduct, obtained at the PBE-D3/pob-TZVP level. Projection perpendicular to the melem stacking direction. C atoms in black, N atoms in blue, H atoms in light gray.

For melam molecules, the rather large standard deviations of 0.03 Å result in experimental bond lengths that range from 1.28 to 1.46 Å. While these values appear unusual, they are within 3σ and are thus not significantly diverging. While numerical values of distances and angles are rather imprecise, the model shows certain general trends in molecular constitution and conformation. In contrast to pure melam, the triazine rings show no corrugation but appear to be flat. Terminal amino groups are only slightly bent out of the ring plane. Analogous to pure melam—but in contrast to compounds of monoprotonated melamium[25,32,33]—melam units in the adduct compound exhibit twisting around the central imide group. The experimentally determined torsion angles of 48° for both molecules, however, are significantly larger than in melam (11° and 14° respectively), or any other melam compound described in literature.[25] Melam molecules form two kinds of hydrogen bonding motifs with neighboring melam units. For once, two symmetrically inequivalent melam molecules with torsion angles of opposite sign facing towards each other with their "backbones" form a dimer through four hydrogen bridges. These involve both imide groups and one terminal amino group per molecule acting as donors, and two ring N atoms per molecule acting as acceptors. An "end-on-end" interaction between two melam molecules facing each other with their short outer sides occurs as a second motif. This enables the formation of two hydrogen bridges. These two motifs form infinitely extended ribbons of melam dimers. Each molecule exhibits one triazine ring lying in the plane, whereas the other is bent out of plane, resulting in roughly "S"-shaped motifs as shown in Figure 4.3. These corrugated ribbons are stacked along [1 0 0].

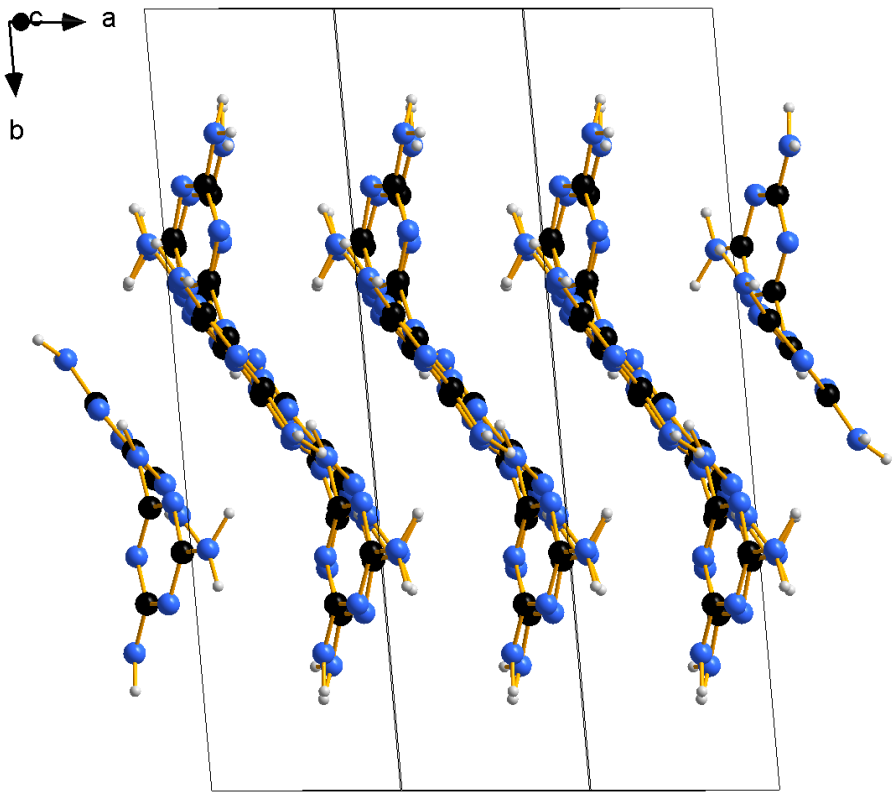

Figure 4.3 Melam cutout structure of the DFT-optimized structure of the melam-melem adduct, obtained at the PBE-D3/pob-TZVP level. Projection perpendicular to the *a*-axis to show stacking motifs. C atoms in black, N atoms in blue, H atoms in light gray.

Both substructures form infinitely extended strands along [0 0 1]. These strands of melam und melem are arranged in an alternating pattern along [0 1 0] (see Figure 4.4). In the melam substructure, molecules are oriented with their backbones facing "inwards" to form hydrogen bridged dimers, whereas the "open" side is facing the next layer of melem substructure. In the latter, the large torsion angle enables the formation of hydrogen bridges towards two layers of melem molecules. This bridging motif towards two melem molecules appears to cause the unusually large torsion angle found for the melam molecules in the adduct compound.

Each melam molecule interacts with three melem molecules, two of which are stacked eclipsing along [1 0 0] and binding one to each of the two triazine rings of one melam molecule. To each of these three melem molecules, melam forms two hydrogen bridges. This leads to a total of six hydrogen bonds towards melem per melam unit and vice versa.

Even though in each of the two substructures there are parallel stacks of molecules, the melam ribbons and melem ribbons are not parallel to each other, but are tilted by about 18°.

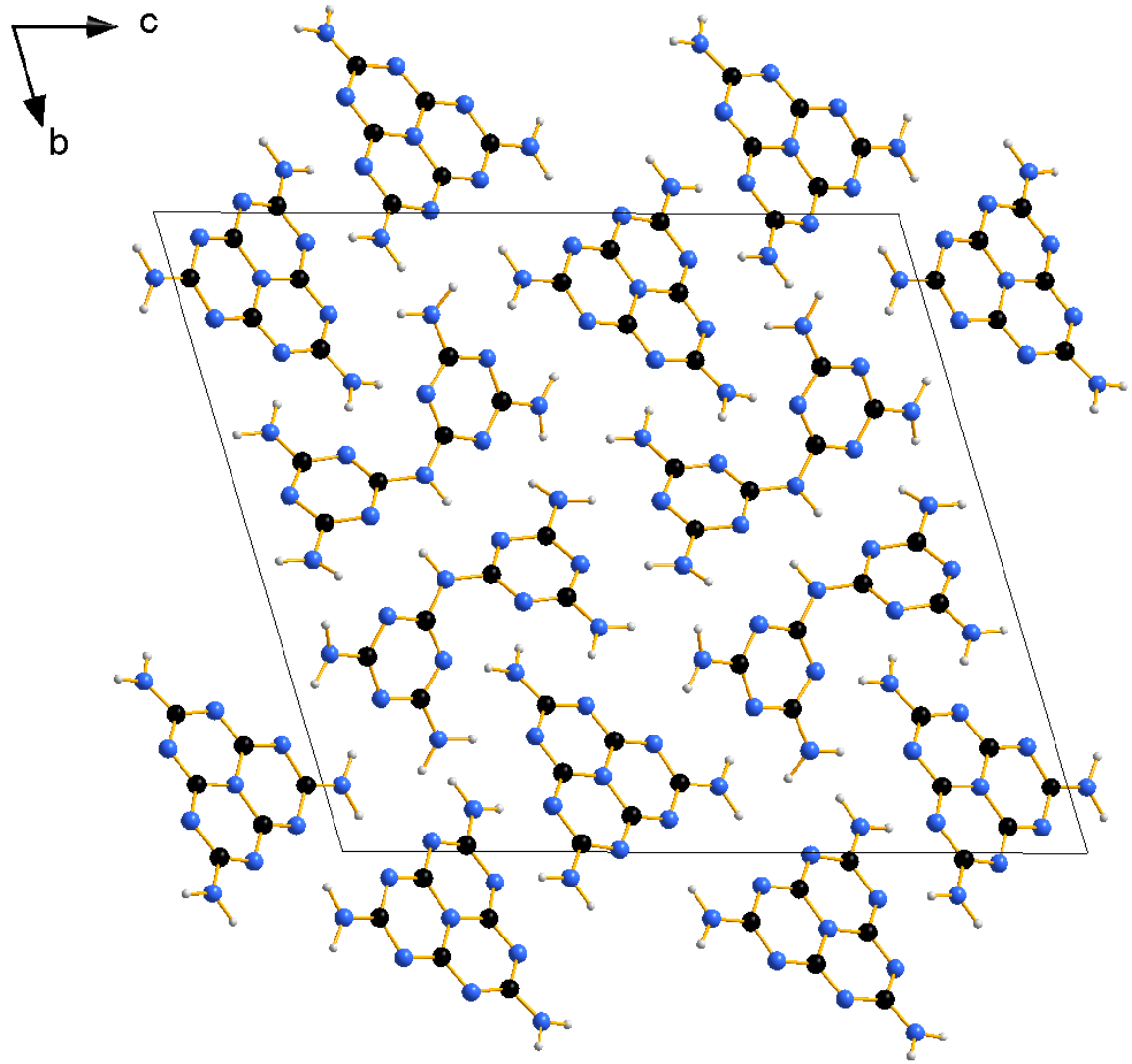

Figure 4.4 Optimized crystal structure of the melam-melem adduct, obtained at the PBE-D3/pob-TZVP level. Projection along [100]. C atoms in black, N atoms in blue, H atoms in light gray.

Quantum-chemical calculations

In order to obtain a more precise structure model than was possible from synchrotron data, we performed a set of structure optimizations at the PBE-D3/pob-TZVP level of theory. These calculations are especially valuable with respect to the positions of H atoms, which could not be obtained from the diffraction data. As the structure is not determined by van der Waals interactions, but hydrogen bridges appear to play a major role in its constitution, these structural parameters are highly important for a deeper understanding of the structure.

Furthermore, structure optimizations of melam and melem as molecular monomers, as well as of a melam dimer, have been performed for comparison at the same level of theory. In addition, crystal structures of pure melam and pure melem were studied.

Table 4.2 Optimized melam structure parameters. Calculated average torsion angles θ [°] between two ring planes in one melam molecule and rotational constants A, B, C [MHz].

system	method	sym.	θ	A	B	C
monomer	PBE/TZVP	C_2	2.4	1029.2	242.2	196.1
	PBE-D3/TZVP	C_2	2.7	1029.5	242.7	196.5
	PBE-D3/QZVP	C_2	3.4	1029.7	242.8	196.5
	PBE0/TZVP	C_2	2.2	1047.8	246.7	199.7
	RPA@PBE/TZVP	C_2	9.9	1033.3	244.9	198.6
	RPA@PBE/QZVP	C_2	6.1	1041.6	246.4	199.5
dimer 1	PBE/TZVP	C_1	35.2	145.0	81.1	59.9
	PBE-D3/TZVP	C_2	35.7	145.0	82.0	60.5
	PBE0/TZVP	C_2	34.1	147.6	81.6	60.3
	RPA@PBE/TZVP	C_1	33.1	144.9	81.6	60.5
dimer 2	PBE/TZVP	C_i	37.4	154.9	79.6	54.1
	PBE-D3/TZVP	C_i	38.9	156.0	80.5	54.7
	PBE0/TZVP	C_i	35.9	156.1	80.3	54.4
	RPA@PBE/TZVP	C_i	39.2	154.1	80.6	54.5

Structure optimizations for a single isolated molecule of melam led to an almost planar C_2-symmetric molecular structure for all methods shown in Table 4.2. Comparison of torsion angles between the ring planes and rotational constants of the melam molecule, which were used as a means to characterize the optimized structure, shows only moderate deviations between the different models. The torsion angle for the monomer does not exceed 10° for any optimized structure. The infrared spectrum in Figure 4.5, simulated with the PBE0 density functional, exhibits bands above 3500 cm^{-1} that result from symmetric and antisymmetric NH_2 stretches, and bands in the range from 1400 to 1700 cm^{-1} that originate from NH_2 bending modes, NH_2 rocking, H rocking on the secondary amino group, C_2NH bending, CN ring vibrations, and combinations thereof. Not all experimentally observed vibration bands[25] could be obtained, which, however, is expected since calculations were done for single molecules in vacuum at a temperature of 0 K. While bands from 1400 to 1700 cm^{-1} are in good agreement with experimental band positions, calculated NH_2 stretching modes are considerably shifted towards higher wave numbers.

For the melam dimer in the gas phase, two possible low energy conformers were found. Using the PBE and RPA method, the most stable dimer **1** exhibits the point group C_1, though the structure is close to the C_2-symmetric transition state, where the weak imaginary mode at 21.35 cm^{-1} (for PBE) belongs to an out-of-plane vibrational mode on two primary amino groups. Using the PBE-D3 and PBE0 functionals, this conformer still is the most stable one and exhibits C_2 symmetry. There is an additional C_i-symmetric dimer **2** for all methods used, around 11 $kJ\,mol^{-1}$ higher in energy. Energy differences obtained by different methods are given in Table 7.3.1 in the Supporting Information. In contrast to

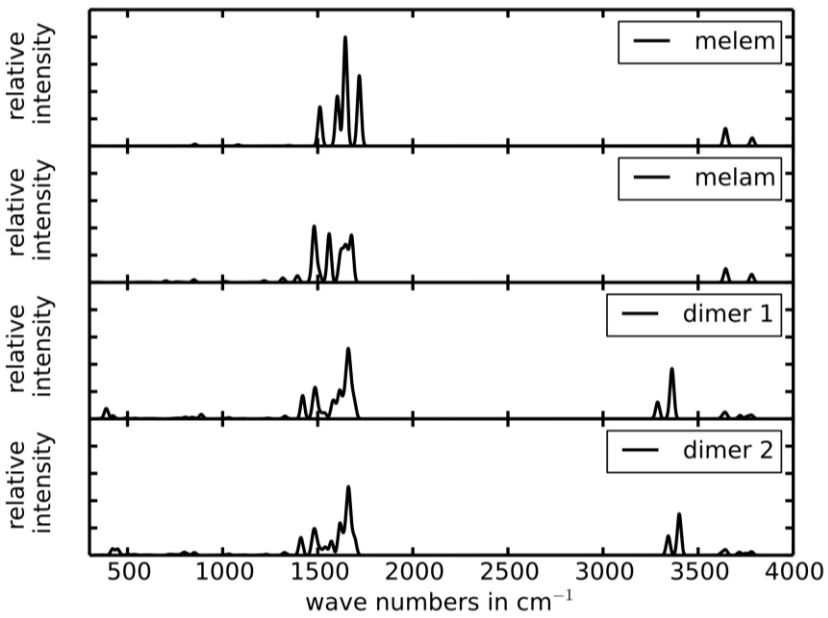

Figure 4.5 Unscaled simulated harmonic vibrational spectra for PBE0/TZVP-optimized gas phase structures of melem, melam, and two melam dimers.

the monomer, both dimers exhibit torsion angles between 33° and 40°, where the torsion in dimer **1** is smaller than in dimer **2**. Since each dimer contains four hydrogen bonds, and since the single melam molecule prefers a small torsion angle, it seems reasonable that dimer **1** is energetically favored compared to dimer **2**. The simulated infrared spectra of both dimers are very similar (see Figure 4.5), however they exhibit additional bands compared to the monomer. The strong bands at 3287 and 3363 cm^{-1} are attributed to secondary and primary amino group N–H···N stretches along hydrogen bonds. This is in good agreement with experimental spectra, which exhibit two distinct signal groups in this region: one consisting of rather sharp signals around 3460 cm^{-1} and a group of rather broad, overlapping signals around 3170 cm^{-1}.

A single melem molecule exhibits D_{3h} symmetry according to the methods PBE, PBE-D3, and PBE0. The simulated infrared spectrum shown in Figure 4.5 exhibits four visible bands between 1500 and 1720 cm^{-1}, as well as two further bands representing symmetric and antisymmetric NH_2 stretches at 3644 and 3784 cm^{-1}. All of these belong to modes of the irreducible representation *e′* and are strict in-plane modes. As for melam, the calculated spectrum differs considerably from experimental solid-state spectra and does not reproduce all observed bands.[24]

Crystal structures were optimized for melam and melem, as well as the melam-melem adduct. The experimentally determined space group of melam is $C2/c$, containing two symmetry inequivalent molecules. One of the melam molecules exhibits C_2 point symmetry while the other one has C_1 symmetry. Optimized cell parameters were obtained from full relaxation applying a PBE-D3/pob-TZVP calculation. As can be seen in Table 4.3 and Table 7.3.2, these show notable deviations from experimental ones, as well as larger mean signed errors. Structure optimization was thus also

Table 4.3 Comparison between lattice parameters from experimental XRD and deviations to PBE-D3/pob-TZVP (DFT) results for melam, melem and the melam-melem adduct. Lengths in Å and angles in °.

	melam		**melem**		**melam-melem adduct**	
parameter	**XRD**	**DFT**	**XRD**	**DFT**	**XRD**	**DFT**
a	18.11	−0.22	7.40	0.10	4.56	−0.17
b	10.87	−0.09	8.65	−0.16	19.34	−0.30
c	13.98	0.10	13.38	−0.06	21.58	−0.33
α	90.00	0.01	90.00	−0.05	73.34	0.95
β	96.31	−0.03	99.91	0.37	89.10	−0.42
γ	90.00	0.04	90.00	0.02	88.40	−1.32

conducted with lattice parameters fixed to experimentally determined values. The resulting hydrogen bond network of the relaxed structure is illustrated in Figure 4.6.

Each asymmetric melam molecule forms ten hydrogen bonds with five melam neighbors including two asymmetric molecules and three C_2-symmetric ones. The C_2-symmetric molecule forms ten hydrogen bonds with six asymmetric melam neighbors. In the latter, the bridging NH group of the C_2-symmetric melam molecule is the only hydrogen donor not involved in the network.

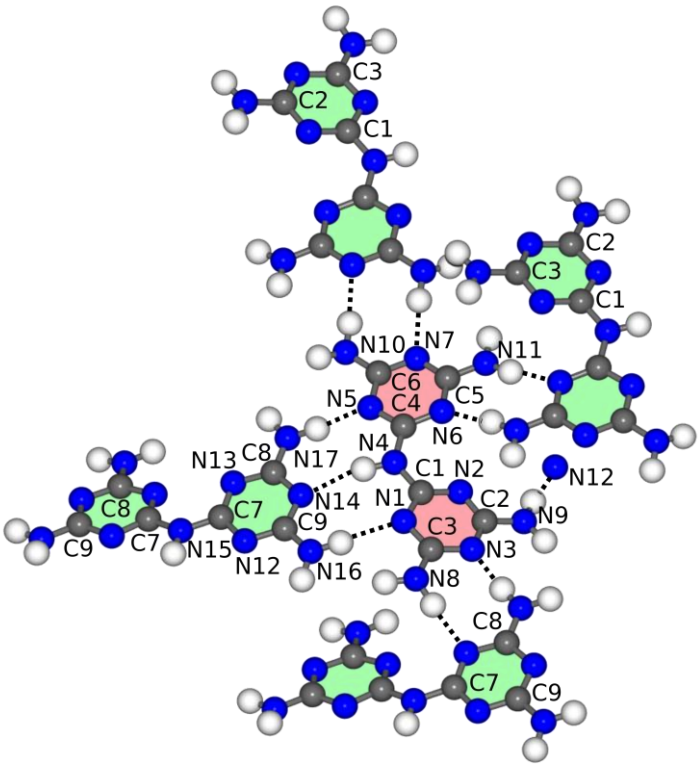

Figure 4.6 Cutout of the melam crystal structure obtained from periodic DFT calculations. C atoms in dark gray, N atoms in blue, H atoms in light gray. Dotted lines show hydrogen donor–acceptor arrangements that indicate possible hydrogen bonds. Melam molecules illustrated in red and green exhibit a negative and positive intramolecular torsion angle between the 1,3,5-triazine rings, respectively. Atom labels indicate symmetry equivalent molecules.

Donor–acceptor distances and N–H–N angles for the experimental and optimized melam structure are listed in Table 7.3.2. Values for both structures are in good agreement with each other and well in line with expected distances in comparable compounds. One hydrogen bond exhibits an unusually small optimized N-H-N angle of only 156.5° and thus probably indicates no, or only a weak interaction, however, it has been included in earlier reports on the experimental structure and thus is listed here for completeness. Intramolecular torsion angles between the triazine ring planes are provided in Table 7.3.3.

Melem crystallizes in space group $P2_1/c$, containing one melem molecule in the asymmetric unit. The molecule is slightly distorted from D_{3h} point symmetry. As for melam, deviations between calculated and measured lattice parameters are notable (see Table 4.3). The calculated relaxed structure using fixed experimental lattice parameters is shown in Figure 4.7. Donor-acceptor distances are given in Table 7.3.4. For one potential hydrogen bond, a distance of 3.66 Å—too large for an interaction—as well as an angle deviating strongly from 180° were found, so that this bond was not considered a hydrogen bond. Therefore, each melem molecule forms eight hydrogen bonds to five neighbors.

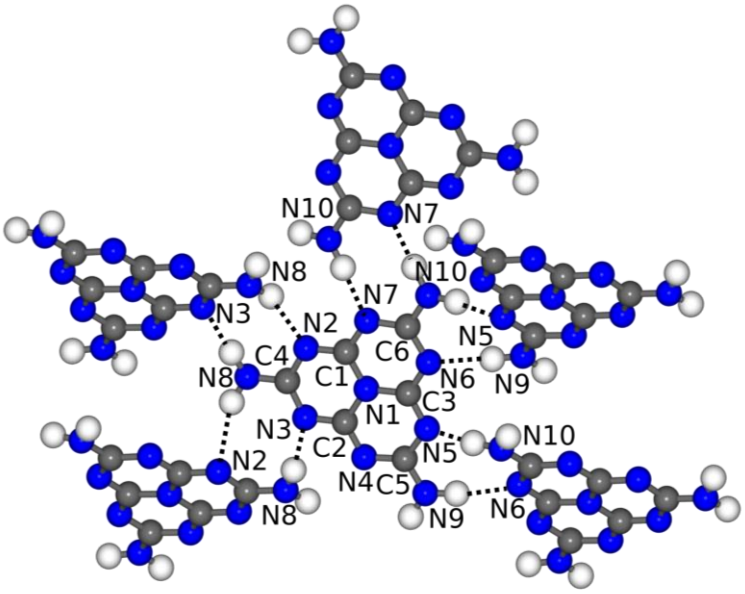

Figure 4.7 Cutout of the melem crystal structure obtained from periodic DFT calculations. C atoms in dark gray, N atoms in blue, H atoms in light gray. Dotted lines show hydrogen donor–acceptor arrangements that indicate possible hydrogen bonds. Atom labels indicate symmetry equivalent molecules.

Optimized structure

The DFT optimized structure of the melam-melem adduct obtained at the PBE-D3/pob-TZVP level of theory enables a close evaluation of structural parameters. Although the experimental model was refined in space group $P\bar{1}$, the calculation applied space group $P1$ due to technical limitations. Lattice parameters for full relaxation (Table 4.3) show deviations between experiment and DFT results that are slightly larger than for the optimized structures of melam and melem due to the larger standard deviation obtained for the adduct. A formation energy of $-6.2\,\mathrm{kJ\,mol^{-1}}$ was predicted for the melam-

melem adduct from pure melam and melem, at zero temperature without zero point vibrational energy correction conducting a PBE-D3/pob-TZVP structure optimization while using experimental lattice parameters. Including lattice relaxation, a formation energy of $-17.2\,\mathrm{kJ\,mol^{-1}}$ was obtained. The dominant energy change between these two results is contributed from the lattice relaxation of the melam-melem structure.

Structure optimization of the melam-melem adduct was performed with lattice parameters fixed to experimental values, since these yielded smaller errors (Table 7.3.5). Bond lengths and angles for comparable parts of molecules that seemed to deviate from each other in the crystallographic model due to its rather large standard deviations exhibit hardly any deviations in the DFT model. In the following, values for lengths and angles as obtained from quantum-chemical calculations are discussed in detail.

For melem molecules, the central N atoms exhibit an average distance of 1.41 Å towards the nearest (inner) C atoms, whereas ring N atoms form bonds of on average 1.33 Å towards inner C atoms and 1.36 Å towards outer C atoms. Angles deviate very little from the regular angle of 120°, with the exception of NCN-angles centered on C atoms bound to terminal amino groups, which show values of 125–126°, and CNC-angles at the outer N atoms with values between 117° and 118°. All of these values, as well as trends, are very well in line with reported values for pure melem, with calculated angles actually closer to regular hexagonal ring symmetry than reported for the pure compound.[24] Amino groups exhibit N–H bond lengths of on average 1.029 Å. HNH-angles are narrowed to 117–118° for the amino groups that form the dimer; other groups exhibit angles close to 120°. Within the dimer, hydrogen bridge donor–acceptor distances of 2.88 and 3.10 Å were found; distances towards the next bound melem unit are slightly longer (3.19 Å). All of these values are well in line with comparable distances in the optimized crystal structure of pure melem, in which similar motifs are found. We thus conclude that hydrogen bonds in both compounds are of comparable strength and contribute comparable binding energies to their respective structure. In contrast, the seeming melem-melem interactions that would elongate the zigzag chains would require two additional hydrogen bridges of lengths of 3.34 and 3.61 Å respectively, to be formed. Furthermore, hydrogen atoms show an orientation that is tilted by 19° to 27° away from their respective potential acceptor atom, making these interactions highly unlikely. Optimized bond distances for each respective hydrogen bond are given in Table 7.3.5.

For melam molecules, average C–N bond lengths of 1.35 Å could be determined for triazine rings, as well as for terminal amino groups. Those ring C–N bonds neighboring the imide bridge are on average 0.01 Å shorter than the remaining bonds. This phenomenon has been described for pure melam as well.[25] Imide bridges exhibit average C–N bond lengths of 1.39 Å and are thus significantly longer. Within the rings NCN-angles of 124–126° and CNC-angles of 114–116° were found. Again, these values are consistent with those reported for pure melam. As can be seen from the DFT model, triazine rings are not planar, but very slightly corrugated.

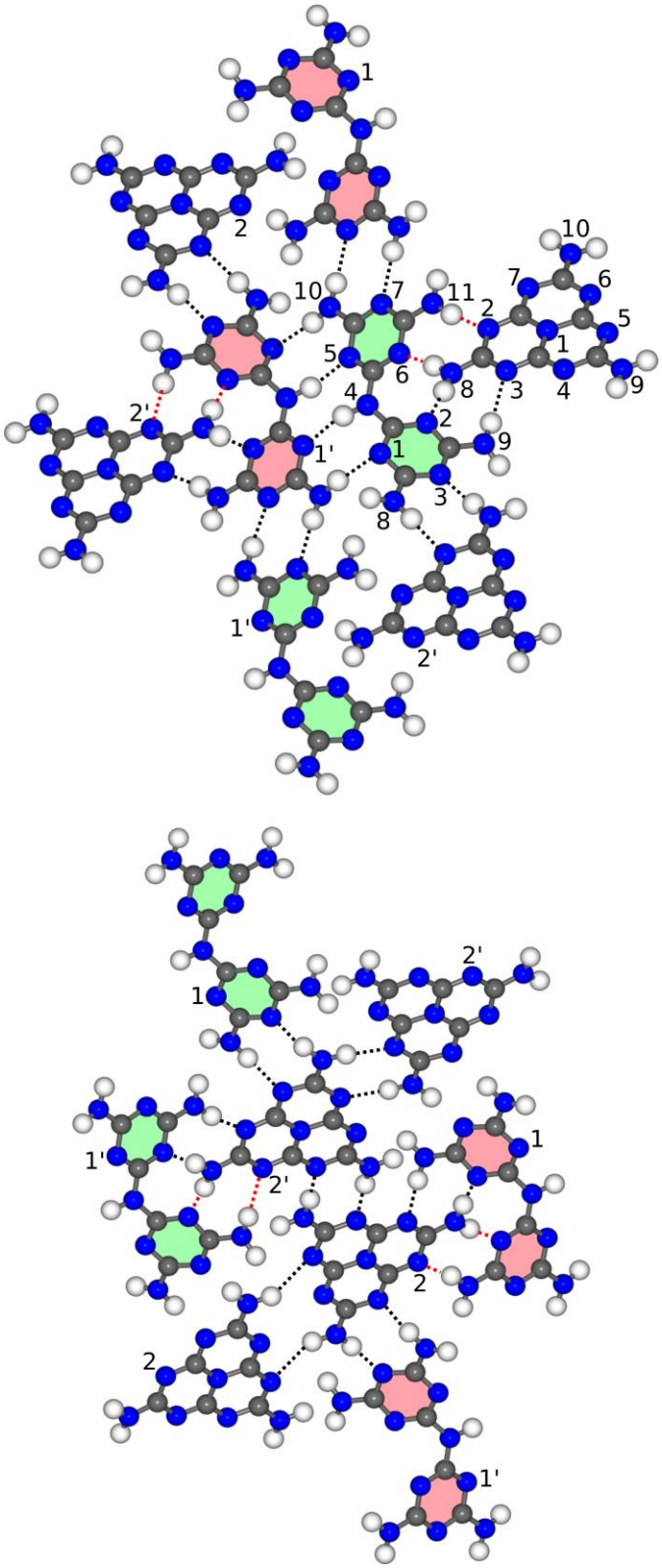

Figure 4.8 Cutout of the melam-melem crystal structure obtained from periodic DFT calculations. C atoms in dark gray, N atoms in blue, H atoms in light gray. Dotted lines show hydrogen donor–acceptor geometries that indicate possible hydrogen bonds. Red dotted lines point to molecules exactly covered by molecules visible in the illustration. Melam molecules illustrated in red and green exhibit a negative and positive intramolecular torsion angle between the 1,3,5-triazine rings, respectively. Atom labels indicate symmetry equivalent molecules.

Terminal amino groups are slightly tilted out of the ring plane with one group above und one group below the ring plane per triazine unit, which was not significant in the synchrotron model. Amino groups exhibit N–H distances of on average 1.03 Å, which appear reasonable in comparison with related compounds. HNH-angles are close to 120° for amino groups that are part of the melam "backbone" structure, however, they are slightly narrower (117–118°) for those groups facing outwards. Torsion angles were found to agree with those obtained from synchrotron data (see Table 7.3.3) within one standard deviation. Hydrogen bridges between two molecules of a melam dimer exhibit donor acceptor distances between 2.98 and 3.10 Å.

For "end-on-end" bonded melam molecules these bonds are slightly weaker, with bond lengths of 3.16 Å. Hydrogen atoms along the backbones of melam dimers are not well aligned between the respective donor and acceptor atoms, tilting out of line by 9–11°. It is unclear whether this represents the actual atomic alignment.

Imide N–H lengths are on average 0.01 Å longer than the respective distances in amino groups. Hydrogen bonding motifs in the melam-melem adduct differ from those in pure melam. Thus, no significant comparison of donor–acceptor distances was possible.

Hydrogen bonds as found in the optimized structure are depicted in Figure 4.8. Between melam and melem molecules, hydrogen bridge donor–acceptor distances ranging from 2.93 to 3.08 Å were found. All H atoms in these bonds appear reasonably well aligned. Comparing these distances to the ones found within the respective substructures, melam-melem interactions appear to be of similar strength to those found within the respective dimers, and slightly stronger than any further melam-melam or melem-melem hydrogen bonds, thus offering a possible explanation for the formation of the alternatingly layered structure.

All of these bond lengths are comparable to those found in various other non-ionic carbon nitride type compounds, for which donor-acceptor distances between 2.85 Å and 3.17 Å have been reported.[24,25,31] Hydrogen bridges are furthermore slightly shorter than in melamine-melem adducts for which average values of 3.1 Å have been found, indicating a stability at least equal to these.[27] Interactions with these distances have been classified as medium strong to weak.[25] All donor–acceptor distances and NHN-angles obtained from XRD, as well as from DFT, are given in Table 7.3.5.

Rietveld refinement

Rietveld refinements on X-ray powder diffractograms of several samples prepared in autoclave reactions as described above agree with the structure model obtained from synchrotron diffraction and quantum-chemical calculations. All of the samples contained the melam-melem adduct as the main phase, with phase contents amounting to 77–88 %. Figure 4.9 exemplarily depicts the Rietveld plot of a melam-melem adduct sample obtained at 450 °C after 9 days of heating under an initial ammonia pressure of 0.2 MPa. The respective sample shows a phase content for melam-melem of 88.0 %. The quantum-chemically optimized model was used for this refinement.

Side phases were identified as melam and melem, whose weight percentages could be refined based on reported structure models.[24,25] Melam proved to be the dominating side phase, with only minor contents of melem in the products.

All reflections appearing in the powder X-ray diffraction pattern could be explained by a combination of the adduct phase, melam and melem. Difference plots show minor problems in fitting certain reflection intensities, indicating some shortcomings of the model. Lattice parameters from powder data (a=4.5098(2), b=19.1556(9) and c=21.3040(9) Å and angles α=73.452(3)°, β=89.447(3)° and γ=88.547(3)°) agree with single-crystal parameters within 3σ.

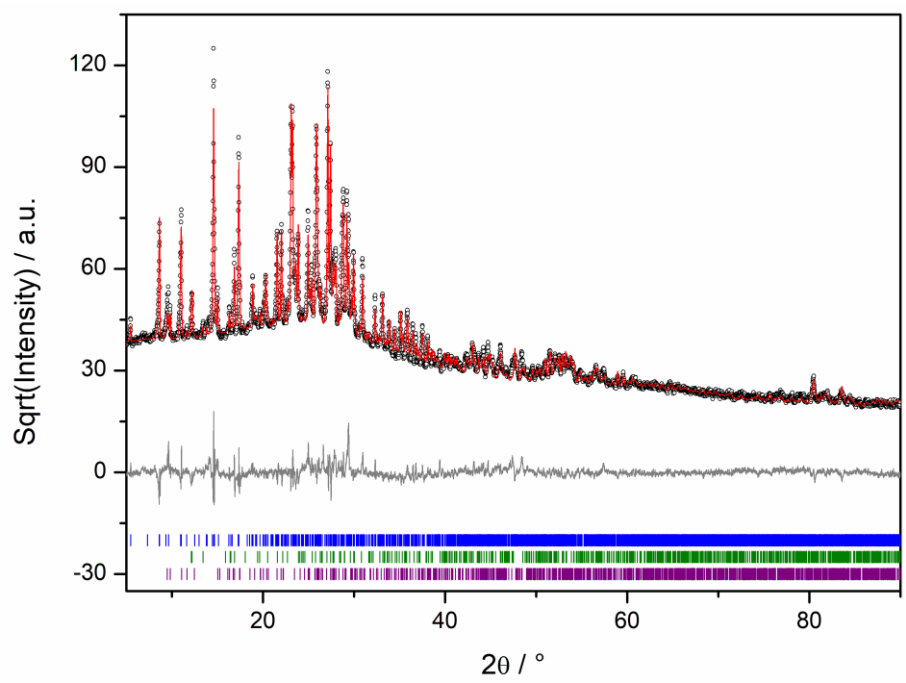

Figure 4.9 Results of the Rietveld refinement on a representative sample from autoclave synthesis. Measured data are displayed as black circles, the calculated model from the fitted pattern is plotted in red. The difference plot is displayed in gray below. Blue reflection markers indicate theoretical Bragg positions of the melam-melem adduct, green markers those of melem, violet markers those of melam.

NMR spectroscopy

NMR spectra of the melam-melem adduct were given in our previous publication.[28] Since chemical shifts are strongly influenced by their local environment and thus structural motifs (e.g., hydrogen bridge motifs), these could not be interpreted up to now since the crystal structure was unknown.

In this work, NMR shifts for local clusters cut from this model were calculated based on the optimized structure model at the B97-2/pcSseg-1 level using the FermiONs++ program package[34-36] and compared to experimental shifts. NMR shifts were calculated for ^{1}H, ^{13}C, and ^{15}N for a melam-dimer and a melem-dimer taken from the central part of the model cluster. Since clusters had to be cut to moderate sizes to make the calculations computationally affordable, only a fraction of the calculated shifts proved to be of significance.

^{1}H shifts of 10.8 to 11.0 ppm were calculated for melam imide H atoms. Shifts for amino H atoms of melam, as well as melem, range from 7.9 to 11.6 ppm. H atoms towards the cluster edges tend to exhibit lower shifts, thus, it is possible that larger clusters might yet yield more consistent shifts. Experimental data, however, show a spectrum consisting of a single, extremely broadened signal; thus a detailed comparison was not possible.

Three different groups of ^{13}C signals were obtained for melam C atoms, melem C atoms bound to amino groups, and inner melem C atoms, respectively. Calculations yield very uniform shifts for each signal group. Melam C atoms were found at about 172.9 ppm, melem outer C atoms at 169.4 ppm, and melem inner C atoms at 160.4 ppm. Compared to experimental spectra, which show resonances at 166.9, 163.4, and 154.4 ppm, this is in excellent agreement when assuming a systematic offset of 6 ppm caused by methodical errors, as well as the limited size of the clusters.

As could be seen from previously published spectra,[28] the pattern of ^{15}N resonances is rather complicated. Three different signal groups can be discerned for melem and melam each, some of which overlap. Additionally, some of these signal groups spread over rather large ranges. For the melem molecules, different signals are expected for the central N atom of the heptazine nucleus (calculated at −214.5 ppm respective to nitromethane), the amino N atoms (found between −253.8 and −264.7 ppm), and outer tertiary N atoms of the heptazine ring (found between −172.3 and −191.69 ppm). In the case of melam, the different signal groups result from the imide N atom (at

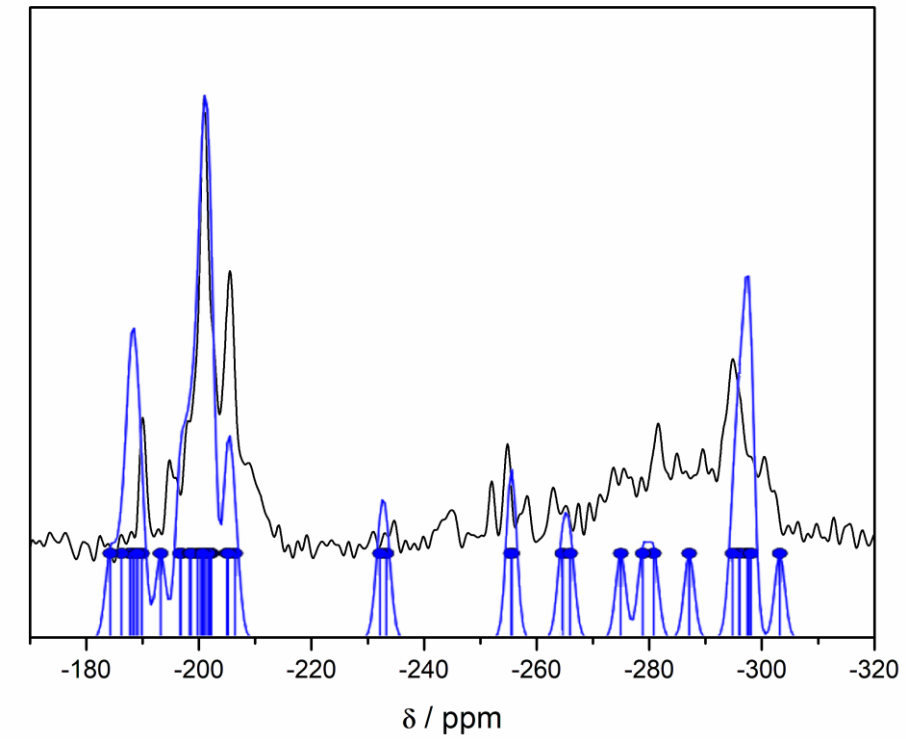

Figure 4.10 Experimental ^{15}N NMR spectrum of the melam-melem adduct in black, and calculated spectrum based on the theoretical model in blue. The theoretical spectrum has been shifted by −14 ppm to account for different environmental conditions.

−241.9 ppm), amino N atoms (between −280.6 and −283.3 ppm), and tertiary N atoms of the triazine rings (between −172.9 and −176.0 ppm).

The huge number of signals, parts of which show strong overlap, make it difficult to assign specific atoms to experimental resonances. However, a comparison between the overall experimental and calculated spectra is possible. As in the ^{13}C NMR spectra, it proved necessary to shift the entire spectrum due to methodical errors, here by −14 ppm. As can be seen in Figure 4.10, the shifted calculated spectrum fits the experimental one reasonably. Certain maxima display minor shifts in position and not all of the less intense experimental signals could be reproduced. We attribute this to the limitation of the cluster sizes, as well as the mediocre signal-to-noise ratio exhibited by the experimental spectrum, which makes unambiguous allocations difficult. Since Rietveld refinements show that samples were not phase pure, it can be assumed that at least part of this is also due to side phase signals.

Figure 7.3.5 compares the ^{15}N NMR spectrum of the adduct to those of side phases melam and melem. It can be seen that several intense signals are exclusive to the melam-melem adduct, and thus not simply caused by a combination of building block intrinsic resonances. A complete list of calculated ^{15}N NMR shifts is given in Tables 7.3.6, 7.3.7 and 7.3.8.

The overall consistency of experimental NMR shifts and shifts calculated based on the optimized structure model is reasonable, which corroborates the validity of this model.

4.3 Conclusions

Melam-melem, an adduct compound that has so far eluded structural elucidation, could be characterized in a combined approach of single-particle synchrotron diffractometry and quantum-chemical calculations. A structure model was obtained from synchrotron data and optimized on the PBE-D3/pob-TZVP level of theory.

The composition of the adduct was determined as melam-melem 1:1. Within the structure, both components form dimers, which are arranged in alternating strands. These strands are stacked along [1 0 0] with a stacking distance equal to the *a* lattice parameter. As in pure melam, the melam-melem adduct exhibits no marked π–π stacking. Van-der-Waals interactions thus seem to play no significant role in the formation of this structure. Instead, we attribute a major role to hydrogen bridge bonds. These are further assumed to be the cause for unusually large dihedral angles of 48° found in melam units. The large angles enable the formation of hydrogen bridges towards melem molecules in different layers of melem stacks and vice versa. However, quantum-chemical structure calculations for a gas phase melam dimer showed dihedral angles that are only slightly smaller than those found in the adduct compound, so these interactions cannot unambiguously be named the reason for the unusually large angle.

NMR shifts were calculated for the optimized structure on the B97-2/pcS-2 level of theory and compared to experimentally obtained shifts. A reasonable agreement between these sets of shifts was found, providing further evidence for the validity to the model.
Rietveld refinements show that the synthesis process for the melam-melem-adduct as described in previous work[28] does not yield phase pure products, but mixtures of the title compound, melam, and melem. This further emphasizes the thermodynamic instability and intermediate role in the condensation process of the adduct compound.

4.4 Experimental Section

Synthesis of the melam-melem adduct: The melam-melem adduct phase was synthesized by heating dicyandiamide (1 g, 11.9×10^{-3} mol, ≥99 %, Avocado) at elevated ammonia pressure (ca. 0.1 to 0.3 MPa) in a Parr stainless steel autoclave with silica glass inlay, to temperatures of 450 to 500 °C. Temperature was held for 9 to 13 days before the autoclave was cooled down at a rate of 1 °C min^{-1} and the pressure released. A sublimate phase of melamine was found at the top of the autoclave, while the melam-melem adduct was found at the bottom of the inlay. No significant influence of respectively chosen reaction parameters on sample composition or quality could be observed within the abovementioned parameter ranges. All herein described measurements were conducted on a sample obtained at 450 °C after 9 days of dwell time with an initial ammonia pressure of 0.2 MPa.
Synchrotron X-ray diffraction: For synchrotron X-ray diffraction, a suitable lath-shaped crystallite of ca. 4 µm diameter and 20 µm length was selected by TEM and characterized by electron diffraction. The same crystallite was used for data collection at beamline ID11 of the European Synchrotron Radiation Facility (ESRF), Grenoble.[37] The TEM grid was mounted on a heavy-duty Huber goniometer at beamline ID11. Fluorescence from the copper crossbars of the TEM grid, which served as “landmarks”, was used to recover the crystallite at the beamline. A single-crystal dataset was measured using a 0.7×2 µm synchrotron beam, microfocused by compound refractive lenses at a wavelength of 0.29464 Å (42.0799 keV, Si(1 1 1) double monochromator). The beam was focused at the tip of the crystallite, where diffraction patterns exhibited the best quality. Data were collected using a Frelon2K detector with 2048×2048 pixels and a dynamic range of 2^{16}. CCDC 1904950 contains the supplementary crystallographic data for this paper. These data can be obtained free of charge from The Cambridge Crystallographic Data Centre.
Quantum-chemical calculations: Structure optimizations of molecular systems were performed using the Perdew–Burke–Ernzerhof (PBE) exchange-correlation functional[38] and the corresponding hybrid functional, PBE0.[39] All DFT calculations were conducted with triple-zeta basis sets plus polarization functions (TZVP).[40] In one selected case, a quadruple-zeta basis (QZVP)[41] was used. Additional PBE calculations included Grimme's dispersion correction, PBE-D3,[42] in energy and gradients. Random phase approximation (RPA) calculations used PBE Kohn–Sham orbitals, indicated

by the term RPA@PBE, and TZVP basis sets. If computationally affordable, then QZVP basis sets were used for RPA in addition. All DFT and RPA calculations in the present work make use of the resolution of the identity (RI) approximation,[43] with the corresponding auxiliary basis sets.[44,45][IR spectra were simulated using unscaled harmonic vibrational frequencies and intensities calculated in the harmonic approximation from analytical derivatives of the dipole moment. Line spectra were convoluted using a Gaussian line shape function.

For crystal structure optimization, TZVP basis sets optimized for solids from *Peintinger et al.* were used.[46] Crystal structure calculations do not use point symmetry. Structures were relaxed starting from experimental ones, once with lattice parameters fixed to experimental values and once with lattice optimization. Calculations with a fixed lattice were conducted using 3×3×3 k-points. For lattice optimizations, the k-point grid was increased for melem and melam-melem adduct crystals to 5×5×5 and 5×3×3, respectively.

Rotational Constants were calculated using Equation 4.1:

$$A = \frac{h}{8\pi^2 I_A} \tag{4.1}$$

with principal moments of inertia I_A, I_B and I_C, obtained from optimized geometries.

Atom site coordinates for melam-melem (1:1) as obtained from these calculations are given in Table 7.3.9.

Acknowledgements

We thank the ESRF, Grenoble, for granting synchrotron beamtime (project HS-4625). Dr. Loredana Erra, Dr. Felix Fahrnbauer and Tilo Schmutzler are acknowledged for their help during the synchrotron measurements. Financial support by the Deutsche Forschungsgemeinschaft DFG (project SCHN 377/15-1) and the Fonds der Chemischen Industrie (FCI) is gratefully acknowledged. A.M.B. acknowledges financial support by a FCI Liebig fellowship. C.O. acknowledges in addition financial support as Max-Planck-Fellow at the MPI-FKF in Stuttgart.

4.5 References

[1] E. Kroke, M. Schwarz, "Novel group 14 nitrides", *Coord. Chem. Rev.* **2004**, *248*, 493-532.

[2] A. Thomas, A. Fischer, F. Goettmann, M. Antonietti, J. O. Müller, R. Schlögl, J. M. Carlsson, "Graphitic carbon nitride materials: variation of structure and morphology and their use as metal-free catalysts", *J. Mater. Chem.* **2008**, *18*, 4893-4908.

[3] A. Schwarzer, T. Saplinova, E. Kroke, "Tri-s-triazines (s-heptazines)—From a “mystery molecule” to industrially relevant carbon nitride materials", *Coord. Chem. Rev.* **2013**, *257*, 2032-2062.

[4] F. K. Kessler, Y. Zheng, D. Schwarz, C. Merschjann, W. Schnick, X. Wang, M. J. Bojdys, "Functional carbon nitride materials — design strategies for electrochemical devices", *Nat. Rev. Mater.* **2017**, *2*, 17030.

[5] X. Li, A. F. Masters, T. Maschmeyer, "Polymeric carbon nitride for solar hydrogen production", *Chem. Commun.* **2017**, *53*, 7438-7446.

[6] T. S. Miller, A. B. Jorge, T. M. Suter, A. Sella, F. Cora, P. F. McMillan, "Carbon nitrides: synthesis and characterization of a new class of functional materials", *Phys. Chem. Chem. Phys.* **2017**, *19*, 15613-15638.

[7] A. Y. Liu, M. L. Cohen, "Prediction of New Low Compressibility Solids", *Science* **1989**, *245*, 841-842.

[8] A. Y. Liu, M. L. Cohen, "Structural properties and electronic structure of low-compressibility materials: β-C_3N_4 and hypothetical β-C_3N_4", *Phys. Rev. B* **1990**, *41*, 10727-10734.

[9] D. M. Teter, R. J. Hemley, "Low-Compressibility Carbon Nitrides", *Science* **1996**, *271*, 53-55.

[10] X. Wang, K. Maeda, A. Thomas, K. Takanabe, G. Xin, J. M. Carlsson, K. Domen, M. Antonietti, "A metal-free polymeric photocatalyst for hydrogen production from water under visible light", *Nat. Mater.* **2009**, *8*, 76-80.

[11] K. Schwinghammer, M. B. Mesch, V. Duppel, C. Ziegler, J. Senker, B. V. Lotsch, "Crystalline Carbon Nitride Nanosheets for Improved Visible-Light Hydrogen Evolution", *J. Am. Chem. Soc.* **2014**, *136*, 1730-1733.

[12] K. Schwinghammer, B. Tuffy, M. B. Mesch, E. Wirnhier, C. Martineau, F. Taulelle, W. Schnick, J. Senker, B. V. Lotsch, "Triazine-based Carbon Nitrides for Visible-Light-Driven Hydrogen Evolution", *Angew. Chem.* **2013**, *125*, 2495-2499; *Angew. Chem. Int. Ed.* **2013,** *52*, 2435-2439.

[13] V. W.-h. Lau, M. B. Mesch, V. Duppel, V. Blum, J. Senker, B. V. Lotsch, "Low-Molecular-Weight Carbon Nitrides for Solar Hydrogen Evolution", *J. Am. Chem. Soc.* **2015**, *137*, 1064-1072.

[14] J. Liu, Y. Liu, N. Liu, Y. Han, X. Zhang, H. Huang, Y. Lifshitz, S.-T. Lee, J. Zhong, Z. Kang, "Metal-free efficient photocatalyst for stable visible water splitting via a two-electron pathway", *Science* **2015**, *347*, 970-974.

[15] V. S. Vyas, V. W.-h. Lau, B. V. Lotsch, "Soft Photocatalysis: Organic Polymers for Solar Fuel Production", *Chem. Mater.* **2016**, *28*, 5191-5204.

[16] G. Zhang, Z.-A. Lan, L. Lin, S. Lin, X. Wang, "Overall water splitting by Pt/g-C_3N_4 photocatalysts without using sacrificial agents", *Chem. Sci.* **2016**, *7*, 3062-3066.

[17] V. W.-h. Lau, V. W.-z. Yu, F. Ehrat, T. Botari, I. Moudrakovski, T. Simon, V. Duppel, E. Medina, J. K. Stolarczyk, J. Feldmann, V. Blum, B. V. Lotsch, "Urea-Modified Carbon Nitrides: Enhancing Photocatalytic Hydrogen Evolution by Rational Defect Engineering", *Adv. Energy Mater.* **2017**, *7*, 1602251.

[18] V. W.-h. Lau, D. Klose, H. Kasap, F. Podjaski, M.-C. Pignié, E. Reisner, G. Jeschke, B. V. Lotsch, "Dark Photocatalysis: Storage of Solar Energy in Carbon Nitride for Time-Delayed Hydrogen Generation", *Angew. Chem.* **2017**, *129*, 525-529; *Angew. Chem. Int. Ed.* **2017**, *56*, 510-514.

[19] K. Bretterbauer, C. Schwarzinger, "Melamine Derivatives – A Review on Synthesis and Application", *Curr. Org. Synth.* **2012**, *9*, 342-356.

[20] Y. Wang, X. Wang, M. Antonietti, "Polymeres graphitisches Kohlenstoffnitrid als heterogener Organokatalysator: von der Photochemie über die Vielzweckkatalyse hin zur nachhaltigen Chemie", *Angew. Chem.* **2012**, *124*, 70-92; *Angew. Chem. Int. Ed.* **2012**, *51*, 68-89.

[21] B. V. Lotsch, M. Döblinger, J. Sehnert, L. Seyfarth, J. Senker, O. Oeckler, W. Schnick, "Unmasking Melon by a Complementary Approach Employing Electron Diffraction, Solid-State NMR Spectroscopy, and Theoretical Calculations—Structural Characterization of a Carbon Nitride Polymer", *Chem. Eur. J.* **2007**, *13*, 4969-4980.

[22] The Market Publishers Ltd., "World Melamine Supply to Exceed 2 Mln Tonnes in 2018, According to In-demand Report by Merchant Research & Consulting", **2014**. Available at: http://www.prweb.com/releases/2014/02/prweb11582781.htm, accessed January 31, 2018.

[23] H. May, "Pyrolysis of melamine", *J. Appl. Chem.* **1959**, *9*, 340-344.

[24] B. Jürgens, E. Irran, J. Senker, P. Kroll, H. Müller, W. Schnick, "Melem (2,5,8-Triamino-tri-s-triazine), an Important Intermediate during Condensation of Melamine Rings to Graphitic Carbon Nitride: Synthesis, Structure Determination by X-ray Powder Diffractometry, Solid-State NMR, and Theoretical Studies", *J. Am. Chem. Soc.* **2003**, *125*, 10288-10300.

[25] B. V. Lotsch, W. Schnick, "New Light on an Old Story: Formation of Melam during Thermal Condensation of Melamine", *Chem. Eur. J.* **2007**, *13*, 4956-4968.

[26] M. Shahbaz, S. Urano, P. R. LeBreton, M. A. Rossman, R. S. Hosmane, N. J. Leonard, "Tri-s-triazine: synthesis, chemical behavior, and spectroscopic and theoretical probes of valence orbital structure", *J. Am. Chem. Soc.* **1984**, *106*, 2805-2811.

[27] A. Sattler, S. Pagano, M. Zeuner, A. Zurawski, D. Gunzelmann, J. Senker, K. Müller-Buschbaum, W. Schnick, "Melamine–Melem Adduct Phases: Investigating the Thermal Condensation of Melamine", *Chem. Eur. J.* **2009**, *15*, 13161-13170.

[28] E. Wirnhier, M. B. Mesch, J. Senker, W. Schnick, "Formation and Characterization of Melam, Melam Hydrate, and a Melam–Melem Adduct", *Chem. Eur. J.* **2013**, *19*, 2041-2049.

[29] E. Mugnaioli, T. Gorelik, U. Kolb, "“Ab initio” structure solution from electron diffraction data obtained by a combination of automated diffraction tomography and precession technique", *Ultramicroscopy* **2009**, *109*, 758-765.

[30] U. Kolb, E. Mugnaioli, T. E. Gorelik, "Automated electron diffraction tomography – a new tool for nano crystal structure analysis", *Cryst. Res. Technol.* **2011**, *46*, 542-554.

[31] E. W. Hughes, "The Crystal Structure of Melamine", *J. Am. Chem. Soc.* **1941**, *63*, 1737-1752.

[32] N. E. Braml, A. Sattler, W. Schnick, "Formation of Melamium Adducts by Pyrolysis of Thiourea or Melamine/NH_4Cl Mixtures", *Chem. Eur. J.* **2012**, *18*, 1811-1819.

[33] F. K. Kessler, T. J. Koller, W. Schnick, "Synthesis and Structure of Melamium Bromide $C_6N_{11}H_{10}Br$ and Melamium Iodide $C_6N_{11}H_{10}I$", *Z. Anorg. Allg. Chem.* **2018**, *644*, 186-192.

[34] J. Kussmann, C. Ochsenfeld, "Pre-selective screening for matrix elements in linear-scaling exact exchange calculations ", *J. Chem. Phys.* **2013**, *138*, 134114.

[35] J. Kussmann, C. Ochsenfeld, "Preselective Screening for Linear-Scaling Exact Exchange-Gradient Calculations for Graphics Processing Units and General Strong-Scaling Massively Parallel Calculations", *J. Chem. Theory Comput.* **2015**, *11*, 918-922.

[36] J. Kussmann, C. Ochsenfeld, "Hybrid CPU/GPU Integral Engine for Strong-Scaling Ab Initio Methods", *J. Chem. Theory Comput.* **2017**, *13*, 3153-3159.

[37] F. Fahrnbauer, T. Rosenthal, T. Schmutzler, G. Wagner, G. B. M. Vaughan, J. P. Wright, O. Oeckler, "Entdeckung und Strukturbestimmung eines ungewöhnlichen Sulfidtellurids mithilfe einer effektiven Kombination von TEM und Synchrotron-Mikrodiffraktion", *Angew. Chem.* **2015**, *127*, 10158-10161; *Angew. Chem. Int. Ed.* **2015**, *54*, 10020-10023.

[38] J. P. Perdew, K. Burke, M. Ernzerhof, "Generalized Gradient Approximation Made Simple", *Phys. Rev. Lett.* **1996**, *77*, 3865-3868.

[39] C. Adamo, V. J. Barone, "Toward reliable density functional methods without adjustable parameters: The PBE0 model ", *J. Chem. Phys.* **1999**, *110*, 6158-6170.

[40] A. Schäfer, C. Huber, R. Ahlrichs, "Fully optimized contracted Gaussian basis sets of triple zeta valence quality for atoms Li to Kr", *J. Chem. Phys.* **1994**, *100*, 5829-5835.

[41] F. Weigend, R. Ahlrichs, "Balanced basis sets of split valence, triple zeta valence and quadruple zeta valence quality for H to Rn: Design and assessment of accuracy ", *Phys. Chem. Chem. Phys.* **2005**, *7*, 3297-3305.

[42] S. Grimme, J. Antony, S. Ehrlich, H. Krieg, "A consistent and accurate ab initio parametrization of density functional dispersion correction (DFT-D) for the 94 elements H-Pu.", *J. Chem. Phys.* **2010**, *132*, 154104.

[43] E. J. Baerends, D. E. Ellis, P. Ros, "Self-consistent molecular Hartree—Fock—Slater calculations I. The computational procedure", *Chem. Phys.* **1973**, *2*, 41-51.

[44] F. Weigend, "Accurate Coulomb-fitting basis sets for H to Rn ", *Phys. Chem. Chem. Phys.* **2006**, *8*, 1057-1065.

[45] C. Hättig, G. Schmitz, J. Koßmann, "Auxiliary basis sets for density-fitted correlated wavefunction calculations: weighted core-valence and ECP basis sets for post-d elements", *Phys. Chem. Chem. Phys.* **2012**, *14*, 6549-6555.

[46] M. F. Peintinger, D. V. Oliveira, T. Bredow, "Consistent Gaussian basis sets of triple-zeta valence with polarization quality for solid-state calculations", *J. Comput. Chem.* **2013**, *34*, 451-459.

5. Polymeric Compounds

5.1 On the Formation of Poly(triazine imide)

From Heptazines to Triazines—On the Formation of Poly(triazine imide)

Fabian K. Kessler, and Wolfgang Schnick

Published in: *Z. Anorg. Allg. Chem.* **2019**, *645*, 857-862.

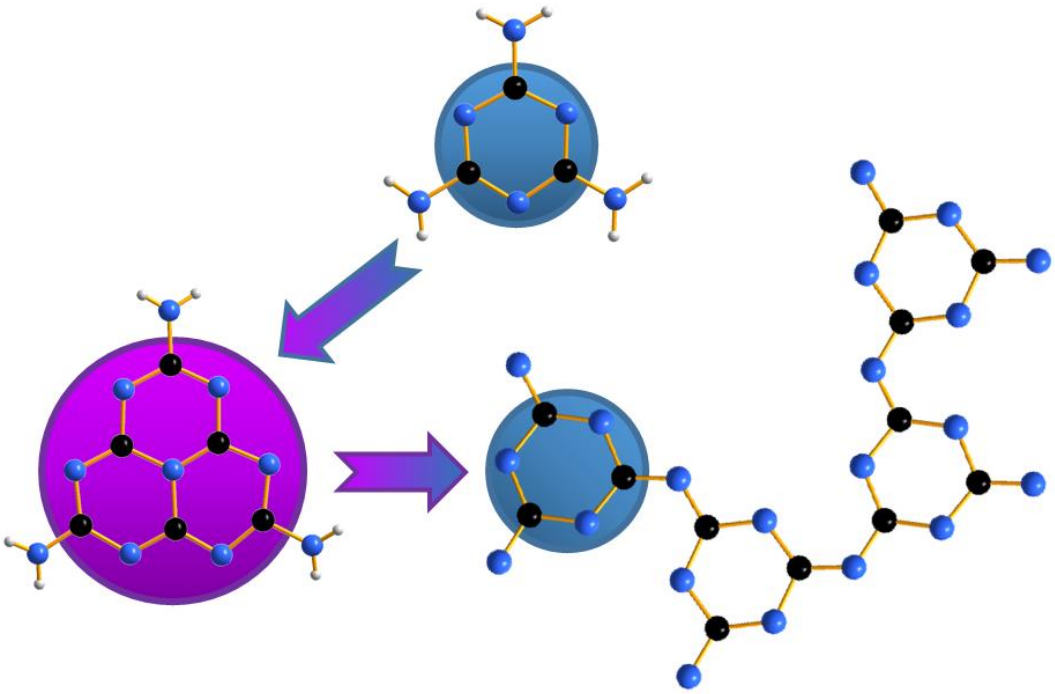

Abstract

Poly(triazine imide), a 2D extended carbon nitride network compound that is obtained from ionothermal synthesis in LiCl/KCl or LiBr/KBr salt melt has been known for over a decade. We now have investigated the formation process of this material starting from various triazine- and heptazine-based precursors as well as the differences between ionothermal and conventional synthesis via thermal condensation. Independent of chosen starting material, melem (triamino-*s*-heptazine) is initially formed from the starting material as the imminent precursor to poly(triazine imide). We

elucidate the impact of various different carbon nitride precursor compounds on the formation process, propose a mechanism for the back reaction of heptazines to triazines, and rationalize the occurring processes.

5.1.1 Introduction

Recent research in carbon nitride chemistry concerns itself almost exclusively with a single compound, namely polymeric carbon nitride (PCN), often also denoted as *Liebig's* melon or misleadingly as graphitic C_3N_4 (g-C_3N_4).[1-3] This material with an approximate composition close to $C_6N_9H_3$ that, however, shows some variability, exhibits electronic properties that make it a promising candidate as a photocatalyst for various applications, such as pollutant degradation for wastewater purification, bacterial disinfection, CO_2 reduction for photochemical fuel generation and most prominently H_2 generation via photocatalytic water splitting.[4,5] The means to optimize PCN for these purposes include nanostructuring, metal and non-metal doping and formation of heterojunctions and composite materials of various kinds.[6-9] While the number of different approaches is large, the basic material almost always stays the same. Other carbon nitride materials, that exhibit very similar properties, are often overlooked due to a more complex synthesis process or simply because they are less known.

One such compound that especially deserves attention is poly(triazine imide) (PTI), an intercalation compound obtained from lithium halide salt melts.[10,11] PTI is a 2D layered material based on sheets of imide-connected triazine rings. This is in stark contrast to PCN, which is generally assumed to be based on heptazine units interconnected by imide groups.[12,13] The structure of poly(triazine imide) contains hexagonal channels along the crystallographic *c* axis in which Li^+ and X^- (X = F, Cl, Br) ions are incorporated.[11,14] Consequently, these compounds are often also denoted as PTI/Li^+X^-. For the carbon nitride network a sum formula of $C_6N_9H_3$ is obtained, which is identical to the formula of heptazine-based melon, an idealized variant of PCN.[15,16] Furthermore, PTI/Li^+Cl^-, the most well characterized compound in this family, is known to possess H/Li disorder, thereby incorporating additional Li^+ ions that substitute imide bound protons, resulting in a formula of $[(C_3N_3)_2(NH_xLi_{1-x})_3 \cdot LiCl]$.[17]

PTI, just as PCN, exhibits an extended conjugated π-system and therefore likewise is a semiconductor, with a bandgap of 2.8 eV.[18] This is very close to PCN, for which a bandgap of 2.7 eV has been reported.[19] However, for PTI it has been shown that the bandgap directly depends on the degree of LiCl loading and drops from 2.8 eV in the absence of LiCl to 2.2 eV for fully loaded PTI/Li^+Cl^-. This should give PTI a significant advantage over PCN concerning photocatalytic applications, since tunability of the bandgap is crucial in the optimization of light harvesting. Photocatalysis experiments showed that crystalline PTI exhibits a 20 % increased hydrogen evolution rate compared to raw melon, as well as an increased oxygen evolution rate in the complementary half-reaction of water

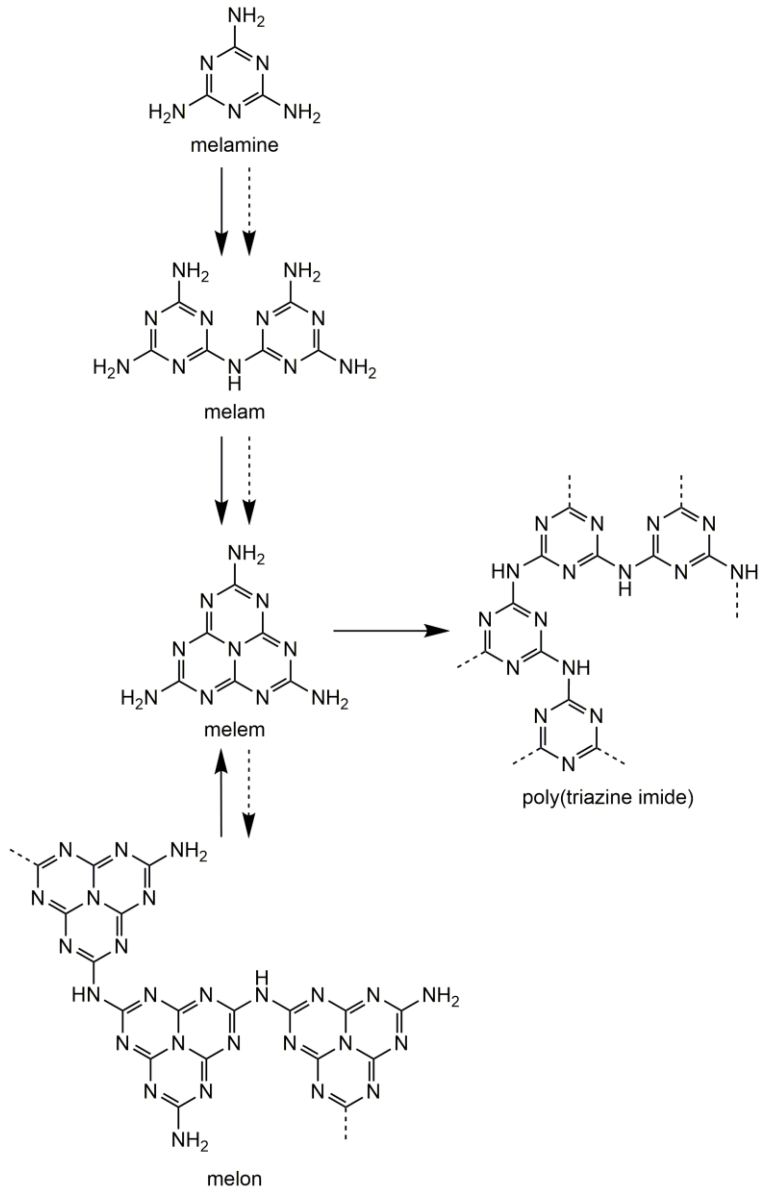

Figure 5.1.1 Carbon nitride compounds and condensation reaction pathways. Dashed arrows indicate reaction pathways of thermal condensation, bold arrows indicate reaction pathways in salt melt.

splitting.[20,21] This can be rationalized not only by more suitable electronic properties, but also a much higher surface area for PTI.[21] Doping of PTI with more carbon-rich heterocycles such as 4-amino-2,6-dihydroxypyrimidine or 2,4,6-triaminopyrimidine further increases the photocatalytic activity to up to 6 times the activity measured for melon-based materials.[20,22] Nanostructuring of PTI via exfoliation is reported to yield PTI nanosheets whose photocatalytic activity is 8 times that of PCN and 17 times the activity of raw melon.[23]

Apart from water splitting, several other potential applications for PTI have been proposed in recent years. In dye-sensitized solar cells PTI-based counter electrodes could replace conventional Pt electrodes, thereby dramatically reducing the prize while maintaining a comparable power conversion efficiency.[24] Due to its porosity, PTI has also been proposed as a N_2-selective membrane for flue gas purification.[25] Furthermore, it deserves mention that an even higher condensed carbon nitride phase of composition C_3N_4 has reportedly been found as a side phase in PTI/Li^+Br^- syntheses. This triazine-based graphitic carbon nitride (TGCN) is noteworthy in that it represents the only known carbon nitride phase that is completely free of hydrogen.[26]

Thus, PTI appears to be a material of great significance. However, apart from the necessity of salt melts in the synthetic process very little is known about its formation. For PCN (or melon) the formation process is well known (Figure 5.1.1). Starting from the molecular precursor melamine (triamino-*s*-triazine) a cascade of thermally induced condensation reactions is started, leading initially

to the formation of the dimeric triazine compound melam [bis(diamino-*s*-triazinyl)amine], which under further deammonation forms melem (triamino-tri-*s*-triazine). At further elevated temperatures melem condenses into heptazine-based polymers that make up PCN.[12,15,27,28]

It should be noted that above temperatures of 380 °C all of the compounds appearing in this reaction cascade are heptazine-based.[28] The formation of triazine-based PTI at 550 °C exemplifies the fundamental influence of salt melts as a reaction medium. This contrast to classic solid-state syntheses makes the investigation of the occurring mechanisms all the more important.

In this work, we have examined the formation mechanism of PTI/Li^+Cl^- and PTI/Li^+Br^- in order to gain further insights into these promising materials as well as the fundamental mechanisms in the formation of carbon nitride compounds in general.

5.1.2 Results and Discussion

In order to elucidate the formation pathway of PTI, several series of synthesis experiments were conducted. PTI/Li^+Cl^- and PTI/Li^+Br^- were synthesized in LiCl/KCl and LiBr/KBr salt melts, respectively, according to literature.[10,14] Mixtures of the respective salt melt and varying carbon nitride precursors—namely dicyandiamide, melamine, melam, melem, and melon—in a weight ratio of 5:1 were sealed in silica glass ampoules, quickly heated to reaction temperature and then rapidly quenched after a defined amount of time by submerging the hot ampoules in ice water. Both salt melts were applied in copious excess. The obtained products were identified by IR spectroscopy and powder X-ray diffractometry. Results of syntheses in LiCl/KCl melt are listed in Table 5.1.1 and for LiBr/KBr melt in Table 5.1.2.

Products obtained after each time step can be seen as intermediate steps in the condensation process of PTI. In the case of the chloride salt melt as well as the bromide salt melt the reactions appear to proceed with only moderate speed so that defined intermediate products, themselves thermodynamically stable compounds, could be isolated. Starting materials with a low degree of condensation yielded especially valuable insights, as they allowed us to map the complete pathway of PTI condensation. In LiCl/KCl, dicyandiamide yielded melam after 5 min and it took up to 20 min to

Table 5.1.1 Products obtained from syntheses in LiCl/KCl melt after defined amounts of time.

Starting material	Product after 5 min	Product after 10 min	Product after 20 min	Product after 30 min	Product after 120 min	Product after 720 min
Dicyan-diamide	Melam	Melem + melam	Melem	Melem	PTI/Li^+Cl^-	PTI/Li^+Cl^-
Melamine	Melamine + melam	Melem + melam	Melem+ melam	Melem	PTI/Li^+Cl^-	PTI/Li^+Cl^-
Melam	Melam	Melem	Melem	Melem	PTI/Li^+Cl^-	PTI/Li^+Cl^-
Melem	Melem	Melem	Melem	Melem	PTI/Li^+Cl^-	PTI/Li^+Cl^-
Melon	Melon	Melon	Melon	Melon	Melon	PTI/Li^+Cl^-

Table 5.1.2 Products obtained from syntheses in LiBr/KBr melt after defined amounts of time.

Starting material	Product after 5 min	Product after 10 min	Product after 20 min	Product after 30 min	Product after 120 min	Product after 720 min
Dicyan-diamid	Melem	Melem	Melem	Melem	PTI/Li^+Br^-	PTI/Li^+Br^- + melem
Melamine	Melem	Melem	Melem	Melem	PTI/Li^+Br^-	PTI/Li^+Br^- + melem
Melam	Melem	Melem	Melem	Melem	PTI/Li^+Br^- + melem	PTI/Li^+Br^-
Melem	Melem	Melem	Melem	Melem	PTI/Li^+Br^- + melem	PTI/Li^+Br^-
Melon	Melon	Melon + melem	Melem	Melem	Melem	PTI/Li^+Br^-

completely convert it to heptazine-based melem. This is, in itself, noteworthy since the condensation pathway from melamine to melem and the role of melam in it has not been unambiguously elucidated, as well. There are indications for a direct conversion of melamine to melem as well as for a route that contains melam as an intermediate in the form of adduct compounds of melamine and melem on the one and melam and melem on the other hand.[29,30] At least for syntheses in salt melts our results seem to favor the latter route.

Comparing reactions in LiCl/KCl to those in LiBr/KBr melt, it appears that in bromide melt at least the initial steps proceed swifter than in chloride melt, in which products of low degrees of condensation (melamine, melam) could still be observed after longer periods of heating. However, it cannot unambiguously be determined whether this is due to a facilitated reaction process in the bromide melt or simply due to concentration effects, considering that under the chosen conditions experiments in bromide melts applied a higher carbon nitride precursor concentration than those in chloride melts.

Independent of the chosen precursor and so observed for both investigated salt melt systems, melem takes a central position in the reaction pathway. Not only is it observed in every series of experiments and the dominating product over a long period of time, it also appears to be the imminent step in the pathway before the formation of the final product PTI. In this, we want to point out the experiment utilizing melon as starting material in LiBr/KBr melt, where depolymerization of melon towards monomeric melem was observed. This is the back reaction of the condensation of melem, which was considered irreversible. The mechanism of this back reaction is yet unclear. However, since melon is derived from melem via condensation and release of ammonia, a source of NH_3 would be required. As the only potential source is melon itself, it has to be assumed that under the chosen reaction conditions a certain degree of decomposition takes place. This would have to yield an additional carbon-rich decomposition product such as graphite or an even higher condensed carbon nitride compound. However, no such byproduct could be detected. It therefore has to be assumed that any further decomposition products are either gaseous or soluble in water and thus removed together with the

salt melt during workup. As the thermodynamic driving force of this back reaction, we propose solvation effects. The suitability of eutectic LiCl/KCl melts as a solvent for nitrides, cyanates, thiocyanates, and cyanides has been shown by *Sundermeyer* as early as 1961.[31-35] Melon is known to exhibit very poor solubility in any solvent due to its polymeric nature and tight hydrogen bridge network. It is highly probable that monomeric melem would possess a better solubility and thus be dissolved in the salt melt, making the depolymerization energetically favorable.

Since all the conducted experiments indicate melem as the precursor compound of PTI—even in case of triazine-based starting materials such as melamine or melam—another aspect requires thorough discussion: the formation of a triazine-based material from a compound exclusively comprised of heptazine nuclei. The formation of heptazine nuclei from triazines is a well known process and although the mechanism of this conversion has not been unambiguously elucidated, several feasible propositions have been discussed in literature.[13] A mechanism based on the addition of cyanamide, generated through decomposition of melamine, to an undecomposed melamine molecule has been proposed by *May*.[36] This is followed by ring closure reactions accompanied by the elimination of ammonia (Figure 5.1.2a). Another postulated mechanism comprises the addition of two molecules of dicyandiamide to melamine, followed by elimination of cyanamide, in analogy to the synthesis of unsubstituted tri-*s*-triazine by *Shahbaz et al.* (Figure 5.1.2b).[13,37]

As mentioned above for the depolymerization of melon, the formation of PTI from melem indicates the reversibility of the formation of the heptazine nucleus. Depending on the mechanism of this reaction, either ammonolysis or nucleophilic addition of cyanamide would be required as a first step in the back reaction, thus a certain amount of ammonia or cyanamide has to be formed in advance to initiate this process. The back reaction step appears to occur for any chosen carbon nitride precursor and thus independent of the autogenic ammonia pressure inside the reaction vessel, which would be created by prior condensation reactions (such as of melamine or melam to melem). A certain degree of decomposition has thus to be assumed, at least for reactions starting from melem or melon. However, since this would potentially lead to a variety of further gaseous compounds, including cyanamide, within the ampoule, no clear preference for any of the above presented mechanisms can be derived. No intermediates of either of the two proposed routes could be isolated—supposedly because they are rather short-lived—thus neither could any indication be obtained in this way. We do tend, however, towards the mechanism depicted in Figure 5.1.2a, as it is easily imaginable for the intermediate to form the carbon nitride network of PTI.

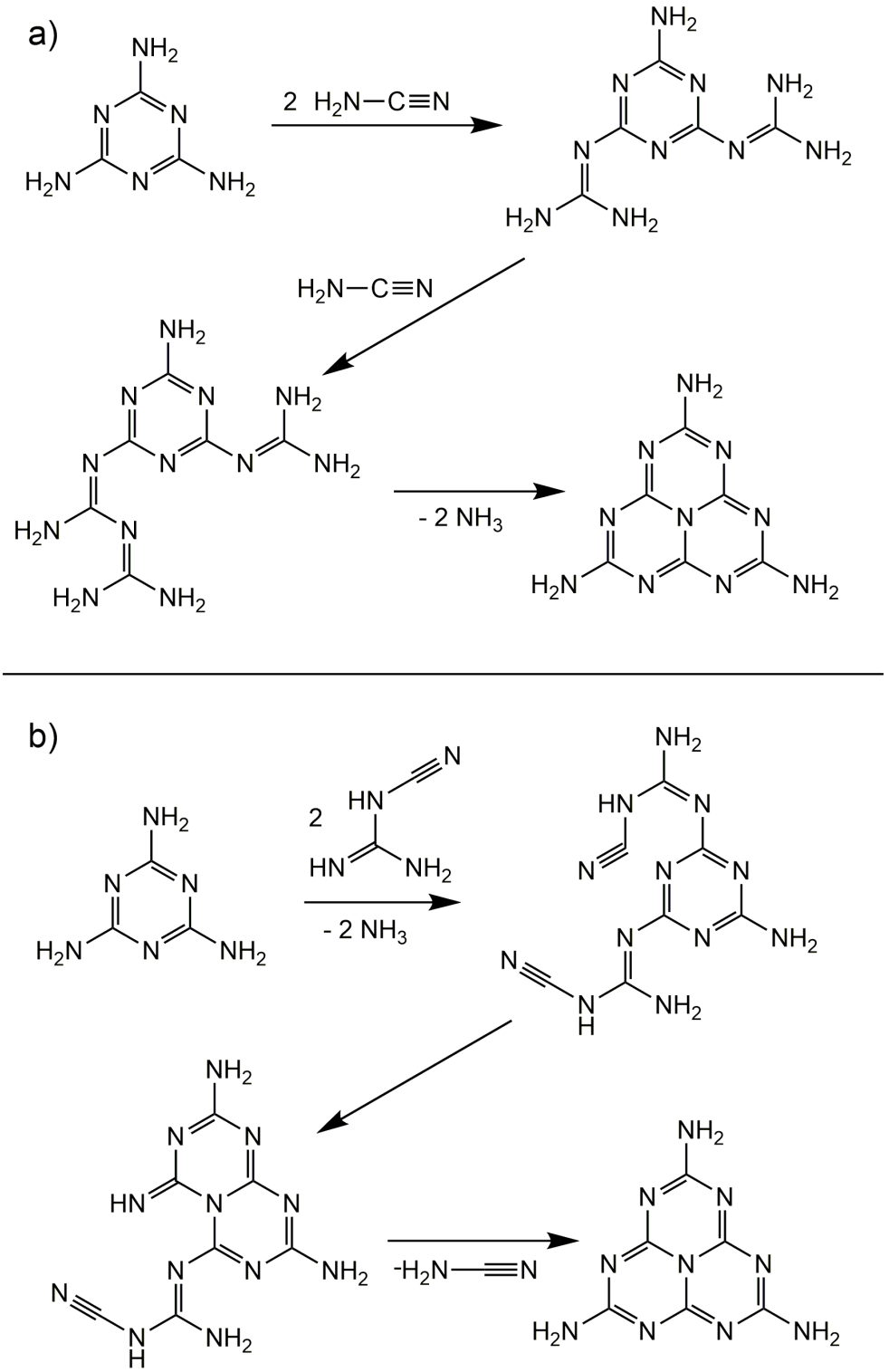

Figure 5.1.2 Proposed reaction mechanisms for the transformation of triazine-based melamine to heptazine-based melem, (a) as proposed by *May*, (b) in analogy to *Shahbaz et al.*[36,37]

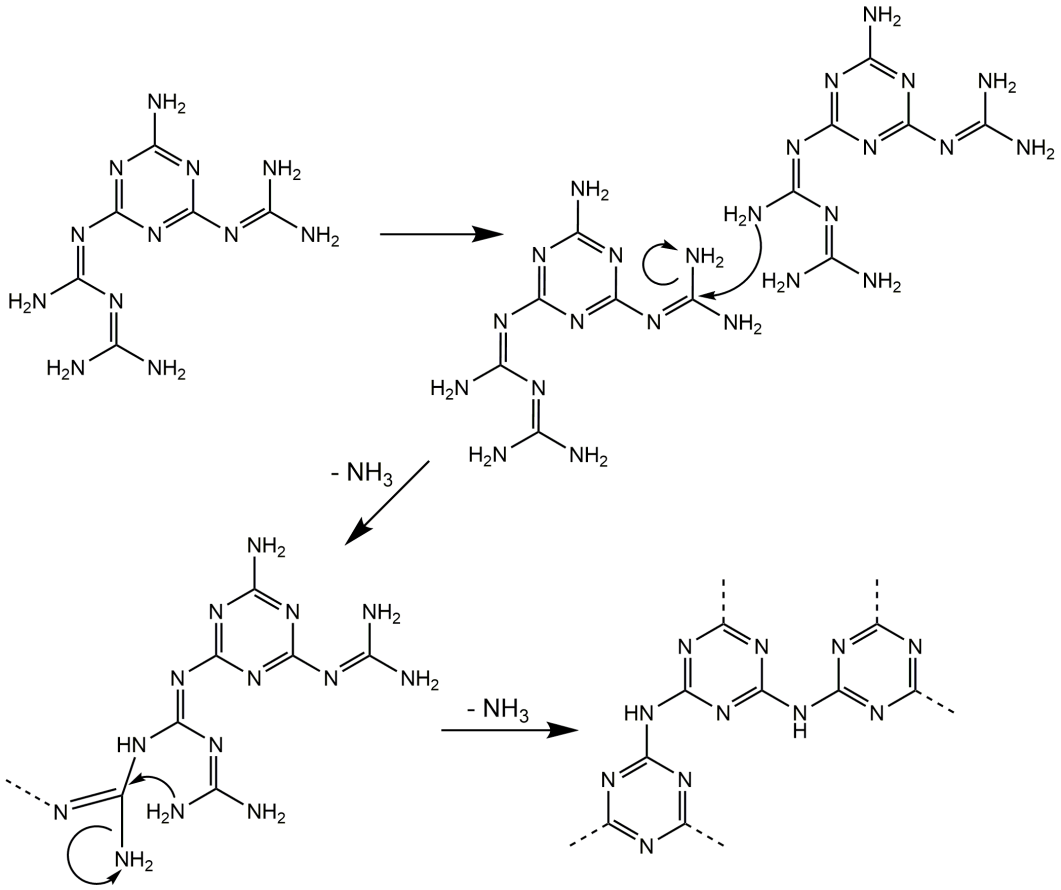

Figure 5.1.3 Reaction mechanism proposed for the formation of poly(triazine imide) from an intermediate of the melamine-to-melem reaction.

We propose a mechanism, in which a ring opening is induced ammonolytically in melem. The 2D network of triazine rings is then formed through condensation of two such intermediates under deammonation (Figure 5.1.3). In this a guanyl C atom is attacked nucleophilically by an amino group and ammonia eliminated from the guanyl group. In a second step, the ring is closed and a second amino group of the guanyl group is eliminated as ammonia. The salt melt would propagate this reaction by stabilizing the intermediate, which should exhibit a greater solubility than melem. As product, 1D zigzag strands of melon-analogous poly(aminoimino)triazine would be obtained. In a final step, these strands could condense along their backbones to form 2D extended sheets of poly(triazine imide).

This mechanism allows to draw analogies to poly(heptazine imide) (PHI), another 2D extended carbon nitride compound. PHI can also be obtained from LiCl/KCl salt melt, however, using substituted triazoles or tetrazoles as starting materials,[38,39] thus requiring a formation mechanism that fundamentally diverges from all herein described mechanisms for C/N/H compound formation. However, the material has also been obtained as a side phase of melon syntheses in closed ampoules under rather harsh conditions and thus a second reaction pathway appears to be viable.[40] Although this process has neither been elucidated, a mechanism is immediately evident when assuming melon as the precursor and the formation of PHI as a further condensation step. This would require just the

same type of polycondensation along the strand backbones that we propose for PTI. Considering the obvious structural relationship between PHI and PTI, it seems only sensible to expect a melon-like precursor for the latter.

5.1.3 Conclusions

We have investigated the formation mechanism of poly(triazine imide) (PTI) in LiCl/KCl and LiBr/KBr salt melt. For this, reactions starting from various different carbon nitride precursor materials were carried out for short durations of time between 5 and 720 min and then quenched and the obtained products analyzed by IR spectroscopy and powder X-ray diffraction.

It could be observed that independent of the chosen precursor melem was formed prior to the formation of PTI. This is remarkable since it necessitates reversing the heptazine formation reaction to obtain triazine-based PTI. To elucidate this curious behavior we thoroughly discussed the formation mechanism of the heptazine core from triazine-based precursors and, based on this, proposed a mechanism for the melem-to-PTI transformation. In this, the melem heptazine nucleus undergoes ring opening via ammonolysis, followed by condensation reactions, in which 1D strands of poly(aminoimino)triazine are formed, which form 2D PTI sheets via polycondensation. The latter part of this is compared to a proposed formation mechanism for poly(heptazine imide) from melon.

The importance of solvation effects in the salt melt is discussed as an explanation for the diverging reaction behavior compared to conventional thermal condensation of carbon nitride compounds, which lead to melon instead. Furthermore, it could be shown that in salt melts melon experiences depolymerization to monomeric melem, which then reacts on towards PTI.

We hope that the insights gained from these investigations lead to greater understanding of the yet only poorly examined processes of carbon nitride condensation and could thus allow a more directed synthesis of carbon nitride materials.

5.1.4 Experimental Section

Chemicals: Dicyandiamide (99 %) was purchased from Avocado, melamine (≥ 99 %) was purchased from Fluka, melam, melem, and melon were prepared according to literature (see below). Lithium chloride (pure) was purchased from AppliChem, lithium bromide (98 %) was purchased from Fluka, potassium chloride (99.5 %) and potassium bromide were purchased from Merck Chemicals GmbH.

Preparation of Melam: Melam was prepared in a two-step synthesis via melamium chloride ammonium chloride.[27,41] Melamine (365 mg, 2.90 mmol) and ammonium chloride (83 mg, 1.56 mmol) were ground together and sealed in a glass ampoule (length 120 mm, inner diameter 11 mm). The ampoule was heated to 723 K in a vertical tube furnace with a rate of 1 K·min^{-1}, held at this temperature for 12 h and cooled to room temperature with 6 K·min^{-1}. The melamium chloride

ammonium chloride adduct sublimed at the upper end of the ampoule was stirred in aqueous ammonia solution (25 %) for 2 h and washed with water. The thus obtained melam hydrate was dried in a muffle furnace at 473 K for 12 h to yield melam as a colorless powder. The product was identified by FT-IR spectroscopy and powder X-ray diffractometry.

Preparation of Melem: Melamine (30.09 g, 239 mmol) in a porcelain crucible covered with a lid was placed in a muffle furnace pre-heated to 473 K and heated to 673 K with 10 K·min^{-1}. It was held at this temperature for 24 h and then cooled to room temperature at 10 K·min^{-1}. The product was ground with mortar and pistil and exposed to the identical temperature program again. Melem was obtained as a pale beige powder. The product was identified by FT-IR spectroscopy and powder X-ray diffractometry.

Preparation of Melon: Melamine (37.82 g, 300 mmol) in a porcelain crucible covered with a lid was placed in a muffle furnace pre-heated to 473 K and heated to 773 K with 10 K·min^{-1}. It was held at this temperature for 24 h and then cooled to room temperature at 10 K min^{-1}. The product was ground with mortar and pistil and exposed to the identical temperature program again. Melon was obtained as a yellow powder. The product was identified by FT-IR spectroscopy and powder X-ray diffractometry.

Synthesis of PTI/Li^{+}Cl^{-}: Carbon nitride precursor material (100 mg) was ground together with 500 mg of a eutectic salt mixture, either LiCl (226 mg, 5.44 mmol) and KCl (274 mg, 3.67 mmol) or LiBr (239 mg, 2.75 mmol) and KBr (261 mg, 2.19 mmol), and sealed in silica glass ampoules (length 120 mm, inner diameter 11 mm). Amounts of salt were chosen well in excess as described in literature.[10,14] Following these protocols, identical weights of chloride melt and bromide melt instead of identical amounts of substance were used for practical reasons, since no significant influence was expected. The ampoules were placed in a vertical tube furnace pre-heated to 773 K and kept there for either 5 min, 10 min, 20 min, 30 min, 120 min, or 720 min. Afterwards, the ampoule was removed from the hot oven and the reaction quenched by submerging in an ice-water mixture. The reaction product was isolated and identified by FT-IR spectroscopy and powder X-ray diffractometry.

General Techniques: FT-IR spectra were recorded with a Perkin–Elmer BX II FT-IR spectrometer equipped with a DuraSampler Diamond ATR (attenuated total reflection) unit. Measurements were conducted at room temperature under exposure to air. Powder X-ray diffractograms were recorded with a Huber Imaging Plate Guinier Diffractometer G670 (guinier geometry, Cu-$K_{\alpha 1}$ radiation, λ = 1.5406 Å) equipped with a CCD camera and an oscillating flat specimen holder.

Acknowledgements

Financial support granted by the Fonds der Chemischen Industrie (FCI) and the Deutsche Forschungsgemeinschaft (DFG) is gratefully acknowledged.

5.1.5 References

[1] I. F. Teixeira, E. C. M. Barbosa, S. C. E. Tsang, P. H. C. Camargo, "Carbon nitrides and metal nanoparticles: from controlled synthesis to design principles for improved photocatalysis", *Chem. Soc. Rev.* **2018**, *47*, 7783-7817.

[2] M. Xiao, B. Luo, S. Wang, L. Wang, "Solar energy conversion on g-C_3N_4 photocatalyst: Light harvesting, charge separation, and surface kinetics", *J. Energy Chem.* **2018**, *27*, 1111-1123.

[3] X. Li, A. F. Masters, T. Maschmeyer, "Polymeric carbon nitride for solar hydrogen production", *Chem. Commun.* **2017**, *53*, 7438-7446.

[4] B. Xu, M. B. Ahmed, J. L. Zhou, A. Altaee, G. Xu, M. Wu, "Graphitic carbon nitride based nanocomposites for the photocatalysis of organic contaminants under visible irradiation: Progress, limitations and future directions", *Sci. Total Environ.* **2018**, *633*, 546-559.

[5] W. Iqbal, B. Yang, X. Zhao, M. Rauf, M. Waqas, Y. Gong, J. Zhang, Y. Mao, "Controllable synthesis of graphitic carbon nitride nanomaterials for solar energy conversion and environmental remediation: the road travelled and the way forward", *Catal. Sci. Technol.* **2018**, *8*, 4576-4599.

[6] A. Sudhaik, P. Raizada, P. Shandilya, D.-Y. Jeong, J.-H. Lim, P. Singh, "Review on fabrication of graphitic carbon nitride based efficient nanocomposites for photodegradation of aqueous phase organic pollutants", *J. Ind. Eng. Chem.* **2018**, *67*, 28-51.

[7] S. Kumar, S. Karthikeyan, A. Lee, "g-C_3N_4-Based Nanomaterials for Visible Light-Driven Photocatalysis", *Catalysts* **2018**, *8*, 74.

[8] J. Fu, J. Yu, C. Jiang, B. Cheng, "g-C_3N_4-Based Heterostructured Photocatalysts", *Adv. Energy Mater.* **2018**, *8*, 1701503.

[9] Z. Zhou, Y. Zhang, Y. Shen, S. Liu, Y. Zhang, "Molecular engineering of polymeric carbon nitride: advancing applications from photocatalysis to biosensing and more", *Chem. Soc. Rev.* **2018**, *47*, 2298-2321.

[10] M. J. Bojdys, J. O. Müller, M. Antonietti, A. Thomas, "Ionothermal Synthesis of Crystalline, Condensed, Graphitic Carbon Nitride", *Chem. Eur. J.* **2008**, *14*, 8177-8182.

[11] E. Wirnhier, M. Döblinger, D. Gunzelmann, J. Senker, B. V. Lotsch, W. Schnick, "Poly(triazine imide) with Intercalation of Lithium and Chloride Ions [$(C_3N_3)_2(NH_xLi_{1-x})_3$·LiCl]: A Crystalline 2D Carbon Nitride Network", *Chem. Eur. J.* **2011**, *17*, 3213-3221.

[12] F. K. Kessler, Y. Zheng, D. Schwarz, C. Merschjann, W. Schnick, X. Wang, M. J. Bojdys, "Functional carbon nitride materials — design strategies for electrochemical devices", *Nat. Rev. Mater.* **2017**, *2*, 17030.

[13] A. Schwarzer, T. Saplinova, E. Kroke, "Tri-s-triazines (s-heptazines)—From a “mystery molecule” to industrially relevant carbon nitride materials", *Coord. Chem. Rev.* **2013**, *257*, 2032-2062.

[14] S. Y. Chong, J. T. A. Jones, Y. Z. Khimyak, A. I. Cooper, A. Thomas, M. Antonietti, M. J. Bojdys, "Tuning of gallery heights in a crystalline 2D carbon nitride network", *J. Mater. Chem. A* **2013**, *1*, 1102-1107.

[15] B. V. Lotsch, M. Döblinger, J. Sehnert, L. Seyfarth, J. Senker, O. Oeckler, W. Schnick, "Unmasking Melon by a Complementary Approach Employing Electron Diffraction, Solid-State NMR Spectroscopy, and Theoretical Calculations—Structural Characterization of a Carbon Nitride Polymer", *Chem. Eur. J.* **2007**, *13*, 4969-4980.

[16] J. Liebig, "Ueber Mellon und Mellonverbindungen", *Justus Liebigs Ann. Chem.* **1844**, *50*, 337-363.

[17] M. B. Mesch, K. Bärwinkel, Y. Krysiak, C. Martineau, F. Taulelle, R. B. Neder, U. Kolb, J. Senker, "Solving the Hydrogen and Lithium Substructure of Poly(triazine imide)/LiCl Using NMR Crystallography", *Chem. Eur. J.* **2016**, *22*, 16878-16890.

[18] E. J. McDermott, E. Wirnhier, W. Schnick, K. S. Virdi, C. Scheu, Y. Kauffmann, W. D. Kaplan, E. Z. Kurmaev, A. Moewes, "Band Gap Tuning in Poly(triazine imide), a Nonmetallic Photocatalyst", *J. Phys. Chem. C* **2013**, *117*, 8806-8812.

[19] X. Wang, K. Maeda, A. Thomas, K. Takanabe, G. Xin, J. M. Carlsson, K. Domen, M. Antonietti, "A metal-free polymeric photocatalyst for hydrogen production from water under visible light", *Nat. Mater.* **2009**, *8*, 76-80.

[20] K. Schwinghammer, B. Tuffy, M. B. Mesch, E. Wirnhier, C. Martineau, F. Taulelle, W. Schnick, J. Senker, B. V. Lotsch, "Triazine-based Carbon Nitrides for Visible-Light-Driven Hydrogen Evolution", *Angew. Chem.* **2013**, *125*, 2495-2499; *Angew. Chem. Int. Ed.* **2013,** *52*, 2435-2439.

[21] Y. Ham, K. Maeda, D. Cha, K. Takanabe, K. Domen, "Synthesis and Photocatalytic Activity of Poly(triazine imide)", *Chem. - Asian J.* **2013**, *8*, 218-224.

[22] M. K. Bhunia, S. Melissen, M. R. Parida, P. Sarawade, J.-M. Basset, D. H. Anjum, O. F. Mohammed, P. Sautet, T. Le Bahers, K. Takanabe, "Dendritic Tip-on Polytriazine-Based Carbon Nitride Photocatalyst with High Hydrogen Evolution Activity", *Chem. Mater.* **2015**, *27*, 8237-8247.

[23] K. Schwinghammer, M. B. Mesch, V. Duppel, C. Ziegler, J. Senker, B. V. Lotsch, "Crystalline Carbon Nitride Nanosheets for Improved Visible-Light Hydrogen Evolution", *J. Am. Chem. Soc.* **2014**, *136*, 1730-1733.

[24] W.-r. Lee, Y.-S. Jun, J. Park, G. D. Stucky, "Crystalline poly(triazine imide) based g-CN as an efficient electrocatalyst for counter electrodes of dye-sensitized solar cells using a triiodide/iodide redox electrolyte", *J. Mater. Chem. A* **2015**, *3*, 24232-24236.

[25] Y. Wang, Q. Yang, C. Zhong, J. Li, "Graphene-like Poly(triazine imide) as N_2-Selective Ultrathin Membrane for Postcombustion CO_2 Capture", *J. Phys. Chem. C* **2016**, *120*, 28782-28788.

[26] G. Algara-Siller, N. Severin, S. Y. Chong, T. Björkman, R. G. Palgrave, A. Laybourn, M. Antonietti, Y. Z. Khimyak, A. V. Krasheninnikov, J. P. Rabe, U. Kaiser, A. I. Cooper, A. Thomas, M. J.

Bojdys, "Triazine-Based Graphitic Carbon Nitride: a Two-Dimensional Semiconductor", *Angew. Chem.* **2014**, *126*, 7580-7585; *Angew. Chem. Int. Ed.* **2014**, *53*, 7450-7455.

[27] B. V. Lotsch, W. Schnick, "New Light on an Old Story: Formation of Melam during Thermal Condensation of Melamine", *Chem. Eur. J.* **2007**, *13*, 4956-4968.

[28] B. Jürgens, E. Irran, J. Senker, P. Kroll, H. Müller, W. Schnick, "Melem (2,5,8-Triamino-tri-s-triazine), an Important Intermediate during Condensation of Melamine Rings to Graphitic Carbon Nitride: Synthesis, Structure Determination by X-ray Powder Diffractometry, Solid-State NMR, and Theoretical Studies", *J. Am. Chem. Soc.* **2003**, *125*, 10288-10300.

[29] E. Wirnhier, M. B. Mesch, J. Senker, W. Schnick, "Formation and Characterization of Melam, Melam Hydrate, and a Melam–Melem Adduct", *Chem. Eur. J.* **2013**, *19*, 2041-2049.

[30] A. Sattler, S. Pagano, M. Zeuner, A. Zurawski, D. Gunzelmann, J. Senker, K. Müller-Buschbaum, W. Schnick, "Melamine–Melem Adduct Phases: Investigating the Thermal Condensation of Melamine", *Chem. Eur. J.* **2009**, *15*, 13161-13170.

[31] W. Sundermeyer, "Hexamethyldisilan", *Z. Anorg. Allg. Chem.* **1961**, *310*, 50-52.

[32] W. Sundermeyer, "Chemische Reaktionen in Salzschmelzen. IV. Neue Darstellungsmethode von Cyaniden, Cyanaten und Thiocyanaten des Siliciums und Kohlenstoffs", *Z. Anorg. Allg. Chem.* **1962**, *313*, 290-295.

[33] W. Sundermeyer, "Salzschmelzen und ihre Verwendung als Reaktionsmedien", *Angew. Chem.* **1965**, *77*, 241-258; *Angew. Chem. Int. Ed. Engl.* **1965**, *4*, 222-238.

[34] W. Sundermeyer, "Chemische Reaktionen in geschmolzenen Salzen", *Chem. Unserer Zeit* **1967**, *1*, 150-157.

[35] W. Verbeek, W. Sundermeyer, "Darstellung von Carbonyl- und Fluorcarbonyl-pseudohalogeniden in der Salzschmelze", *Angew. Chem.* **1967**, *79*, 860-861; *Angew. Chem. Int. Ed. Engl.* **1967**, *6*, 871-872.

[36] H. May, "Pyrolysis of melamine", *J. Appl. Chem.* **1959**, *9*, 340-344.

[37] M. Shahbaz, S. Urano, P. R. LeBreton, M. A. Rossman, R. S. Hosmane, N. J. Leonard, "Tri-*s*-triazine: synthesis, chemical behavior, and spectroscopic and theoretical probes of valence orbital structure", *J. Am. Chem. Soc.* **1984**, *106*, 2805-2811.

[38] D. Dontsova, S. Pronkin, M. Wehle, Z. Chen, C. Fettkenhauer, G. Clavel, M. Antonietti, "Triazoles: A New Class of Precursors for the Synthesis of Negatively Charged Carbon Nitride Derivatives", *Chem. Mater.* **2015**, *27*, 5170-5179.

[39] A. Savateev, S. Pronkin, J. D. Epping, M. G. Willinger, C. Wolff, D. Neher, M. Antonietti, D. Dontsova, "Potassium Poly(heptazine imides) from Aminotetrazoles: Shifting Band Gaps of Carbon Nitride-like Materials for More Efficient Solar Hydrogen and Oxygen Evolution", *ChemCatChem* **2017**, *9*, 167-174.

[40] M. Döblinger, B. V. Lotsch, J. Wack, J. Thun, J. Senker, W. Schnick, "Structure elucidation of polyheptazine imide by electron diffraction-a templated 2D carbon nitride network", *Chem. Commun.* **2009**, 1541-1543.

[41] N. E. Braml, A. Sattler, W. Schnick, "Formation of Melamium Adducts by Pyrolysis of Thiourea or Melamine/NH_4Cl Mixtures", *Chem. Eur. J.* **2012**, *18*, 1811-1819.

5.2 Synthesis of C/N/H Compounds in Lewis-Acidic Salt Melts

5.2.1 Introduction

The ionothermal synthesis approach in C/N/H chemistry, first proposed by *Bojdys et al.* in 2008,[1] has shown to be a useful asset and valuable addition to the preparative repertoire for C/N/H compounds, opening up the route to novel compounds of high degrees of condensation that were previously unobtainable. The main advantage of this route as opposed to conventional syntheses via thermal condensation lies in the differences between solid-state syntheses and syntheses in solution. The latter allows for diffusion rates exceeding those in solids by several orders of magnitude, resulting in faster and more homogeneous reactions at lower temperatures.[2] Most C/N/H compounds are known for their poor solubility in almost any kind of common solvent and themselves do not melt but rather tend to either sublimate or directly decompose prior to any phase transition. This significantly complicates the realization of liquid-state synthesis for this group of materials. Various molten salts, however, do not only exhibit substantial dissolving power for C/N/H precursor compounds, but also thermal stability up to the rather high temperatures required to induce transformation reactions in C/N/H compounds.[3-5]

Inorganic salts, however, have also found application in a completely different function in C/N/H chemistry. Lewis-acidic salts, such as $ZnCl_2$, have been shown to catalyze the trimerization of nitriles to form triazine rings. This method has found application in the preparation of covalent organic frameworks that use triazine building blocks as linkers, so called covalent triazine frameworks (CTFs).[6-8] Such salts thus fulfill not one but two functions within the transformation process of C/N/H precursor materials. In the following chapter, experiments in lewis-acidic salt melts are presented that were conducted specifically with this twofold functionality in mind. Central questions concerned the influence these salt melts would have on the reaction process in contrast to salt melts without any particular catalytic activity, such as the lithium halide melts used in PTI syntheses; the nature of the thus obtained C/N/H compounds; and the roles that either of these two effects play in the reaction process. To this end a series of experiments was conducted in $ZnCl_2$ or $ZnCl_2$-containing salt melts. Similar experiments were furthermore conducted in $CdCl_2$-containing salt melts, since $CdCl_2$ is not only chemically closely related to $ZnCl_2$, but ^{113}Cd is a useful nucleus for NMR measurements, which have shown to be a suitable tool for the structural investigation of C/N/H compounds. Experiments applying only catalytic amounts of lewis-acidic salts were conducted to elucidate the role of the salt melt as a solvent and the influence of a liquid reaction regime on the formation of C/N/H compounds. In the following, three compounds obtained in these syntheses as well as the insights gained into the reaction processes taking place are presented and discussed.

5.2.2 Synthesis of C/N/H compounds in $ZnCl_2$ salt melt

Compound **(1)** was initially encountered in a series of experiments analogous to those conducted in the investigation of the formation mechanism of poly(triazine imide) using a eutectic $ZnCl_2$/NaCl mixture as the reaction medium. It was shown, however, that the reaction would likewise proceed in pure $ZnCl_2$ melt, since the formation of **(1)** appears to depend exclusively on the presence of the lewis-acidic compound and no reduction of the melting point was necessary due to the already low melting point of $ZnCl_2$ of about 322 °C.[9] Typical synthesis protocols used mixtures of 100 mg of $C_2N_4H_4$ (1.19 mmol) and 500 mg of salt melt (either 94.5 mg NaCl (1.62 mmol) / 405.5 mg $ZnCl_2$ (3.00 mmol) or 500 mg $ZnCl_2$ (3.70 mmol)) with the melt in copious excess. Although experiments showed that **(1)** is also formed for weight ratios for $C_2N_4H_4$ to $ZnCl_2$ of up to 1 : 1, the products obtained from such experiments exhibited significantly poorer crystallinity as well as band broadening in FT-IR spectroscopy, which are interpreted as indications of a less well-defined material with inferior long-range order. These reaction mixtures were intimately ground and sealed in evacuated silica glass ampoules with lengths of 10 to 13 cm, inner diameters of 11 mm and a wall thickness of 2 mm, which were subsequently placed in a tube furnace. When applying temperatures below 500 °C for durations up to 12 h an amorphous material was obtained that exhibited an FT-IR spectrum that indicated an unknown yet ill-defined phase. However, at temperatures above 525 °C **(1)** was formed as a beige to brown polycrystalline and caked material. Experiments under varying reaction conditions showed **(1)** to be a thermodynamically favorable compound that was obtained at temperatures between 525 and 675 °C, dwell times as short as 2 h and cooling rates between 6 and 0.05 K min^{-1}. The standard program exhibiting the best reproducibility and product quality consisted of heating the ampoule to 550 °C with a rate of 6 K min^{-1}, a dwell time of 12 h and a cooling rate of 6 K min^{-1}. The product was afterwards recovered and washed in boiling water to remove excess salt.

Optimization of the synthesis procedure towards better crystallinity and more defined IR absorption bands was attempted, however, no unambiguous correlation between reaction temperature, dwell time or cooling rate and these factors could be observed. However, product quality according to abovementioned criteria was significantly increased by post-synthetic tempering of the recovered product in $ZnCl_2$. For this, 100 mg of **(1)** and 100 mg of $ZnCl_2$ were mixed, sealed in an evacuated silica glass ampoule and heated to 650 °C for 12 h. The material obtained by this second reaction step is denoted as **(1b)** in the following, while the as-obtained product shall be referred to as **(1a)**. It has to be noted, however, that this tempering process brought the compound close to the point of thermal decomposition and several samples of **(1b)** contained $ZnCN_2$, which is interpreted as a decomposition product of **(1)**, as a side product. Thus, no post-treatment experiments at temperatures higher than 650 °C were attempted.

$ZnCl_2$ is very hygroscopic and thus had to be dehydrated before use and stored under a protective inert gas atmosphere to prevent H_2O and thus oxygen to participate in the reaction. In this series of experiments, $ZnCl_2$ was either handled in a Schlenk tube and thus shortly exposed to air while

weighing out; or weighing was performed in a glovebox under Ar atmosphere to completely avoid hydrate water. However, no significant difference in sample quality was observed between the two methods.

Ampoule synthesis of **(1)** did often yield small amounts of sublimate at the top end of the ampoule while the target phase was found at the bottom. Sublimate phases typically consisted of either known C/N/H compounds such as melam, or of **(1)** as well, however, were always poorly crystalline and in general not unambiguously identifiable. Sublimate phases were thus discarded and further investigations focused on the more ordered residuum phase.

The composition of compounds **(1a)** as well as **(1b)** was determined by a combination of combustion analysis for H, C and N, titration for Cl and energy dispersive X-ray spectroscopy (EDX) for Zn and Cl. Cl content values, which were determined as the most precise, were used to normalize values from different methods. The obtained values are found in Table 5.2.1.

Table 5.2.1 Elemental composition of **(1)** obtained by different synthesis routes. All values in w%.

	C	N	H	Zn	Cl
(1a), in air	16.63	28.84	1.29	40.74	5.52
(1a), glovebox	16.32	28.96	1.09	32.36	14.17
(1b)	12.42	20.53	1.24	41.65	7.48

From these values, an approximate sum formula of '$C_6N_9H_{5\text{-}7}$' can be deduced. The N : C ratio is fairly consistent over all measurements and comes to approximately 1.5 : 1 (when calculated in atomic percent). This value is equal to the respective ratios in melon, $[C_6N_7(NH)_2(NH)]_n$, and poly(triazine imide), $[(C_3N_3)_2(NH)_3]_n$, and thus indicates a highly condensed, potentially polymeric C/N/H network for **(1)**. However, for a highly condensed C/N/H polymer, hydrogen contents are unusually high. Furthermore, there are significant deviations in hydrogen content between individual samples, which should not occur without changes in the N : C ratio. Possible explanations for this behavior are discussed below. Zn and Cl contents are subject to even larger variations, not only between different samples, but also within samples as could be shown by EDX measurements at several selected spots throughout each sample. It is thus assumed that **(1)** is not an intercalation compound with a defined amount of coordinated Zn^{2+} and Cl^- ions, as is the case in PTI/Li^+Cl^- or PTI/Li^+Br^-, but that observed Zn and Cl contents rather represent residual salt melt, potentially trapped within C/N/H structures and thus not elutable by treatment in boiling water. Furthermore, it has to be noted that while the $ZnCl_2$ salt melt is the exclusive source for both Zn and Cl, their elemental ratio significantly deviates from 1 : 2. Furthermore, contents of C, N, H, Zn and Cl as obtained from elemental analyses do not add up to 100 w% and EDX detected additional oxygen that might account for these differences. It is thus assumed that hydrolysis of $ZnCl_2$ takes place during aqueous workup, potentially resulting in a broad variety of zinc oxides and hydroxides such as ZnO, $Zn(OH)_2$ or Zn(OH)Cl, which would account not only for variations in Zn and Cl contents, but might also explain the varying and overall too high H content throughout the samples of **(1)**. It is thus reasonable to assume an actual composition of the

C/N/H network of $C_6N_9H_3$—the same stoichiometry that is observed in melon and PTI—and additional side phases of zinc oxides, hydroxides and chlorides that could not be removed completely during workup. It is also conceivable that a certain amount of zinc chloride is intercalated within the structure of **(1)** in analogy to PTI, however, the presence of further phases containing these ions makes a determination of such intercalates through elemental analysis alone impossible.

Comparing samples of **(1a)** and **(1b)**, it has been noted as a general trend that the N : C ratios obtained for **(1b)** are slightly smaller, indicating a higher degree of condensation. This might be explained by the higher temperatures und longer dwell times promoting a more complete condensation reaction, which results in larger extended sheets or chains. A similar behavior has been observed for melon, in the synthesis of which reaction conditions drastically determine chain lengths and thereby also properties.[10, 11]

FT-IR spectra of **(1)** were recorded in pure substance at room temperature and in air on a Perkin-Elmer BX II FT-IR spectrometer equipped with a DuraSampler Diamond ATR (attenuated total reflection) unit. The characteristic spectrum of **(1)** as depicted in Figure 5.2.1 contains only a small number of absorption bands, indicating a high structural symmetry of the compound. Almost all bands are found in the fingerprint area below 1600 cm^{-1}. ν(N-H) vibrations in the area around 3350 cm^{-1} form a single, extremely broad and flat absorption band that in some samples is almost indiscernible from the background. The two main bands are found at 1298 and 1195 cm^{-1} and are of equal intensity. They are both attributed to C-N or C=N ring vibrations. In some samples, the latter of these peaks shows rather strong tailing towards lower wavenumbers. A characteristic band at 808 cm^{-1} is attributed to the ring out-of-plane breathing mode of triazine or heptazine rings and identifies **(1)** as a C/N/H compound build from one of these building blocks. A band of medium intensity at 1573 cm^{-1} might result from δ(N-H) vibrations, but could also indicate further C-N vibrations. Often, another band of low to medium intensity is encountered at ca. 2050 cm^{-1}. This band results from C≡N vibrations, which, however, do not belong to **(1)** but to a side phase that has been identified as $ZnCN_2$. Minor amounts of this compound are often formed during the synthesis of **(1)**.

No absorption band is detected in the area around 1250 cm^{-1}, where vibrations of CNHC units of bridging imido groups are expected. However, a similar gap is observed in PTI, which does exhibit imido bridging and a band shifted hypsochromically to 1289 cm^{-1}. Thus, the lack of such a band does not necessarily contradict the hypothesis of **(1)** being formed from a highly condensed, imido bridged C/N/H network. Several further similarities between the spectra of **(1)** and PTI can be observed indicating a close relation between these two compounds. However, bands in **(1)** are more narrow and distinct than in PTI and some of them are shifted towards lower wavenumbers. No unambiguous explanation for these correlations can be deduced from vibrational spectroscopy alone.

Just as PTI, **(1)** is a well-crystalline compound that shows narrow and distinct reflections in X-ray powder diffraction. Polymeric C/N/H compounds such as melon or poly(heptazine imide) typically exhibit rather poor crystallinity and are often amorphous except for an intense stacking reflection that

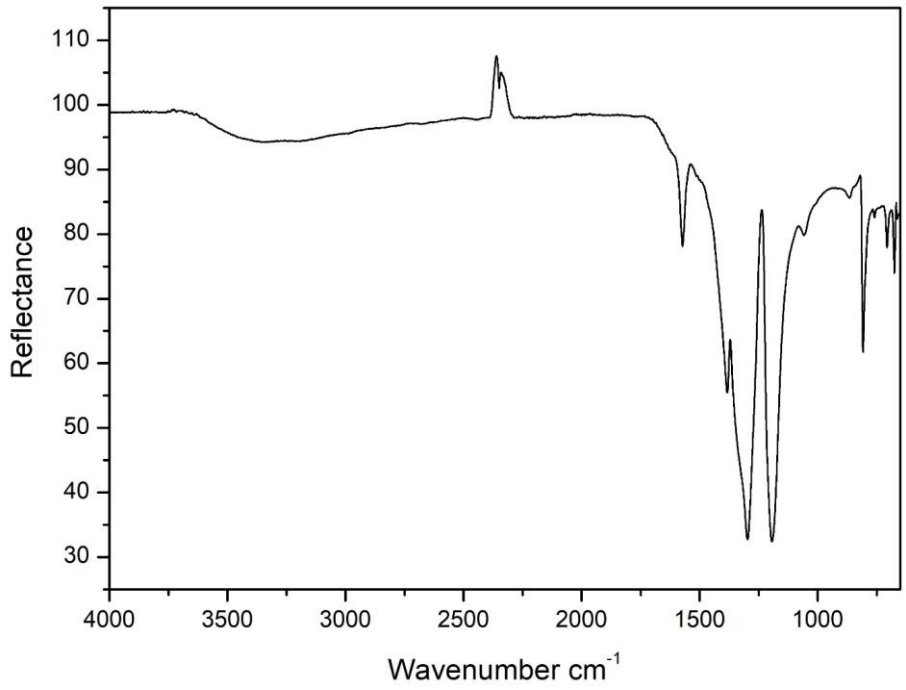

Figure 5.2.1 FTIR-ATR spectrum of **(1)**.

corresponds to a characteristic stacking distance between sheets or strands that is defined by van-der-Waals interactions. **(1)**, however, shows a distinct pattern of reflections, which is depicted in Figure 5.2.2.

Although the pattern looks highly symmetric, it was not possible to index any diffractograms of **(1)** and determine a unit cell. It is unclear, however, whether this results from any yet unidentified side phase—so that certain reflections were in fact not part of the pattern—whether the compound suffers from texturization, so that certain reflections are missing, or whether another effect not yet taken into consideration causes these issues. A typical side phase that often occurs in synthesis of **(1)** and could be detected via PXRD in several samples is $ZnCN_2$. Furthermore, as can be seen from a hill-shape in the background between 10° and 40° in Fig 5.2.2, products typically contain amorphous side phases.

It is noteworthy that in contrast to most other C/N/H compounds, no stacking reflection at $2\theta \approx 27°$ is present in the diffractogram of **(1)**. This is unusual for C/N/H compounds, particularly for polymeric compounds that are typically build up from 2D extended layers, whose distance is defined by van-der-Waals interactions and thus ranges from 3.2 to 3.4 Å, as is also found in graphite. The absence of a corresponding reflection in **(1)** might either indicate that the compound possesses a different form of interlayer interactions, potentially even a 3D network; or could result from texture effects, which might reduce the intensity of the stacking reflection. As mentioned above, texturization is one plausible explanation for the failure in indexing the diffraction pattern. Stacking directions in C/N/H compounds are typically oriented along a single preferred cell direction, with the [002] stacking reflection in melon as the most prominent example.[11] Should the compound exhibit strong preferred orientation effects, this could potentially result in a complete loss of intensity for reflections

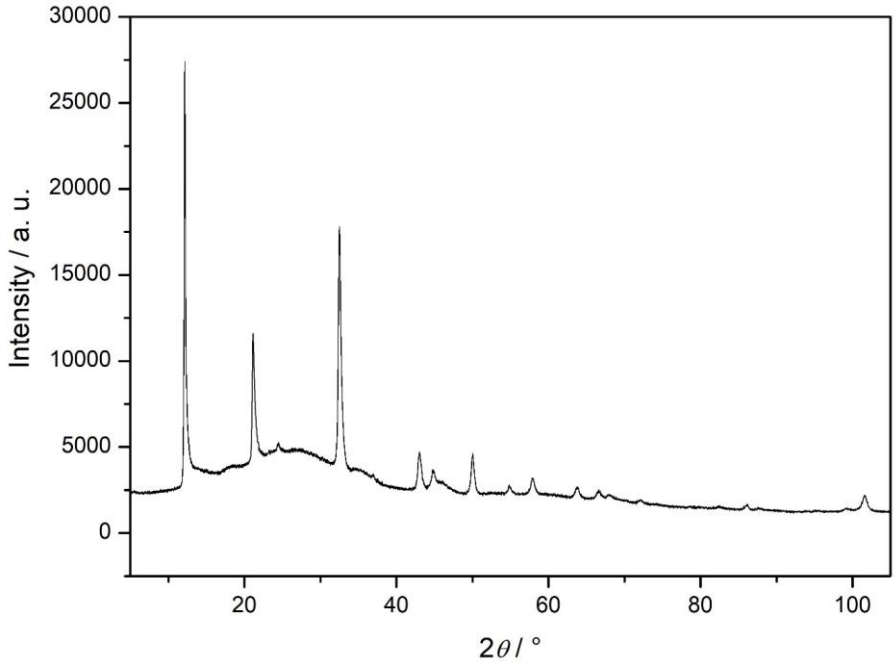

Figure 5.2.2 Powder X-ray diffractogram of **(1)**, Cu-$K_{\alpha 1}$ radiation (1.54056 Å).

corresponding to one respective direction and thus account for the expected though not observable reflections in the diffraction pattern of **(1)**.

The most intense reflection in the pattern of **(1)** is found at $2\theta = 12.2°$, corresponding to a *d*-spacing of 7.3 Å. This reflection is also commonly found in other C/N/H compounds such as melon and interpreted as the length of one repetition unit $-C_6N_7(NH_2)(NH)-$ of the heptazine chain. Finding a comparable spacing in the diffraction pattern of **(1)** might indicate the presence of similar structural elements. It is furthermore remarkable that the diffraction pattern exhibits reflections of fairly high intensity up to diffraction angles of $2\theta = 101.6°$. This is completely unusual for C/N/H compounds, as the structure factor of the light atoms comprising these compounds dramatically drops towards higher angles, resulting in hardly any intensity for such reflections. Intensities as observed for **(1)** would require the presence of heavier atoms, of which Zn is the obvious choice. Since no reflections in the pattern of **(1)** could be assigned to any known Zn containing compound—in particular those expected from EDX measurements, which are thus assumed to be present in an amorphous form—this can be seen as an indication of incorporation of Zn (and potentially also Cl) within the structure.

To further elucidate structural features of **(1)**, the compound was investigated by solid-state MAS-NMR spectroscopy. Measurements were conducted at the University of Bayreuth in the group of Prof. Dr. J. Senker on a Bruker Avance III HD 400 spectrometer with a B_0 field of 9.4 T. ^{1}H and ^{13}C shifts are referenced to TMS, ^{15}N shifts to nitromethane. ^{13}C and ^{15}N spectra were measured applying ^{1}H decoupling and cross polarization (CP) pulse sequences. In the case of ^{15}N, varying CP contact times

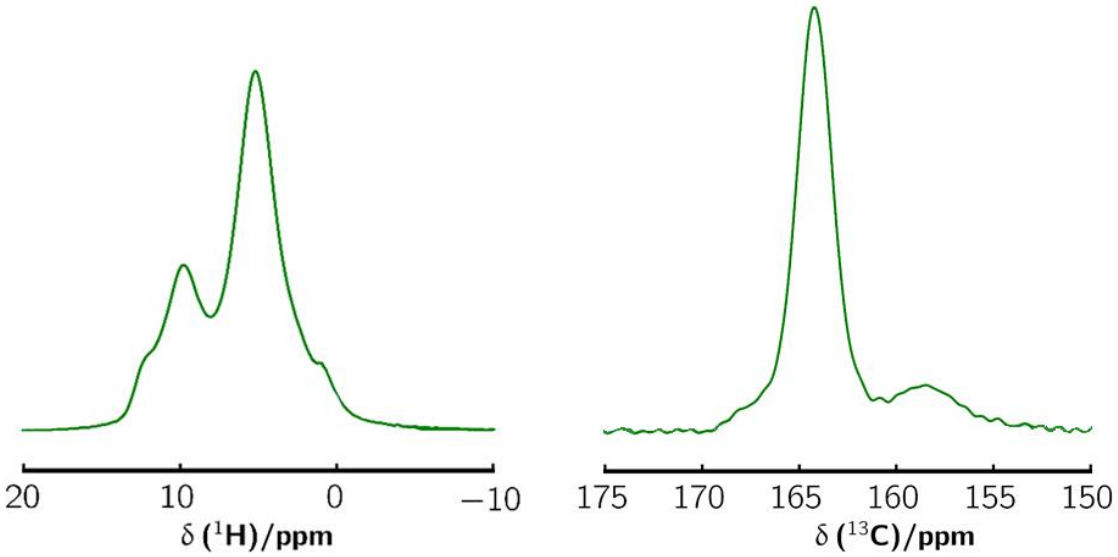

Figure 5.2.3 Solid-state MAS-NMR spectra of **(1)**. Left: ^{1}H spectrum. Right: ^{13}C-CP spectrum.

were used to elucidate proton environments of the respective signal groups.

In ^{1}H NMR spectra (Figure 5.2.3 left), three signal groups could be observed at 5.1 ppm, 9.9 ppm and 12.1 ppm with the latter two showing a rather high degree of overlap. The signal at 5.1 ppm is interpreted as an amino group signal in accordance with related amino group comprising triazine and heptazine compounds. The small shoulder at 12.1 ppm most likely results from protonation of ring N atoms of C/N/H heterocycles, which are known to exhibit rather high chemical shifts due to their acidity. Interpretation of the signal at 9.9 ppm is more ambiguous. With respect to the observed chemical shift, it could either stem from further ring protonation, or from imide groups that bridge the respective nuclei. The former are typically expected in a range between 10.5 and 12.5 ppm, while the latter are usually found between 8.0 and 9.0 ppm. Both interpretations appear feasible. Further elucidation of this issue would require ^{1}H-^{15}N correlation 2D NMR experiments, which, however, could not be conducted in this study.

Two signals can be distinguished in the ^{13}C spectrum of **(1)** (Figure 5.2.3 right). The major signal peaks at 164.2 ppm while a second, smaller but fairly broad signal is found at 158.5 ppm. Both are located in a range where signals for C/N/H compounds are expected. No further signals that might indicate carbon-containing impurities, could be detected.. Signals between 160 and 170 ppm in C/N/H compounds typically result from ring $CN_2(NH_2)$ or $CN_2(NH)$ atoms while signals between 155 and 160 ppm are generally attributed to CN_3 carbon atoms. The latter are usually part of heptazine nuclei, since bridging tertiary N atoms are very rare in C/N/H chemistry. However, a resonance at 157.9 ppm has also been reported for PTI/Li^+Cl^-, which does not contain any CN_3 groups.[12] Thus, an analogous assumption for **(1)** would be reasonable. The low number of ^{13}C signals observed in the spectrum of **(1)** supports the hypothesis of a highly symmetric structure as deduced from PXRD and FT-IR spectroscopy.

^{15}N resonances were found at -176 ppm, -200 ppm, -239 ppm and -251 ppm (Figure 5.2.4). Multiple spectra were recorded with different CP contact times between 1 and 10 ms to observe intensity buildup and thus deduce the proton environment of the respective N atoms. Signal intensities for resonances at -176 ppm and -200 pm are more or less independent from contact time and are thus attributed to tertiary N atoms of the ring systems. This is also in good agreement with their respective chemical shifts. On the other hand, the resonances at -239 ppm and -251 ppm both loose intensity with increasing contact time, indicating proximity to protons. These signals are assigned to imide N atoms according to their chemical shift. No signal is found in the range between -225 and -235 ppm, where the resonance for the central N atom of a heptazine nucleus would be expected. Neither were any amino N signals observed, which are expected between -280 and -300 ppm.

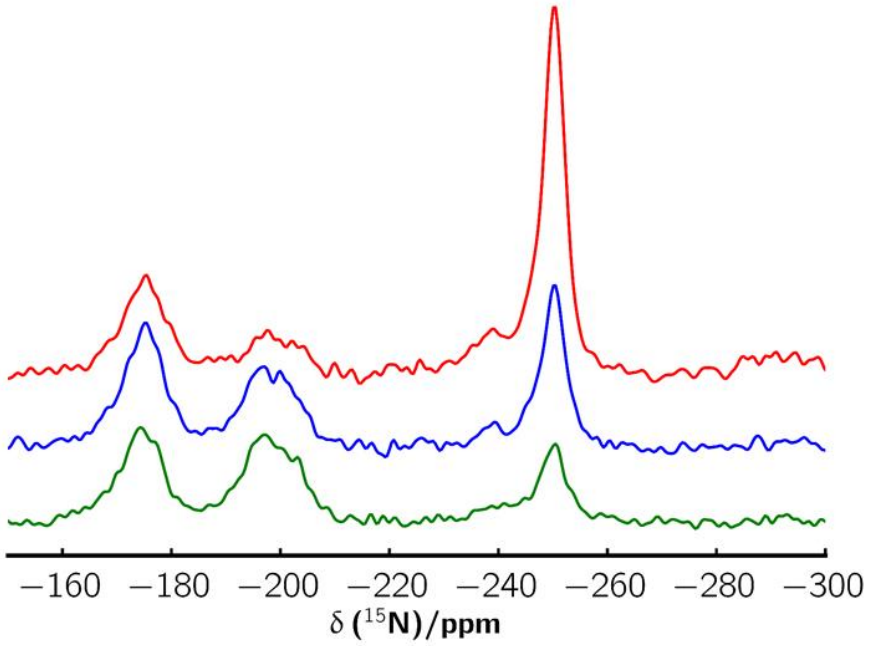

Figure 5.2.4 ^{15}N solid-state CP-MAS-NMR spectra of **(1)**, recorded with different CP contact times. Red: t = 1 ms; blue: t = 5 ms; green: t = 10 ms.

Several conclusions can be drawn when combining the findings obtained through this multitude of analytic experiments. The low number of signals in X-ray powder diffractograms, IR as well as NMR spectra suggest high crystallographic as well as molecular symmetry. The elemental composition, in particular the N : C ratio indicates a high degree of condensation. Since triazine- and heptazine-based compounds typically are planar, high symmetry would require extended condensation in two dimensions, resulting in networks similar to PTI or PHI. Such a network could be constructed from either triazine or heptazine building blocks. While a ^{13}C signal at 158.5 ppm might indicate CN_3 units and thus heptazine rings, comparable signals have also been observed in triazine-based PTI. Furthermore, no ^{15}N signal for the characteristic central N atom of heptazine was detected. A weak signal at -239 ppm that is potentially close to the expected range was shown to result from imide groups by variation of CP contact times. These results indicate a compound based on triazine rings.

^{15}N NMR signals—in particular the intense resonance located at -251 ppm—further indicate these nuclei to be interconnected by bridging imide groups. Since the ^{13}C NMR signal at 164.2 ppm thus has to be assigned to C atoms adjacent to these groups and no ^{15}N NMR signal in the range between -280 and -300 ppm was observed, amino groups can be ruled out as part of the structure. This is also in good agreement with the very low ν(NH) signal observed in FT-IR spectra. The intense ^{1}H NMR signal at 5.1 ppm, which shows a shift comparable to amino groups in C/N/H compounds, thus most likely results from side phases, e.g. hydroxides. Elemental analysis did confirm hydrogen containing side phases since the observed hydrogen content was too high for the observed N : C ratio of **(1)**.
A 2D extended network of triazine rings interconnected by imide units is realized in PTI and indeed does **(1)** show several similarities to this compound. FT-IR spectra exhibit partial resemblance, as do NMR spectra. In particular, the resemblance of ^{15}N NMR spectra has to be mentioned. PTI shows the same imide resonance as **(1)**, as well a broad signal in the shift range expected for tertiary N atoms, which would envelope the two signals observed for **(1)**. No imminent explanation for the presence of two distinct signals in this region in **(1)** is evident from the supposed structure. Furthermore, a PTI-like network would only account for a single C atom signal in ^{13}C NMR. However, for PTI, the occurrence of multiple resonances has been explained with different protonation patterns as well as Li^+/H^+ disorder. A more ordered protonation pattern for ring N atoms could explain the second ^{13}C resonance as well as the clear distinction of the two ^{15}N signals. However, no unambiguous model of the C/N/H network can be deduced from these data alone. Further measurements, e.g. 2D NMR correlation experiments, would be required to determine the connectivity of the respective atoms. Moreover, no prediction can be made concerning the role and location of Zn^{2+} and Cl^- ions within the structure. A zinc chloride containing compound supposedly comprising a poly(triazine imide) network has been reported on by *Fettkenhauer et al.*,[13] however, neither PXRD nor FT-IR measurements of this compound show any resemblance to **(1)**.

5.2.3 Synthesis of C/N/H compounds in $CdCl_2$ salt melt

Syntheses under various different conditions analogous to those described in the previous chapter were also conducted in $CdCl_2$/KCl melt. $CdCl_2$ was synthesized from $CdCO_3$ as described in *Inorganic Syntheses*.[14] 1723.9 mg (10.0 mmol) of $CdCO_3$ were dissolved in 20 mL of concentrated hydrochloric acid and the solvent evaporated. The residue was refluxed in 20 mL of thionyl chloride under N_2 atmosphere for several hours. Thionyl chloride was afterwards removed in vacuum and the product washed twice in boiling acetone and then dried over KOH. $CdCl_2$ is very hygroscopic and was thus handled in a glovebox or under inert gas atmosphere using Schlenk techniques.
Compound **(2)**, which shall be described in this subchapter, was obtained by the following synthesis route: 100 mg of $C_2N_4H_4$ (1.19 mmol) and 500 mg of a eutectic mixture of $CdCl_2$ and KCl (296.5 mg $CdCl_2$ (1.63 mmol, 37.2 a%) and 203.5 mg KCl (2.77 mmol, 62.8 a%)) were ground together in a glovebox

under Ar protective atmosphere and sealed in an evacuated silica glass ampoule (lengths 12 cm, inner diameter 11 mm, wall thickness 2 mm). The ampoule was placed in a tube furnace and heated to 550 °C with a rate of 6 K min^{-1}, held at this temperature for 2 h and cooled to room temperature with a rate of 0.1 K min^{-1}. **(2)** was recovered as a caked light to dark brown residuum. The compound was exclusively handled under protective inert gas atmosphere.

(2) was only formed in the presence of excess salt melt. Experiments with reduced amounts of $CdCl_2$ are described in chapter 5.2.4. Dicyandiamide could also be substituted for ammonium dicyanamide $NH_4^+C_2N_3^-$ in the synthesis of **(2)**. Furthermore, the compound was synthesized from ^{15}N enriched dicyandiamide.

Elemental analysis was conducted without any prior workup to remove the salt melt, thus rather low values for C, N and H were obtained. Since samples still contained residual salt, no determination of Cd, K or Cl contents in **(2)** could be conducted. Measured C, N, and H contents are as follows: N: 9.96 w%, C: 5.50 w%, H: 0.85 w%. This would roughly equate to a sum formula of '$C_6N_{9.3}H_{11.0}$'. The N : C ratio of 1.81 is slightly above the ratios found in melon or PTI, both $C_6N_9H_3$, but still rather low, thus indicating a compound of relatively high degree of condensation. The observed hydrogen content is drastically higher than expected for a highly condensed C/N/H compound, however, weighing out samples for combustion analysis required handling the sample in air. Due to the hygroscopicity of $CdCl_2$, the detected H content is thus not reliable and might result from hydration of the salt. Additionally, although $CdCl_2$ was only handled under Ar atmosphere, the possibility of the material being slightly contaminated by a corresponding hydrate cannot be excluded completely.

Aqueous workup of **(2)** in order to remove remaining salt and so isolate the compound and determine its composition without hindering influence of $CdCl_2$ and KCl could not be performed due to sensitivity of the compound towards hydrolysis. An experiment to test for stability against hydrolysis was conducted, in which a sample of **(2)** was ground and suspended in 75 mL of deionized H_2O, which was then heated to the boiling point. The insoluble solid was isolated by filtration and analyzed by FT-IR spectroscopy and PXRD. It could be shown that the sample underwent significant changes during the experiment. The main FT-IR bands of the product closely resemble those of melem, $C_6N_{10}H_6$, however, several additional low intensity bands suggest either the presence of further phases or a completely different product. Deviations from the starting material **(2)** are so significant that any partial agreements between the band patterns is interpreted as purely coincidental. No agreement at all could be observed between the powder X-ray diffractograms of the compound before and after aqueous treatment. Neither, however, did the diffractogram of the hydrolyzed compound show any resemblance to melem or melem hydrate, which would have been expected regarding the abovementioned FT-IR spectrum. No unambiguous assumptions on the processes occurring in H_2O can thus be made. However, it is obvious that **(2)** is a sensitive compound that has to be handled with care and exposure to water has to be avoided at any cost. This, however, makes isolation of the

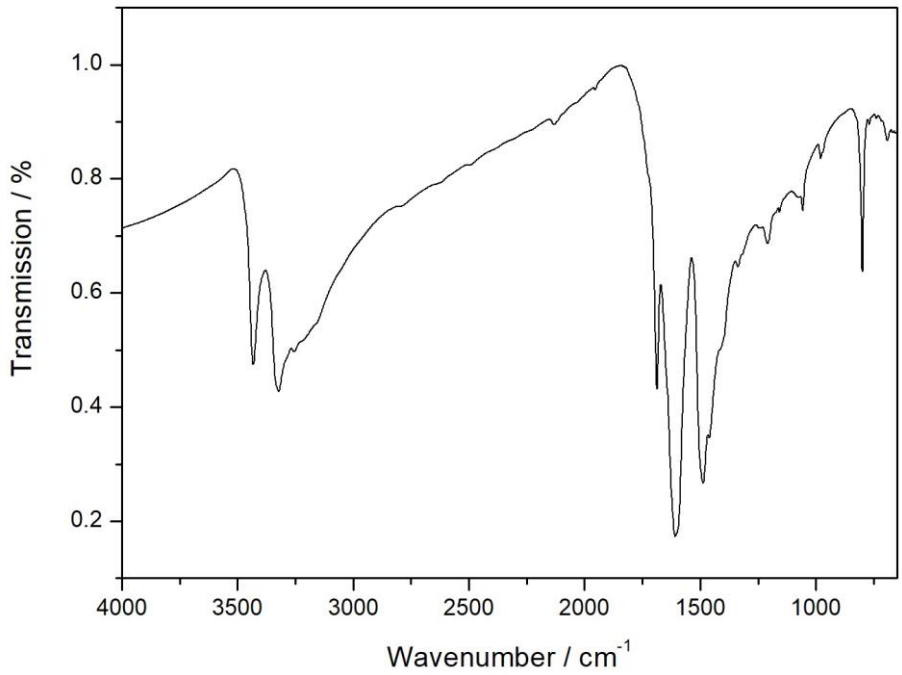

Figure 5.2.5 FTIR-ATR spectrum of **(2)**.

compound difficult and necessitates conduction of analyses to take place in the presence of residual salt.

The FT-IR spectrum of **(2)** (Figure 5.2.5) shows a band pattern that exhibits little resemblance to any other ionothermally obtained C/N/H compound. Most characteristic for **(2)** is a rather narrow and well-defined band in the ν(NH) region at 3431 cm^{-1} that indicates a well ordered environment for an amino or imido group. Most C/N/H compounds show rather broad signals without any distinct peaks in this spectral range. Further intense signals are found at 1687 cm^{-1}, 1608 cm^{-1}, and 1489 cm^{-1} in the fingerprint region. No specific assignment of these signals is possible. The characteristic triazine or heptazine ring out-of-plane breathing mode is found at a frequency of 798 cm^{-1}, which is slightly lower than expected for typical highly condensed C/N/H compounds, but in good agreement with e.g. melem.

The powder X-ray diffractogram of **(2)** is depicted in Figure 5.2.6. Reflections are remarkable narrow and well developed, indicating a highly crystalline compound with large domain sizes. It was not possible to index the pattern, however, the large number of signals suggests a crystallographic system of low symmetry, which in general complicates powder indexing. Relatively high signal intensities at high angles suggest the presence of heavy atoms, most likely Cd and Cl, within the structure. The most intense peak at 27.1° is interpreted as a stacking reflection. The corresponding *d*-spacing of 3.29 Å is absolutely reasonable for van-der-Waals distances between C/N/H ring systems. No reflections belonging to $CdCl_2$, KCl, mixtures thereof or the respective hydrates could be identified, although salt melts had not been removed from the samples. It is thus assumed that these salts form amorphous glasses during solidification of the melt.

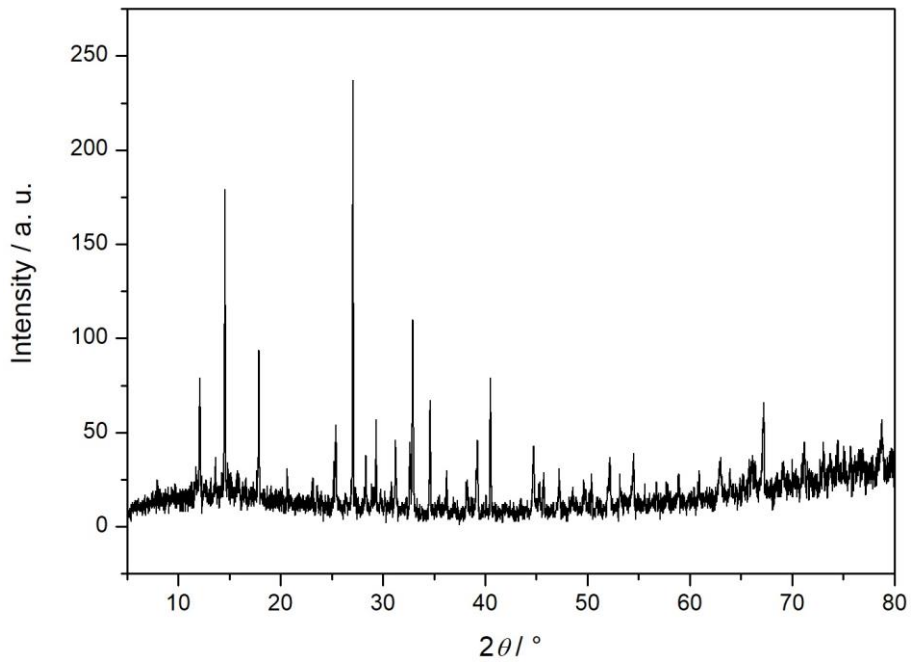

Figure 5.2.6 Powder X-ray diffractogram of **(2)**, Cu-$K_{\alpha1}$ radiation (1.54056 Å).

It has to be mentioned that relative peak intensities could not always be reproduced. This might be an indication either for several phases that make up the sample—which is to be expected, considering the presence of residual salt melt—or for texturization effects within the sample. However, no experimental evidence for either of these potential explanations could be obtained.

A ^{15}N enriched sample of **(2)**—synthesized from dicyandiamide ^{15}N enriched to about 25 %—was investigated by ^{1}H, ^{13}C, ^{15}N and ^{113}Cd solid-state MAS NMR spectroscopy. Measurement parameters were identical to those described for compound **(1)**. ^{13}C, ^{15}N and ^{113}Cd spectra depicted in Figures 5.2.7 and 5.2.8 were recorded using CP pulse sequences. ^{15}N and ^{113}Cd spectra were additionally recorded without cross polarization and shall be discussed later.

The ^{1}H spectrum of **(2)** (Figure 5.2.7 left) shows two resonances as well as a broad background signal of about 20 ppm width. One resonance at 6.7 ppm is interpreted as an amino group signal. No obvious explanation can be found for the second resonance at 0.0 ppm, which is completely atypical for C/N/H compounds. It is thus assumed that this signal results from hydrogen containing species formed in the salt melt, e.g. hydrates from (short) exposure to air or amides formed from eliminated ammonia. Elemental analysis did detect a hydrogen content significantly higher than expected for the observed degree of condensation. It is thus reasonable to assume additional hydrogen containing species within the sample, from which the second resonance as well as the broad underlying background signal might result. No signals indicating bridging imido groups (expected between 8 and 9 ppm) or protonation of ring systems (expected between 10 and 13 ppm) could be observed.

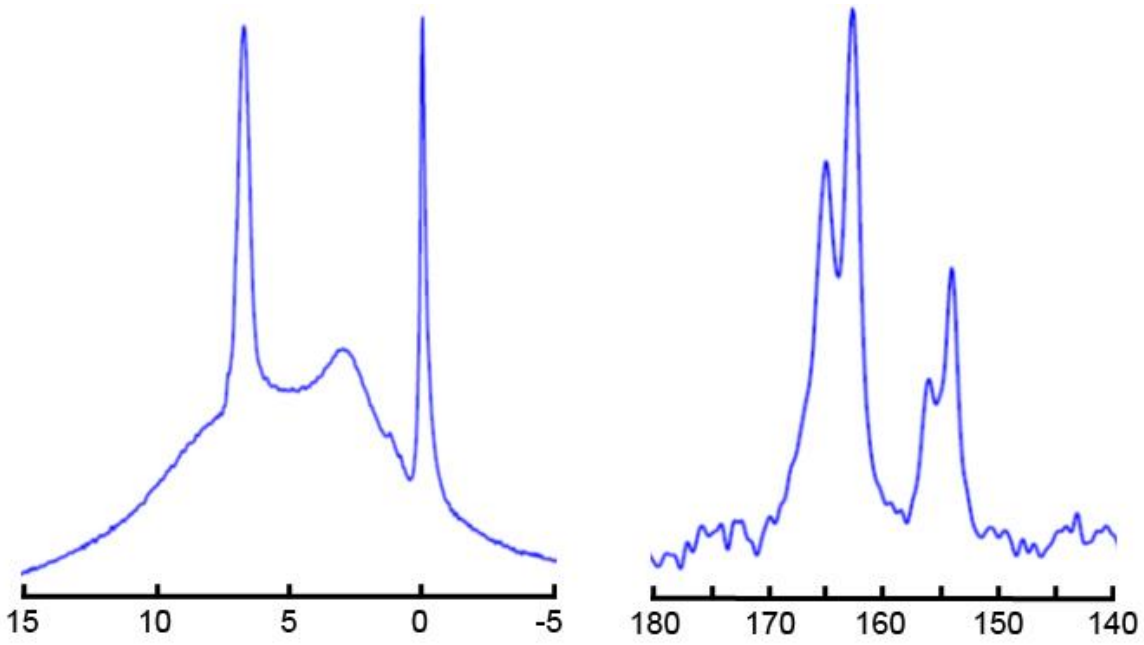

Figure 5.2.7 Solid-state MAS-NMR spectra of **(2)**. Left: ^{1}H spectrum. Right: ^{13}C-CP spectrum.

The ^{13}C-CP NMR spectrum of **(2)** exhibits four signals at 164.9, 162.6, 156.4 and 154.0 ppm, respectively, which can be divided into two signal groups. It is noticeable that the intensity ratio of the signals within one group is about equal for both groups and that the same can be stated for shifts between the signals within each group. Although in general integration of signal intensities is not valid in CP experiments since the intensity depends on proton proximity as well as on the number of magnetically equivalent atoms, it is reasonable to assume comparable chemical environments for resonances within the same signal group, thus allowing for interpretation of these observations. The chemical shifts observed for the signal groups are indicative for heptazine building blocks, with the low field signal group attributable to outer—i.e. amino bond—C atoms and the high field shifted group to inner C atoms bonded to the central N atom. The two signals per signal group could thus be interpreted as two heptazine nuclei of slightly different chemical environment within the structure.
Seven resonances are observed in the ^{15}N spectrum of **(2)**, which could be assigned to different building blocks by their respective chemical shift. Signals at -200.8 ppm and -212.5 ppm are attributed to tertiary N atoms. The low-intensity signal at -235.7 ppm is interpreted as the central N atom of a heptazine nucleus, as this chemical shift is very characteristic. While the signal is barely noticeable in the CP experiment, direct excitation experiments yield a significantly higher intensity. This is in accordance with expectations since the heptazine central N atom is the atom in the nucleus furthest from any protons and thus receives hardly any additional intensity from cross-polarization. The most intense signal group in the CP spectrum, exhibiting three resonances at – 273.8, -279.6 and -292.5 ppm, is found in the region attributed to primary amino groups. Consequently, these signals show significantly lower intensities in experiments without cross-polarization, confirming their proximity to protons. A final signal is observed at -354.9 ppm, which is identified by its chemical shift as an

ammonium resonance. This is remarkable since no other analysis did indicate an ionic compound. However, it is not possible to determine whether the ammonium ion is part of compound **(2)** itself or rather belongs to a side phase formed in the melt from eliminated ammonia. No signal is found in the range between -240 and -260 ppm, in which imido group resonances would be expected, thus confirming the absence of such building blocks as has already been noticed from FT-IR spectroscopy.

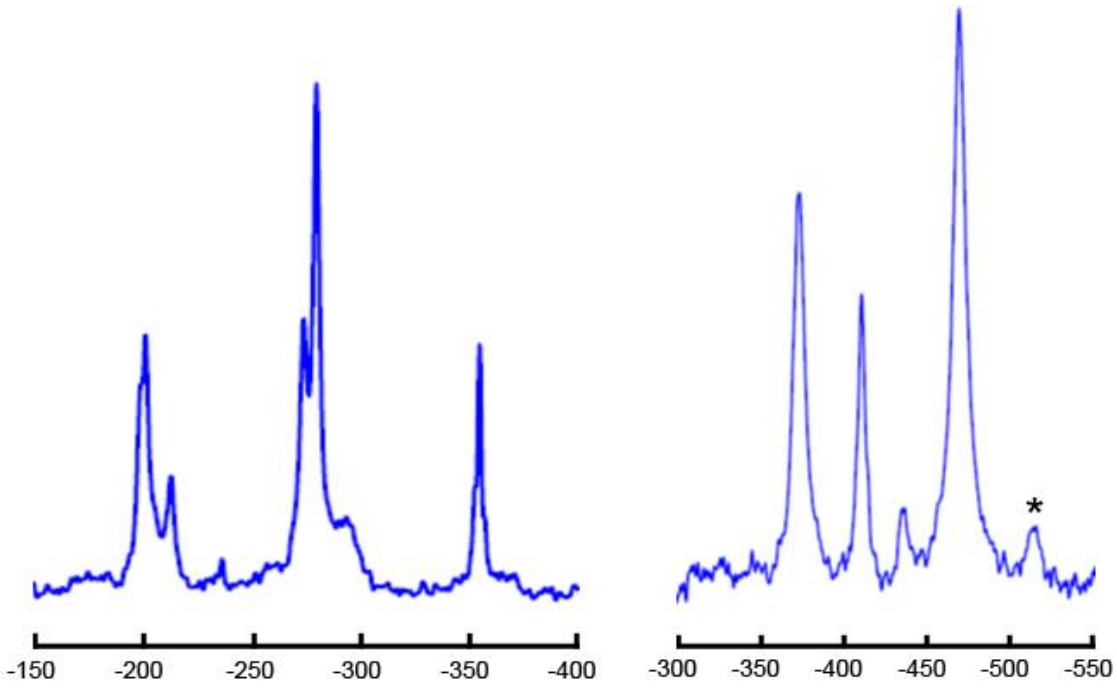

Figure 5.8 Solid-state MAS-NMR spectra of **(2)**. Left: ^{15}N-CP spectrum. Right: ^{113}Cd-CP spectrum. The asterisk marks a spinning side band.

^{113}Cd NMR spectroscopy yielded four signals at -373.2, -410.8, -435.6 and -469.7 ppm. Direct excitation yields high intensities for the resonances at -410.8 and -435.6 ppm while the signals at -373.2 and -469.7 ppm possess hardly any intensity. Comparing this to the CP experiment as depicted in Figure 5.2.8 indicates that the latter two signals belong to proton containing species. However, since the cadmium species formed in the salt melt are unknown, it is not possible to unambiguously assign any of the four signals to a definite species.

As for **(1)**, no unambiguous data that would allow for structure elucidation of the compound—such as single-crystal or powder X-ray diffraction structure solution and refinement—could be obtained for **(2)**. However, spectroscopic data allow for certain conclusions concerning composition and structural elements of the compound. Elemental analysis indicated a degree of condensation that is lower than the one found in melon (or other polymeric C/N/H compounds), but higher than in molecular melem. However, the low overall measured contents of carbon and nitrogen caused by the presence of residual salt melt—and potentially additional side phases formed within this melt—make these calculations rather imprecise. Furthermore, the N : C ratio is only valid as a measure of the degree of condensation when assuming that none of the other phases within the reaction mixture does contain C or N. More telling information were obtained spectroscopically. IR as well as NMR spectroscopy both verified the

presence of amino groups and the absence of imide groups, which would be expected as bridging elements in a polymeric C/N/H compound. NMR shifts for ^{13}C and ^{15}N further show the fundamental building block of **(2)** to be the heptazine nucleus. This agrees well with the observed reaction behavior in aqueous medium, in which melem was formed as the primary product. It was thus concluded that **(2)** is a compound based on isolated triamino-heptazine units. However, IR spectra and powder X-ray diffractograms, which deviate fundamentally from those of melem, imply further structural elements. In accordance with related C/N/H compounds it is assumed that these deviations are caused by ions from the salt melt, which either form adducts or intercalates with triamino-heptazine units, or form ionic compounds in which the C/N/H building blocks themselves are anionic or cationic, e.g. in the form of melemium ions. Furthermore, the presence of ammonium might indicate a salt containing multiple cations or an adduct compound between a meleminium salt and an ammonium salt—as has been observed for melamium chloride ammonium chloride.[15]

5.2.4 On the influence of salt melts on the reaction behavior of C/N/H compounds

Salt melts are generally deployed in excess since they are supposed to fulfill the role of solvent and C/N/H starting materials only possess a limited solubility in them. However, as could be shown in the previous chapters, salt melts often also fulfill additional roles, for which no excess of the material is necessary: those of reactant or of catalyst. To investigate the role of salt melts as solvents, experiments in $ZnCl_2$ and $CdCl_2$/KCl melts were conducted with successively smaller amounts of salt up to a point at which an influence on the reaction behavior caused by this reduction was observable.

In continuing with synthesis protocols designed priorily for syntheses in excess salt melts, experiments were conducted with a fixed weight ratio of C/N/H starting material to overall salt melt. Dicyandiamide was chosen as the C/N/H precursor in all experiments. In a typical experiment, either 100 or 200 mg (1.19 resp. 2.38 mmol) of $C_2N_4H_4$ were ground together with 10 to 1000 mg of the respective salt or salt mixture. $ZnCl_2$ was used as a pure salt, all other salts investigated in this study were mixed with KCl in a eutectic ratio to lower their melting points. Different dicyandiamide to salt melt ratios investigated in this study are listed in Table 5.2.2. Molar ratios are listed for better comparability.

All syntheses were conducted in sealed and evacuated silica glass ampoules. A default temperature program as described in previous chapters (heating to 550 °C with a rate of 6 K min^{-1}, 2 h dwell time, cooling rate of 0.1 K min^{-1}) was used. Starting materials as well as products were handled in an Ar-filled glovebox to protect them from moisture. No workup to remove residual salt was performed, thus all samples are expected to contain side phases and/or residues of the salt melt. A more detailed

Table 5.2.2 Starting material to salt melt ratios and obtained products.

Weight ratio $C_2N_4H_4$: overall salt melt	**Molar ratio $C_2N_4H_4$: salt melt**	**Obtained product**
$ZnCl_2$ 1:10	1 : 6.17	(1)
$ZnCl_2$ 1:5	1 : 3.08	(1)
$ZnCl_2$ 1:1	1 : 0.62	(1)
$ZnCl_2$ 2:1	1 : 0.31	(3)
$ZnCl_2$ 5:1	1 : 0.12	(3)
$ZnCl_2$ 10:1	1 : 0.06	(3)
$CdCl_2$/KCl 1:5	1 : 1.36 / 1 : 2.29	(2)
$CdCl_2$/KCl 1:1	1 : 0.27 / 1 : 0.46	(3)
$CdCl_2$/KCl 2:1	1 : 0.14 / 1 : 0.23	(3)
$CdCl_2$/KCl 5:1	1 : 0.05 / 1 : 0.09	(3)
$CdCl_2$/KCl 10:1	1 : 0.03 / 1 : 0.05	(3)
AgCl/KCl 5:1	1 : 0.10 / 1 : 0.04	(3)
AgCl/KCl 10:1	1 : 0.05 / 1 : 0.02	(3)
LiCl/KCl 5:1	1 : 0.18 / 1 : 0.12	(3)
LiCl/KCl 10:1	1 : 0.09 / 1 : 0.06	(3)

description of synthesis protocols has been given in the previous subchapters.

Several experiments listed in Tab. 5.2.2 have already been discussed in subchapters 5.2.2 and 5.2.3. The products obtained under those conditions are the abovementioned compounds **(1)** and **(2)**. It can be seen that these compounds are exclusively formed below a certain ratio of dicyandiamide to overall salt melt. This ratio is larger than 1.0, which on the one hand speaks of a high solubility of the C/N/H precursor in the respective salt melt, on the other hand has to be taken with caution, since $C_2N_4H_4$ will start to condense to higher C/N/H compounds before the respective salt mixture is molten, thus lowering the actual molar ratio.

Above a certain molar ratio of starting material to salt, an unknown compound is formed that shall herein be denoted as **(3)**. This compound is formed independent of the used salts and has not only been observed in syntheses using the previously described systems $ZnCl_2$ and $CdCl_2$/KCl, but also with further halide mixtures such as AgCl/KCl and also LiCl/KCl, from which—although at lower ratios—PTI has been initially obtained. It is thus evident that no incorporation of ions from any of these compounds is necessary for the formation of **(3)**. However, the presence of the salt might have a catalytic effect and thus influence the formation of the compound.

As shown in Tab. 5.2.2, **(3)** was obtained under various different conditions. Thus, samples that are denominated as **(3)** throughout this chapter do show slight deviations in composition as well as properties as a result of their respective synthesis process. Overall similarity of these samples, however, is sufficient to classify them as the same compound or at least as containing this compound as the main phase. Since phase purity could not be established for any of these samples, this makes determination of the composition of **(3)** by elemental analysis rather tenuous and limits the

significance of such measurements. However, at least general trends could be determined reliably. Table 5.2.3 contains compositional data as obtained from combustion analysis for some exemplarily selected samples.

Table 5.2.3 Composition of samples of **(3)** in w%.

Sample	N	C	H	N : C ratio
$ZnCl_2$ 2:1	33.80	17.17	2.48	1.97
$ZnCl_2$ 5:1	50.36	26.44	2.45	1.90
$ZnCl_2$ 10:1	54.04	29.67	2.09	1.82
$CdCl_2$/KCl 5:1	47.52	26.59	1.85	1.79

The apparent degree of condensation—measured as a lower N : C ratio for the respective samples—was found to increase with reduced salt content. Likewise, the overall H content—similarly indicative of the degree of condensation—declines for lower amounts of salt. While this trend could be observed for all investigated samples, it has to be taken into account that larger amounts of salt may also allow for the formation of larger amounts of nitrogen and hydrogen containing side phases, e.g. amines or ammonium salts. With phase analysis impossible by the available methods, no unambiguous evidence for a trend within the group of compounds denominated as **(3)** can be established. It could be observed, however, that independent of chosen salt mixture for very small amounts of salt, N : C weight ratios appear to converge towards a value slightly below 1.8. This is close to the value observed for polymeric C/N/H compounds such as melon or poly(triazine imide) of 1.75 and thus indicates a highly condensed, most likely polymeric compound. This is also supported by the reaction conditions under which **(3)** is formed, which include relatively high temperatures, at which the formation of highly condensed materials is expected. Such a polymeric structure would also account for the variance in composition in dependence of reaction conditions, since polymers of different lengths would show such deviations from the ideal formula of an infinite polymeric chain.

FT-IR spectroscopy further supports this assumption. The spectrum of **(3)** (Figure 5.2.9) shows remarkable similarities over most of the fingerprint region to the spectrum of melon. Between 1700 and 1250 cm^{-1} spectra are virtually identical apart for some minor differences in relative intensities. Below 1250 cm^{-1}, however, melon shows an intense imide bridge band tailing extremely broadly towards lower wavenumbers, while little of this is seen in **(3)**. Additional differences can be observed in the N-H stretching vibration region, where **(3)** shows two distinct bands at 3450 and 3425 cm^{-1} that are completely missing in melon. Furthermore, it has to be noted that all bands in the spectrum of **(3)** are generally more narrow and well defined than observed for melon.

Regardless of these minor differences, the spectra suggest not only a close relation between melon and **(3)**, but rather a more or less identical structure. **(3)** is thus interpreted as a variant of melon, exhibiting the same building blocks and bond structure, but possibly possesses a more distinct long-range order as indicated by more narrow bands.

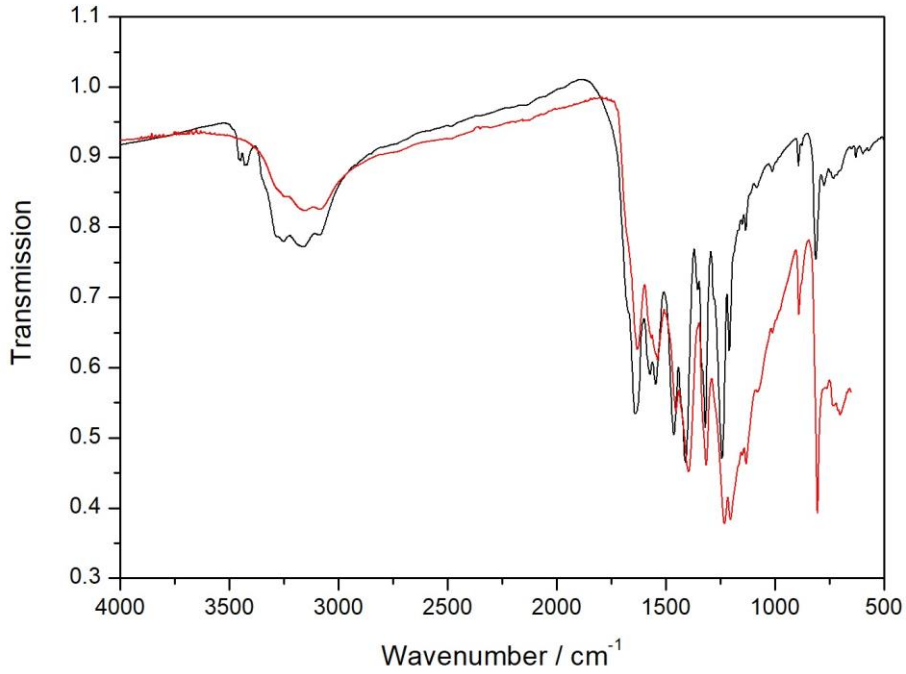

Figure 5.2.9 FTIR spectra of (3) (black) and melon (red) for comparison.

Obtaining melon in these syntheses would not be remarkable, considering that long established synthesis protocols for this compound use comparable temperature programs, which thus could fully account for the formation of this material. The salt or salt mixtures were thus unnecessary and their effect on the reaction of C/N/H precursor material negligible. However, while melon is well known to be a compound of extremely poor crystallinity with even the diffractograms of optimized samples exhibiting barely more than the stacking reflection, **(3)** shows a very well defined diffraction pattern of numerous intense and narrow reflections (Figure 5.2.10). As for melon the most intense reflection with a maximum at 2θ = 27.9° is attributed to the stacking distance between two layers of C/N/H network. Several further reflections of high intensity are found between 2θ = 12° and 35°. Towards higher angles, intensities drop rapidly, indicating no heavy scatterers present within the structure. Attempts to index the diffraction pattern were not successful. Thus, no information concerning the crystallographic structure could be obtained and no cell parameters determined and compared to those of melon from conventional synthesis.

The sample selected for Figure 5.2.10 does only contain reflections, which were observed in every sample that was identified as compound **(3)**. However, several other samples did contain additional reflections of minor intensity, which were interpreted as side phases formed from the molten salts. None of this side phases could be identified, however. Interestingly, no sample showed reflections originating from the pure salt. This might, however, be explained by the low initial amount of salt, which might result in overall salt contents below the detection limit of the X-ray detector; or by the molten salts solidifying amorphously or as a nanoscale material, thus not showing any distinct and intense reflections.

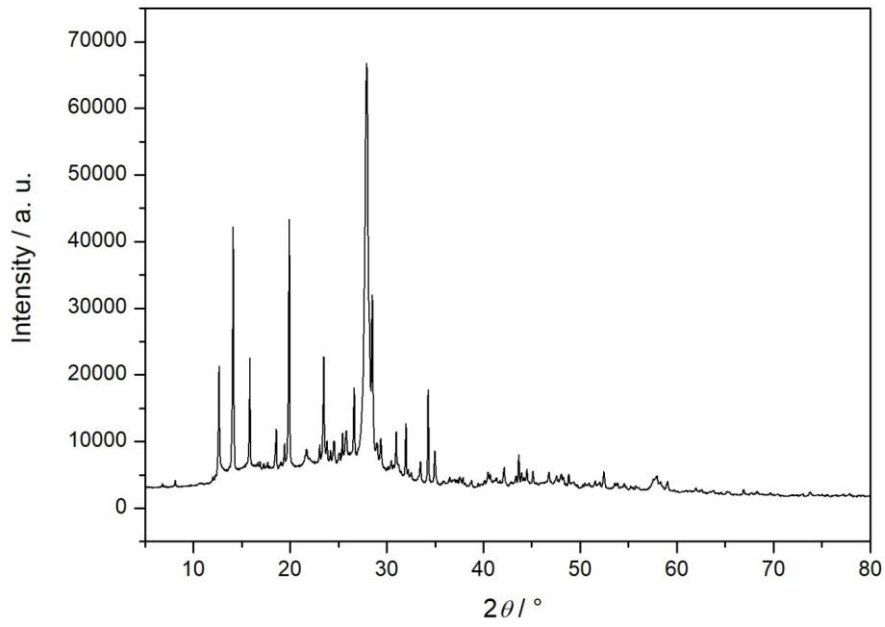

Figure 5.2.10 Powder X-ray diffractogram of **(3)**, Cu-$K_{\alpha 1}$ radiation (1.54056 Å). Sample prepared from $ZnCl_2$ salt melt (ratio 10:1).

Compound **(3)** was further investigated by solid-state MAS-NMR spectroscopy of nuclei ^{1}H, ^{13}C and ^{15}N (Figure 5.2.11). As described for previous experiments, cross polarization was used for ^{13}C and ^{15}N measurements to obtain improved signal-to-noise ratios.

Three signals could be discerned in the ^{1}H spectrum, possessing chemical shifts of 8.5, 4.2 and 0.9 ppm. The first resonance is attributed to protons located on bridging imide groups, while the shift of the second resonance is well in line with those found for terminal amino groups in C/N/H compounds. No unambiguous designation of the third resonance was possible. Furthermore, although the signal bands are rather broad, no signal could be discerned around 11 ppm, where H atoms protonating triazine or heptazine nuclei would be expected.

The ^{13}C spectrum exhibits two signal groups: a single band with a maximum at 156.6 ppm and two overlapping signals at 163.3 and 165.2 ppm. This pattern is in exceptional good agreement with shifts reported for melon. Literature describes one signal group around 157 ppm and another one between 163 and 165 ppm.[11] Likewise, reported spectra exhibit two signals for the latter group and but a single band for the former. The resonances are thus assigned in analogy with the designation reported for melon: the signal at 156.6 ppm is assigned to CN_3 carbon atoms of the heptazine nucleus, while the more low-field shifted signals result from C atoms located either next to the terminal amino groups or the bridging imide groups.

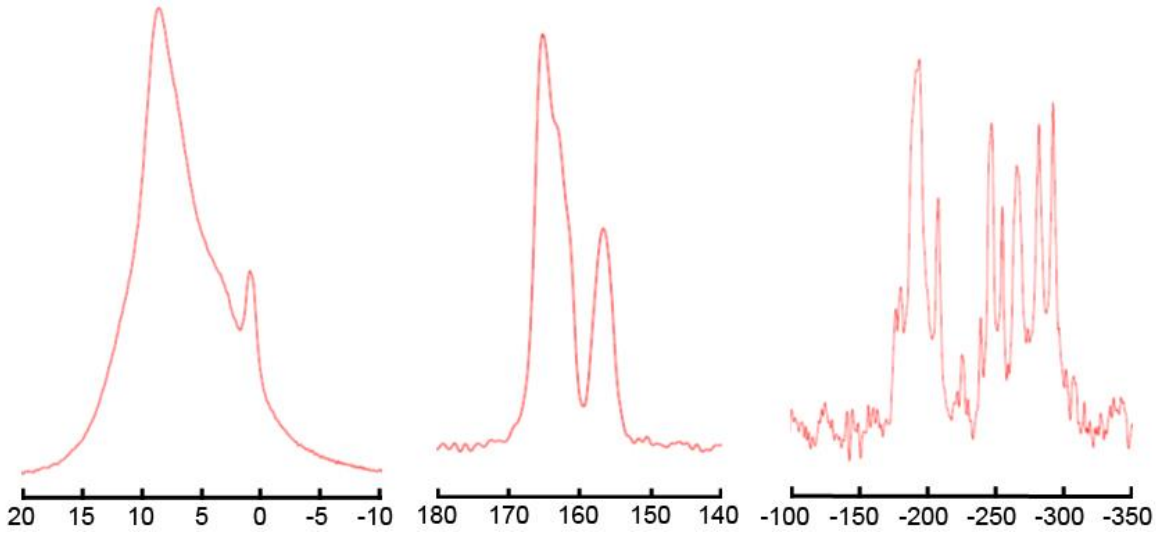

Figure 5.2.11 Solid-state MAS-NMR spectra of **(3)**. Left: ^{1}H spectrum. Middle: ^{13}C-CP spectrum. Right: ^{15}N-CP spectrum.

^{15}N NMR shows ten signals, which can be divided into four signal groups. In the region generally assigned to tertiary N atoms, three signals at -180.5, -194.2 and 208.0 ppm were observed. A single low-intensity signal at -225.6 ppm is identified as heptazine central N atom due to the characteristic chemical shift. The third group, consisting of four signals with shifts of -239.3, -247.3, -255.1 and 265.7 ppm results from imido N atoms. Finally, two signals at -282.1 and -292.4 ppm were assigned to terminal amino groups. Although no further structural information could be obtained from these experiments alone, they are well in line with expectations for melon and thus confirm the assumed identity of **(3)**.

All evidence suggests that **(3)**, obtained from syntheses with addition of very minor amounts of inorganic salts, is fundamentally identical to melon. Solid-state NMR spectroscopy identified the building blocks of melon and the obvious similarities in NMR as well as FT-IR spectra between the two compounds indicate an identical bonding pattern. Exposing pure dicyandiamide to temperature programs as used in the here described experiments would yield melon as well and, in fact, is rather close to commonly applied synthesis protocols. In contrast to the synthesis of various poly(triazine imides) or the above described compounds **(1)** and **(2)** the salt melt thus does not fundamentally change the course of the reaction. Reducing the amount of salt melt—i.e. solvent—will inevitably lead to only incomplete dissolution of the C/N/H starting material. Thus, adding only small amounts of salt will result in the reaction taking place not in solution but rather in solid state and thus proceeding along the typical reaction path of C/N/H compounds in the solid state, which is the condensation cascade described previously. It thus comes as little surprise that at temperatures of 550 °C melon is obtained as the product. It is, however, remarkable that the obtained product is highly crystalline and well ordered as observed by PXRD and very narrow bands in FT-IR as well as NMR spectra. The addition of inorganic salts thus does influence the reaction even when not leading to the formation of a novel product. Melon is well known as a material that exhibits strong stacking disorder and is thus

of notoriously poor crystallinity.[11,16] Crystallinity, however, has been shown to have great influence on the performance of the material in photocatalytic applications. Crystalline materials such as PTI or PHI surpass raw melon in e.g. hydrogen evolution rate by an order of magnitude.[17-19] The possibility to increase the crystallinity of the benchmark material melon might thus be of great advantage for more application-oriented research on C/N/H compounds. Based on the herein described observations, **(3)** is assumed to represent a more ordered variant of melon, possibly missing the stacking disorder observed in melon obtained via conventional synthesis routes. Since the primary difference between these syntheses and those presented herein is the presence of inorganic salts, it is postulated that salt ions exert a structure directing effect throughout the synthesis that leads to the formation of this well ordered material.

5.2.5 References

[1] M. J. Bojdys, J. O. Müller, M. Antonietti, A. Thomas, "Ionothermal Synthesis of Crystalline, Condensed, Graphitic Carbon Nitride", *Chem. Eur. J.* **2008**, *14*, 8177-8182.

[2] D. E. Bugaris, H.-C. zur Loye, "Materials Discovery by Flux Crystal Growth: Quaternary and Higher Order Oxides", *Angew. Chem.* **2012**, *124*, 3844-3876; *Angew. Chem. Int. Ed.* **2012**, *51*, 3780-3811.

[3] W. Sundermeyer, "Chemische Reaktionen in Salzschmelzen. IV. Neue Darstellungsmethode von Cyaniden, Cyanaten und Thiocyanaten des Siliciums und Kohlenstoffs", *Z. Anorg. Allg. Chem.* **1962**, *313*, 290-295.

[4] W. Sundermeyer, "Salzschmelzen und ihre Verwendung als Reaktionsmedien", *Angew. Chem.* **1965**, *77*, 241-258; *Angew. Chem. Int. Ed. Engl.* **1965**, *4*, 222-238.

[5] W. Sundermeyer, "Chemische Reaktionen in geschmolzenen Salzen", *Chem. Unserer Zeit* **1967**, *1*, 150-157.

[6] S. Hug, M. E. Tauchert, S. Li, U. E. Pachmayr, B. V. Lotsch, "A functional triazine framework based on N-heterocyclic building blocks", *J. Mater. Chem.* **2012**, *22*, 13956-13964.

[7] S. Hug, M. B. Mesch, H. Oh, N. Popp, M. Hirscher, J. Senker, B. V. Lotsch, "A fluorene based covalent triazine framework with high CO_2 and H_2 capture and storage capacities", *J. Mater. Chem. A* **2014**, *2*, 5928-5936.

[8] S. Hug, L. Stegbauer, H. Oh, M. Hirscher, B. V. Lotsch, "Nitrogen-Rich Covalent Triazine Frameworks as High-Performance Platforms for Selective Carbon Capture and Storage", *Chem. Mater.* **2015**, *27*, 8001-8010.

[9] G. J. Janz, R. P. T. Tomkins, C. B. Allen, J. R. Downey, G. L. Garner, U. Krebs, S. K. Singer, "Molten salts: Volume 4, part 2, chlorides and mixtures—electrical conductance, density, viscosity, and surface tension data", *J. Phys. Chem. Rev. Data* **1975**, *4*, 871-1178.

[10] V. W.-h. Lau, M. B. Mesch, V. Duppel, V. Blum, J. Senker, B. V. Lotsch, "Low-Molecular-Weight Carbon Nitrides for Solar Hydrogen Evolution", *J. Am. Chem. Soc.* **2015**, *137*, 1064-1072.

[11] B. V. Lotsch, M. Döblinger, J. Sehnert, L. Seyfarth, J. Senker, O. Oeckler, W. Schnick, "Unmasking Melon by a Complementary Approach Employing Electron Diffraction, Solid-State NMR Spectroscopy, and Theoretical Calculations—Structural Characterization of a Carbon Nitride Polymer", *Chem. Eur. J.* **2007**, *13*, 4969-4980.

[12] E. Wirnhier, M. Döblinger, D. Gunzelmann, J. Senker, B. V. Lotsch, W. Schnick, "Poly(triazine imide) with Intercalation of Lithium and Chloride Ions $[(C_3N_3)_2(NH_xLi_{1-x})_3 \cdot LiCl]$: A Crystalline 2D Carbon Nitride Network", *Chem. Eur. J.* **2011**, *17*, 3213-3221.

[13] C. Fettkenhauer, J. Weber, M. Antonietti, D. Dontsova, "Novel carbon nitride composites with improved visible light absorption synthesized in $ZnCl_2$-based salt melts", *Rsc Adv.* **2014**, *4*, 40803-40811.

[14] A. R. Pray, R. F. Heitmiller, S. Strycxer, V. D. Aftandilian, T. Muniyappan, D. Choudhury, M. Tamres, "Anhydrous Metal Chlorides", in *Inorganic Syntheses, Vol. V* (Ed.: T. Moeller), McGraw-Hill Book Company, Inc., New York, **1957**, pp. 153-156.

[15] N. E. Braml, A. Sattler, W. Schnick, "Formation of Melamium Adducts by Pyrolysis of Thiourea or Melamine/NH_4Cl Mixtures", *Chem. Eur. J.* **2012**, *18*, 1811-1819.

[16] L. Seyfarth, J. Seyfarth, B. V. Lotsch, W. Schnick, J. Senker, "Tackling the stacking disorder of melon—structure elucidation in a semicrystalline material", *Phys. Chem. Chem. Phys.* **2010**, *12*, 2227-2237.

[17] K. Schwinghammer, B. Tuffy, M. B. Mesch, E. Wirnhier, C. Martineau, F. Taulelle, W. Schnick, J. Senker, B. V. Lotsch, "Triazine-based Carbon Nitrides for Visible-Light-Driven Hydrogen Evolution", *Angew. Chem.* **2013**, *125*, 2495-2499; *Angew. Chem. Int. Ed.* **2013,** *52*, 2435-2439.

[18] K. Schwinghammer, M. B. Mesch, V. Duppel, C. Ziegler, J. Senker, B. V. Lotsch, "Crystalline Carbon Nitride Nanosheets for Improved Visible-Light Hydrogen Evolution", *J. Am. Chem. Soc.* **2014**, *136*, 1730-1733.

[19] D. Dontsova, S. Pronkin, M. Wehle, Z. Chen, C. Fettkenhauer, G. Clavel, M. Antonietti, "Triazoles: A New Class of Precursors for the Synthesis of Negatively Charged Carbon Nitride Derivatives", *Chem. Mater.* **2015**, *27*, 5170-5179.

6. Discussion and Outlook

This thesis concerned itself with C/N/H compounds based on the triazine nucleus, predominantly with compounds containing the melam and melaminium molecular or molecular ionic building blocks, but to a lesser degree also with oxo substituted ionic compound ammelinium and polymeric poly(triazine imide). As has been stated in the introductory chapter of this work, several chief questions were aimed to be elucidated in the conducted investigations. Triazine compounds are of only limited thermal stability and typically undergo condensation to form heptazines above certain temperatures. However, as has been shown by the example of poly(triazine imide)—a highly condensed yet triazine-based compound obtained at temperatures of 550 °C and above[1]—temperature is not the only factor influencing the triazine-to-heptazine transition and further factors must also be involved in constituting the stability of the respective nuclei. The first aim of this work thus was the elucidation of aspects that either favor the formation of triazines or increase the stability of triazine-based compounds towards further condensation reactions. In particular, preparative approaches for the targeted synthesis of (thermally) stable triazine-based compounds were subject of these studies. Especial attention was paid to additives to the reaction mixture, typically inorganic salts that would act on the occuring processes in a multitude of ways. The different roles of such salts—as a solvent in the form of melts, as a catalyst or as a reactant in the formation of ionic triazine compounds—and the importance of each of these in individual syntheses represent a second topic that has been under investigation. Furthering the knowledge on these roles might open up new synthetic routes and allow for a more directed preparation of further triazine-based compounds in the future.

Apart from preparative aspects, structural investigations constituted a major point of interest of this thesis. In contrast to typical inorganic compounds—e.g. oxides, nitrides, etc.—C/N/H compounds do not tend to form isostructural crystal structures, even when closely related regarding their constituents. Being molecular or molecular ionic in nature, the structure of C/N/H compounds is dominated by various inter- and intramolecular interactions, the most prominent of which are van-der-Waals interactions, hydrogen bridge bonds, and in the case of charged constituents, ionic interactions. The importance of each of these interactions and their structure directing effects, however, do vary from compound to compound. It was thus tried to work out general trends and preferences through comparison of different kinds of triazine-based compounds and thus gain insight in the fundamental principles that lead to the formation of observed structural motifs.

6.1 On the preparation of triazine-based compounds

As described in chapters 3 and 4, the central projects of this thesis were concerned with the synthesis and investigation of compounds based on melam or its protonated form melamium. Melam is an especially interesting compound regarding preparative considerations, since its direct synthesis is challenging due to competing processes taking place under similar reaction conditions. It has often been described as a reactive intermediate in the condensation process of melamine towards melem and has only been obtained from the condensation cascade in very small amounts and often contaminated with melamine, melem or adducts thereof.[2] This, in general, has been attributed to a very narrow temperature range between the formation temperature required for melam formation and the onset of melem condensation—the latter a process that has not been unambiguously elucidated itself. Quantitative synthesis of melam has been reported for syntheses in autoclaves under elevated ammonia pressure that impedes the formation of melem, which requires the elimination of one equivalent of ammonia, according to the principle of *Le Chatelier*.[3] The same principle has been successfully applied in this work in the synthesis of a melam-melem (1:1) adduct as described in chapter 4. These two syntheses do neither differ in applied temperature nor pressure nor starting material, but exclusively in the duration for which the compound was exposed to these conditions. Melam was obtained after dwell times of 4 - 5 days while 9 - 13 days were necessary for the formation of the adduct.[3,4] It has thus been concluded that under the chosen conditions elevated ammonia pressure does not completely impede the formation of melem, but only slows the reaction down, so that isolation of the intermediates melam and melam-melem (1:1) is possible. For both compounds, reaction temperatures significantly exceeded the commonly reported formation temperature of melam for thermal condensation in open systems of about 360 °C. However, only melamine is obtained as a product when performing analogous autoclave reactions at such low temperatures, since the formation of melam from melamine is accompanied by elimination of ammonia as well and thus also hindered. Significantly higher temperatures are thus necessary for even the decelerated reaction to take place. It is very much conceivable that the same principle can be applied for the synthesis of dimers or oligomers of melem by further raising the temperature to enter the regime of melem condensation. Such oligomers have shown to be promising materials for photocatalytic applications.[5] However, if extrapolation from the melam-to-melem condensation is possible, temperatures of well beyond 500 or even 600 °C would be required for such experiments, which are not accessible with commercially available autoclaves. Special high temperature autoclaves would thus be required to validate the feasibility of such an approach.

Before this thesis, reports on compounds containing the melamium cation have been scarce. To the author's best knowledge, only three publications on such salts did exist. In 1977, *Gavrilova et al.* reported on the synthesis of melamium chloride, nitrate, sulfate, phosphate and perchlorate through treatment of melam in diluted mineral acids, however, did not characterize any of the obtained

compounds.[6] The perchlorate salt could later be reproduced and characterized spectroscopically as well as crystallographically.[2] For the chloride as well as nitrate salt, however, it was shown that instead of melamium salts, salts of ammelinium, a product of melam hydrolysis, are actually formed. It was thus concluded that the proposed synthesis route is not suitable to obtain melamium salts of strong mineral acids, since these induce acidic hydrolysis of the precursor material.[7] This was further validated in this thesis through the example of ammelinium sulfate cyanuric acid and ammelinium sulfate monohydrate, both of which have been obtained from treatment of melam in diluted sulfuric acid, as described in chapter 3.3. In contrast to this observation, however, the proposed synthesis route seems to work quite well for weak mineral acids. As mentioned above the synthesis of melamium perchlorate via this route has been confirmed and experiments in diluted phosphoric acid in this thesis did show the formation of a colorless solid that did exhibit vibration bands unequivocally attributable to melamium imide groups. In these cases, the treatment of melam in aqueous mineral acids seem indeed to represent a viable synthesis routes towards the respective melamium salts.

A completely different synthetic approach has been reported on in the third of the abovementioned publications. For this, ampoules charged with either thiourea or a mixture of melamine and ammonium chloride were heated to elevated temperatures in a tube furnace and adducts of melamium thiocyanate and melamine or of melamium chloride and ammonium chloride were obtained, respectively.[8] It has been discussed in previous works that the formation of these compounds and inhibition of the formation of melem—which would be expected at the respective temperatures in thermal condensation reactions—results from the in situ generation of a Brønsted-acidic compound (HCl and HSCN in the here mentioned cases). The formation of melam, which is supposedly significantly more basic than melem or melamine, would thus be preferred since it is protonated more readily.[9,10] In this thesis, ampoule syntheses were used for the preparation of melamium bromide, melamium iodide and melamium thiocyanate melam, as described in chapters 3.1 and 3.2. In these syntheses, mixtures of dicyandiamide and ammonium bromide, ammonium iodide or ammonium thiocyanate were used, respectively. Each of these salts is able to liberate a corresponding hydroacid HBr, HI or HSCN, which are gaseous at the respective decomposition temperature of their ammonium salts.[11] No such compounds could be obtained in analogous reactions using ammonium sulfate or ammonium phosphate, both of which do decompose at the chosen temperature as well, however, would not liberate the respective (oxo)acid but rather their decomposition products. The presence of a (hydro)acid thus seems essential for the formation of melamium, supporting the hypothesis of the formation of melam being favorable under such conditions due to its strong basicity. Analogous to autoclave reactions, the melamium salts synthesized in this work were obtained at temperatures of 450 °C, well above the onset of melem formation under conventional—i.e. salt-free—conditions. Nevertheless, not even traces of melem could be detected in any sample of these compounds and the formation of the melamium salt appears to be quantitative. Both approaches thus seem feasible to expand the thermal stability range of melam(ium) and with it, of the triazine nucleus. While this may

come as little surprise in the case of the autoclave reactions since the interplay of temperature and pressure in chemical reaction is a well-established physicochemical principle, the stability of melamium (pseudo-)halide salts against further thermally induced condensation reactions—especially in comparison to other triazine-based materials—is quite remarkable. Thermoanalytic investigations showed these compounds to only undergo further condensation towards polymeric melon at significantly elevated temperatures. The expected intermediate phase melem appears to be skipped completely, which leads to the conclusion that these salts are thermodynamically preferable to melem, which itself is well known as a thermodynamic sink in the condensation cascade of C/N/H compounds. Only even more stable melon seems to be energetically favored over these melamium salts. It is noteworthy that comparable thermal stabilities in triazine compounds have also been reported for several other ionic compounds, such as tricyanomelaminates.[12,13] With the ionic character of the compounds as the common feature, it is concluded that salt-like triazine compounds are particularly stable against further thermally induced condensation or decomposition reactions and that ionic interactions and high lattice energies are suitable means to stabilize the triazine nucleus even at elevated temperatures.

It is tempting to add poly(triazine imide)—itself a triazine-based compound incorporating ions from inorganic salt melts and obtained at temperatures of 550 °C and above—to this category of compounds and apply the same argumentation. However, investigations into the formation mechanism of PTI, which have been described in chapter 5.1, show that the triazine nucleus is actually not conserved under the respective reaction conditions—an ionothermal reaction in LiCl/KCl or LiBr/KBr salt melt—but instead heptazine nuclei are formed from triazines, only for this formation to be reversed in the following reaction step. PTI is thus no example of a compound, in which the triazine nucleus is stabilized against thermally induced reactions and the condensation to heptazines suppressed. Rather, the fact that heptazine-based melem decomposes to form PTI is a testimony to the stability of this network structure, which is preferential to melem and melon even under these harsh reaction conditions. Several different reasons for this stability are conceivable. The presence of ions to be intercalated within the cavities of the network appears to be a necessary condition for the formation of PTI, independent of chosen synthetic approach.[1,14,15] However, it is rather unlikely that ionic interactions between the C/N/H network and the intercalated ions are the main reason for the stability of PTI. In contrast to aforementioned melamium or other C/N/H salts, the PTI network is at least formally uncharged, since intercalated ions compensate their respective charges and the protonation of ring nitrogen atoms appears to be compensated by deprotonation of imide groups.[16] Furthermore, Li^+ and Cl^- could be removed from cavities in PTI/Li^+Cl^- without the network collapsing, thus, these ions do not appear to be essential for the structural integrity of PTI.[4,17] Thus, while intercalated ions most certainly contribute to the stability of PTI and likely possess a structure directing effect that leads to the formation of the C/N/H network, ionic interactions do not appear to be the dominating effect for the preference of triazine nuclei in PTI. Another aspect that deserves closer notice is the

high degree of condensation realized in PTI. The idealized C/N/H network (neglecting any substitution of H^+ by Li^+) possesses the same sum formula and thus the same degree of condensation as melon. The formation of triazine based PTI from heptazine based melem is thus still accompanied by release of ammonia and thus means an increase in entropy. Compared to melon, PTI shows a 2D network as opposed to 1D chains. This more rigid structure might be energetically favorable at higher temperatures. Lastly, a 2D network comprised of heptazine rings in a PTI-analogous fashion—i.e. poly(heptazine imide), PHI—which would not require the decomposition of heptazine nuclei to be formed from melem, would possess a significantly larger cavity than PTI and would thus be unsuitable to accommodate Cl^- ions. In the reported case of PHI obtained as a side phase in melon formation, PHI exhibits a melamine molecule located in the respective cavity. Thus, in the presence of Cl^- or Br^- ions the formation of PTI is assumed to be energetically favorable, explaining the reversion of heptazine formation in the PTI formation process. Further aspects concerning the role of the salt melt as a liquid reaction medium shall be discussed further below. Thus, while several reasons for the unexpected formation of triazine-based PTI from heptazine-based melem are conceivable, the obtained data do not allow for the unambiguous explanation of this phenomenon.

6.2 On the influence of inorganic salts on C/N/H synthesis

Most of the experiments described throughout this thesis employed mixtures of a C/N/H precursor compound and one or more inorganic salts, with the latter fulfilling various different roles in different series of experiments. Salts were used as Lewis- or Brønsted-acidic catalysts, as a source for (hydro)acids for the protonation of C/N/H molecules and the respective counter ions, as well as as solvent for reactions in liquid phase in the form of salt melts. In all of these roles, the presence of the salt(s) greatly influenced the reaction process and was necessary for the formation of the respective product. For melamium salts, the role of ammonium salts added to the starting material has already been discussed in the previous chapter and is easily comprehensible. These salts liberate a Brønsted-acidic compound, which is then able to protonate the C/N/H compound—here melam—and furthermore provides the respective counter ion for salt formation. Apart from stabilization of the basic molecule melam as mentioned above, no further contribution is attributed to the salt.

A more thorough analysis is required for experiments conducted in excess salt melt as described in chapters 5.1 and 5.2. Here, additional criteria have to be taken into consideration, since reaction conditions in solid state and solution may differ fundamentally. In solution, free diffusion of molecules or molecular building blocks is possible, influencing the kinetics of such reactions and potentially leading to different products. Furthermore, solubilities of different compounds—e.g. triazines and heptazine—in the respective solvent have to be considered. Since reactions in solution are expected to proceed significantly faster than reactions in solid state, precursor compounds or building blocks of high solubility would clearly be favored in such processes. In water, triazine-based compounds such

as melamine exhibit a higher solubility than their heptazine-based counterparts due to a larger dipole moment. A similar behavior can be expected in salt melts, which are polar solvents as well. Thus, compounds such as PTI might be favored in salt melts for reasons of solubility.

Experiments in various salt melts described in chapter 5.2 showed that rather small amounts of salt melt are sufficient to obtain these effects. In particular, investigations in molten $ZnCl_2$ did show that less than 1 mol of $ZnCl_2$ per mol of precursor compound dicyandiamide was necessary to obtain the same product as was formed in excess salt melt. This might either indicate an astonishing solubility for dicyandiamide in molten $ZnCl_2$, or signify that although dissolution of the starting material is incomplete, the reaction in liquid medium is favored to a degree that allows to dominate the entire process, e.g. through precipitation of the formed product and dissolution of further starting material as well as any intermediates eventually formed in solid state.

Furthermore, it could be shown that in this type of reaction, inorganic salt melts act not only as solvents, but fulfill multiple roles at once and the choice of salt is thus essential. In previously reported syntheses of PTI/Li^+Cl^- and PTI/Li^+Br^-, chloride and bromide based salt melts did, in essence, yield identical products and lead to the formation of the same C/N/H network.[1,14] The choice of cation, however, appears to be of more significance, as has been shown by the examples of compounds **(1)** and **(2)** obtained from $ZnCl_2$ and $CdCl_2$/KCl melt, respectively. While the compound obtained from $ZnCl_2$ is assumed to be structurally closely related—although not identical—to PTI as obtained from Li^+-containing melts, $CdCl_2$/KCl melts instead had little effect on the reaction at all, as seen by the formation of a melem-like product—as would have been expected in salt-free synthesis. It is conceivable that different dissolving powers of the respective melts play a role in this, however, whether these alone account for different reaction behavior or whether further effects such as ion incorporation are relevant, remains to be elucidated in further studies.

A third effect of inorganic salts on the reaction behavior of C/N/H compounds was observed in experiments with substoichiometric amounts of $ZnCl_2$. In these syntheses, a very melon-like material was obtained, which, however, showed signs of well-developed long-range order and crystallinity. This is completely unlike any other reports on melon, which is notorious for its disorder phenomena and commonly exhibits but a single reflection in powder X-ray diffractograms, which is attributed to stacking distances. However, no indication for incorporation of any ions could be found. Furthermore, the observed effect was independent of the total amount of salt additive—so long as this amount did not exceed the minimum amount to enter the regime of liquid phase reaction that would result in the formation of compound **(1)**—thus giving further evidence that the salt does not participate in the reaction as a reactant. The effect could also be reproduced with a variety of different salts, namely $CdCl_2$/KCl, AgCl/KCl and LiCl/KCl and thus appears to be largely independent of a specific compound, but rather depend on the presence of any (halide) salt at all. For neither of these any indication of ion incorporation or dependence on stoichiometry was detected. It is thus assumed that the effect leading to the formation of this ‘crystalline melon’ is catalytic in nature. However, since no elucidation of the

crystal structure of the thus obtained material was possible and thus no structural feature responsible for the observed crystallinity can be identified, no catalytic mechanism can be named either. Further—in particular: crystallographic—investigations will have to be conducted to gain deeper insight into this effect.

6.3 On structural motifs and interactions in C/N/H substructures

Novel preparative approaches for C/N/H materials, as have been reported on in literature as well as described in this work, often tend to yield compounds of unexpected composition, e.g. adduct compounds in which the parallel existence of multiple different molecular or molecular ionic building units is not imminently explicable. Examples from literature for such compounds include three different melamine-melem adducts,[18] melemium melem perchlorate,[19] and melamium thiocyanate melamine.[8] This thesis added several additional compounds to this range, namely melamium thiocyanate melam, melam-melem (1:1) and ammelinium sulfate cyanuric acid. In the cases of melamium bromide and melamium iodide the here obtained compounds show compositions that would be expected for the utilized preparative route, however, diverge from the previously described compound melamium chloride ammonium chloride, which has been prepared in an analogous approach.[8] Unexpected compositions in C/N/H compounds typically manifest in coexistence of several species of C/N/H molecules or molecular ions, even when thermodynamics would suggest only one of them to be stable; protonation of only parts of the molecules of a C/N/H species, even with the protonating acid present in excess; or formation of double salts with additional species.

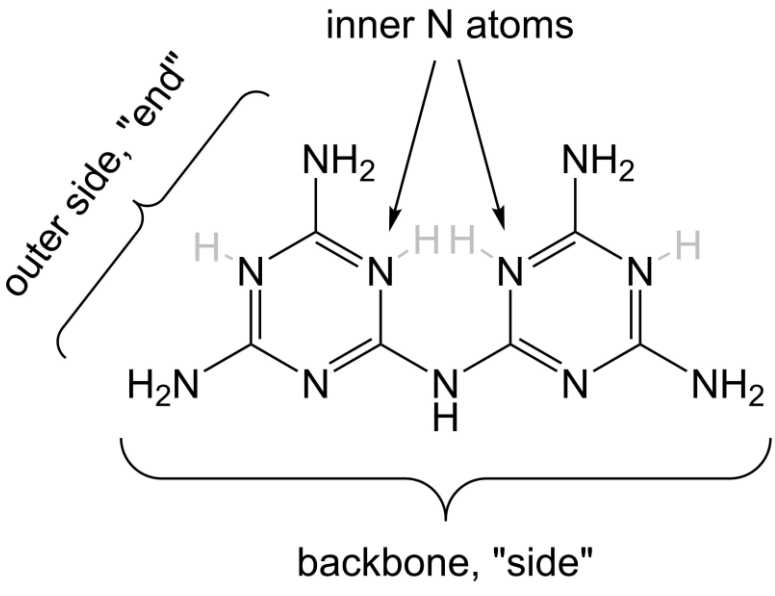

Figure 6.1 Definitions of different parts of the melam molecule. H atoms in light grey represent potential protonation sites.

Reasons for the formation of these compounds of unexpected composition were sought in their crystallographic structures. The structures of C/N/H compounds are generally determined by several

different types of intra- and intermolecular interactions, most prominent of which are van-der-Waals interactions, hydrogen bridge bonds and—in the case of salt-like compounds—ionic interactions. The latter, however, shall herein be neglected and the following discussion be focused on interactions between C/N/H units, exclusively. Neither shall covalent interactions—e.g. the formation of networks in polymeric compounds, such as PTI—be discussed in this place.

The majority of (monomeric) compounds studied in this thesis comprise the melam or melamium unit. This molecule is structurally interesting due to its low symmetry in comparison to e.g. melamine or melem molecules, which both exhibit D_{3h} symmetry in their idealized form.[20] This allows for several non-equivalent orientations of melam(ium) units within a structure, which result in a multitude of possible interaction patterns between structural units. Furthermore, melam possesses free rotatability around the imide bridge, resulting in a variable dihedral angle between the triazine ring planes. In contrast to melamine, melem and their derivatives, this allows melam(ium) to significantly deviate from molecular planarity, resulting in structural motifs exclusively available to this C/N/H representative. In pure melam, for example, molecular building blocks are arranged in helical motifs instead of in stacked layers.[2] These dihedral angles are typically rather small—11° to 14° in pure melam—however, the adduct compound melam-melem (1:1) elucidated in this work showed angles of up to 48° and quantum-chemical calculations for a hypothetical isolated melam dimer in the gas phase yielded dihedral angles of up to 39°, thus illustrating the structural flexibility the molecule possesses due to this rotational degree of freedom. In the melam-melem adduct large dihedral angles allow single melam molecules to form hydrogen bridge bonds towards melem molecules located in different layers of the melem substructure, while in the case of the dimer steric reasons are assumed for the large angle. The moderate dihedral angles in pure melam are interpreted as being favorable, since they allow for a maximum number of interactions within the 3D network of the melam structure. In contrast, melamium is typically planar or exhibits only small dihedral angles between the triazine ring planes. Melamium possesses three structurally different triazine ring N atoms that could potentially be protonated. However, it has been shown in previous work that protonation preferentially occurs at the ‘inner’ N atom next to the imide bridge (Figure 6.1). This allows for an intramolecular hydrogen bridge between this protonated N atom and the opposite inner N atom of the second triazine ring. However, formation of this hydrogen bridge requires a torsion angle close to 0°. Although hydrogen atoms could not be established from structure solution for melamium compounds investigated in this thesis and thus were geometrically constructed, planarity of the melamium ions indicate a protonation pattern identical to those observed in other melamium salts. For melamium iodide, melamium thiocyanate and one of two melamium ions in melamium bromide almost perfect planarity was observed while the remaining melamium ion in melamium bromide exhibited but a small dihedral angle of less than 7°. The latter might be an indication of a deviating protonation pattern, however, no unambiguous proton positions could be determined due to proximity to bromide ions. Nevertheless, the trend towards planarity for melamium ions is evident.

Three different hydrogen bridge binding motifs between melam(ium) molecules and ions have been observed, as depicted in Figure 6.2. Molecules can be oriented with their backbones towards each other, as is the case in melam-melem (1:1) or in melamium chloride ammonium chloride as well as in melamium thiocyanate melamine. This motif allows for the formation of four hydrogen bridge bonds with one amino group and one imide group per melam(ium) unit acting as donor and two triazine ring N atoms per melam(ium) unit as acceptor group. In a second motif, one melam(ium) molecule is oriented with the short, 'outer' side of a diamino triazine subunit towards the backbone side of a second melam(ium) unit. This 'side-on-end' motif results in three hydrogen bridges with two terminal amino groups of the 'end-facing' melam(ium) and the imide group of the 'side-facing' unit acting as hydrogen bridge donors and respective opposite triazine ring N atoms in both molecules as the acceptors. 'Side-on-end' motifs have been observed in pure melam[2] and melam hydrate,[3] but never before in ionic melamium compounds. In this thesis, the motif has been observed in melamium bromide, melamium iodide and melamium thiocyanate melam. The third motif is formed from two melam(ium) units facing each other with their outer sides. Two hydrogen bridges are realized in this motif. These occur between a triazine ring N atom acceptor and an amino group donor, respectively. The two melam(ium) units in these motif are typically connected through inversion. Such 'end-on-end' motifs have been observed for pure melam,[2] melam hydrate,[3] melamium chloride ammonium chloride[8] as well as for the herein described compounds melamium bromide, melamium iodide, melamium thiocyanate melam and melam-melem (1:1).

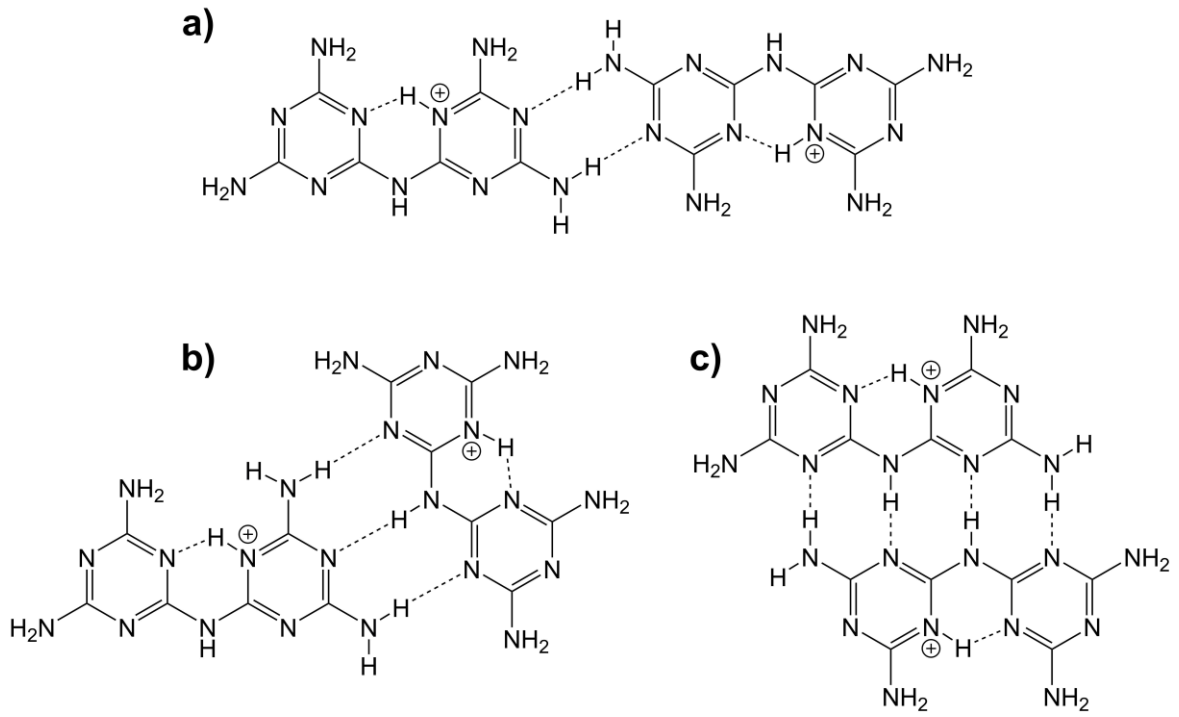

Figure 6.2 Hydrogen binding motifs in melam and melamium compounds. **a)** end-on-end motif; **b)** side-on-end motif; **c)** side-on-side or backbone motif.

The strength of hydrogen bridge bonds is correlated with the respective donor-acceptor distances, which are easily accessible from the structure and therefore represent a good measure for bond strengths. Certain general trends can be deduced when comparing hydrogen bonds as found in the different binding motifs. In side-on-end and side-on-side motifs, bonds originating from amino groups were always found shorter than those involving imide groups, the latter being in average 0.2 Å longer and thus supposedly weaker. Donor-acceptor distances in end-on-end motifs, exclusively showing amino groups as hydrogen bridge donors, are slightly longer than amino group involving distances in the other two motifs. Side-on-side and side-on-end motifs thus appear to not only represent stronger hydrogen networks due to their higher number of bonds, but also due to the strengths of at least a part of these bonds. A second trend that was observed lies in ionic melamium expressing hydrogen bonds with shorter donor-acceptor-distances than uncharged melam. This trend is true for all binding motifs and has been observed for pure melam, melam hydrate as well as the adduct compound melam-melem (1:1). A reasonable explanation might be that depletion of electron density in the positively charged melamium cations increases the electron affinity of N atoms and thus strengthens intermolecular interactions.

Although they apparently represent the weakest hydrogen bridge interactions, end-on-end motifs occur in every structurally known melam or melamium compound. The only exception in this is the melamium thiocyanate melamine adduct,[8] in which, however, analogous interactions occur between melamium and melamine. This omnipresence might be rationalized by the fact that each melam(ium) unit allows for the formation of two such sets of interactions and these thus are structurally readily available. Each of the investigated compounds furthermore expresses a second motif of hydrogen bridge interactions, either the side-on-end or the side-on-side motif. These two, however, are mutually exclusive since their co-presence would require multiple crystallographically independent melam(ium) units and different crystallographic environments, which is seldom realized in C/N/H compounds. No such limitations occur for the combination of the end-on-end motif with any of these other motifs.

No correlation could be observed between the presence or absence of ionic interactions and the amount of hydrogen bridge interactions. While in melamium perchlorate hydrate melamium does exclusively interact with the anion and water molecules, dense hydrogen networks have been observed e.g. in melamium bromide and while the melam-melem (1:1) adduct shows a multitude of hydrogen bridge interactions between melam and melam as well as between melam and melem (and between melem and melem), no such dense networks have been reported for pure melam or melam hydrate. This observation is attributed to interactions between melamium and the respective anion typically taking place at the ‘inner’ part of the C/N/H structure, which is not involved in any of the observed melam-melam interactions, and thus do not impair these.

Apart from pure melam and the melam-melem (1:1) adduct, all other structurally characterized melam(ium) compounds—including those elucidated in this thesis—are layered. Such layers can be

either planar or corrugated with multiple examples found for both cases. It is noteworthy that in the case of corrugated layers, the melamium molecules themselves are more or less planar and corrugation only occurs through their orientation. No conclusive criteria for the formation of corrugation or planarity could be deduced from any observed structural feature. In fact, melamium iodide and melamium thiocyanate melam show identical network arrangements of melamium units, however, layers within the former are planar while they are corrugated within the latter. It is thus assumed that corrugation only plays a minor role in the structural stability of these compounds.

Layered compounds are common in the group of C/N/H materials since such arrangements allow for the formation of π-π interactions between the conjugated π-systems of aromatic triazine rings. In this regard, C/N/H compounds behave very similar to graphite. Next to hydrogen bridge interactions, these van-der-Waals interactions are the second major group of intermolecular interactions that define the constitution of C/N/H structures. To obtain the greatest interaction, ring systems have to be arranged in an eclipsing stacking pattern. In melam and melamium compounds, eclipsing, partially eclipsing as well as non-eclipsing arrangements of the ring systems are realized. Van-der-Waals interactions are thus expected to be of different importance for each of these structures. In the herein investigated compounds, no correlation between the degree of overlap or the interlayer distance as a means to measure the strength of such interactions, and the amount of hydrogen interactions could be observed. Neither was a preference for π-stacks observed for either ionic or non-ionic compounds. Structural features of the investigated C/N/H compounds appear to depend much more on the formation of hydrogen bridge interactions, so van-der-Waals interactions are interpreted as less important.

Interactions in ammelinium salts shall only be discussed briefly. For both ammelinium sulfate cyanuric acid and ammelinium sulfate monohydrate only moderate amounts of hydrogen bridge interactions between the C/N/H ions were observed. In the former case, hydrogen bridges are formed exclusively in triangular motifs consisting of one cyanuric acid molecule surrounded by three ammelinium ions. These motifs, however, are isolated from each other. In the latter compound, only one of two crystallographically independent ammelinium ions does form hydrogen bridge interactions towards other ammelinium units at all. The second type of ammelinium ions exclusively interacts with sulfate groups and water molecules. No continuous network of hydrogen bridged C/N/H units could be observed for any ammelinium compound. This is caused by a lack of hydrogen bridge donor groups since the keto group of ammelinium in contrast to the substituted amino group acts as an acceptor. Isolated units are thus much more common than in melam(ium) compounds. However, a multitude of hydrogen bridge interactions towards sulfate groups or water could be observed for both compounds. These apparently replace the interactions between ammelinium units and are interpreted as having a major influence on the structural arrangement within these compounds.

To conclude, it can be stated that throughout this thesis the binding behavior or melam and melamium compounds was extensively studied and valuable insights into occurrence and importance of different types of interactions could be achieved. Melam(ium), although lacking the threefold symmetry of

related C/N/H compounds melamine and melem, was shown to be a highly flexible hydrogen bridge donor as well as acceptor. Comparison to ammelinium-based compounds, which form hydrogen bridge bonds much more reluctantly, illustrated the particular advantage of the melam building block to lie within the near even number of accessible hydrogen bridge donor and acceptor sites and their alternating arrangement, allowing melam to form dense hydrogen bridged networks with itself. In contrast to other molecular C/N/H compounds, melam is able to not only form multiple different motifs due to its lower symmetry, but also to form a greater number of such bonds, e.g. in fourfold bonded side-on-side motifs. Another aspect that increases the flexibility of this molecule lies within the rotational degree of freedom around the imide bridge, as could be shown in melam-melem (1:1). Melam—as opposed to melamine or melem—is thus not limited to hydrogen network formation within a plane, but able to form 3D structures and even interconnect multiple layers of planar substructure. Various melamium salts as well as hydrates studied in this thesis furthermore showed the readiness of the molecule to not only form hydrogen bridges towards itself but also to coordinate anionic groups or hydrate water molecules. This vast array of options would make melam and melam-based compounds a very attractive choice for supramolecular chemistry and crystal engineering, e.g. in analogy to the famous adducts of melamine and cyanuric acid studied by *Whitesides et al.*[21,22] The coordination behavior of melam towards metal ions has not been investigated in this thesis, however, the literature example of a melam zinc chloride adduct compound,[2] in which melam coordinates to Zn^{2+}, gives rise to the expectation that future work might yield additional such compounds and thus further expand the structural diversity of this flexile ligand. Metal coordination would also open up further areas of application for melam, e.g. in metal organic frameworks.

Several projects attempted in this thesis could not be brought to a close and require to be tackled in future studies. Attempts were undertaken on the synthesis of melamium phosphate according to the route described by *Gavrilova et al.*,[6] however, no single crystals of the compound could be obtained and the composition could not unambiguously be determined. This compound might be of great interest, since phosphoric acid just as perchloric acid is a weak acid and thus might actually yield a melamium salt as opposed to ammelinium salts obtained with strong acids such as sulfuric, nitric or hydrochloric acid through this synthesis route. Furthermore, melamium perchlorate is structurally interesting in that no melamium-melamium interactions at all are expressed in this compound. Additional related compounds might thus shed further light on the structural behavior of melam and melamium compounds. The formation mechanism of triazine based 2D extended polymer PTI in salt melts could be elucidated, however, the discovery of synthesis routes for PHI from triazoles or tetrazoles in LiCl/KCl melts in recent years did show that salt melts could also propagate the formation of heptazine based compounds. A deeper understanding of the ongoing processes in these reactions could grant further insights in the underlying principles and allow for a comparison with the formation mechanism of PTI. Furthermore, several compounds obtained from Lewis acidic salt melts that have been described in chapter 5.2 still lack structural elucidation. Since no single crystals of these

compounds could be obtained and attempts on structure solution from powder X-ray diffraction were not fruitful, alternative methods have to be tested in order to make progress on these projects. More advanced diffraction methods such as electron diffraction or synchrotron X-ray diffraction or spectroscopic methods such as 2D correlation NMR experiments might prove useful in these investigations.

Although this thesis is far from unambiguously answering the entirety of initially posed questions, several valuable contributions could be made to the understanding of C/N/H material structures and underlying interactions and mechanisms. In a time, in which structural elucidation of these materials plays less and less of a role, while an exclusive focus on material properties and application comes to the fore, the author hopes to have shown that despite of almost two centuries of investigations, C/N/H chemistry still holds the potential for completely novel materials and fundamental questions to be answered.

[1] E. Wirnhier, M. Döblinger, D. Gunzelmann, J. Senker, B. V. Lotsch, W. Schnick, "Poly(triazine imide) with Intercalation of Lithium and Chloride Ions $[(C_3N_3)_2(NH_xLi_{1-x})_3 \cdot LiCl]$: A Crystalline 2D Carbon Nitride Network", *Chem. Eur. J.* **2011**, *17*, 3213-3221.

[2] B. V. Lotsch, W. Schnick, "New Light on an Old Story: Formation of Melam during Thermal Condensation of Melamine", *Chem. Eur. J.* **2007**, *13*, 4956-4968.

[3] E. Wirnhier, M. B. Mesch, J. Senker, W. Schnick, "Formation and Characterization of Melam, Melam Hydrate, and a Melam–Melem Adduct", *Chem. Eur. J.* **2013**, *19*, 2041-2049.

[4] E. Wirnhier, "Solvothermal and Ionothermal Approaches to Carbon Nitride Chemistry", Doctoral Thesis, University of Munich (LMU), **2013**.

[5] V. W.-h. Lau, M. B. Mesch, V. Duppel, V. Blum, J. Senker, B. V. Lotsch, "Low-Molecular-Weight Carbon Nitrides for Solar Hydrogen Evolution", *J. Am. Chem. Soc.* **2015**, *137*, 1064-1072.

[6] N. K. Gavrilova, V. A. Gal'perin, A. I. Finkel'shtein, A. G. Koryakin, "Synthesis of Melam and its Salts with Mineral Acids", *Zh. Org. Khim.* **1977**, *13*, 669-670.

[7] B. V. Lotsch, W. Schnick, "Synthesis and Structural Characterization of the Ammelinium Salts $[C_3H_6N_5O]Cl$, $[C_3H_6N_5O]Br$, and $[C_3H_6N_5O]NO_3$", *Z. Anorg. Allg. Chem.* **2006**, *632*, 1457-1464.

[8] N. E. Braml, A. Sattler, W. Schnick, "Formation of Melamium Adducts by Pyrolysis of Thiourea or Melamine/NH_4Cl Mixtures", *Chem. Eur. J.* **2012**, *18*, 1811-1819.

[9] B. V. Lotsch, "From Molecular Building Blocks to Condensed Carbon Nitride Networks: Structure and Reactivity", Doctoral Thesis, University of Munich (LMU), **2006**.

[10] A. Sattler, "Investigations into s-Heptazine-Based Carbon Nitride Precursors", Doctoral Thesis, University of Munich (LMU), **2010**.

[11] M. Ohta, S. Hirai, H. Kato, V. V. Sokolov, V. V. Bakovets, "Thermal Decomposition of NH_4SCN for Preparation of Ln_2S_3 (Ln = La and Gd) by Sulfurization ", *Mater. Trans.* **2009**, *50*, 1885-1889.

[12] E. Irran, B. Jürgens, W. Schnick, "Synthesis, crystal structure determination from X-ray powder diffractometry and vibrational spectroscopy of the tricyanomelaminate monohydrates $M_3[C_6N_9]\cdot H_2O$ (M=K, Rb)", *Solid State Sci.* **2002**, *4*, 1305-1311.

[13] B. Jürgens, E. Irran, J. Schneider, W. Schnick, "Trimerization of NaC_2N_3 to $Na_3C_6N_9$ in the Solid: Ab Initio Crystal Structure Determination of Two Polymorphs of NaC_2N_3 and of $Na_3C_6N_9$ from X-ray Powder Diffractometry", *Inorg. Chem.* **2000**, *39*, 665-670.

[14] S. Y. Chong, J. T. A. Jones, Y. Z. Khimyak, A. I. Cooper, A. Thomas, M. Antonietti, M. J. Bojdys, "Tuning of gallery heights in a crystalline 2D carbon nitride network", *J. Mater. Chem. A* **2013**, *1*, 1102-1107.

[15] Z. Zhang, K. Leinenweber, M. Bauer, L. A. J. Garvie, P. F. McMillan, G. H. Wolf, "High-Pressure Bulk Synthesis of Crystalline $C_6N_9H_3\cdot HCl$: A Novel C_3N_4 Graphitic Derivative", *J. Am. Chem. Soc.* **2001**, *123*, 7788-7796.

[16] M. B. Mesch, K. Bärwinkel, Y. Krysiak, C. Martineau, F. Taulelle, R. B. Neder, U. Kolb, J. Senker, "Solving the Hydrogen and Lithium Substructure of Poly(triazine imide)/LiCl Using NMR Crystallography", *Chem. Eur. J.* **2016**, *22*, 16878-16890.

[17] E. J. McDermott, E. Wirnhier, W. Schnick, K. S. Virdi, C. Scheu, Y. Kauffmann, W. D. Kaplan, E. Z. Kurmaev, A. Moewes, "Band Gap Tuning in Poly(triazine imide), a Nonmetallic Photocatalyst", *J. Phys. Chem. C* **2013**, *117*, 8806-8812.

[18] A. Sattler, S. Pagano, M. Zeuner, A. Zurawski, D. Gunzelmann, J. Senker, K. Müller-Buschbaum, W. Schnick, "Melamine–Melem Adduct Phases: Investigating the Thermal Condensation of Melamine", *Chem. Eur. J.* **2009**, *15*, 13161-13170.

[19] A. Sattler, W. Schnick, "Preparation and Structure of Melemium Melem Perchlorate $HC_6N_7(NH_2)_3ClO_4\cdot C_6N_7(NH_2)_3$", *Z. Anorg. Allg. Chem.* **2008**, *634*, 457-460.

[20] B. Jürgens, E. Irran, J. Senker, P. Kroll, H. Müller, W. Schnick, "Melem (2,5,8-Triamino-tri-s-triazine), an Important Intermediate during Condensation of Melamine Rings to Graphitic Carbon Nitride: Synthesis, Structure Determination by X-ray Powder Diffractometry, Solid-State NMR, and Theoretical Studies", *J. Am. Chem. Soc.* **2003**, *125*, 10288-10300.

[21] G. Whitesides, J. Mathias, C. Seto, "Molecular self-assembly and nanochemistry: a chemical strategy for the synthesis of nanostructures", *Science* **1991**, *254*, 1312-1319.

[22] G. M. Whitesides, E. E. Simanek, J. P. Mathias, C. T. Seto, D. Chin, M. Mammen, D. M. Gordon, "Noncovalent Synthesis: Using Physical-Organic Chemistry To Make Aggregates", *Acc. Chem. Res.* **1995**, *28*, 37-44.

7. Appendix

7.1 Supporting Information for Chapter 3.2: Melamium Thiocyanate Melam

Contents:

- Optical microscope image of $C_6N_{11}H_{10}SCN{\cdot}C_6N_{11}H_9$.
- Impedance spectrum of $C_6N_{11}H_{10}SCN{\cdot}C_6N_{11}H_9$.
- Bond lengths in Å for $C_6N_{11}H_{10}SCN{\cdot}C_6N_{11}H_9$, excluding unrefinable thiocyanate anions.
- Angles in ° for $C_6N_{11}H_{10}SCN{\cdot}C_6N_{11}H_9$, excluding unrefinable thiocyanate anions.
- Atom coordinates x, y, z and isotropic displacement parameters U_{iso} for $C_6N_{11}H_{10}SCN{\cdot}C_6N_{11}H_9$.
- Crystal structure of "$C_6N_{11}H_{9.5}$".
- ^{1}H, ^{13}C and ^{15}N solid-state MAS-NMR spectra of $C_6N_{11}H_{10}SCN{\cdot}C_6N_{11}H_9$.
- Quantification of thiocyanate through UV-Vis spectroscopic measurements
- Summary of Rietveld refinement for $C_6N_{11}H_{10}SCN{\cdot}C_6N_{11}H_9$.

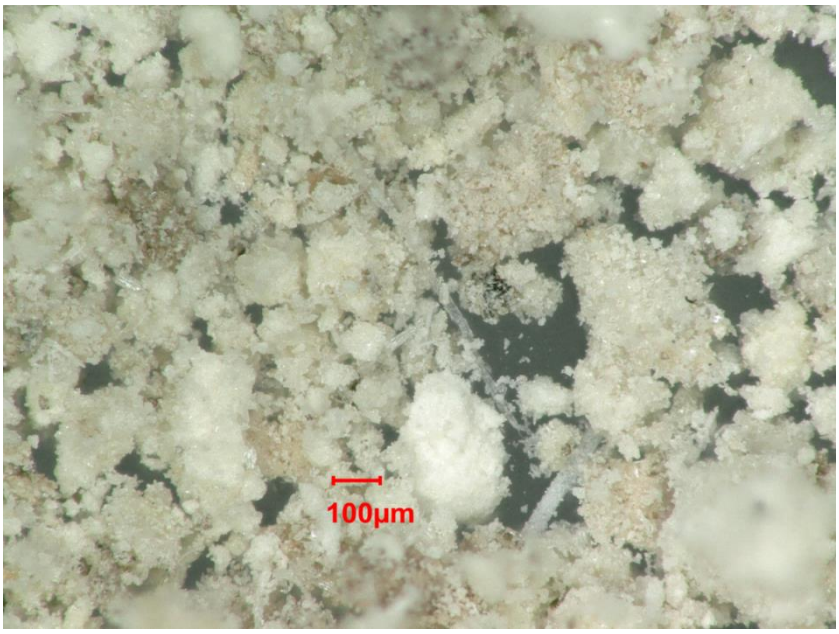

Figure 7.1.1 Optical microscope image of a representative sample of $C_6N_{11}H_{10}SCN{\cdot}C_6N_{11}H_9$. Needle-shaped single crystals can be seen amidst the polycrystalline material.

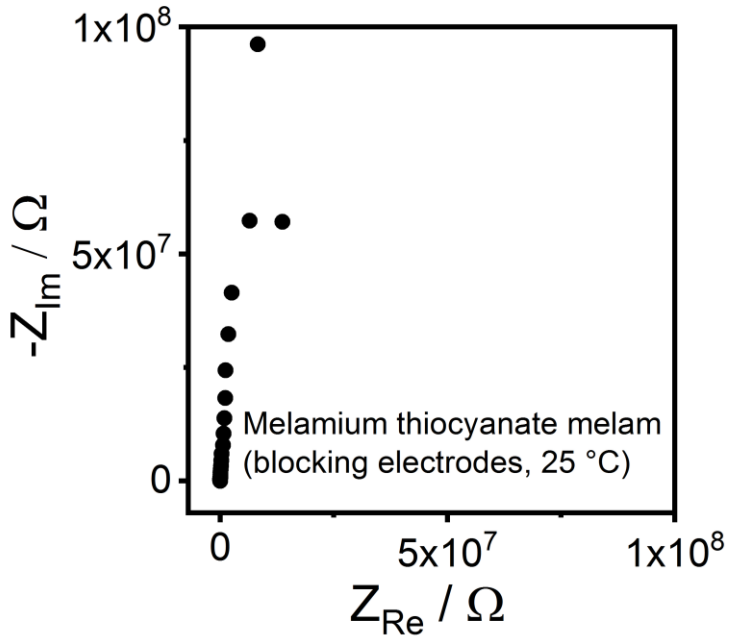

Figure 7.1.2 Impedance spectrum of $C_6N_{11}H_{10}SCN{\cdot}C_6N_{11}H_9$ measured between blocking electrodes (stainless steel) in the frequency range of 1 MHz to 1 Hz at 25 °C. A steep increase resembles the behavior of an insulating material. Neither ionic nor electronic conductivity could be observed.

Table 7.1.1 Bond lengths in Å for $C_6N_{11}H_{10}SCN{\cdot}C_6N_{11}H_9$, excluding unrefinable thiocyanate anions.

N01-C03	1.339(10)
N01-C02	1.366(10)
N02-C05	1.305(11)
N02-C03	1.344(11)
N03-C02	1.330(11)
N03-H01	0.8801
N03-H02	0.8800
N04-C01	1.329(11)
N04-C04	1.374(12)
N04-H03	0.8801
N05-C03	1.361(10)
N05-H04	0.8801
N05-H05	0.8800
N06-C04	1.339(12)
N06-H06	0.8802
N06-H07	0.8800
N07-C01	1.358(10)
N07-C05	1.415(11)
N07-H10	0.8801
N08-C06	1.315(11)
N08-H12	0.8800
N08-H13	0.8800
N09-C04	1.317(12)
N09-C06	1.352(11)
N10-C02	1.334(11)
N10-C05	1.358(11)
N10-H11	0.7003
N11-C01	1.335(10)
N11-C06	1.346(11)

Table 7.1.2 Angles in ° for $C_6N_{11}H_{10}SCN{\cdot}C_6N_{11}H_9$, excluding unrefinable thiocyanate anions.

C03-N01-C02	112.1(7)
C05-N02-C03	113.2(7)
C02-N03-H01	118.3
C02-N03-H02	121.6
H01-N03-H02	120.0
C01-N04-C04	113.4(7)

C01-N04-H03	122.7
C04-N04-H03	123.7
C03-N05-H04	119.7
C03-N05-H05	120.1
H04-N05-H05	120.0
C04-N06-H06	118.1
C04-N06-H07	121.9
H06-N06-H07	120.0
C01-N07-C05	130.3(7)
C01-N07-H10	114.9
C05-N07-H10	114.9
C06-N08-H12	120.4
C06-N08-H13	119.5
H12-N08-H13	120.0
C04-N09-C06	115.3(7)
C02-N10-C05	114.2(7)
C02-N10-H11	105.0
C05-N10-H11	139.5
C01-N11-C06	114.1(7)
N04-C01-N11	127.0(8)
N04-C01-N07	118.8(7)
N11-C01-N07	114.2(7)
N03-C02-N10	117.3(7)
N03-C02-N01	117.0(7)
N10-C02-N01	125.6(8)
N01-C03-N02	128.2(7)
N01-C03-N05	114.4(7)
N02-C03-N05	117.4(7)
N09-C04-N06	119.2(9)
N09-C04-N04	125.2(8)
N06-C04-N04	115.6(9)
N02-C05-N10	126.7(8)
N02-C05-N07	116.8(7)
N10-C05-N07	116.4(7)
N08-C06-N11	118.7(8)
N08-C06-N09	116.4(8)
N11-C06-N09	124.9(8)

Table 7.1.3 Atom coordinates x, y, z and isotropic displacement parameters U_{iso} for $C_6N_{11}H_{10}SCN{\cdot}C_6N_{11}H_9$, excluding unrefinable thiocyanate anions.

Atom name	x	y	z	U_{iso}
N01	1.089(2)	0.2595(2)	0.9196(7)	0.038(2)
N02	0.710(2)	0.2536(2)	0.7176(7)	0.036(2)
N03	1.252(2)	0.1906(3)	1.0233(7)	0.044(2)
H01	1.355975	0.208284	1.085420	0.052
H02	1.256606	0.159925	1.030619	0.052
N04	0.586(2)	0.1075(3)	0.7255(7)	0.042(2)
H03	0.708813	0.119001	0.794858	0.051
N05	0.911(3)	0.3246(3)	0.8060(7)	0.061(3)
H04	0.797809	0.338647	0.738692	0.073
H05	1.015659	0.341317	0.869763	0.073
N06	0.597(3)	0.0332(3)	0.8068(10)	0.078(3)
H06	0.554106	0.002934	0.797888	0.094
H07	0.714457	0.044234	0.877568	0.094
N07	0.532(2)	0.1808(2)	0.6342(7)	0.0363(19)
H10	0.447389	0.196520	0.566250	0.044
N08	-0.004(3)	0.0565(3)	0.4128(8)	0.059(3)
H12	-0.103073	0.075254	0.352525	0.070
H13	-0.040722	0.026084	0.406295	0.070
N09	0.287(2)	0.0432(3)	0.6090(7)	0.046(2)
N10	0.896(2)	0.1844(2)	0.8328(6)	0.042(2)
H11	0.952101	0.161532	0.850175	0.050
N11	0.264(2)	0.1200(2)	0.5203(7)	0.039(2)
C01	0.459(2)	0.1341(3)	0.6281(8)	0.033(2)
C02	1.078(3)	0.2117(3)	0.9218(8)	0.034(2)
C03	0.901(2)	0.2770(3)	0.8141(7)	0.029(2)
C04	0.484(3)	0.0612(3)	0.7098(9)	0.045(3)
C05	0.724(2)	0.2082(3)	0.7322(8)	0.036(2)
C06	0.185(3)	0.0739(3)	0.5155(8)	0.036(2)

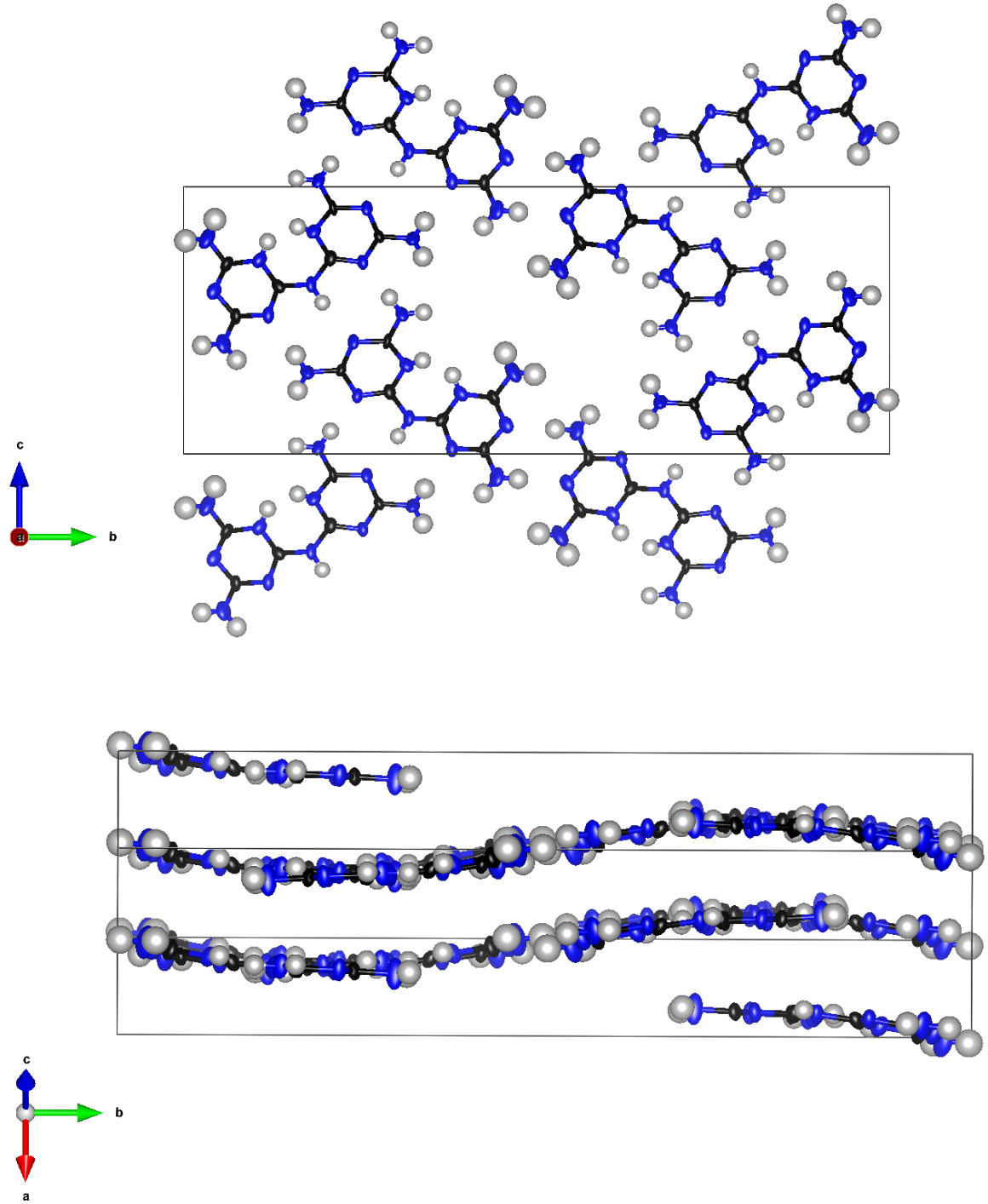

Figure 7.1.3 Crystal structure of "$C_6N_{11}H_{9.5}$" (melamium thiocyanate melam refined excluding thiocyanate anions). C atoms in black, N atoms in blue, H atoms in gray. Top: viewing direction along *a*. Bottom: viewing direction perpendicular to the layers.

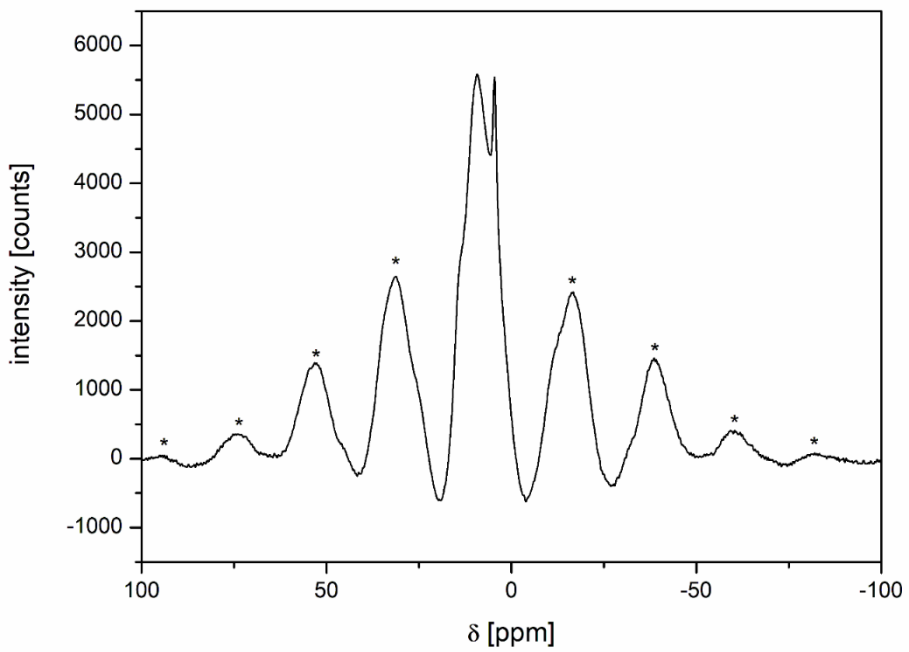

Figure 7.1.4 ^{1}H solid-state MAS-NMR spectrum of $C_6N_{11}H_{10}SCN{\cdot}C_6N_{11}H_9$. Asterisks mark spinning side bands.

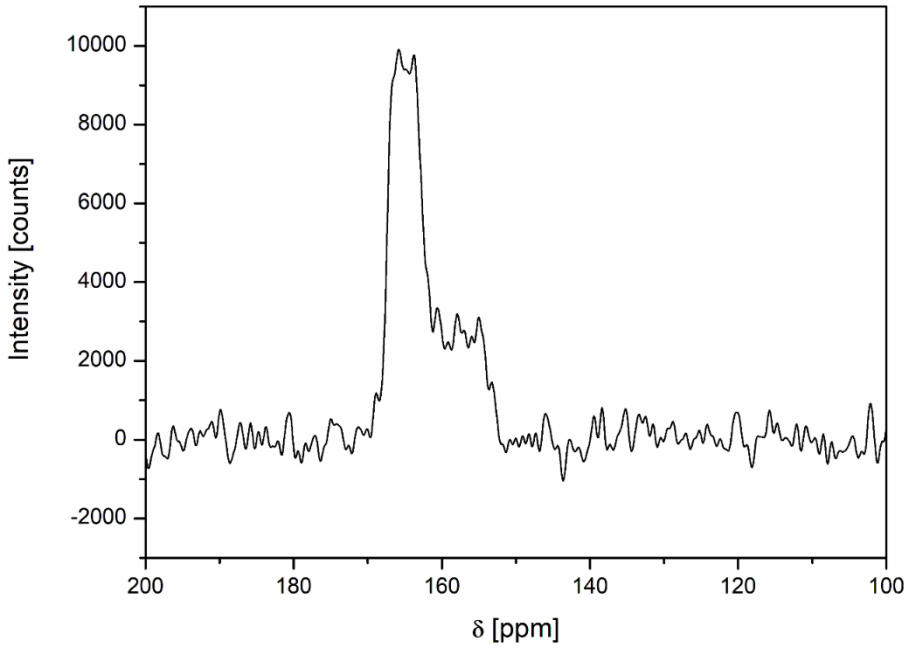

Figure 7.1.5 ^{13}C solid-state MAS-NMR spectrum of $C_6N_{11}H_{10}SCN{\cdot}C_6N_{11}H_9$.

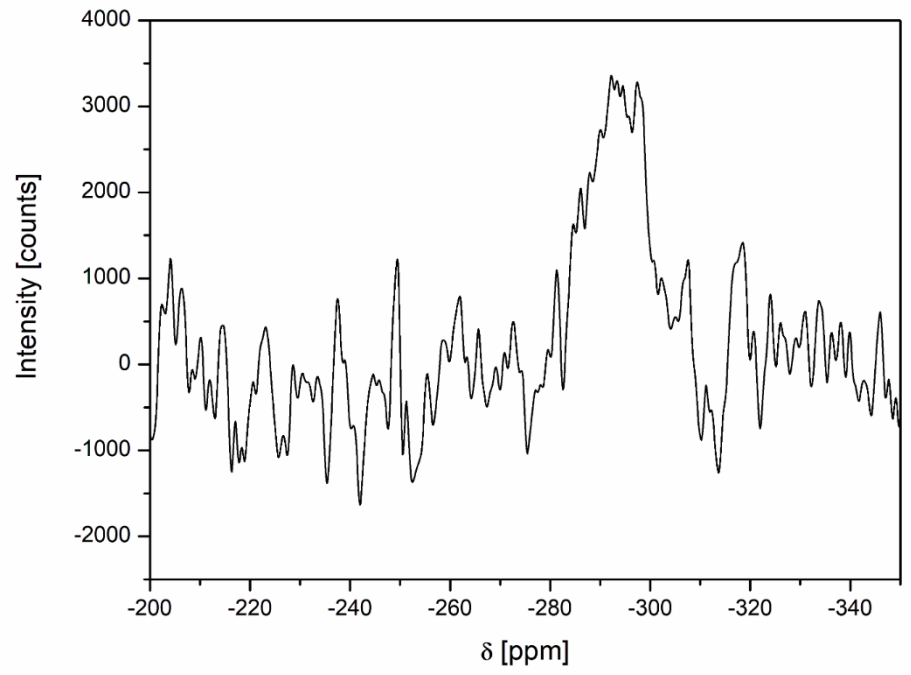

Figure 7.1.6 ^{15}N solid-state MAS-NMR spectrum of $C_6N_{11}H_{10}SCN{\cdot}C_6N_{11}H_9$.

Quantification of thiocyanate through UV-Vis spectroscopic measurements Thiocyanate eluted from a sample of melamium thiocyanate melam was quantified in the form of $[Fe(SCN)(H_2O)_5]^{2+}$ through measurement of absorption intensities in UV-Vis spectroscopy. Elution of thiocyanate from 50.0 mg of melamium thiocyanate melam was performed as described in the Experimental section (chapter 3.2.4). The sample was further diluted to a total volume of 90.4 mL and the pH adjusted to pH = 7 using HCl (aq.) to prevent precipitation of $Fe(OH)_3$. For reference, solutions of ammonium thiocyanate with concentrations of 0.01, 0.02, 0.05 and 0.10 mg mL^{-1} were prepared. 2 mL of thiocyanate solution and 1 mL of Fe^{3+} solution (from $FeCl_3{\cdot}6H_2O$ dissolved in deionized water, c = 2.33 mg mL^{-1}) were filled in a cuvette with a lengths of 1.0 cm for UV-Vis measurements. Absorption is expected to linearly depend on the concentration of $[Fe(SCN)(H_2O)_5]^{2+}$ according to the Beer-Lambert law (Eq. 7.1.1).

$$E_\lambda = -\lg\left(\frac{I}{I_0}\right) = \varepsilon_\lambda \cdot c \cdot d \qquad (7.1.1)$$

where E_λ is the absorbance at wavelength λ, I and I_0 the transmitted and initial light intensity, ε_λ the molar extinction coefficient of the species at wavelength λ, c the concentration of the species and d the optical path length through the medium.

Absorption maxima were determined for four references as well as the sample of unknown concentration from plotted spectra. A slight shift of absorption maxima towards higher wavelengths with increasing concentration was observed. Intensities at the absorption maximum were plotted against concentration of SCN^- for wavelengths of all five absorption maxima. Plots deviated from linearity for the reference solution of concentration 0.10 mg mL^{-1}, however, agreed well to the Beer-

Lambert law for all other values. The concentration of the melamium thiocyanate melam sample was determined for all five plots and an average formed. A concentration of 0.548 mmol L^{-1} (0.0325 mg mL^{-1}) equating to a total of 2.94 mg of 'SCN$^-$' for 50.0 mg of sample was found. From the sum formula $C_6N_{11}H_{10}SCN{\cdot}C_6N_{11}H_9$ a mass fraction of 11.0% equating 5.50 mg would have been expected. It is thus assumed that only partial elution of thiocyanate from melamium thiocyanate melam is possible, which is also supported by the presence of a ν(C≡N) vibration band in IR spectra of the residue.

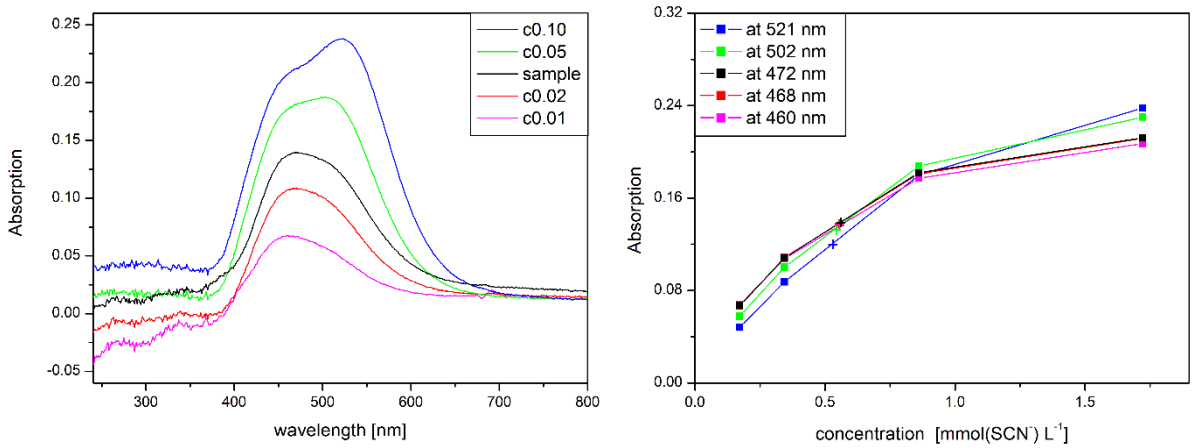

Figure 7.1.7 Quantification of eluted thiocyanate through UV-Vis spectroscopy. Left: UV-Vis spectra of NH_4SCN solutions with concentrations of c = 0.01, 002, 0.05 and 0.010 mg mL^{-1} and the sample of unknown concentration (labelled 'sample'). Right: plots of absorption intensity at absorption curve maxima versus concentration. Squares indicate data from reference measurements, crosses mark intensities of the unknown sample.

Table 7.1.4 Rietveld refinement of $C_6N_{11}H_{10}SCN{\cdot}C_6N_{11}H_9$.

Empirical formula	$C_6N_{11}H_{10}SCN{\cdot}C_6N_{11}H_9$
Formula weight [g mol−1]	529.57
Crystal system	Monoclinic
Space group	*Pc* (no. 7)
Radiation, λ [ppm]	Cu-Kα_1, 1.5406
a [Å]	3.6402
b [Å]	28.457
c [Å]	10.901
β [°]	98.605
V [Å³]	1116.6
Z	4
Density (calcd.) [g cm^{-1}]	3.150
Temperature [K]	297
Diffraction range [°]	$5 \leq \theta \leq 112$
R_{wp}	19.572
R_{exp}	0.833
R_{bragg}	5.7309

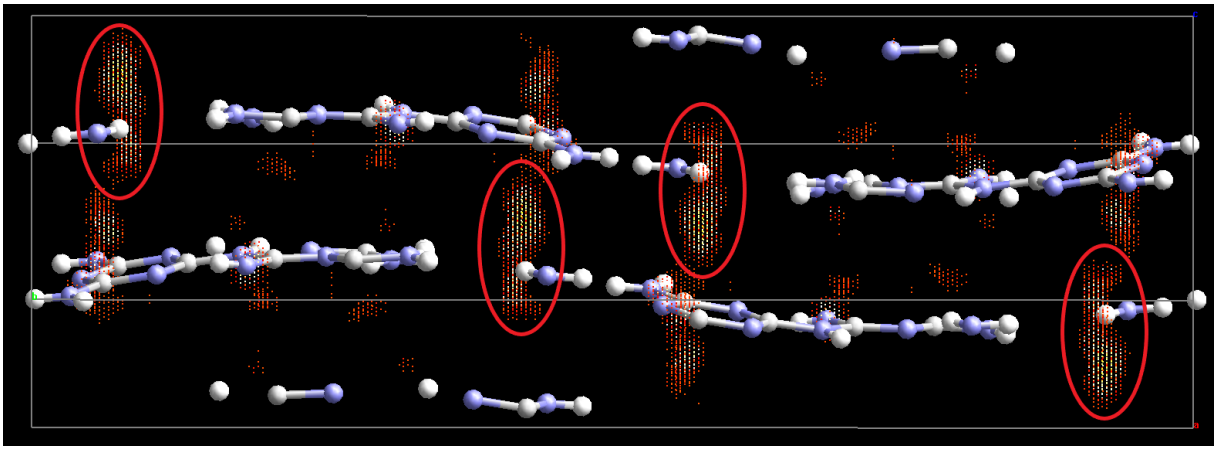

Figure 7.1.8 Difference Fourier plot of the Rietveld fit of melamium thiocyanate melam, utilizing the model from single crystal XRD data excluding SCN^- anions. Red circles mark continuous columns of electron density attributed to disordered thiocyanate anions.

7.2 Supporting Information for Chapter 3.3: Ammelinium Sulfate Cyanuric Acid and Ammelinium Sulfate Monohydrate

Contents:

- Optical microscope images of crystals of $6C_3N_5H_6O^+ \cdot 3SO_4^{2-} \cdot 1⅔C_3N_3H_3O_3 \cdot H_2O$.
- Comparison of different layers of the $6C_3N_5H_6O^+ \cdot 3SO_4^{2-} \cdot 1⅔C_3N_3H_3O_3 \cdot H_2O$ crystal structure.
- Atomic coordinates and bond lengths for $6C_3N_5H_6O^+ \cdot 3SO_4^{2-} \cdot 1⅔C_3N_3H_3O_3 \cdot H_2O$.
- Precession image of the h0l-plane of $6C_3N_5H_6O^+ \cdot 3SO_4^{2-} \cdot 1⅔C_3N_3H_3O_3 \cdot H_2O$.
- Hydrogen bridge network for $2C_3N_5H_6O^+ \cdot SO_4^{2-} \cdot H_2O$.
- Atomic coordinates and bond lengths for $2C_3N_5H_6O^+ \cdot SO_4^{2-} \cdot H_2O$.
- ^1H solid-state MAS NMR spectrum of $6C_3N_5H_6O^+ \cdot 3SO_4^{2-} \cdot 1⅔C_3N_3H_3O_3 \cdot H_2O$.
- Rietveld refinement for $6C_3N_5H_6O^+ \cdot 3SO_4^{2-} \cdot 1⅔C_3N_3H_3O_3 \cdot H_2O$.

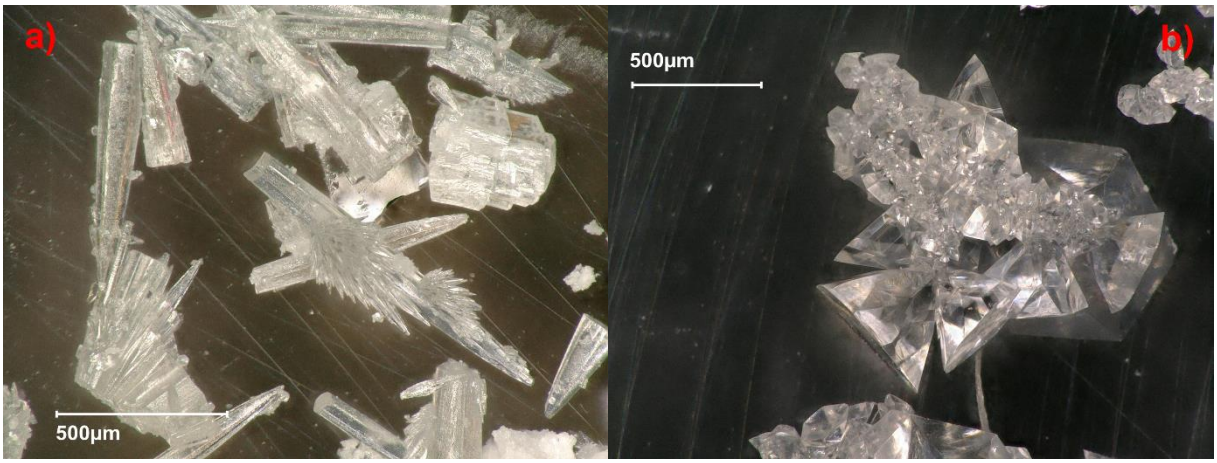

Figure 7.2.1 Optical microscope images of crystals of $6C_3N_5H_6O^+ \cdot 3SO_4^{2-} \cdot 1⅔C_3N_3H_3O_3 \cdot H_2O$. a) crystals with needle shaped habitus. b) crystals with hexagonal-pyramidal habitus.

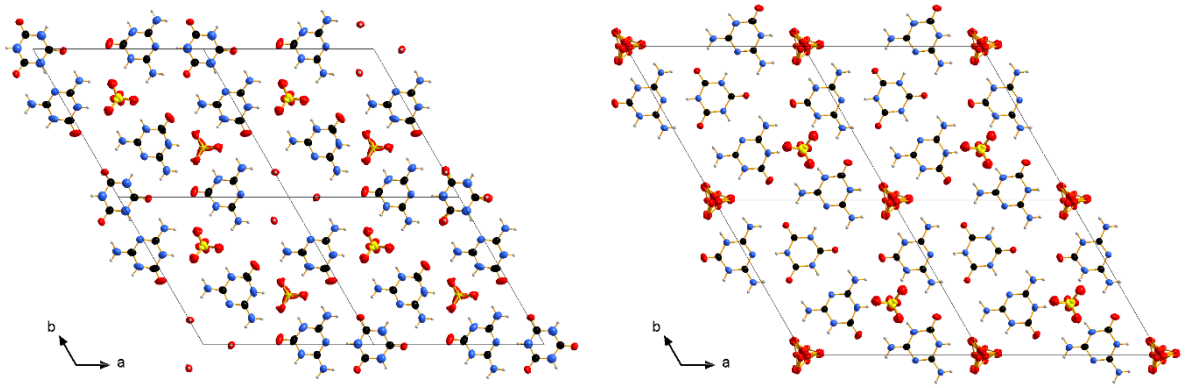

Figure 7.2.2 Comparison of different layers of the $6C_3N_5H_6O^+ \cdot 3SO_4^{2-} \cdot 1⅔C_3N_3H_3O_3 \cdot H_2O$ crystal structure. Left: layer of type 1. Right: layer of type 2. Viewing direction along *c*. Sulfate anions drawn as disordered groups with occupancy of ⅓ for all atoms. C atoms in black, N atoms in blue, H atoms in gray, O atoms in red, S atoms in yellow. Ellipsoids drawn at 50 % probability.

Table 7.2.1 Atomic coordinates x, y, z, isotropic displacement parameters U_{iso} and occupancies for $6C_3N_5H_6O^+ \cdot 3SO_4^{2-} \cdot 1⅔C_3N_3H_3O_3 \cdot H_2O$.

Atom name	Wyckoff position	x	y	z	U_{iso}	occupancy
S1	2a	0.9980(16)	1.0023(15)	0.4920(4)	0.0509(18)	0.2222
O2D	6c	0.909(2)	0.896(2)	0.4755(17)	0.046(4)	0.2222
O2E	6c	1.095(2)	1.009(2)	0.454(3)	0.054(4)	0.2222
O2F	6c	0.979(2)	1.080(2)	0.440(2)	0.058(4)	0.2222
O3	6c	1.009(3)	1.0245(13)	0.6028(8)	0.058(5)	0.2222
S1A	2a	1	1	0.4435(5)	0.0285(17)	0.3333
O2A	6c	0.9201(19)	0.9034(19)	0.499(2)	0.019(6)	0.1111
O2B	6c	1.011(3)	1.095(2)	0.496(2)	0.033(7)	0.1111
O2C	6c	1.1037(17)	1.004(3)	0.4446(17)	0.040(7)	0.1111
O3A	6c	0.9650(17)	0.997(2)	0.3365(12)	0.035(6)	0.1111
S3	6c	0.6664(5)	0.3347(6)	0.2774(2)	0.0458(13)	0.3333
O8A	6c	0.5720(9)	0.2360(9)	0.2979(15)	0.053(7)	0.3333
O8B	6c	0.7575(11)	0.3282(11)	0.307(2)	0.053(8)	0.3333
O8C	6c	0.6638(13)	0.4183(11)	0.3327(17)	0.056(7)	0.3333
O10	6c	0.6723(17)	0.3569(16)	0.1693(5)	0.073(8)	0.3333
O1	6c	1.1611(3)	0.4824(3)	0.4252(4)	0.0474(9)	1
S2	6c	0.6634(18)	0.335(2)	0.6360(3)	0.0492(13)	0.3333
O5A	6c	0.765(2)	0.416(2)	0.679(3)	0.059(10)	0.3333
O5B	6c	0.577(2)	0.340(2)	0.688(2)	0.059(8)	0.3333
O5C	6c	0.651(2)	0.230(2)	0.6530(17)	0.054(6)	0.3333
O6	6c	0.661(4)	0.353(3)	0.5266(5)	0.048(5)	0.3333
O7	6c	0.7549(3)	0.6277(3)	0.4574(4)	0.0607(11)	1
O9	6c	1.0351(5)	1.5701(4)	0.6536(5)	0.0829(19)	1
N1	6c	0.9324(3)	0.7273(3)	0.4557(4)	0.0406(8)	1
H1	6c	0.92997	0.7857	0.46403	0.049	1
N2	6c	1.0375(3)	0.6484(3)	0.4326(3)	0.0355(9)	1
C1	6c	1.2416(4)	0.5688(4)	0.4242(4)	0.0361(10)	1
N3	6c	1.2398(3)	0.6605(3)	0.4244(4)	0.0386(9)	1
H2	6c	1.17782	0.65655	0.42472	0.046	1
C2	6c	1.0967(9)	1.0919(8)	0.7195(10)	0.063(3)	0.6667
N4	6c	1.0902(8)	0.9960(8)	0.7262(8)	0.068(2)	0.6667
H3	6c	1.14831	0.99321	0.73504	0.082	0.6667
O4	6c	1.1824(15)	1.1696(18)	0.7120(11)	0.048(2)	0.6667
O4A	6c	1.167(4)	1.162(4)	0.735(3)	0.048(2)	0.3333
H4A	6c	1.152(10)	1.128(9)	0.669(6)	-0.001(16)	0.3333
H4B	6c	1.156(8)	1.145(8)	0.806(6)	-0.001(16)	0.3333
N5	6c	1.1133(3)	0.8277(3)	0.4478(5)	0.0451(10)	1

H4	6c	1.17576	0.83379	0.43953	0.054	1
H5	6c	1.10789	0.88436	0.45686	0.054	1
C3	6c	1.0282(3)	0.7341(4)	0.4465(4)	0.0359(9)	1
C4	6c	0.8394(3)	0.6329(4)	0.4525(4)	0.0386(9)	1
N6	6c	0.8529(3)	0.5473(3)	0.4415(4)	0.0470(11)	1
H6	6c	0.79634	0.4843	0.43982	0.056	1
C5	6c	0.9487(4)	0.5541(4)	0.4329(4)	0.0370(10)	1
N7	6c	0.9529(3)	0.4686(3)	0.4195(4)	0.0478(11)	1
H7	6c	1.0141	0.4722	0.41019	0.057	1
H8	6c	0.89447	0.40697	0.4197	0.057	1
N8	6c	1.1943(5)	1.3719(5)	0.6941(5)	0.0656(15)	1
H9	6c	1.1907	1.3109	0.7051	0.079	1
H10	6c	1.25609	1.42954	0.68772	0.079	1
C6	6c	1.1084(5)	1.3768(4)	0.6871(5)	0.0478(12)	1
N9	6c	1.1158(5)	1.4726(4)	0.6703(5)	0.0633(15)	1
H11	6c	1.17872	1.52833	0.66195	0.076	1
C7	6c	1.0298(6)	1.4850(5)	0.6659(5)	0.0616(17)	1
N10	6c	0.9355(5)	1.3933(4)	0.6782(4)	0.0526(11)	1
H12	6c	0.87683	1.39597	0.67795	0.063	1
N11	6c	1.0156(4)	1.2893(4)	0.6968(4)	0.0474(10)	1
C8	6c	0.9296(5)	1.2979(4)	0.6909(4)	0.0473(12)	1
N12	6c	0.8360(4)	1.2141(4)	0.7011(4)	0.0530(12)	1
H13	6c	0.82997	1.15198	0.71185	0.064	1
H14	6c	0.77911	1.21996	0.69723	0.064	1

Table 7.2.2 Bond lengths in Å for $6C_3N_5H_6O^+ \cdot 3SO_4^{2-} \cdot 1⅔C_3N_3H_3O_3 \cdot H_2O$.

S1-O2B	1.28(3)
S1-O2A	1.32(3)
S1-O2E	1.465(10)
S1-O2F	1.466(10)
S1-O2D	1.469(10)
S1-O3	1.480(10)
S1-O2C	1.66(3)
S1-O3A	2.088(18)
O2D-S1A	1.50(3)
O2E-S1A	1.34(3)
O2F-S1A	1.35(3)
O3-S1A	2.113(12)
S1A-O3A	1.487(16)
S1A-O2C	1.492(17)
S1A-O2B	1.495(16)
S3-O8B	1.440(7)
S3-O8A	1.440(7)
S3-O8C	1.440(7)
S3-O10	1.447(7)
O1-C1	1.224(6)
S2-O6	1.464(7)
S2-O5C	1.471(7)
S2-O5A	1.472(7)
S2-O5B	1.472(7)
O7-C4	1.203(6)
O9-C7	1.220(8)
N1-C3	1.361(6)
N1-C4	1.373(6)
N1-H1	0.88
N2-C3	1.340(6)
N2-C5	1.342(6)
C1-N3	1.356(6)
C1-N3	1.363(6)
N3-H2	0.88
C2-O4	1.21(2)
C2-N4	1.361(14)
C2-N4	1.377(15)
N4-H3	0.88

O4A-H4A	0.96(8)
O4A-H4B	0.96(8)
N5-C3	1.313(6)
N5-H4	0.88
N5-H5	0.88
C4-N6	1.370(6)
N6-C5	1.360(6)
N6-H6	0.88
C5-N7	1.295(6)
N7-H7	0.88
N7-H8	0.88
N8-C6	1.298(8)
N8-H9	0.88
N8-H10	0.88
C6-N11	1.328(7)
C6-N9	1.369(8)
N9-C7	1.362(10)
N9-H11	0.88
C7-N10	1.371(9)
N10-C8	1.366(7)
N10-H12	0.88
N11-C8	1.328(8)
C8-N12	1.312(8)
N12-H13	0.88
N12-H14	0.88

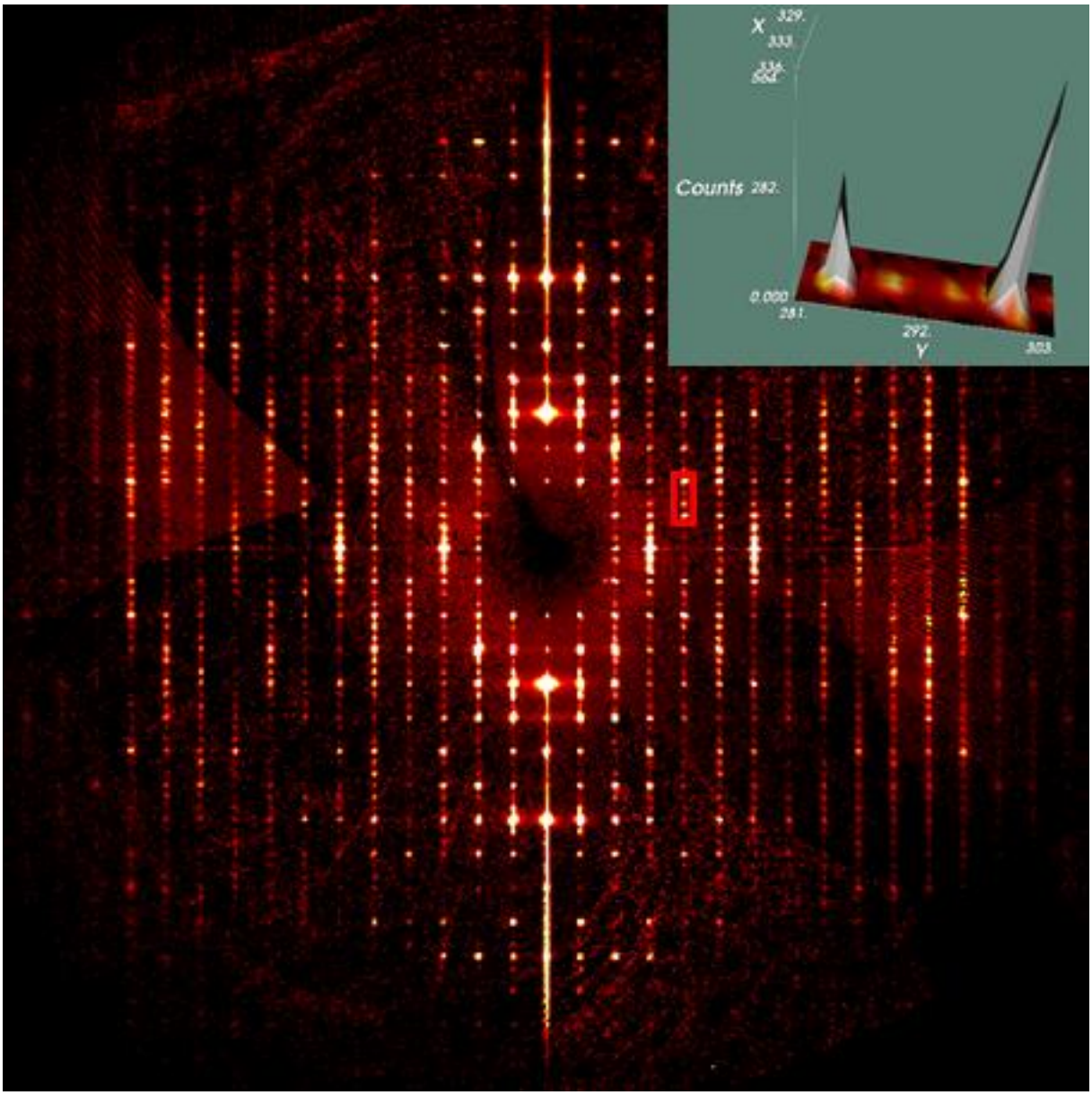

Figure 7.2.3 Precession image of the h0l-plane of $6C_3N_5H_6O^+ \cdot 3SO_4^{2-} \cdot 1⅔C_3N_3H_3O_3 \cdot H_2O$. Inset shows a 3D xy vs. intensity plot of the area within the red frame.

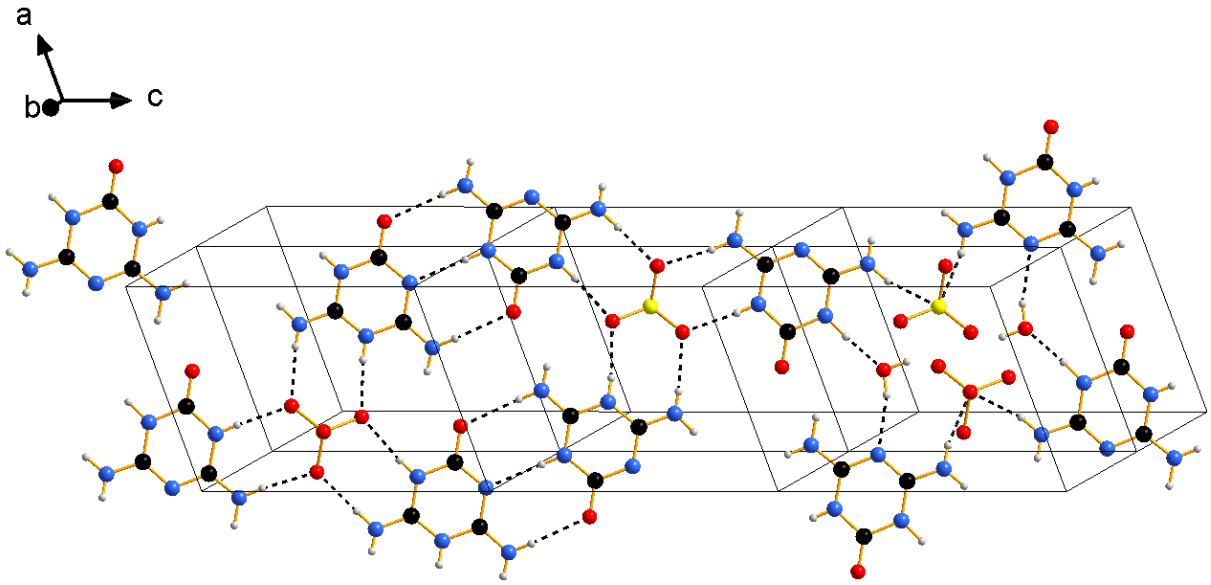

Figure 7.2.4 Complete repetition unit of a layer of **(2)**, viewing direction perpendicular to the layer plane. C atoms in black, N atoms in blue, H atoms in gray, O atoms in red, S atoms in yellow. Dashed black bonds indicate hydrogen bridge interactions. O/N disorder omitted. 2x3 unit cells plotted.

Table 7.2.3 Atomic coordinates x, y, z, isotropic displacement parameters U_{iso} and occupancies for $2C_3N_5H_6O^+ \cdot SO_4^{2-} \cdot H_2O$.

Atom name	Wyckoff position	x	y	z	U_{iso}	occupancy
S1	2i	0.75240(10)	0.22687(8)	0.56716(7)	0.0155(2)	1
O1	2i	-0.2244(11)	0.481(4)	0.160(3)	0.016(3)	0.59(3)
N10A	2i	-0.2372(17)	0.463(7)	0.151(5)	0.016(3)	0.41(3)
H10A	2i	-0.255(11)	0.513(7)	0.082(7)	0.019	0.41(3)
H10B	2i	-0.298(10)	0.485(8)	0.203(7)	0.019	0.41(3)
O2	2i	0.4529(3)	0.2012(2)	0.9374(2)	0.0233(5)	1
O3	2i	0.6975(3)	0.3131(2)	0.4416(2)	0.0298(6)	1
O4	2i	0.6336(3)	0.2583(2)	0.6546(2)	0.0228(5)	1
O5	2i	0.9564(3)	0.2596(2)	0.6526(2)	0.0214(5)	1
O6	2i	0.7236(3)	0.0785(2)	0.5231(2)	0.0203(5)	1
O7	2i	0.4121(3)	0.0663(3)	1.2469(2)	0.0249(5)	1
N1	2i	0.0075(3)	0.4087(3)	0.3529(2)	0.0145(5)	1
H1	2i	-0.077(6)	0.389(5)	0.389(5)	0.017	0.62(3)
C1	2i	0.1935(4)	0.3798(3)	0.4166(3)	0.0158(6)	1
N2	2i	0.3199(3)	0.4014(3)	0.3482(2)	0.0151(5)	1
H2	2i	0.431(4)	0.372(4)	0.381(4)	0.018	0.77(3)

C2	2i	0.2607(4)	0.4458(3)	0.2132(3)	0.0132(6)	1
C3	2i	-0.0532(4)	0.4544(3)	0.2179(3)	0.0134(6)	1
N3	2i	0.0739(3)	0.4732(2)	0.1489(2)	0.0142(5)	1
H3	2i	0.033(7)	0.493(5)	0.064(3)	0.017	0.61(3)
N4	2i	0.6900(4)	0.1363(3)	1.1347(3)	0.0174(6)	1
H4	2i	0.586(6)	0.119(4)	1.174(4)	0.047(11)	1
C4	2i	0.6213(4)	0.1813(3)	0.9973(3)	0.0167(6)	1
N5	2i	0.7600(3)	0.2029(3)	0.9376(3)	0.0161(6)	1
H5	2i	0.720(5)	0.223(4)	0.858(4)	0.036(11)	1
C5	2i	0.9484(4)	0.1776(3)	1.0053(3)	0.0143(6)	1
N6	2i	1.0706(4)	0.2018(3)	0.9380(3)	0.0158(5)	1
H6A	2i	1.202(5)	0.182(3)	0.985(4)	0.030(9)	1
H6B	2i	1.030(5)	0.224(4)	0.852(4)	0.030(10)	1
C6	2i	0.8776(4)	0.1083(3)	1.1981(3)	0.0147(6)	1
N7	2i	1.0102(3)	0.1313(2)	1.1372(2)	0.0157(5)	1
N8	2i	0.9281(4)	0.0583(3)	1.3259(3)	0.0196(6)	1
H8A	2i	1.036(6)	0.029(4)	1.361(4)	0.031(10)	1
H8B	2i	0.843(5)	0.053(4)	1.373(4)	0.030(10)	1
N9	2i	0.2488(4)	0.3294(3)	0.5429(3)	0.0196(6)	1
H9A	2i	0.155(5)	0.302(4)	0.578(4)	0.031(10)	1
H9B	2i	0.353(5)	0.309(3)	0.579(3)	0.017(9)	1
N10	2i	0.389(2)	0.467(5)	0.1519(19)	0.014(3)	0.59(3)
H10C	2i	0.347(7)	0.474(6)	0.064(4)	0.017	0.59(3)
H10D	2i	0.502(6)	0.450(5)	0.196(5)	0.017	0.59(3)
O1A	2i	0.370(3)	0.449(6)	0.143(2)	0.014(3)	0.41(3)
H11	2i	0.294(6)	0.087(4)	1.231(4)	0.038(11)	1
H12	2i	0.449(6)	0.047(4)	1.332(5)	0.054(14)	1

Table 7.2.4 Bond lengths in Å for $2C_3N_5H_6O^+ \cdot SO_4^{2-} \cdot H_2O$.

S1 O3	1.474(2)
S1 O4	1.475(2)
S1 O5	1.478(2)
S1 O6	1.479(2)
O1 C3	1.242(7)
N10A C3	1.305(4)
N10A H10A	0.83(3)
N10A H10B	0.83(3)
O2 C4	1.212(3)
O7 H11	0.87(4)
O7 H12	0.83(5)
N1 C1	1.351(4)
N1 C3	1.365(4)
N1 H1	0.84(3)
C1 N9	1.305(4)
C1 N2	1.347(4)
N2 C2	1.360(3)
N2 H2	0.84(3)
C2 O1A	1.242(7)
C2 N10	1.304(4)
C2 N3	1.353(4)
C3 N3	1.353(4)
N3 H3	0.84(3)
N4 C6	1.359(4)
N4 C4	1.385(4)
N4 H4	0.99(4)
C4 N5	1.364(4)
N5 C5	1.364(4)
N5 H5	0.78(4)
C5 N6	1.316(4)
C5 N7	1.339(4)
N6 H6A	0.96(4)
N6 H6B	0.85(4)
C6 N8	1.317(4)
C6 N7	1.335(4)
N8 H8A	0.82(4)
N8 H8B	0.90(4)
N9 H9A	0.91(4)

N9 H9B	0.77(3)
N10 H10C	0.83(3)
N10 H10D	0.83(3)

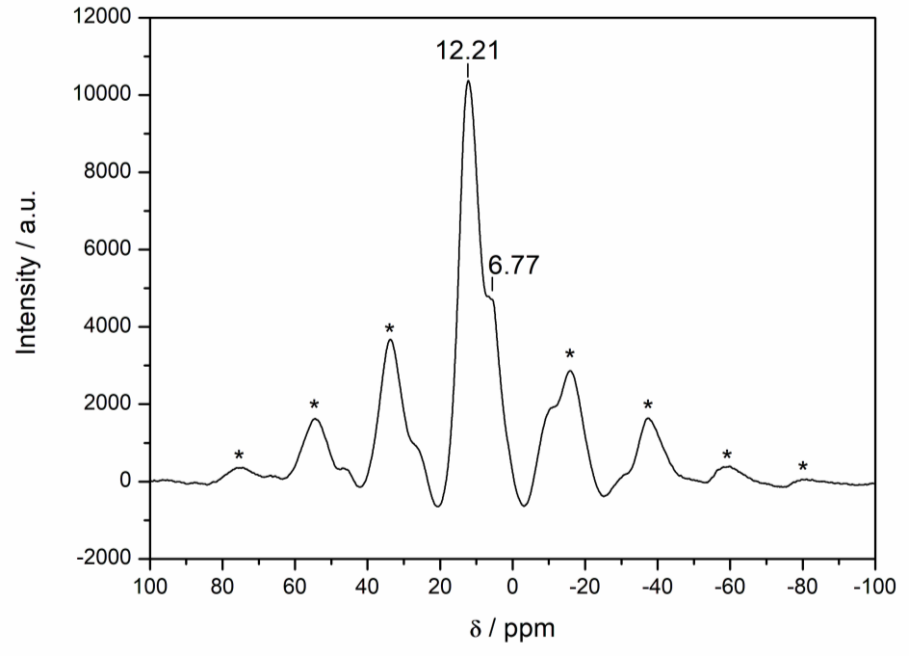

Figure 7.2.5 ^{1}H solid-state MAS NMR spectrum of $6C_3N_5H_6O^+ \cdot 3SO_4^{2-} \cdot 1⅔C_3N_3H_3O_3 \cdot H_2O$.

Table 7.2.5 Rietveld refinement for $6C_3N_5H_6O^+ \cdot 3SO4^{2-} \cdot 1⅔C_3N_3H_3O \cdot H_2O$.

Empirical formula	$C_{22}N_{34}H_{44}S_3O_{24}$
Formula weight [g mol^{-1}]	1265.09
Crystal system	hexagonal
Space group	$P6_3$ (no. 173)
Radiation, λ [Å]	Cu-Kα_1, 1.54060
a [Å]	14.64540(39)
c [Å]	13.12999(35)
V [Å^3]	2438.91(14)
Z	2
Temperature [K]	297
Diffraction range [°]	$5 \leq \theta \leq 101$
R_{wp}	0.08636
R_{exp}	0.01666
R_{bragg}	0.03675

7.3 Supporting Information for Chapter 4: Molecular Adduct Compounds: Melam-Melem (1:1)

Contents:

- Melem partial structure of the melam-melem adduct
- Melam partial structure of the melam-melem adduct
- Comparison of the DFT optimized structure and the structure obtained from synchrotron XRD data for the melam-melem adduct
- Relative energy E_r [kJ/mol] of melam gas phase dimers
- PBE optimized structures of melam and melem
- Comparison of melam donor-acceptor distances from XRD and PBE-D3/pob-TZVP
- Intramolecular torsion angles for melam and melam-melem (XRD and PBE-D3/pob-TZVP)
- Comparison of melem donor-acceptor distances from XRD and PBE-D3/pob-TZVP
- Comparison of melam-melem donor-acceptor distances from XRD and PBE-D3/pob-TZVP
- Calculated ^{15}N NMR shemical shifts for melam, melem and the melam-melem adduct
- Simulated ^{15}N NMR spectra of melam, melem and the melam-melem adduct as obtained from DFT calculations
- Atom site coordinates for the optimized crystal structure of the melam-melem adduct

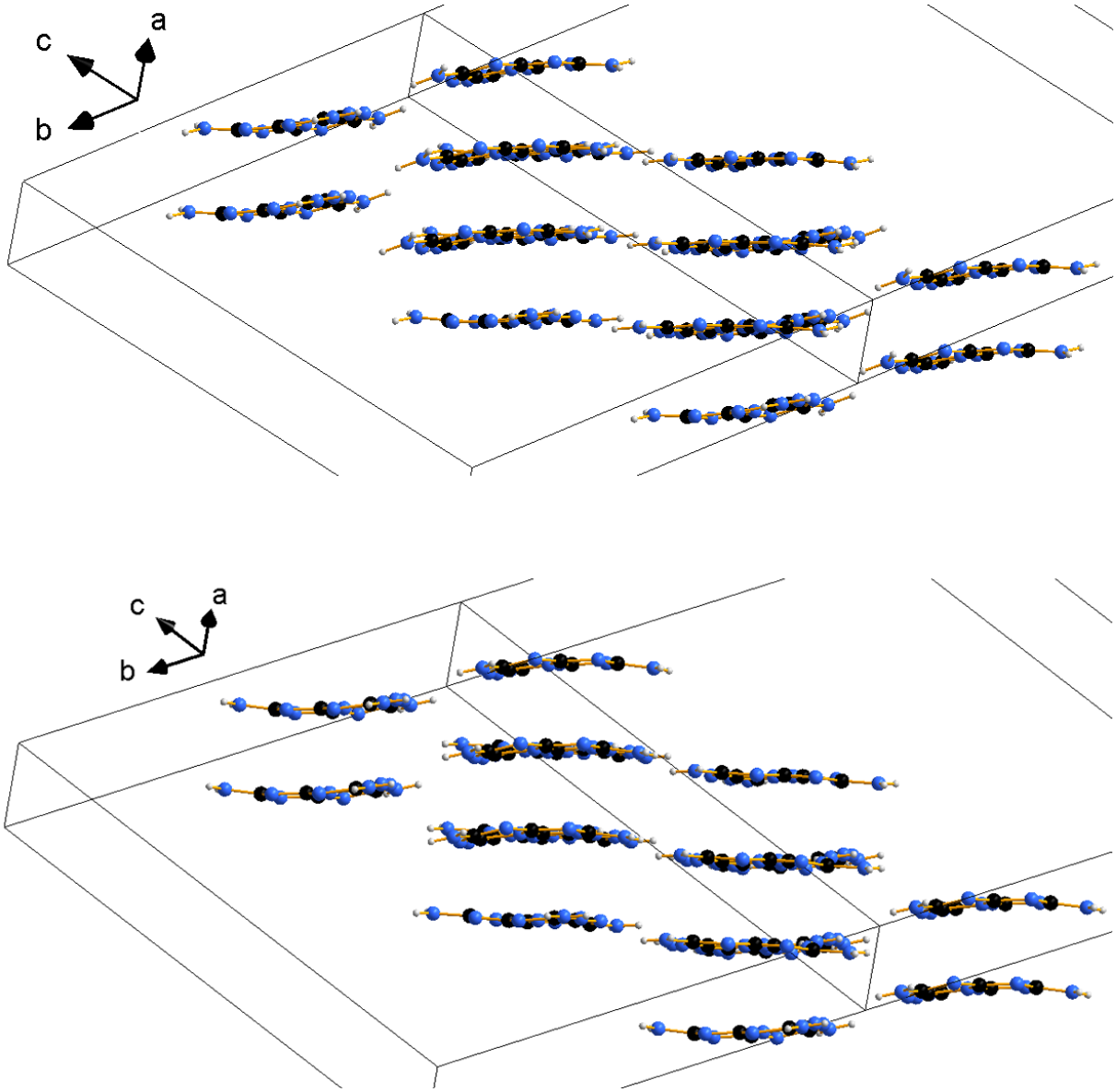

Figure 7.3.1 Melem partial structure of the melam-melem adduct. Projection perpendicular to the melem stacking direction. C atoms in black, N atoms in blue, H atoms in light gray. Comparison of the DFT optimized structure (top) and the structure obtained from synchrotron XRD data (bottom).

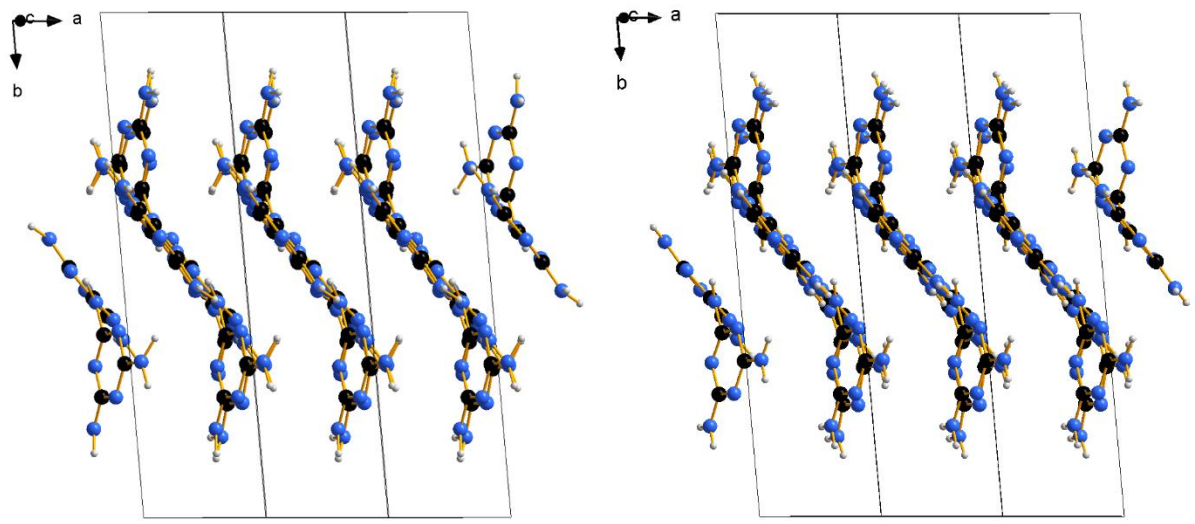

Figure 7.3.2 Melam partial structure of the melam-melem adduct. Projection perpendicular to the *a* axis to show stacking motifs. C atoms in black, N atoms in blue, H atoms in light gray. Comparison of the DFT optimized structure (left) and the structure obtained from synchrotron XRD data (right).

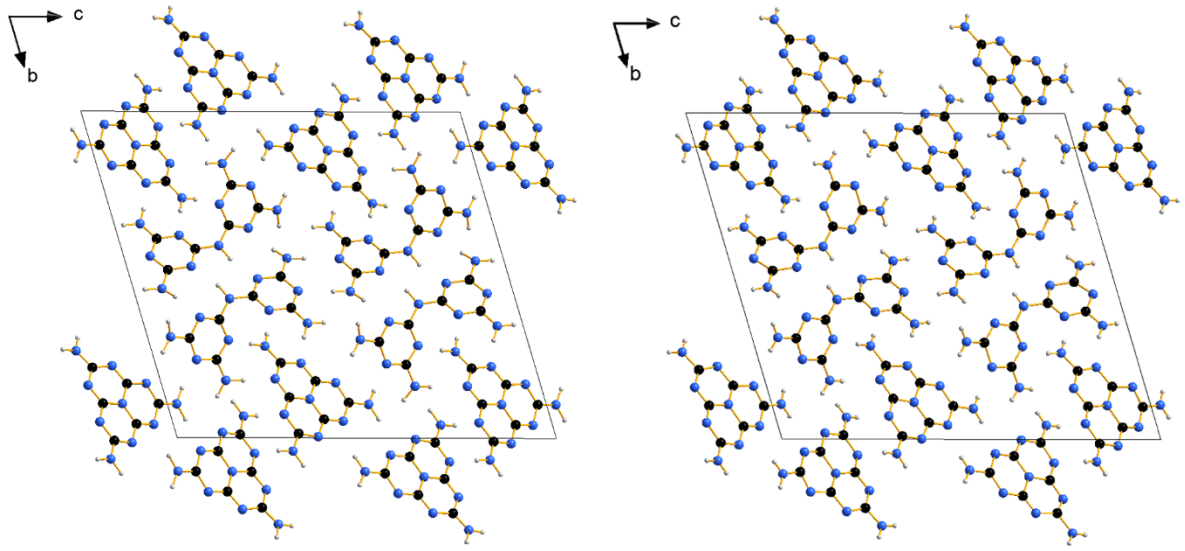

Figure 7.3.3 Crystal structure of the melam-melem adduct, projection along [100]. C atoms in black, N atoms in blue, H atoms in light gray. Comparison of the DFT optimized structure (left) and the structure obtained from synchrotron XRD data (right).

Table 7.3.1 Relative energy E_r [kJ/mol] of melam gas phase dimer **2** with respect to dimer **1** and harmonic zero-point vibrational energy corrections (ΔZPVE).

method	***Er***	**ΔZPVE**
PBE/TZVP	10.8	---
PBE-D3/TZVP	10.9	+1.0
PBE0/TZVP	11.3	<+0.1
RPA@PBE/TZVP	8.9	---

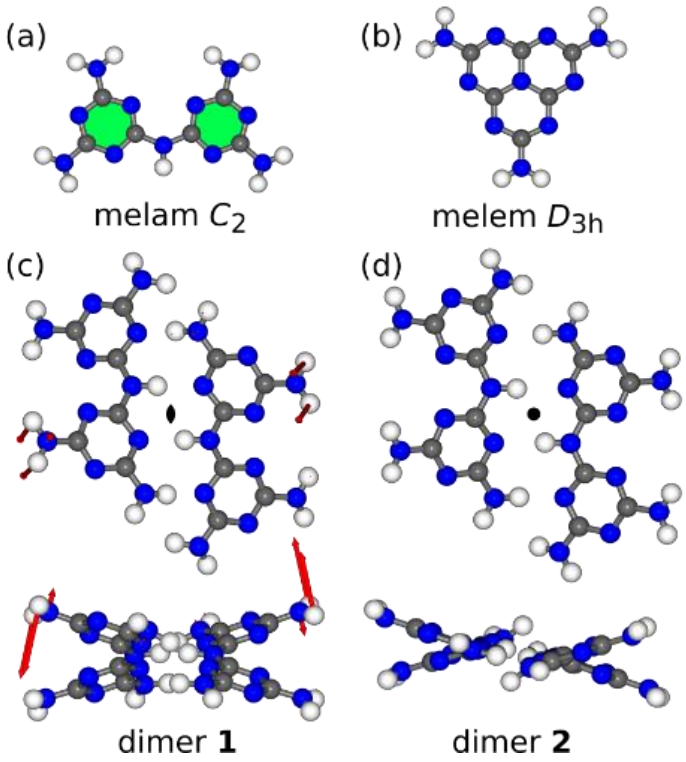

Figure 7.3.4 PBE optimized structures. Nitrogen atoms in blue, hydrogen atoms in white. (a) and (b) are gas-phase structures of melam and melem molecule. The melam torsion angle is defined as angle between the normal vectors of the planes defined by the green area in the rings. (c) and (d) are gas-phase dimers of melam, each from two different perspectives; filled lense and circle represent position of C_2 axis and inversion center, respectively; The C_2-symmetric structure (c) is determined as a transition state for PBE, for which a slight distortion along the very weak eigenmode of imaginary frequency (shown as arrows) virtually yields the asymmetric minimum (see chapter 4.2).

Table 7.3.2 Melam crystal. Distances d (in Å) between hydrogen donor (D) and acceptor (A) atoms from experimental XRD and deviations of PBE-D3/pob-TZVP (DFT) results. N–H–N angles α from DFT. MSE = mean signed error, Max = maximum signed error.

D-A	d(XRD)	d(DFT)	α(DFT)
N17-N5	2.99	−0.04	175.4
N4-N14	3.33	−0.05	156.5
N16-N1	3.26	−0.04	174.6
N8-N13	3.12	−0.07	172.3
N17-N3	2.97	−0.04	172.9
N9-N12	3.11	−0.01	173.6
N11-N6 ×2	3.00	−0.05	173.5
N10-N7 ×2	3.11	−0.06	173.8
MSE	–	−0.045	–
Max	–	−0.07	–

Table 7.3.3 Intramolecular torsion angles (in °) between the 1,3,5-triazine rings from experimental XRD and deviations (in °) of PBE-D3/pob-TZVP (DFT) results. Atom labels define the torsion angles.

labels	XRD	DFT
melam crystal		
C8-N12-N12-C8	21.4	−0.3
C2-N1-N5-C5	−19.5	+0.3
melam-melem crystal		
C2-N1-N5-C5	48.4	−0.9
C2'-N1'-N5'-C5'	−48.1	+2.4

Table 7.3.4 Melem crystal. Distances d (Å) between hydrogen donor (D) and acceptor (A) atoms from experimental XRD and deviations of PBE-D3/pob-TZVP (DFT) results. N–H–N angles α from DFT. MSE = mean signed error, Max = maximum signed error.

D-A	d(XRD)	d(DFT)	α(DFT)
N8-N2 ×2	3.71	−0.05	157.6
N8-N3 ×2	3.29	−0.10	168.1
N9-N6 ×2	3.18	−0.08	170.8
N10-N5 ×2	2.81	0.06	172.3
N10-N7 ×2	3.02	−0.11	172.2
MSE	–	−0.056	–
Max	–	−0.11	–

Table 7.3.5 Melam–melem adduct: Distances d (Å) between hydrogen donor (D) and acceptor (A) atoms from experimental XRD and deviations of PBE-D3/pob-TZVP (DFT) results of fixed and optimized unit cells. N–H–N angles α from DFT. MSE = mean signed error, Max = maximum signed error.

D-A	d(XRD)	d(DFT, fixed)	α(DFT, fixed)	d(DFT, opt)	α(DFT, opt)
melam dimer					
N1-N8'	3.04	−0.06	166.0	−0.11	164.0
$N8_{melem\ top}$-N2	3.00	−0.04	174.3	−0.14	173.3
N4-N1'	3.18	−0.11	162.7	−0.24	164.8
N4'-N5	3.10	0.00	163.4	-0.14	165.8
$N8_{melem\ bottom}$-N6	2.99	0.06	176.5	0.00	176.8
N10-N7 ×2	3.01	0.15	178.2	0.05	177.1
N9-$N3_{melem\ top}$	3.02	−0.09	177.1	−0.15	176.1
N10-N5'	3.20	−0.16	166.3	−0.25	165.0
N11-$N2_{melem\ bottom}$	3.03	−0.09	173.6	−0.16	174.1
N9'$_{melem}$-N3	2.95	−0.01	169.9	−0.07	171.6
N8-N4'$_{melem}$	3.14	−0.06	173.7	−0.15	173.8
N2'-N8'$_{melem\ top}$	3.12	0.04	175.1	-0.05	176.2
N8'$_{melem\ bottom}$-N6'	3.09	−0.07	175.7	−0.21	174.1
N8'-N3' ×2	3.17	0.07	176.9	-0.09	176.7
N9'-N3'$_{melem\ top}$	2.98	−0.07	173.4	−0.12	173.6
N11'-N2'$_{melem\ bottom}$	3.35	−0.13	164.6	−0.33	169.5
N7'-$N10_{melem}$	3.12	−0.06	174.4	−0.18	175.5
N10'-$N7_{melem}$	3.11	−0.05	177.5	−0.15	177.7
intermelem bonds in melem dimer					
N10'-N4	3.24	−0.14	177.7	-0.25	177.2
N9-N7'	2.93	−0.04	173.2	-0.08	174.0
N10-N5 ×2	3.28	0.06	153.0	-0.17	157.0
N9'-N5' ×2	3.18	0.01	167.7	-0.16	170.1
MSE	–	−0.03	–	-0.15	–
Max	–	−0.16	–	-0.33	–

Table 7.3.6 Melam: Calculated ^{15}N NMR chemical shifts for melam obtained on B97-2/pcSseg-1 level of theory. Values have not been corrected for methodical errors, shifts thus differ by about 14 ppm from values found in literature.

Label	NMR Chemical Shielding [ppm]	NMR Chemical Shift [ppm]
N2	45.23	-177.01
N13	50.79	-182.57
N1	51.31	-183.09
N12	53.38	-185.16
N6	54.19	-185.97
N5	54.72	-186.50
N7	58.16	-189.94
N14	58.41	-190.19
N3	63.14	-194.92
N15	101.30	-233.07
N4	108.34	-240.11
N11	134.03	-265.81
N17	140.21	-271.99
N8	146.83	-278.60
N9	154.25	-286.03
N10	160.74	-292.52
N16	162.54	-294.32

Table 7.3.7. Melem: Calculated ^{15}N NMR chemical shifts for melem obtained on B97-2/pcSseg-1 level of theory. Values have not been corrected for methodical errors, shifts thus differ by about 14 ppm from values found in literature.

Label	NMR Chemical Shielding [ppm]	NMR Chemical Shift [ppm]
N3	48.13	-179.91
N4	52.18	-183.96
N2	53.39	-185.17
N6	57.23	-189.00
N7	58.55	-190.33
N5	61.33	-193.11
N1	87.24	-219.02
N10	116.70	-248.47
N8	135.37	-267.15
N9	145.46	-277.23

Table 7.3.8 Melam-melem adduct: Calculated ^{15}N NMR chemical shifts for the melam-melem-adduct obtained on B97-2/pcSseg-1 level of theory. Values have not been corrected for methodical errors, shifts thus differ by about 14 ppm from values found in literature.

Label	Origin	NMR Chemical Shielding [ppm]	NMR Chemical Shift [ppm]
N2	Melam	45.23	-177.01
N3	Melem	48.13	-179.91
N4	Melem	52.18	-183.96
N13	Melam	50.79	-182.57
N1	Melam	51.31	-183.09
N2	Melem	53.39	-185.17
N12	Melam	53.38	-185.16
N6	Melam	54.19	-185.97
N5	Melam	54.72	-186.50
N6	Melem	57.23	-189.00
N7	Melem	58.55	-190.33
N7	Melam	58.16	-189.94
N14	Melam	58.41	-190.19
N5	Melem	61.33	-193.11
N3	Melam	63.14	-194.92
N1	Melem	87.24	-219.02
N15	Melam	101.30	-233.07
N4	Melam	108.34	-240.11
N10	Melem	116.70	-248.47
N8	Melem	135.37	-267.15
N11	Melam	134.03	-265.81
N17	Melam	140.21	-271.99
N9	Melem	145.46	-277.23
N8	Melam	146.83	-278.60
N9	Melam	154.25	-286.03
N10	Melam	160.74	-292.52
N16	Melam	162.54	-294.32

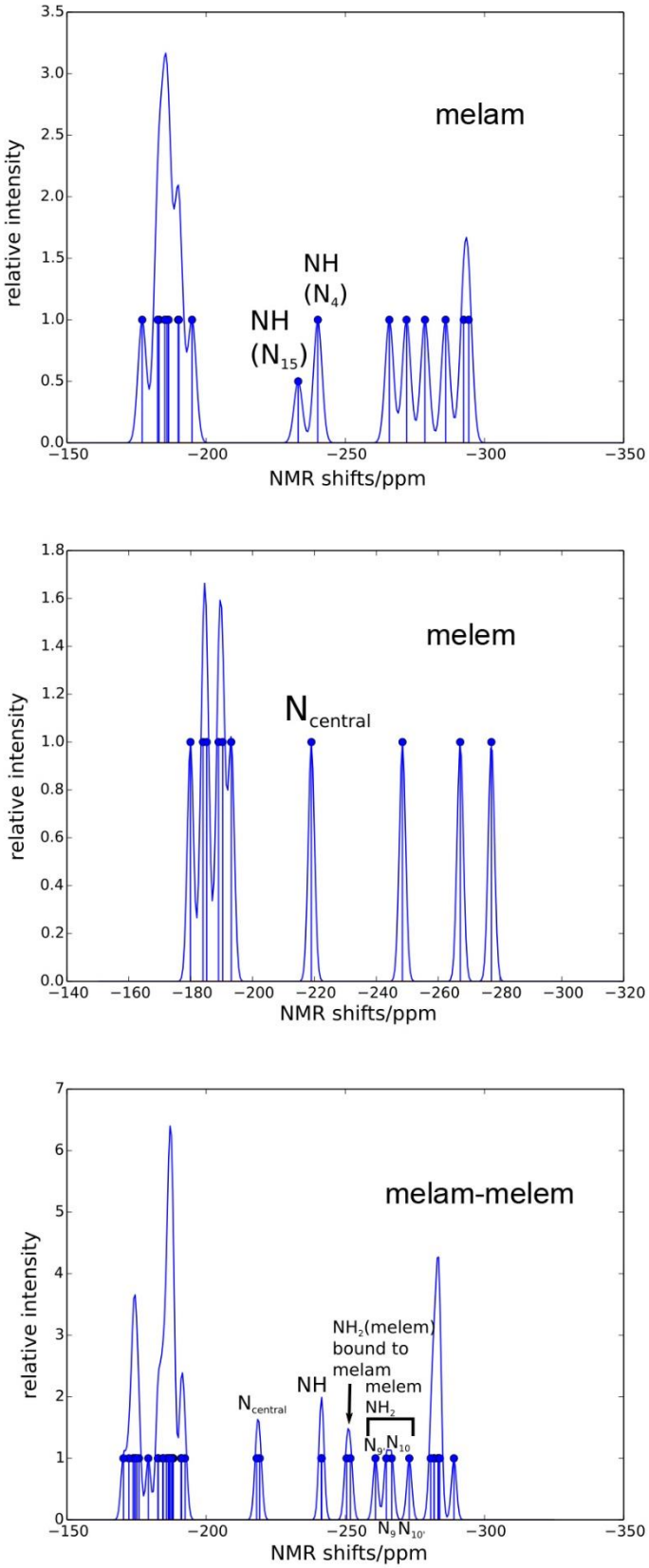

Figure 7.3.5 Simulated ^{15}N NMR spectra of melam, melem and the melam-melem adduct as obtained from DFT calculations. Spectra have not been corrected for methodical errors, shifts thus differ by about 14 ppm from values found in literature.

Table 7.3.9 Melam-melem adduct: atom site coordinates *x*, *y*, *z* for the optimized crystal structure obtained at the PBE-D3/pob-TZVP level.

Cell parameters				
a	4.56000			
b	19.3340			
c	21.5800			
α	73.34			
β	89.1			
γ	88.4			
Atom site label	**Atom type**	***x***	***y***	***z***
N1	N	0.54773813873284	0.60862836607480	0.34146463006187
C1	C	0.43638551153140	0.60116351340295	0.40191683910540
N2	N	0.51923695942744	0.64845634694994	0.43297582181672
H1	H	0.65427257178543	0.69106988001197	0.41257057100306
H2	H	0.42488433136252	0.64643253199353	0.47621561729499
N3	N	0.24719359869270	0.54969978066837	0.43282089905447
C2	C	0.16233740962273	0.50541946270601	0.39852980360822
N4	N	0.99252406369003	0.44915025788536	0.42927328621105
H3	H	0.90996413215320	0.44946155603619	0.47395072289854
H4	H	0.88192850795471	0.42385598439695	0.40105893576374
N5	N	0.23653068967031	0.51286569616337	0.33547241700896
C3	C	0.42809107885010	0.56556369085408	0.31015156474422
N6	N	0.51186051532241	0.57383491714735	0.24636435685662
H5	H	0.46435095743449	0.53272805673599	0.22625664395640
C4	C	0.59802330101209	0.63800414120106	0.20281831784017
N7	N	0.77147372725066	0.63147541674528	0.15352396344505
C5	C	0.84235276813199	0.69499742882569	0.10995009945892
N8	N	0.02789546053340	0.69111614672392	0.06123076764432
H6	H	0.09699552012435	0.73815687129286	0.02876745321703
H7	H	0.15082806775658	0.64481411245189	0.06712953522157
N9	N	0.74373657226489	0.76101958489656	0.11183213422009
C6	C	0.57624418299536	0.76102924420652	0.16428259774639
N10	N	0.48005530626719	0.82418290107822	0.17279605787687
H8	H	0.50095250653161	0.87268291975931	0.13853174356917
H9	H	0.40737388065732	0.82395807729253	0.21864155274557
N11	N	0.49597283211518	0.70058990494642	0.21081371902083
N12	N	0.97387178927282	0.37978195112534	0.16231647848907
C7	C	0.07847352699017	0.39041954744367	0.10075250882149
N13	N	0.99549226043293	0.34459200571479	0.06836815799763
H10	H	0.86675061707029	0.30062429513997	0.08879248561381
H11	H	0.08422486072965	0.34908919874919	0.02407378844431

N14	N	0.26035404169661	0.44378748874534	0.07004506329622
C8	C	0.34964919885620	0.48592728385410	0.10587737268004
N15	N	0.51331964574740	0.54368110133294	0.07568554590672
H12	H	0.59028442132223	0.54602835118055	0.03007151010150
H13	H	0.62886242257138	0.56767995182704	0.10425068243275
N16	N	0.28541009618828	0.47490822642732	0.16996732839176
C9	C	0.09603612320459	0.42141827054320	0.19459165458835
N17	N	0.01798063556286	0.41100644346079	0.25910854835952
H14	H	0.06115886751504	0.45208707535261	0.27948708938517
C10	C	0.91470305929373	0.34810888499447	0.30144892523742
N18	N	0.74558025655739	0.35687328438306	0.35056002605936
C11	C	0.65072997820299	0.29477999672152	0.39271619643126
N19	N	0.46517910187309	0.30167396630180	0.44043247731681
H15	H	0.35609997397404	0.34994629071823	0.43401559046827
H16	H	0.37938432274346	0.25647198180712	0.47277569530604
N20	N	0.72652160757870	0.22738084436703	0.39011557920150
C12	C	0.90092222580766	0.22538755446596	0.33928432386425
N21	N	0.98120002978645	0.15963765959968	0.33241787809948
H17	H	0.99756668986869	0.11669123596667	0.37262007522045
H18	H	0.10670981814599	0.15809850762852	0.29298748995999
N22	N	0.99890991912918	0.28393102643644	0.29329411603506
N23	N	0.91158252814918	0.77086387357032	0.38426234592685
N24	N	0.03125583769360	0.71899793606631	0.30250815298574
H19	H	0.18358310746441	0.71215612820212	0.26837970393111
H20	H	0.86631712143430	0.68208054095662	0.31745259157807
C13	C	0.07668120068258	0.77016643927023	0.33116494988293
N25	N	0.28655140007309	0.81920830242215	0.30414262736337
C14	C	0.31470340833120	0.87547518249929	0.32706819189684
N26	N	0.50440085476601	0.92765074608753	0.30055755301667
C15	C	0.49920360565602	0.98671346302875	0.32337369675913
N27	N	0.67765197013779	0.04036811583529	0.29490416574572
H21	H	0.67829617204616	0.08479621101546	0.31122300002165
H22	H	0.82290956985899	0.03926979381622	0.25766851918553
N28	N	0.32816992095168	0.99604782419580	0.37261031665309
C16	C	0.14823325300915	0.94302094359420	0.40172910419922
N29	N	0.97970580516682	0.94825020930863	0.45083455323446
C17	C	0.80831473830855	0.89166775878965	0.47974201394255
N30	N	0.64817036144456	0.89672230488597	0.53094176463473
H23	H	0.66216937035697	0.94201477671352	0.54597312049330
H24	H	0.51174346413701	0.85590262102886	0.55523791476280
N31	N	0.78231670974135	0.83057645311170	0.46060023015174

C18	C	0.93926523865128	0.82600677436335	0.40890599169333
N32	N	0.13603506998814	0.88127483569205	0.37941368896362
N33	N	0.62731820419350	0.21975205459097	0.11625687954942
C19	C	0.45320224938330	0.21420291761998	0.16930547760707
N34	N	0.47193134532375	0.26524986553753	0.19934545393671
H25	H	0.62748934467241	0.30448694602642	0.18529921738135
H26	H	0.31442943392981	0.26943374481653	0.23318496120883
N35	N	0.26300653732452	0.15954782439911	0.19444095323288
C20	C	0.27170027515554	0.10423654680421	0.16936398849628
N36	N	0.09815317812009	0.04760646318319	0.19192294028653
C21	C	0.14048270159603	0.98989220983717	0.16836439576912
N37	N	0.96508065566278	0.93376900750318	0.19188377068357
H27	H	0.80861154446392	0.93264060568832	0.22706519447612
H28	H	0.99159823647178	0.88974525640358	0.17558825646813
N38	N	0.34424200541034	0.98404724543374	0.12342957476265
C22	C	0.50800695536236	0.04131628315123	0.09705616558829
N39	N	0.70881635397236	0.04052948792863	0.05178743285026
C23	C	0.84713344249442	0.10338170848138	0.02292389677231
N40	N	0.03826902790503	0.10345445522683	0.97536859235597
H29	H	0.13134552922086	0.15141633784358	0.94884860542397
H30	H	0.08971554683062	0.05638099052908	0.96422714907666
N41	N	0.81166522152140	0.16613824080997	0.03968770360361
C24	C	0.63922022387631	0.16489292954180	0.09061075037747
N42	N	0.46981924309041	0.10365507387374	0.11851564305071
N43	N	0.45225979605777	0.39137206762349	0.65853462479191
C25	C	0.56361696982187	0.39883610306272	0.59808316046488
N44	N	0.48076432366891	0.35154193019423	0.56702435797177
H31	H	0.34573088648459	0.30892918333132	0.58742813529338
H32	H	0.57511672257871	0.35356545288497	0.52378468792453
N45	N	0.75280529760414	0.45029853378648	0.56717863313865
C26	C	0.83766057448853	0.49457992135842	0.60146932192216
N46	N	0.00747698401987	0.55084940315899	0.57072648527479
H33	H	0.09003660126686	0.55053980715786	0.52604846884589
H34	H	0.11806768079765	0.57614340570154	0.59894053898156
N47	N	0.76346900850354	0.48713459686346	0.66452687984508
C27	C	0.57191655829960	0.43443679436249	0.68984725115997
N48	N	0.48813892532659	0.42616458299652	0.75363518717097
H35	H	0.53564716791671	0.46727101252054	0.77374253257890
C28	C	0.40197515690327	0.36199542775316	0.79718229537739
N49	N	0.22852849018201	0.36852397329389	0.84647698626587
C29	C	0.15765175251979	0.30500099996713	0.89005054357937

N50	N	0.97210536182244	0.30888284090089	0.93877021294466
H36	H	0.90299931270054	0.26184283104041	0.97123429849687
H37	H	0.84917769287878	0.35518497818629	0.93287028017809
N51	N	0.25626681963352	0.23897896405501	0.88816814351319
C30	C	0.42375597423944	0.23897038144434	0.83571727435786
N52	N	0.51994364933022	0.17581699766629	0.82720365644370
H38	H	0.49905323528496	0.12731706186653	0.86146724380899
H39	H	0.59262375765796	0.17604025133704	0.78135908659768
N53	N	0.50402706633129	0.29940984775897	0.78918665166473
N54	N	0.02612983987990	0.62021789825485	0.83768376048460
C31	C	0.92152570615243	0.60958126376461	0.89924773109691
N55	N	0.00450501578658	0.65540909905200	0.93163120090223
H40	H	0.13324781062596	0.69937635820205	0.91120881045695
H41	H	0.91577538179201	0.65091218899667	0.97592600572873
N56	N	0.73964650141284	0.55621363221192	0.92995593671877
C32	C	0.65035300009866	0.51407332288448	0.89412388662414
N57	N	0.48667901654130	0.45631907338037	0.92431478386389
H42	H	0.40971235913150	0.45396994317802	0.96992944548845
H43	H	0.37114086121588	0.43232077488568	0.89574953601348
N58	N	0.71458974963986	0.52509153746114	0.83003340678108
C33	C	0.90395777635096	0.57858178707181	0.80540902370368
N59	N	0.98202001662301	0.58899460447558	0.74089175166168
H44	H	0.93884273904261	0.54791433451199	0.72051365227471
C34	C	0.08529908839091	0.65189207312001	0.69854990566721
N60	N	0.25441569603246	0.64312783206304	0.64943889776965
C35	C	0.34926584876807	0.70522226360260	0.60728316373628
N61	N	0.53481719556747	0.69832747786958	0.55956697093687
H45	H	0.64389302109967	0.65005590564158	0.56598457983371
H46	H	0.62061788457374	0.74352807342053	0.52722259061607
N62	N	0.27347706886402	0.77262128522632	0.60988440408196
C36	C	0.09907716270343	0.77461332549340	0.66071548428058
N63	N	0.01879660525409	0.84036202348213	0.66758199797845
H47	H	0.00242854842056	0.88330926855217	0.62738078858601
H48	H	0.89329302884742	0.84190373542855	0.70701204448713
N64	N	0.00108801611609	0.71606939252749	0.70670544745690
N65	N	0.08841774664850	0.22913647421906	0.61573776473142
N66	N	0.96874362400376	0.28100039082061	0.69749142795475
H49	H	0.81641924718720	0.28784403508770	0.73162051350775
H50	H	0.13368246167326	0.31791966399235	0.68254744289516
C37	C	0.92331626592949	0.22983400869218	0.66883508095851
N67	N	0.71344967924414	0.18079212404632	0.69585729855010

C38	C	0.68529572657180	0.12452415869508	0.67293179869735
N68	N	0.49560146791694	0.07234969392734	0.69944280063066
C39	C	0.50079719138013	0.01328674092068	0.67662631409604
N69	N	0.32235340236093	0.95963235552613	0.70509569679769
H51	H	0.32170450660047	0.91520459283267	0.68877763006469
H52	H	0.17709609422539	0.96073006695641	0.74233109814412
N70	N	0.67183031327676	0.00395224176286	0.62738940335639
C40	C	0.85176539440352	0.05697885841104	0.59827096413811
N71	N	0.02029564224562	0.05174928648070	0.54916478495191
C41	C	0.19168316484609	0.10833245388379	0.52025811187308
N72	N	0.35182676691365	0.10327779697513	0.46905897927174
H53	H	0.33783472915544	0.05798590152854	0.45402755097287
H54	H	0.48825377263563	0.14409753195729	0.44476198950607
N73	N	0.21768428565622	0.16942508422574	0.53939922279137
C42	C	0.06073522660267	0.17399392839493	0.59109317431405
N74	N	0.86396741234243	0.11872596365150	0.62058635131118
N75	N	0.37268534355515	0.78024841228132	0.88374310949759
C43	C	0.54680001185632	0.78579733820552	0.83069505824036
N76	N	0.52806935246204	0.73475120686508	0.80065473179592
H55	H	0.37251178305156	0.69551311012818	0.81470029100735
H56	H	0.68556880189832	0.73056559869891	0.76681449491360
N77	N	0.73698949654337	0.84045193354622	0.80555908670083
C44	C	0.72829552791522	0.89576372608638	0.83063646153627
N78	N	0.90184073268194	0.95239301720517	0.80807721960765
C45	C	0.85951345886295	0.01010637192238	0.83163583483329
N79	N	0.03491763588816	0.06623148101281	0.80811690701523
H57	H	0.19138620313422	0.06735972240766	0.77293542027637
H58	H	0.00840193148256	0.11025396204803	0.82441150471599
N80	N	0.65575924509991	0.01595102588004	0.87657086816312
C46	C	0.49199364717461	0.95868231171051	0.90294390223673
N81	N	0.29118319321786	0.95946953165535	0.94821325239705
C47	C	0.15287099921822	0.89661728177481	0.97707545303026
N82	N	0.96173289251117	0.89654514812832	0.02463072072215
H59	H	0.86865377468694	0.84858411799900	0.05115096306294
H60	H	0.91028359200303	0.94361687057793	0.03577339411366
N83	N	0.18833846714717	0.83386070956250	0.96031221043231
C48	C	0.36078391771177	0.83510731701031	0.90938943568612
N84	N	0.53017913605186	0.89634400088083	0.88148431381911

7.4 List of Publications

I. Published as Part of this Thesis

1. Synthesis and Structure of Melamium Bromide $C_6N_{11}H_{10}Br$ and Melamium Iodide $C_6N_{11}H_{10}I$

Fabian K. Kessler, Thaddäus J. Koller, and Wolfgang Schnick

Published in: *Z. Anorg. Allg. Chem.* **2018**, *644*, 186-192.

Conceptualization and analyses were performed by Fabian K. Kessler, who also wrote the manuscript. Syntheses were performed by Thaddäus J. Koller under instruction of Fabian K. Kessler. Wolfgang Schnick supervised the project. Revision of the original manuscript was done by Fabian K. Kessler and Wolfgang Schnick.

2. Structure Elucidation of a Melam–Melem Adduct by a Combined Approach of Synchrotron X-ray Diffraction and DFT Calculations

Fabian K. Kessler, Asbjörn M. Burow, Gökcen Savasci, Tobias Rosenthal, Peter Schultz, Eva Wirnhier, Oliver Oeckler, Christian Ochsenfeld, and Wolfgang Schnick

Published in: *Chem. Eur. J.* **2019**, *25*, 8415-8424.

Project organization, the major part of formal analyses and part of the syntheses were done by Fabian K. Kessler. Asbjörn M. Burow performed quantum-chemical structure optimizations of melam, melem and the melam-melem adduct. Further quantum-chemical calculations, in particular of NMR shifts, were done by Gökcen Savasci. Microfocussed X-ray data were recorded by Tobias Rosenthal and the structure solved and refined from these by Peter Schultz. Eva Wirnhier is responsible for most of the syntheses and original conceptualization. Oliver Oeckler supervised the microfocus X-ray analysis of the adduct compound. Christian Ochsenfeld supervised all quantum-chemical calculations. Wolfgang Schnick supervised the project. The manuscript was written by Fabian K. Kessler in a leading role with support of Asbjörn M. Burow and Oliver Oeckler. Revision of the original manuscript was performed by Fabian K. Kessler, Gökcen Savasci, Oliver Oeckler, Christian Ochsenfeld and Wolfgang Schnick.

3. Ammelinium Sulfate Monohydrate and Ammelinium Sulfate Cyanuric Acid – Synthesis and Structural Characterization

Fabian K. Kessler, and Wolfgang Schnick

Published in: *Z. Anorg. Allg. Chem.* **2019**, *645*, 848-856.

Conceptualization, syntheses and analyses were done by Fabian K. Kessler. The manuscript was written by Fabian K. Kessler. Wolfgang Schnick supervised the project. Both authors revised the manuscript.

4. From Heptazines to Triazines – On the Formation of Poly(triazine imide)
Fabian K. Kessler, and Wolfgang Schnick
Published in: *Z. Anorg. Allg. Chem.* **2019**, *645*, 857-862.

Conceptualization, syntheses and analyses were done by Fabian K. Kessler. The manuscript was written by Fabian K. Kessler. Wolfgang Schnick supervised the project. Both authors revised the manuscript.

5. Melamium Thiocyanate Melam, a Melamium Salt with Disordered Anion Sites
Fabian K. Kessler, Alexander M. Schuhbeck, and Wolfgang Schnick
Published in: *Z. Anorg. Allg. Chem.* **2019**, *645*, 840-847.

Conceptualization, analyses and part of the syntheses were performed by Fabian K. Kessler. Most of the syntheses were performed by Alexander M. Schuhbeck under instruction of Fabian K. Kessler. Wolfgang Schnick supervised the project. The manuscript was written by Fabian K. Kessler. Revision of the original manuscript was done by Fabian K. Kessler and Wolfgang Schnick.

II. Further Publications

6. Functional carbon nitride materials — design strategies for electrochemical devices
Fabian K. Kessler, Yun Zheng, Dana Schwarz, Christoph Merschjann, Wolfgang Schnick, Xinchen Wang and Michael J. Bojdys
Published in: *Nat. Rev. Mater.* **2017**, *2*, 17030.

Fabian K. Kessler and Wolfgang Schnick are responsible for the chapter on 'Formation of carbon nitride materials'. The chapter on 'Applications in electronics and catalysis' was written by Yun Zheng and Xinchen Wang. Dana Schwarz and Michael J. Bojdys wrote the chapter on 'Carbon nitride photocatalysts'. Christoph Merschjann contributed a paragraph on analytical methods. Conceptualization and project organization were performed by Michael J. Bojdys. All authors revised the manuscript.

7.5 CSD and CCDC numbers

Crystallographic data for compounds elucidated in this thesis have been deposited with the Cambridge Crystallographic Data Centre, CCDC, 12 Union Road, Cambridge CB21EZ, UK or with the Fachinformationszentrum Karlsruhe, FIZ, 76344 Eggenstein-Leopoldshafen, Germany (Fax: +49-7247-808-666; E-Mail: crysdata@fiz-karlsruhe.de, http://www.fiz-karlsruhe.de/request for deposited data.html). Copies of the data can be obtained free of charge on quoting the CCDC depository numbers for CCDC and CSD depository numbers for FIZ.

$C_6N_{11}H_{10}Br$	CSD-433426
$C_6N_{11}H_{10}I$	CSD-433427
$6C_3N_5H_6O^+ \cdot 3SO_4^{2-} \cdot 1⅔C_3N_3H_3O_3 \cdot H_2O$	CCDC-1898048
$2C_3N_5H_6O^+ \cdot SO_4^{2-} \cdot H_2O$	CCDC-1898049
$C_6N_{11}H_{10}SCN \cdot C_6N_{11}H_9$	CCDC-1898050
$C_6N_{11}H_9 \cdot C_6N_{10}H_6$	CCDC-1904950

7.6 Contributions to Conferences

1. Synthese von CN-Netzwerksverbindungen in lewisaciden Salzschmelzen

2. Obergurgl-Seminar Festkörperchemie, **2016**

2. Ionothermalsynthese von Kohlenstoff(IV)-Stickstoff-Verbindungen in $ZnCl_2$-Schmelze

45. Hirschegg-Seminar Festkörperchemie, **2016**

3. Synthese und Charakterisierung von Melamiumsalzen

3. Obergurgl-Seminar Festkörperchemie, **2018**

4. Synthese und Charakterisierung von Melamiumsalzen

47. Hirschegg-Seminar Festkörperchemie, **2018**

5. Neues aus der CN-Chemie: (Melamium- und) Ammeliniumsalze

4. Obergurgl-Seminar Festkörperchemie, **2019**